Conception and optimization of supercritical CO2 Brayton cycles for coal-fired power plant application

Qiao Zhao

ÉCOLE DOCTORALE RESSOURCES PROCÉDÉS PRODUITS ENVIRONNEMENT
LABORATOIRE RÉACTION ET GÉNIE DES PROCÉDÉS

THÈSE DE DOCTORAT

Présentée par

Qiao ZHAO

Pour l'obtention du grade de

Docteur en Science de l'Université de Lorraine
Spécialité : Génie des Procédés et des Produits

Conception and optimization of supercritical CO_2 Brayton cycles for coal-fired power plant application

Présentée et soutenue publiquement le 15 mai 2018 à Nancy

Directeur de thèse : Jean-Noël JAUBERT
Co-directeur de thèse : Romain PRIVAT

Tuteurs industriels : Mounir MECHERI, Thibaut NEVEUX

Composition du jury :

Rapporteurs	Prof. Claire ADJIMAN	Imperial College
	Prof. Xavier JOULIA	Université Toulouse (ENSIACET)
Examinateurs	Prof. Jean-Noël JAUBERT	Université de Lorraine (ENSIC)
	Dr. Romain PRIVAT	Université de Lorraine (ENSIC)
Invités	Prof. Jean-Marc COMMENGE	Université de Lorraine (ENSIC)
	Mounir MECHERI	EDF R&D
	Dr. Thibaut NEVEUX	EDF R&D

LRGP - Laboratoire **R**éactions et **G**énie des **P**rocédés
1 rue Grandville - 54001 Nancy Cedex

Acknowledgment

I would like to first thank my tutors and professors, who have guided me with patience throughout this scientific adventure during three years. Thank Prof. Jean-Noël Jaubert and Dr. Romain Privat for their expertise and devotion in thermodynamic. Their criticism and strictness on academy impressed me and their modifications on my papers helped me to make progress. Thank Mounir Mecheri, my industrial supervisor at EDF, for the support on my decisions and the patience on my growth since my first day in EDF. His initial research on SC-CO_2 Brayton cycle has set cornerstones to start this thesis. Thanks to my other industrial supervisor, the foresighted, talented Dr. Thibaut Neveux for his suggestions on this thesis. His insight on process synthesis inspired me to think more, which finally makes it possible to accomplish all the ambitious goals defined during this PhD.

I would like to express my gratitude to the members of the jury for agreeing to judge my dissertation. I would especially like to thank Prof. Claire Adjiman and Prof. Xavier Joulia for the careful reading of my dissertation and accepting the role of reporter.

I thank Electricité de France (EDF) for having funded my thesis. Thanks to Julien Najac and Albannie Cagnac, respectively the head of group I8F and the project manager of "advanced cycle", for trusting me in carrying out this thesis. I would like to thank all the members of the group for their welcome within the team, their experience and the everyday interesting discussions, this three years' experience could not have been such fulfilling without them. I also take advantage to thank Dr. Yann Le Moullec, for trusting me and selecting me for this innovative topic. Without his confidence in me, I would never have courage to get a PhD.

Finally, I would dedicate my thanks to my solid backing, my family. The passion of my parents in their work gives me more reasons to pursue higher and to work harder with dedication. I thank my grandmothers, who support me without any reason since I was a child. Thank my dear husband, Dr. Tianyuan Wang, for our everyday constructive talks on science and life, for his invaluable emotional support when I felt frustrated. I appreciate so much to have you in my journey for the past, right now and in the future. My lovely friends, Guangze, Ting, Yusong, Shen, Yanni, Hongjie..., I also thank them for letting me realize my merits and defects, encouraging me to become be a better person.

Résumé en français des travaux menés et des résultats obtenus

L'amélioration des systèmes énergétiques est considérée comme un levier technologique pour répondre aux défis liés à la croissance de la demande d'électricité et des émissions des gaz à effet de serre. Les futures centrales devraient présenter une intégration thermique plus flexible, des niveaux de température et de pression plus élevés et des sources de chaleur mixtes possibles.

Une des solutions fiables consiste à remplacer le cycle conventionnel de Rankine à vapeur d'eau (H2O) par un cycle de Brayton au CO_2 supercritique (CO_2 -SC), où un bon compromis entre les gains d'efficacité et la simplicité du cycle ont déjà été soulignés [1]. Un tel cycle à haut rendement est théoriquement prometteur pour les applications nucléaires, fossiles et solaires thermiques.

La polyvalence du cycle de Brayton au CO_2-SC a d'abord été révélée en 1967 [2]. Deux ans plus tard, Angelino [3] a approfondi ses investigations concernant la configuration du cycle. Alors que le potentiel de cette technologie a été mis en évidence pour la production de l'énergie, son développement a été freiné pour des raisons technologiques : les turbines à gaz présentaient à l'époque une faible efficacité et des défauts de fiabilité en raison des limitations métallurgiques (conditions de haute pression et haute température).

La thèse de Dostal en 2004 [4] est considérée comme la première étude de faisabilité des cycles de Brayton au CO_2-SC pour l'industrie du nucléaire dans des conditions réelles. Grâce à ses conclusions en matière de rendement et de dimensionnement du cycle, les avantages de cette technologie ont été mis en évidence et quantifiés : le cycle de Brayton au CO_2-SC permet d'utiliser de petites turbomachines par rapport au cycle à vapeur d'eau dans les mêmes conditions de température et pression.

Un des principaux obstacles au déploiement du cycle de Brayton au CO_2-SC est de justifier sa faisabilité, sa viabilité et son potentiel à l'échelle industrielle. D'un côté, des chercheurs et entreprises se concentrent sur les aspects fondamentaux de cette technologie comme l'optimisation paramétrique ainsi que le contrôle des turbomachines. D'un autre côté, la configuration du système à l'échelle industrielle reste inconnue.

Objectifs de la thèse

Dans ce contexte, l'objectif de cette thèse est de fournir une conception et une optimisation du cycle de Brayton au CO_2-SC afin d'évaluer le potentiel de cette technologie.

Dans le contexte des centrales de charbon, cette thèse a pour but d'évaluer la performance énergétique et les coûts de cette technologie innovante avant l'étape d'industrialisation. L'ambition principale de cette thèse est de proposer une nouvelle méthodologie pour l'optimisation des centrales électriques, permettant de sélectionner automatiquement le procédé optimal parmi une grande quantité de configurations possibles.

Résultats de la thèse

Choix de l'équation d'état pour représenter le dioxyde de carbone supercritique

Les propriétés physiques du CO_2 au voisinage de son point critique (dans des états sub- ou supercritiques) peuvent varier de manière abrupte. Par exemple, la capacité calorifique isobare (c_p) du CO_2 tend vers l'infini au niveau du point critique alors qu'un effet mémoire de cette divergence peut être observé dans la région supercritique (voir la Figure 1). Cet effet mémoire se traduit par une courbe à l'allure caractéristique (en forme de cloche) obtenue, en traçant la propriété cp en fonction de la température à 11,8 MPa. Dans la première partie de la thèse, une procédure rigoureuse a été proposée afin de sélectionner une équation d'état (EoS) capable de représenter les propriétés d'intérêt du CO_2-SC au voisinage de son point critique et dans le domaine supercritique. Plusieurs types d'équations d'état ont été considérées : entre autres, des équations d'état de type cubique ou de type SAFT, fréquemment utilisées pour la simulation de procédés, mais également des modèles spécifiques au CO_2. Le but de cette partie était donc également de quantifier la perte de précision induite par le passage d'une équation d'état spécifique au CO_2 à une équation d'état de type SAFT ou cubique afin de réaliser un choix de modèle thermodynamique éclairé pour les simulations de la centrale à charbon à venir dans les étapes ultérieures de la thèse.

En comparant la densité, la capacité calorifique isobare, les vitesses du son avec des données expérimentales pour six équations d'état différentes, l'équation d'état de Span Wagner (SW) a été identifiée – comme cela était attendu - comme l'équation d'état la plus précise pour le CO_2. Bien que la capacité calorifique isobare soit un critère conventionnel de comparaison, la vitesse du son est rarement prise en compte pour la sélection de l'équation d'état. Les résultats de la comparaison impliquent que la vitesse du son peut être un critère de validation exigeant et pertinent pour la sélection d'une équation d'état pour une application donnée.

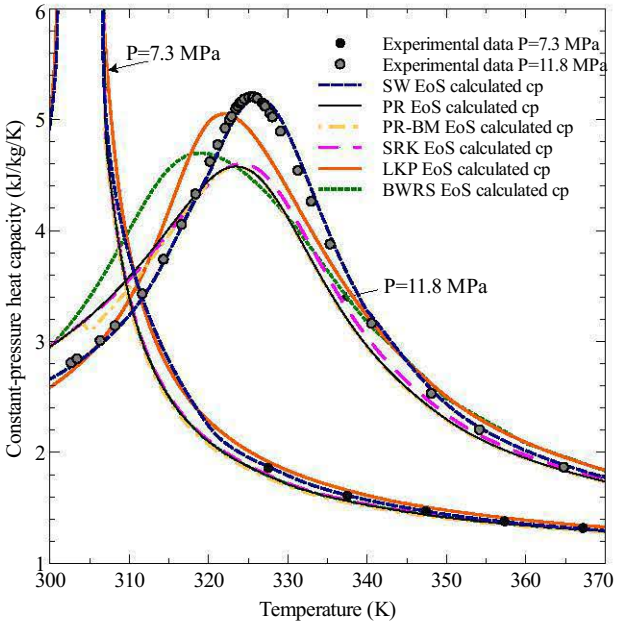

Figure 1: Comparaison de la capacité calorifique isobare expérimentale du CO_2 avec les valeurs calculées à deux pressions proches de la pression critique à partir de six équations d'état différentes

Impact de l'équation d'état sur la modélisation du cycle de Brayton au CO_2-SC

La sélection de l'équation d'état pour représenter le CO_2 est une étape nécessaire pour garantir la précision des estimations des propriétés fluides aux divers points de fonctionnement du cycle de Brayton. Ceci étant fait, nous nous sommes intéressés à quantifier l'impact de l'imprécision de l'équation d'état choisie sur le dimensionnement du procédé du cycle de Brayton ainsi que sur l'estimation du rendement. En effet, les résultats des étapes de simulation et d'optimisation du procédé dépendent de la précision de l'équation d'état retenue. Nos études démontrent que l'incertitude de l'équation d'état a des impacts non négligeables sur l'optimisation ou le dimensionnement du cycle de Brayton au CO_2-SC étudié (voir Figure 2).

A la lumière de ces résultats, il a été décidé de conserver l'équation de SW pour les simulations et optimisations à venir dans le reste de la thèse.

Optimisation de la configuration du cycle de Brayton selon une approche « process design »

Cette partie a un double objectif : (1) proposer une méthodologie de type « process design » reposant sur l'optimisation d'une « superstructure » (ce terme est défini par la suite) appliquée à la conception d'une centrale électrique et (2) l'appliquer afin de concevoir une centrale optimale reposant sur un cycle de Brayton au CO_2-SC. Il est à noter que la méthodologie « process design

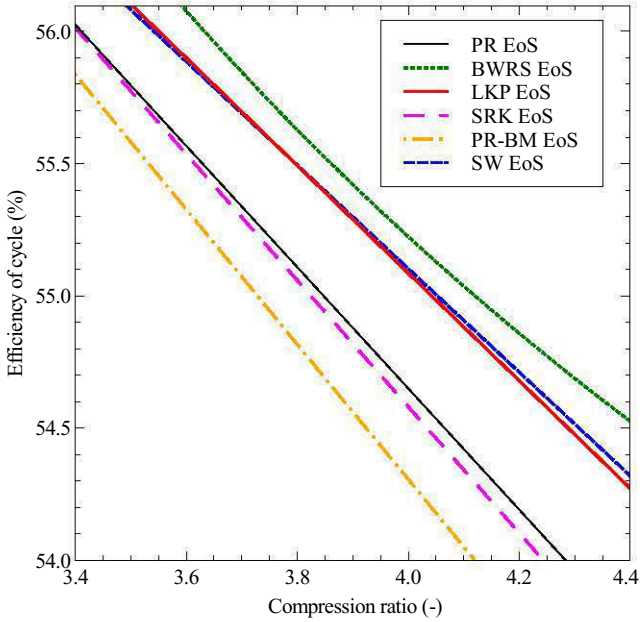

Figure 2: Influence du choix de l'équation d'état sur l'estimation du rendement du cycle de Brayton

» proposée va permettre de comparer différentes technologies innovantes possibles pour mettre en évidence la technologie optimale.

Plus précisément, on commence par définir une superstructure qui est un schéma de procédé contenant les opérations unitaires du cycle de Brayton et des interrupteurs (permettant d'autoriser ou d'interdire des flux de matière). En jouant sur la position (ouvert/fermé) de ces interrupteurs, on peut obtenir des milliers de configurations différentes (contenant en particulier, toutes celles que l'on souhaite tester). Les paramètres opératoires réels (niveaux de pression, débits ...) et entiers (caractère ouvert/fermé de chaque interrupteur) sont déterminés à travers une procédure d'optimisation. On parle alors d'un problème mathématique d'optimisation de type MINLP (Mixed Integer NonLinear Programming).

Dans cette thèse, un simulateur de procédé commercial, ProSimPlus, a été utilisé pour mettre en œuvre la méthodologie. Ce dernier dispose d'une interface graphique permettant de dessiner la superstructure désirée. L'avantage de la méthodologie proposée est de permettre d'identifier automatiquement la configuration optimale du cycle parmi un très grand nombre de possibilités.

La méthodologie proposée dans cette thèse permet pour la première fois (à la connaissance de l'auteur) de gérer entièrement la boucle d'optimisation à travers l'interface d'un simulateur de procédé. Les variables continues ainsi que les variables entières discrètes sont optimisées simultanément dans cette boucle. La méthode d'optimisation choisie repose sur un algorithme

évolutionnaire type colonies de fourmis (elle se nomme MIDACO). Par sa formulation générale, notre méthodologie pourrait être appliquée à d'autres problèmes de synthèse de procédés.

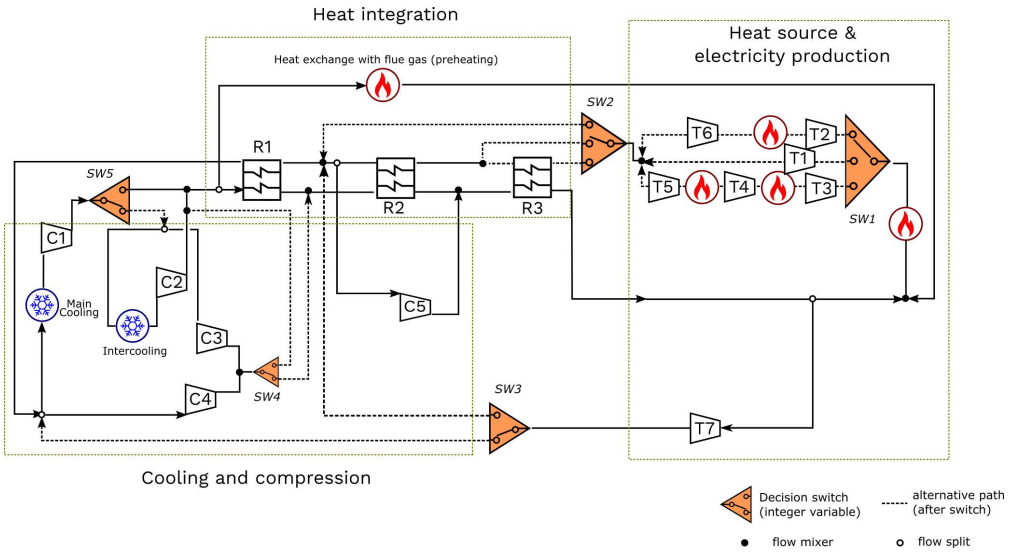

Figure 3: Superstructure SS2 conçue pour l'optimisation du cycle de Brayton au CO_2-SC ($2^7 \times 3^2 = 1152$ alternatives)

La méthodologie proposée a été appliquée au contexte industriel des centrales à charbon au CO_2-SC. Une superstructure contenant plus de 1000 alternatives a été conçue ; une optimisation a été effectuée dans le but de trouver la configuration maximisant le rendement énergétique du cycle (voir la Figure 3). La configuration la plus prometteuse a été identifiée comme une configuration de double resurchauffe-recompression (voir la Figure 4) associée à un rendement net de 51,4 % -pts ; il s'agirait a priori du cycle de Brayton au CO_2-SC le plus performant connu dans les conditions de température et de pression considérées. En considérant d'autres sources chaudes, le rendement du cycle pourrait atteindre 52,1 % -pts démontrant ainsi que la nature de la source chaude influence la performance du cycle de Brayton.

Couplage des critères énergétiques et économiques pour déterminer la configuration optimale du cycle de Brayton

Dans cette partie, la configuration optimale du cycle est déterminée de manière à maximiser son rendement énergétique (comme précédemment) mais de plus, on cherche simultanément à minimiser les coûts du procédé ; on parle alors d'optimisation multi-objectifs.

L'analyse technico-économique joue un rôle important dans la procédure d'évaluation d'une technologie. Pour ce faire, des fonctions de coût internes à EDF et propres aux cycles de Brayton au CO_2-SC ont été utilisées afin de permettre l'estimation des coûts d'investissement (CAPEX),

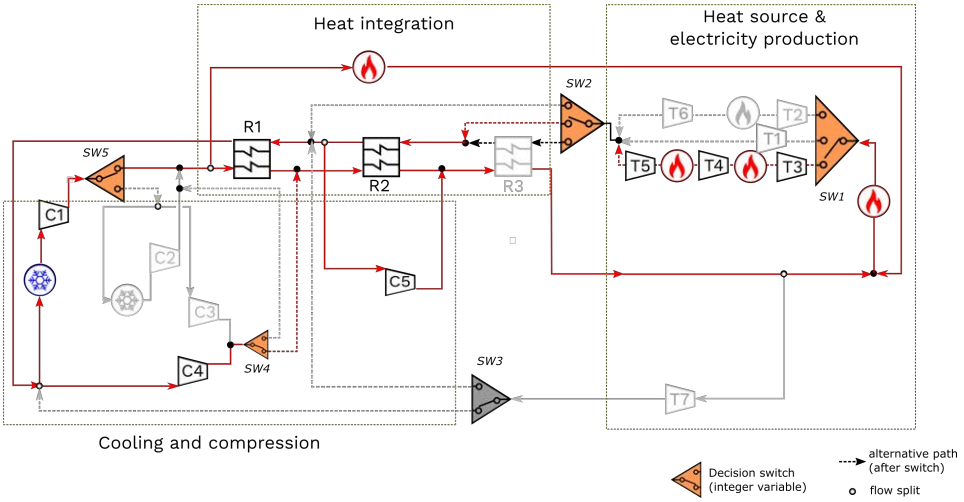

Figure 4: Procédé optimal obtenu après l'optimisation superstructure énergétique

des dépenses opérationnelles (OPEX) et du coût actualisé de l'électricité (LCOE).. Les critères pris en compte pour l'optimisation multi-objectif du cycle sont : le LCOE (jugé comme critère prioritaire) ainsi que le CAPEX et l'efficacité du cycle. Les résultats de cette optimisation sont reportés sur la Figure 5 sous la forme d'un front de Pareto.

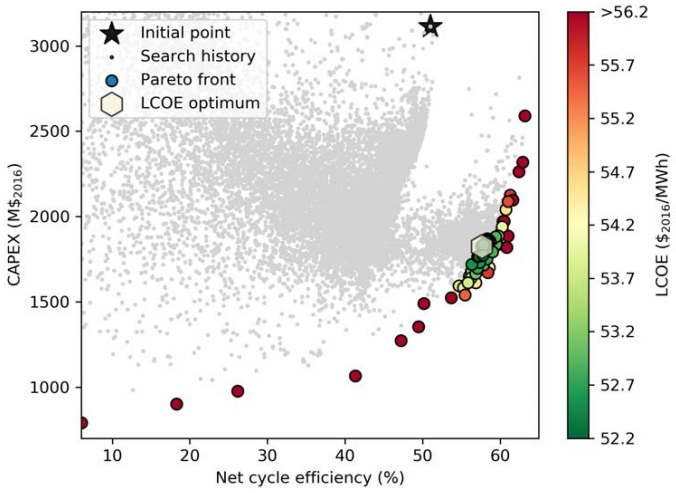

Figure 5: Résultats de l'optimisation technico-économique illustrée par le tracé d'un front de Paréto (influence conjuguée ducoût d'investissement et du rendement du cycle sur le LCOE)

Le point initial de l'optimisation multi-objectifs (60,9 $ / MWh LCOE, 3124 M $ de CAPEX, 51%-pts d'efficacité nette du cycle) est le meilleur résultat obtenu pendant l'optimisation mono-objectif (rendement du cycle). L'optimisation multi-objectifs conduit à un LCOE de 52,3 $ /

MWh (CAPEX de 1826 M$, une efficacité nette du cycle de 57 %-pts). La configuration optimale est nommée « simple resurchauffe-recompression avec refroidissement intermédiaire» et est représentée sur les Figures 5 et 6.

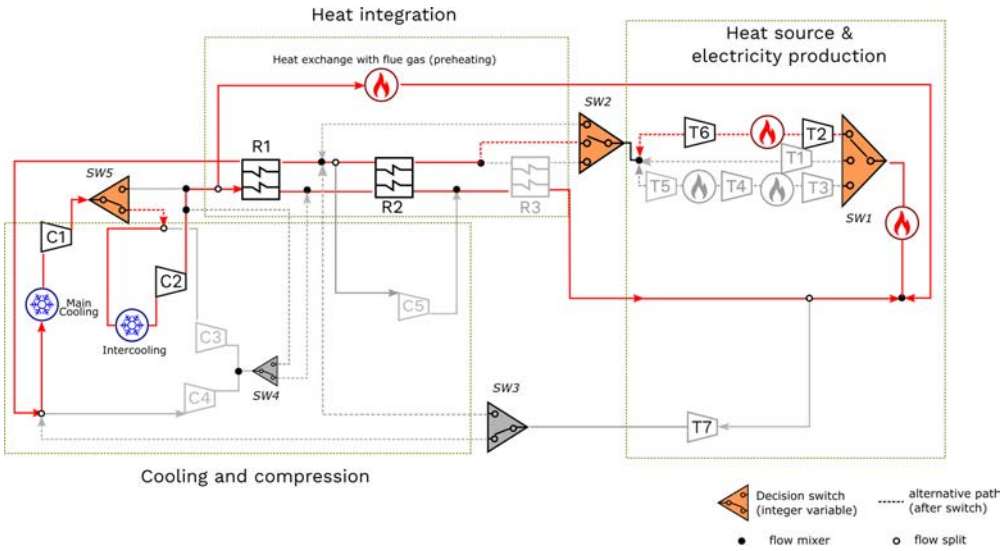

Figure 6: Procédé optimal obtenu après l'optimisation technico-économique de la superstructure

Cette réduction de 8 $ / MWh sur le LCOE représente une économie d'environ 67,5 M$ / an pour une centrale de 1000 MWe. Avec une durée de vie de 40 ans, la centrale optimisée permet de réaliser une économie de 2700 M$. Par conséquent, le LCOE optimisé et le front de Pareto reflètent non seulement le compromis entre les critères économiques et énergétiques, mais également le potentiel de cette technologie en matière de performance économique.

Référence:

[1] M. Mecheri and Y. Le Moullec. Supercritical CO_2 Brayton cycles for coal-fired power plants. Energy, 103:758–771, 2015.

[2] E.G. Feher. The supercritical thermodynamic power cycle Douglas Paper No.4348. In Proceedings of the Intersociety Energy Conversion Engineering Conference, pages 13–17, Miami Beach, August 1967.

[3] G. Angelino. Carbon dioxide condensation cycles for power production. ASME. J. Eng. Power., 1968.

[4] V. Dostal, M.J. Driscoll, and P. Hejzlar. A supercritical carbon dioxide cycle for next generation nuclear reactors. PhD thesis, MIT, 2004.

Contents

List of Figures

List of Tables

Nomenclature

Latin symbols

a	Attractive parameter of a cubic EoS (J m^3mol^{-2})
	or Helmholtz energy (J mol^{-1})
	or Discout rate (-)
A	Heat echanger area (m^2)
a_i	Coefficient in SW EoS (-)
$a', b', c', d', e', f', g', h'$	Coefficients of BWRS EoS (-)
A_i	Coefficient in SW EoS (-)
A_j	Universal coefficients in BWRS EoS (-)
b	Covolume (m^3mol^{-1})
b_i	Coefficient in SW EoS (-)
B_i	Coefficient in SW EoS (-)
B_j	Universal coefficients in BWRS EoS (-)
b_{1-4}, c_{1-4}	Universal coefficients in LKP EoS (-)
c	Parameter of Boston-Mathias alpha function (-)
C	Cost (M$)
c_i	Coefficient in SW EoS (-)
c_v	Specific heat at constant volume (kJ $kg^{-1}K^{-1}$)
c_p	Specific heat at constant pressure (kJ $kg^{-1}K^{-1}$)
d	Parameter of Boston-Mathias alpha function (-)
D	Rotor diameter (m)
d_1, d_2	Universal coefficients in LKP EoS (-)
d_i	Coefficient in SW EoS (-)
d_s	Dimensionless specific diameter (-)
f_a	Discout factor (-)
f_T	Material factor on temperature (-)
f_P	Material factor on pressure (-)
g	Molar Gibbs energy (J mol^{-1}))
	or Gravitational constant (m s^{-2}
h	Molar enthalpy (J mol^{-1}))
H_{-1}	Adiabatic head (J $s^2kg^{-1}m^{-1}$)
L, M, N	Parameters of the Twu alpha function (-)
m	Parameter of the Soave alpha function (-)
	or number of elementary segments (-)
	or mass flowrate (kg s^{-1})
n_i	Coefficient in SW EoS (-)
n_s	Dimensionless specific speed (-)
P	Pressure (Pa) or Power (MW)
Q	Quantity of echanged heat (W)or (W kg s^{-1})
R	Gas constant (J $mol^{-1}K^{-1}$)
s	Molar internal entropy (J $mol^{-1}K^{-1}$)
S_i	Stream i (-)

t_i	Coefficient in SW EoS (-)
T	Absolute temperature (K)
u	Molar internal energy (J mol^{-1})
U	Overall heat transfer coefficient (W $m^{-2}K^{-1}$)
v	Molar volume (m^3s^{-1})
V	Volumetric flowrate (m^3mol^{-1})
w	Speed of sound (ms^{-1})
W	Mechanical work (W)or (W $kg^{-1}s^{-1}$)
x	State variable (-) or continuous variable
Z	Compressibility factor (-)

Greek letters

α	Alpha function of cubic EoS (-)
α', γ'	Coefficient in BWRS EoS (-)
α_i	Coefficient in SW EoS (-)
β_i	Coefficient in SW EoS (-)
β	Universal coefficient in LKP EoS (-)
ϵ_i	Coefficient in SW EoS (-)
η	Energy efficiency (-)
η_{sC}	Isentropic efficiency of compression
η_{sT}	Isentropic efficiency of expansion
γ	Universal coefficient in LKP EoS (-) or isentropic coefficient (-)
γ_i	Coefficient in SW EoS (-)
$\phi(x, y)$	Objective function (-)
ρ	Density ($kg.m^{-3}$)
τ	Inverse reduced temperature in SW EoS(-)
δ	Reduced density in SW EoS (-) or Mean deviation between calculated and experimental value
Δ	Distance function defined in SW EoS (-)or difference between two value
ω	Pure-component acentric factor (-) or shaft speed (rpm)
Ω	Oracle parameter in MIDACO (-)
Ω_a	Universal constant of cubic EoS (-)
Ω_b	Universal constant of cubic EoS (-)
φ	Dimensionless Helmholtz function (-)

Subscript

alt	Alternator
aux	Auxiliary
c	Critical property
e	Electric
EQP	Equipement
hot	Absorbed heat energy
in	Input
net	Net power
out	Output
$O\&M$	Operating and maintenance
r	Reduced property
R	Reference fluid
RA	Racket
S	Isentropic property

T	Isotherm property
th	Thermal
ρ	Density constant property

Exponents

0	Simple fluid
o	Ideal-gas part
*	Real fluid
R	Reference fluid
res	Residual function

Acronym

ACO	Ant Colony Optimization
BM	Boston-Mathias alpha function
Btoe	Billion tones of oil equivalent
BWR	Benedict-Webb-Rubin
CAPEX	Capital expenditure
BWRS	Benedict-Webb-Rubin modified by Starling-Nishiumi
CSP	Concentrated Solar Power
EoS	Equation of State
GHG	Green House Gases
GWP	Global Warming Potential
HP	High Pressure
LP	Low Pressure
LCOE	Levelized Cost Of Electricity
IP	Intermediary Pressure
IGCC	Integrated Gasification Combined Cycle
LHV	Low Heating Value
LKP	Lee-Kesler-Plöcker
LMTD	Log Mean Temperature Difference
LNG	Liquified Natural Gas
MAPE	Mean Absolute Percentage Errors
MIDACO	Mixed Integer Distributed Ant Colony Optimization
Mtce	Million tones of coal equivalent
MINLP	Mixed Integer Non Linear Programming
NLP	Non Linear Programming
OPEX	Operational Expenditure
P-v-T	Pressure-Volume-Temperature
PR	Peng-Robinson
RC	Recuperated Cycle
RK	Redlich-Kwong
SAFT	Statiscal Associating Fluid Theory
SC-CO_2	Supercritical CO_2
SRK	Soave modified Redlich-Kwong
SS	Superstructure
SW	Span Wagner
SW_i	Switcher
USC	Ultra-supercrtical
vdW	Van der Waals

CHAPTER 1

Introduction

1.1 CHALLENGE IN THE ENERGY SECTOR

1.1.1 General context

The modern world of 6.8 billion people is running with energy of different forms: food, clean water, health, lighting, transportation, heating and cooling (Armaroli and Balzani, 2010). Primary energy, both non-renewable and renewable resources, plays a key role in any type of goods and is needed to produce any kind of service. Coal, oil, natural gas and nuclear are defined as non-renewable resources while hydropower, geothermal, solar, wind are classified as renewable energy. The worldwide total amount of primary energy before conversion, denoted world total primary energy supply (TPES), has raised from 6.1 Btoe (billion tonnes of oil equivalent) to 13.6 Btoe between 1973 and 2015, as depicted in the Figure 1.1. On one point, this growth in world energy demand comes from fast-growing emerging economies, especially from China and India. Another factor is the increasing world population. The world's population is projected to reach 8.8 billion people by 2035 with an annual increase of 1.1% (RPB, 2018). Hence, both the exploitation of primary resources and their simultaneous transformation into end-user energy (i.e., electricity, gasoline or natural gas) are necessary.

Electricity represents one important form of end-user energy and is often considered as an indicator of the economic growth (Ang, 2007; Shiu and Lam, 2004). Nearly two thirds of the increasing demand in global primary energy mentioned in the previous paragraph is consumed for electrical power generation. The share of energy used for electrical power generation is expected to rise from 42% in 2015 to 47% by 2035 (BP, 2017).

This rising share partly reflects a shift in consumer preferences towards electricity as an energy that is clean and convenient at the point of use, showing that human lifestyle and public awareness could have impact on both energy end-use and energy-mix. The society is hence

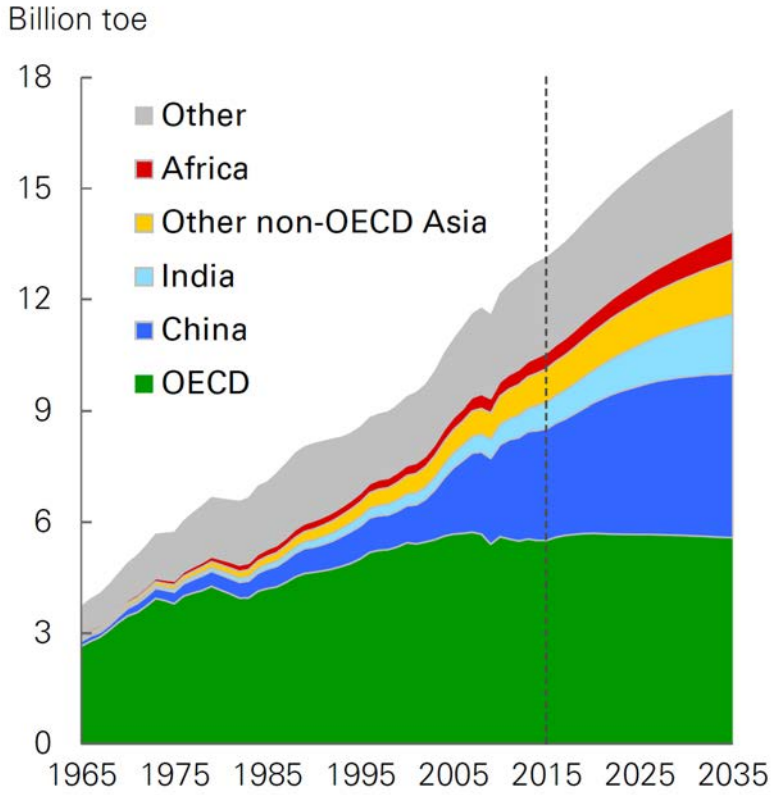

*1 billion toe $= 1.163 \times 10^7$GWh

Figure 1.1: Global energy picture: total primary energy supply from 1965-2035 (IEA, 2015b; BP, 2017)

facing an era where both issues and opportunities exist.

Recently, more public attention has been paid on air pollution, the emission of greenhouse gases (GHG), and resource availability (Jacobson, 2008). Electricity and heat production account for around 40% of global greenhouse gas emissions, meaning that the electricity production sector must be at the heart of global actions. Furthermore, a commitment of limiting the global average temperature increase by 2 °C has been made by 195 countries, which corresponds to a reduction of the CO_2 emissions by almost 60% by 2050 compared with the 2013 level (IEA, 2015a). Such policies can tighten the existing standard as well as to force to improve the technology level in energy sector (IEA, 2015a). Yet for the policy maker (decision maker), more supporting information and solutions are necessary to take better decisions in order to tackle with the climate change (Jacobson, 2008).

To summarize, one of the most important scientific and technological challenges of the twenty-first century is to ensure the rapidly growing electricity need in a more sustainable way (Armaroli and Balzani, 2010; Wang et al., 2014b). The most immediate course ahead is searching for reliable alternatives for energy conversion based on existing sources of energy.

1.1.2 The role of coal

The world's energy mix, i.e. the group of different primary energy sources from which secondary energy (usually electricity) is produced, is gradually changing while renewable source supply is growing up. The growth in global coal demand is slowing down and is expected to reach a peak in the mid-2020s, (IEA, 2017). However, coal remains the dominant source of energy and plays a crucial role in many sectors such as iron and steel industries, (BP, 2017).

The world demand for coal is currently over 5 357 Mtce (million tonnes of coal equivalent). Coal-fired power plants contribute to 41% of the world's electricity production, see the Figure 1.2, and is forecasted to continue to supply a strategic share over the next three decades. For example, an accumulative capacity of 400 GW_e is under construction for coal-fired power generation from today to 2040, suggesting that the predominance of coal in developing countries is likely to continue in next decades (IEA, 2017). Unfortunately, the coal combustion is largely contributing the emission of GHG gases. Developing technologies that help to improve the efficiency of coal-fired plants can hence bridge to prospect of low-GHG power production.

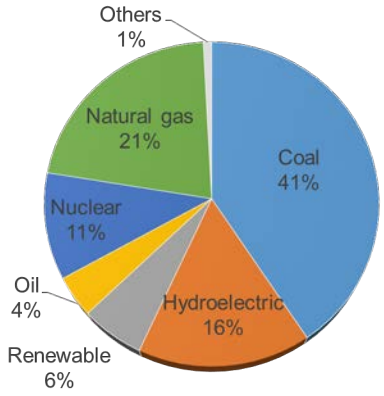

Figure 1.2: Share of global electricity produced by means of production (primary source), IEA (2015a)

The actual thermal energy conversion technology for electricity, i.e. power plants technologies, are listed in Table 1.1. It can be seen that ultra-supercritical (USC) pulverized coal-fired plants (state-of-the-art) design efficiency reaches 45%-pts (LHV), which is higher than the efficiency of other technologies such as natural gas, nuclear and CSP (Concentrating Solar Power) plants. Yet, the world's average efficiency for today's coal-fired plants is only 33%-pts due to many factors such as the coal quality, the conversion technology applied along with the aging degradation in the structure or component (IEA, 2012). This efficiency improvement of 12%-pts (between USC and basic coal power plants) means that less coal is consumed at a given

electricity production rate which represents a reduction of 18% to 22% of the CO_2 emission to the atmosphere.

The principle of thermal power plants mainly focuses on the applied power cycles (thermodynamic cycle), and thus, their performances highly depend on the thermodynamic conditions but also on the technology maturity explaining the need for advanced technologies to improve power cycles (IEA, 2017). In this context, there is an attractive prospect for developing highly efficient, low-carbon power plants and adapting their technologies to different sources of energy.

Table 1.1: Typical efficiency of different thermal power technology

Primary source	Technology	power plant efficiency*
Coal	Pulverized-coal power plants	29-35%-pts (world's average)
	Supercritical pulverized coal	38-42%-pts
	Ultra-supercritical pulverized coal (state-of-the-art)	45%-pts
	Integrated Gasification Combined Cycle (IGCC)	43%-pts
Natural gas	Natural Gas fired power plants (including LNG fired)	32-38%-pts
Nuclear	Nuclear plants	33%-pts (average efficiency)
Renewable	Solar thermal plant (CSP)	18%-pts
	Biomass	34-41%-pts

**efficiency base on lower heating value (LHV) of the fuel.*

1.2 POWER CYCLE

Thermal power plants mainly produce a net power output by converting the heat received (from combustion, or nuclear reaction) into mechanical work (usually in the form of a rotating shaft). Then, the mechanical work is converted into electric power through an alternator. The following sections deal with different power cycle operation characteristics, classification and their main parameters.

1.2.1 Definition

The production of power (work) in a system involves different thermodynamic *processes*, where the initial system undergoes some changes and passes from one initial state to another different state. For electricity generation, the involved processes are usually divided in four basic steps:

compression, heat absorption (heat addition), expansion and heat rejection. At the end of these processes, the system eventually returns to its initial state and the whole state changes exercised as well as their sequence are defined as **power cycles**. Power cycles as well as refrigeration cycles are one kind of **thermodynamic cycles**.

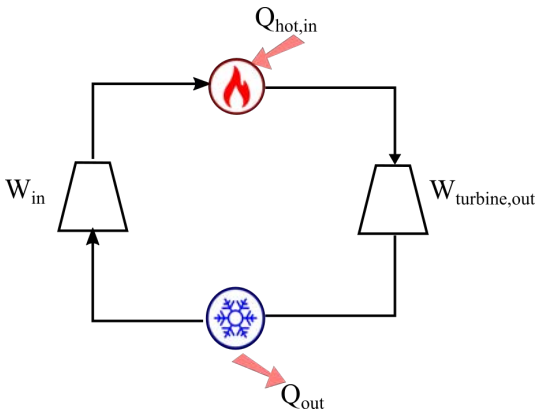

Figure 1.3: Schematic representation of basic power cycle

A power cycle (e.g., Figure 1.3) consists of producing a net power by converting the heat addition ($\dot{Q}_{hot}$) into work through expansion in a turbine. The net power is then defined as the output work of turbine ($\dot{W}_{out}$) subtracted by the work consumed by the system (e.g., compressors, pumps) within the power cycle ($\dot{W}_{in}$):

$$\dot{W}_{net} = \dot{W}_{out} - \dot{W}_{in} \tag{1.1}$$

The thermal efficiency, seen as the performance of the power cycle is then defined as in Eq 2.

$$\eta_{\text{cycle}} = \dot{W}_{net}/\dot{Q}_{hot} \tag{1.2}$$

The Carnot cycle efficiency $\eta_{\text{ideal carnot}} = 1 - T_{cooling}/T_{heat\ source}$ (temperature in Kelvin) is known to be the maximal theoretical performance limit (ideal) for a given couple of cooling and heat source temperature. The Carnot cycle involves reversible processes (isothermal heat transfers and isentropic pressure changes). In reality, this performance is not reachable because it would be impractical to have an isothermal heat transfer at variable pressures (Çengel and Boles, 1989) and the realistic pressure changes are not isentropic (irreversibilities). However, this ideal Carnot cycle efficiency definition indicates that there is at least two ways to achieve higher efficiency for these thermodynamic power cycles: increase the average temperature at which heat is transferred to the working fluid, or decrease the average temperature at which

heat is rejected from the working fluid in the condenser.

The terms “ideal” denotes that all the process is reversible (Carnot cycle) whereas in a “real” power cycles, *irreversibilities* exist. The term of *irreversibilities* refers to the difference between the reversible work and the useful work. For the turbomachinery such as pumps, turbines and compressors, the source of irreversibilities refers to the unrestrained or fast expansion or compression of a fluid. For example, a real compressor requires a greater work input than an ideal compressor and a real turbine produces a smaller work output than an ideal turbine as a result of internal irreversibilities. Another cycle irreversibility comes from the fluid friction, which causes pressure drops in the boiler, the heat exchangers, and the piping between various components (Çengel and Boles, 1989).

1.2.2 Power cycle classifications

Power cycles can be classified depending on the cycle configuration (*closed* or *open* cycle) or depending on the state of the working fluid (*two-phase* cycle, *gas* cycle).

In *closed* cycles, the working fluid is returned to the initial state at the end of the cycle and is recirculated. In *open* cycles there is no cooler (no pipes between the expansion and compression steps), the working fluid is released to the atmosphere at the end of the expansion step instead of being recirculated through a cooler towards the compression step (e.g., air in gas turbines).

Depending on the state of working fluid, power cycles can be sorted into: *two-phase* (liquid-vapor) cycle and *gas* cycle (Çengel and Boles, 1989; Kato et al., 2004). In *two-phase* cycles (e.g., Rankine cycles), the working fluid goes through both vapor phase and liquid phase (or at its phase equilibrium). Whereas in *gas* cycles, the working fluid remains in the gaseous phase throughout the entire cycle.

In addition, the unit operations (components) involved in these two kinds of cycles are different. In two-phase cycles, the pressure rise is performed by pumps (the working fluid being liquid at this step) whereas in gas cycles compressors are used. In the absence of specific steps such as "moisture separation" and "steal extractions" systems required by the working fluid changing phase, gas turbines are much simpler than that of the two-phase turbine (Kato et al., 2004).

In recent decades, it has been possible to use working fluids beyond their critical point, i.e., into their supercritical region. The terms of transcritical cycle and supercritical cycle are hence generated. They could be sorted respectively into the category of two-phase cycle (transcritical cycle) and gas cycle (supercritical cycle), depending on whether a phase change (condensation) is occurring or not.

Rankine cycle

The steam Rankine cycle is the most deployed *two-phase* cycle for electricity production since the 90's. This cycle is a "two-phases" process where the water is evaporated with the heat from boiler and is later condensed into the liquid phase after the turbine expansion, (Çengel and Boles, 1989). A classical ideal Rankine cycle consists of the following four basic processes, see the Figure 1.4:

1-2 Isentropic compression in a pump

2-3 Constant pressure heat addition from a heat source (e.g., boiler)

3-4 Isentropic expansion in a turbine

4-1 Constant pressure heat rejection in a condenser

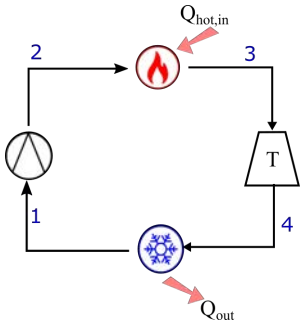

Figure 1.4: Schematic representation of Rankine cycle

The actual application of Rankine cycle extends to all kinds of thermal power plants and is listed in Table 1.1. Several improvement of the basic Rankine cycle exist (superheating, reheating, steam extraction, thermal integration....) in (Çengel and Boles, 1989) and are not detailed here. The state-of-the-art Rankine cycle applied in USC-steam coal-fired plant is using a "two-stages" turbine with a reheating step, an example of its deployment is detailed in Section 1.3.1.

Brayton cycle

Brayton cycle is a basic thermodynamic cycle that is commonly used in both electrical power-generation and mechanical-drive (propulsion system) applications (Çengel and Boles, 1989; McDonald and Wilson, 1996). However, in the 1940's, the first deployment of gas turbines in combined-cycle power plant for electricity production suffered from low efficiency and poor reliability due to metallurgical limitations (on pressure and temperature). Brayton cycles can be designed as stand-alone cycles or as combined cycle when used in conjunction with a steam

power cycle (Çengel and Boles, 1989).

Brayton cycles can be applied in the form of simple *open* cycle with air as working fluid. An ideal air Brayton cycle consists of three basic stages: isentropic compression of the working fluid up to around 1.5 MPa (typical case), constant pressure fuel-air combustion in the combustion chamber, isentropic expansion through a back-pressure turbine to generate mechanical work, and heat rejection to the atmosphere, see the Figure 1.5 a. *A Closed* Brayton cycle is composed by a compressor, a heat source, a turbine and a cooler in order to bring the fluid back to the initial state, see the Figure 1.5 b. Çengel and Boles (1989). While an *open* Brayton cycle is restricted with air as working fluid (at atmospheric pressure at the turbine outlet), a *closed* Brayton cycle can use a selection of potential working fluids different from the air (Fuller, 2010).

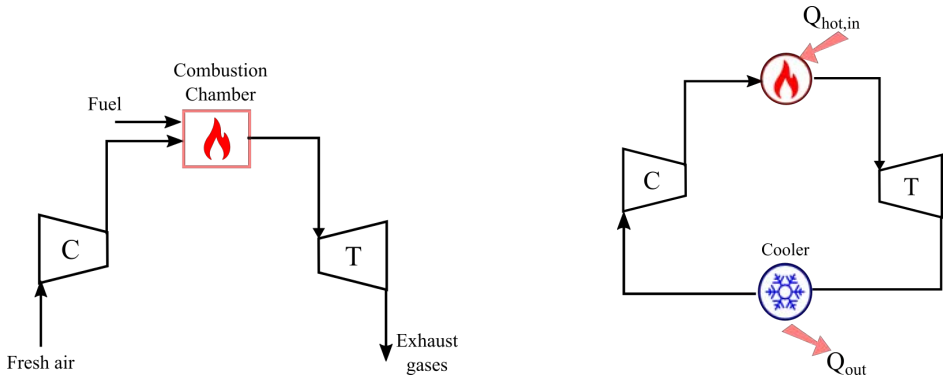

a) Open Brayton cycle b) Closed Brayton cycle

Figure 1.5: Schematic of Brayton cycle system: a) open Brayton cycle b) closed Brayton cycle

Working fluid study Due to the presence of compressors, the fluid selection is then limited to those fluids known to be stable and that remains a gas at working temperatures from 200 K to 1073.15 K, (Fuller, 2010). For the material compatibility, a non-reactive, stable and inert gas is beneficial. The properties of the fluids classically considered are compared by Dostal et al. (2004) in Table 2, in which helium and nitrogen were added for this dissertation, Table 1.2.

Meanwhile, the Global Warming Potential (GWP) is regarded as a selection criterion in this table in the context of sustainable development. GWP is a relative measure of how much heat a greenhouse gas traps in the atmosphere and it is expressed as a factor of carbon dioxide (whose GWP is standardized to 1). A fluid with a high GWP means that it traps a large quantity of heat with a long atmospheric lifetime. Candidates such as CF_4, N_2O and SF_6 are eliminated because of their high GWP.

The rest of candidates in Table 1.2: nitrogen, helium and carbon dioxide (CO_2), possess

more accessible critical conditions (T_c and P_c) in comparison with water. Studies (Cachon et al., 2012; Alpy et al., 2014) have considered nitrogen as working fluid for SFR (Sodium Fast Reactor) application in order to avoid sodium-CO_2 reaction, whereas helium has been regarded as a potential working fluid for advanced nuclear and space systems (Wright et al., 2006; Zhao and Peterson, 2008; Sánchez et al., 2013). However, nitrogen and helium Brayton cycles are demonstrated to be less efficient and potentially more costly than CO_2 Brayton cycle in the similar operating conditions (Dostal et al., 2004; Ahn and Lee, 2014; Brun et al., 2017). Furthermore, extreme turbomachinery design challenges may occur for helium cycles due to its low molecular weight, (Fuller, 2010). Together with its cost and its limited reserve in the nature, it is difficult to have a scale-up helium power cycle for industrialization.

Table 1.2: comparisons of different fluids for closed Brayton system

Fluid Name	Formula	Critical Temperature T_c (K)	Critical Pressure P_c (MPa)	critical density ρ_c (kg/m3)	GWP*
Helium	He	5.22	0.23	69.6	0
Carbon dioxide	CO_2	304.21	7.38	467.6	1
Tetrafluoromethane	CF_4	351.26	5.78	424.0	650
Nitrous oxide	N_2O	309.7	7.27	452.0	298
Nitrogen	N_2	126.2	3.4	313.3	0
Sulphur hexafluoride	SF_6	318.71	3.76	742.3	16300
Water steam	H_2O	647.04	22.10	322	0

*:for 100-year time horizon, (UNCC, 2018)
**: number extracted from Ravishankara et al. (2009)

Due to high carbon dioxide density, more compact turbomachinery is expected with CO_2 in comparison with nitrogen and helium, Brun et al. (2017). CO_2 has good overall thermodynamic parameters (critical temperature close to the ambient temperature, low GDP, high availability, chemical stability...) and could be a promising working fluid. Next sections describe the supercritical CO_2 (SC-CO_2) Brayton cycles.

1.3 SUPERCRITICAL CO_2 BRAYTON CYCLE

Historical development and current state-of-the-art

Feher (1967) has firstly revealed the versatility of Brayton cycle by proposing a cycle that operates over the critical point of the working fluid. In his opinion, the supercritical CO_2 (SC-CO_2) Brayton cycle has potential to overwhelm the Rankine steam cycle in similar conditions (high turbine inlet temperature and pressure). Meanwhile, Angelino (1969) performed an extensive

review of various configurations of SC-CO_2 Brayton cycles, which highlights the potential cycle efficiency improvement during the cycle configuration modification.

The dissertation of Dostal et al. (2004) is considered to be the first SC-CO_2 industry feasibility investigation with integration of cycle efficiency enhancement and machinery sizing. Thanks to his study, the benefits of higher cycle efficiency and smaller turbomachinery components of SC-CO_2 Brayton cycle are revealed and quantified. From then, worldwide studies focus on its fundamental aspects as well as technical limitations of the crucial components, such as turbomachinery and heat exchangers, see Table 1.3. Rather than roughly describing past work in the area of SC-CO_2 power cycles, this dissertation organizes numerous studies in different categories.

The Table 1.3 lists various studies regarding different industrial applications. They are classified according to their investigation area and industrial application. Meanwhile, many of cited papers have been supported by the existing test facilities, detailed in Table 1.4. Notably, a scaled up test loop of 1 MW_e has been under preparation with the SunShot initiative funding (DOE, 2015) in order to better assess existing technical risks in the industrial adoption.

Firstly, it can be concluded that this cycle has no discrimination on different application fields. SC-CO_2 Brayton cycle can be integrated in nuclear, concentrate solar power (CSP) and fossil application, (see Tables 1.3 and 1.4). The main difference between these various applications is the diverse industrial constraints such as the heat source temperature, the cooling technology and its temperature. For example, in desert dry regions where water resource is highly limited, the dry air cooling is favorable, resulting in higher cooling temperature hence decreases the cycle efficiency. CSP application with tower/central receiver technology can reach maximum temperatures of 773 K-1273 K (Chacartegui et al., 2011; Ma and Turchi, 2011); while parabolic technology can only reach a inlet turbine temperature of 673 K-773 K (Singh et al., 2013a). An advanced Generation IV nuclear reactor (Dostal et al., 2004) can heat the inlet turbine temperature to 1153 K, whereas a medium temperature nuclear reactor (Jeong et al., 2011a) and sodium-cooled fast reactor (Moisseytsev and Sienicki, 2009) can reach reactor outlet temperature of 823-923 K. For pulverized coal-fired plant application carried by Mecheri and Le Moullec (2015), SC-CO_2 Brayon cycle has a maximum temperature of 893 K, which corresponds to the condition of actual advanced ultra supercritical steam (USC-steam) boiler technology. For an application of IGCC, the SC-CO_2 leaving the boiler can theoretically achieve 1477 K and 30 MPa, (Weiland and White, 2018).

Nevertheless, as it can be seen from Tables 1.3 and 1.4, there is still strong need in researches of SC-CO_2 Brayton cycle. Only a limited number of SC-CO_2 power cycle test facilities (Table 1.4)

Table 1.3: Review on SC-CO_2 Brayton cycle studies

	Nuclear power application	CSP application	Fossil Application*	General
Review		Roux et al. (2013)Wang et al. (2017) Dunham and Iverson (2014)		Ahn et al. (2015) Li et al. (2017)Crespi et al. (2017)
Off-design modeling	Dostal et al. (2004) Cha et al. (2008) Sarkar (2009) Wright et al. (2011, 2010) Pham (2015)	Chacartegui et al. (2011) Garg et al. (2013) Iverson et al. (2013)	Thimsen (2014) Le Moullec (2013b) Mecheri and Le Moullec (2015) Zhao et al. (2018) Bai et al. (2018); Park et al. (2018)	
Parametric Optimization (fixed configuration)	Dostal et al. (2004) Floyd et al. (2013) Akbari and Mahmoudi (2014)	Garg et al. (2013) Mohagheghi and Kapat (2013) Reyes-Belmonte et al. (2016) Li et al. (2015) Roux et al. (2014) Milani et al. (2017)	Mecheri and Le Moullec (2015)	Ma et al. (2017) Sarkar and Bhattacharyya (2009) Sánchez-Orgaz et al. (2010) Besarati et al. (2010) Wang et al. (2010) Cheng et al. (2017); Kim et al. (2018)
Dynamic modeling	Moisseytsev and Sienicki (2008) Cha et al. (2008) Wright et al. (2010, 2011)	Iverson et al. (2013) Singh et al. (2013b) Milani et al. (2017)		
Turbomachinery	Kato et al. (2004); Cha et al. (2008) Wright et al. (2010) Wright et al. (2011) Lee et al. (2014)	Qi et al. (2016)		Bidkar et al. (2016) Holaind et al. (2017)
Heat exchangers	Cha et al. (2008)	Gkountas et al. (2017)		Tsuzuki et al. (2007) Kim et al. (2016); Guo (2016) Meshram et al. (2016) Hinze et al. (2017)Lee et al. (2017)
Techno-economic	Dostal et al. (2004)		Park et al. (2018)	Hinze et al. (2017) Marchionni et al. (2017)
Material				Fleming et al. (2014) Mahaffey et al. (2014)
*Process configuration evaluation***	Dostal et al. (2004) Ahn and Lee (2014); Pham (2015) Moisseytsev and Sienicki (2009) Ahn and Lee (2014)	Chacartegui et al. (2011) Turchi et al. (2012) Dunham and Iverson (2014) Neises and Turchi (2014) Binotti et al. (2017)		Angelino (1968) Crespi et al. (2017) Marchionni et al. (2017) Heo et al. (2017)
Test loop	Wright et al. (2011, 2010) Cho et al. (2016) Lee et al. (2012)Vesely et al. (2014)	Iverson et al. (2013) DOE (2015)		Persichilli et al. (2012) Aritomi et al. (2010)
SC-CO_2 Mixture	Wright et al. (2011); Jeong et al. (2011b) Vesely and Dostal (2014)			

*Fossil applications include pulverized coal, gasification of coal and natural gas
** No structural optimization present

Table 1.4: Existing test facilities in the world

Year	Laboratory	Country	Production Capacity	Application
2010 - 2011	Sandia National Laboratory	US	260 kW_{th}	Nuclear
2010	Sandia National Laboratory	US	1 MW_{th}	Nuclear
2010	Echogen Power System LLC	US	6 - 8 MW_e	Heat Recuperation
2010	Tokyo Institute of Technology	Japan	10 kW_e	General
2013 - 2016	KIER	South Korea	80 kW_e	Nuclear
2013	KAERI, KASIT & PSOTECH	South Korea	730 kW_{th}	Nuclear
2015	Czech Technical University Research Center Rez	Czech Republic	500 kW_{th}	General

exist around the world and they are rather classified as micro- or small-scale test loops. More key test results and numerical research are necessary to support the development of technology.

1.3.1 Motivation for integrating SC-CO_2 Brayton cycle into pulverized coal-fired plant

Current state-of-the-art of coal-fired plant

Figure 1.6 shows a simplified process flowsheet of a current state-of-the-art pulverized coal-fired plant. It is composed of three main blocks: boiler, electricity generation and flue gas treatment blocks. The power cycle applied in the coal-fired plant is a Rankine cycle with a superheating (Hirn cycle) and reheating. Firstly, the pulverized coal is injected with preheated air in the boiler where the combustion takes place. The heat is then recovered by the water (steam) circulating in the boiler and transforms the steam to its supercritical phase. In the electricity generation block, the working fluid is feeding the turbines at different pressure level (HP/IP/LP turbines) in order to generate electricity (conversion of the mechanical rotating energy to electricity through the alternator). The last block, purification block, serves to denitrify, desulphurise and remove dust from the combustion flue gas before it is released to the atmosphere.

The current average *cycle efficiency* (η_{cycle}) of applied ultra-supercritical (USC) steam Rankine cycle is around 47%-pts, with steam parameters of 30 MPa/873 K/893 K. The condition of superheated steam is beyond its critical point (647 K and 22.1 MPa). It is recalled that in Table 1.1, the *overall plant net efficiency* within the lower heat value (LHV) consideration ($\eta_{\text{LHV plant}}$) of 45%-pts is listed. The difference is due to the consideration of the boiler efficiency in the overall plant efficiency. Along this dissertation, the boiler block is considered as a heat source, but its inside structure as well as the coal combustion are not considered in the power cycle study.

Under the context of growing energy demands and sustainable development, current studies on pulverized coal-fired plant focus on developing more efficient power plants. By considering a higher steam temperature (over 873 K), hence higher pressure, (Weitzel, 2011; Le Moullec, 2013a; Wang et al., 2014b; Long et al., 2017) a theoretical improvement of 5%-pts on cycle efficiency is foreseen. Relatively expensive materials (high-nickel alloys) are then necessary to be considered (Thimsen, 2014) in order to bear the steam at such extreme conditions. Meanwhile, Wang et al. (2014a) focus on the coal-fired plant retrofit in "Boiler block" and "Electricity generation block". Cycle configuration/architecture improvement (i.e., Boiler block and Electricity generation block) is demonstrated to be another potential solution in efficiency enforcement.

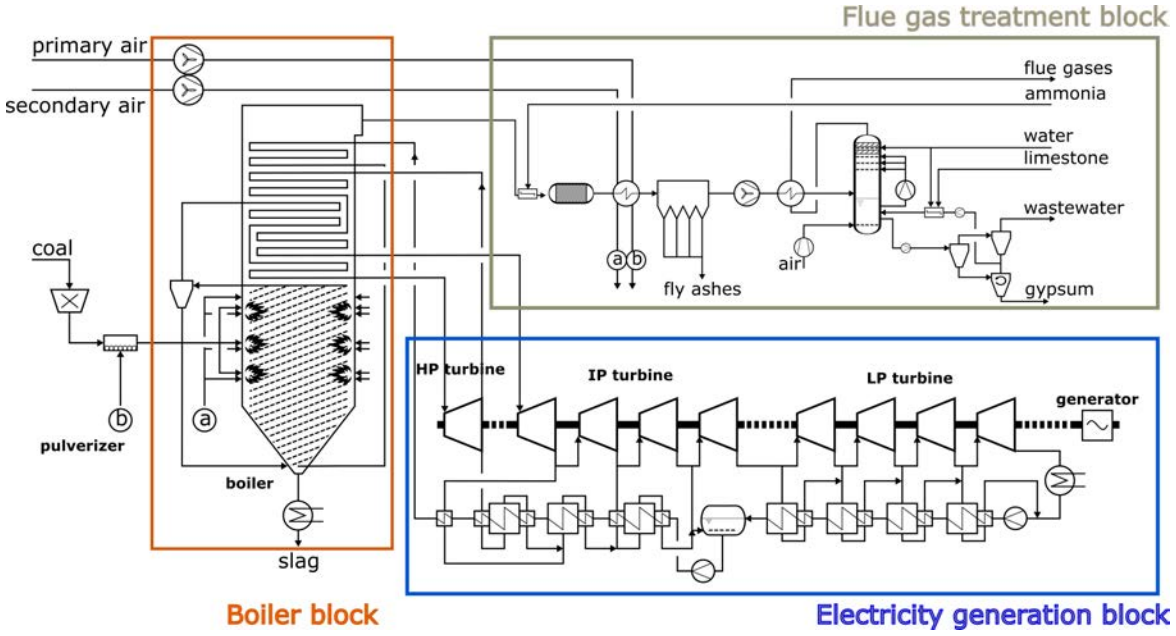

Figure 1.6: Process flow sheet of an ultra supercritical pulverized coal-fired plant of steam extracted from Hagi (2014)

Motivation

In comparison to a water steam Rankine cycle, for identical operating condition, Brayton cycles with CO_2 as working fluid can more easily go over its critical conditions. Therefore, CO_2 remains in supercritical state in the whole cycle process (which is not the case in USC-steam cycles).

Furthermore, SC-CO_2 Brayton cycle has simpler layout than steam Rankine since there is no moisture separator, steam extraction systems, (Rovira et al., 2013). The first concept of coal-fired supercritical CO_2 Brayton cycle is suggested by Le Moullec (2013a) from EDF company, where CO_2 required in the power cycle came from the post combustion carbon capture. Later on, Mecheri and Le Moullec (2015) firstly quantified that the SC-CO_2 Brayton cyle has a 5-7%-pts

higher thermal efficiency in comparison with the current steam Rankine cycle under the same operation conditions (30 MPa/893 K). Since then, the SC-CO_2 Brayton cycle applied to coal-fired power plants has then received more attention, yet the elaborated literature review showed that only a few studies exist regarding this topic (Table 1.3) to support its future deployment (Park et al., 2018; Bai et al., 2018; Mecheri and Le Moullec, 2015; Le Moullec, 2013a,b; Thimsen, 2014).

1.3.2 Technology improvement and this dissertation

Overall cycle configuration

Meanwhile, the overall cycle configuration improvement is also a key strategy to enlarge the potential of SC-CO_2 Brayton cycle technology. Although some investigations devoted to propose new Brayton cycle configurations/architectures (row Process configuration evaluation in Table 1.3), no quantified comparison has been carried out yet. As an example, Crespi et al. (2017) identified forty-two different possible stand-alone SC-CO_2 Brayton and thirty-eight for combined power cycles mentioned in the existing publication. This large quantity of possible cycle configurations seems to be promising yet, reviewing those published process evaluations is less rewarding since each of them has been assessed in different conditions and hypothesis.

In order to avoid time consuming modeling of each cycle conception, there is interest for this thesis to review large quantities of cycle topology/configurations and even create new cycle configurations by the approach of process synthesis.

Based on the 42 stand-alone SC-CO_2 Brayton cycles listed by Crespi et al. (2017), this dissertation selected 11 of them. These selected cycle configurations remain in the supercritical phase (no liquid phase) and have no specific heat source employment. Four main categories are identified: intercooling, heat integration, recompression and reheating. In most cases, the advanced Brayton cycle processes combine several process modifications to achieve certain efficiency improvement. The complete classification of individual process modifications to be studied in this thesis is presented in Figure 1.7.

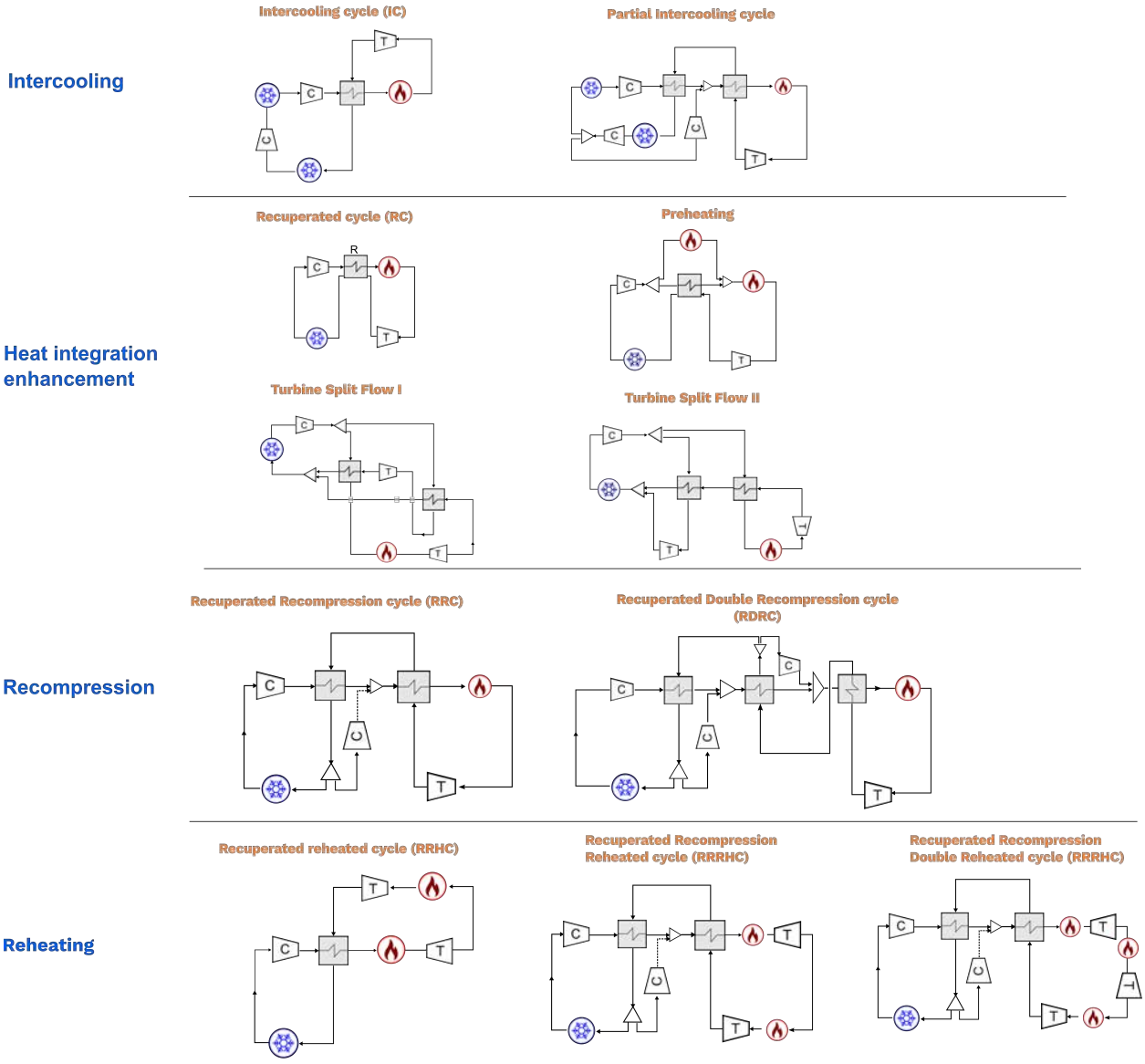

Figure 1.7: Classification of a few individual process modifications of SC-CO_2 Brayton cycle (Angelino, 1968; Mecheri and Le Moullec, 2015; Crespi et al., 2017)

Optimization

Preliminary optimization focuses on sensitivity analysis study in which some operating parameters (e.g., temperature, pressure...) are scanned one by one manually. Some interesting process information and cycle performance improvement can be drawn from sensitivity diagram reading (Mecheri and Le Moullec, 2015; Pham, 2015; Ma et al., 2017). Some advanced SC-CO_2 optimization investigations have applied some optimizers to find operating parameters than meeting the defined criterion (e.g., cycle efficiency, investment cost...) (depicted in row "parametric optimization" in Table 1.3). However, different cycle performance comparisons

focus on optimizing one cycle by one and systematic structural (configuration) optimization has not received any attention. A systematic way would be brought out through a **process synthesis** study, where both generation of alternatives configurations and key parameters are directly guided by the chosen criterion. In this thesis, optimization-based process synthesis will enlighten the industrialization of SC-CO_2 Brayton cycle by showing the most promising configuration of SC-CO_2 Brayton cycle and its corresponding operating parameters at given operating conditions constraints.

Material and key component development

More experimental tests and numerical research are identified to leapfrog several technology gaps. For example, suitable materials for high-temperature and high pressure plant design are still under development and long-term material data of CO_2 are also necessary considering the erosion phenomena in some component, (D. Hofer , 2016; Brun et al., 2017). The need in component development such as turbomachinery and heat exchangers is also highlighted by D. Hofer (2016): the technology gap in turbomachinery relies in the development of advanced seals and the transient management; while finding cost-effective heat exchangers (compromise between size, performance, pressure drops, costs) is identified as the key feature to support the industrialization of SC-CO_2 Brayton cycle.

The aforementioned material and component development are important features for the future commercialization of SC-CO_2 Brayton cycle. Nevertheless, this thesis does not intend to bring forward their state-of-the-art but rather applied current published studies as assumptions.

OBJECTIVES OF THIS THESIS

The aim of this PhD is therefore to respond to demands in the conception of supercritical CO_2 Brayton cycle for coal-fired power plant application and overall power cycle configuration design optimization. Based on the conceptual study of Le Moullec (2013b); Mecheri and Le Moullec (2015), this thesis is brought out with a more rigorous modeling, simulation and advanced optimization in order to access towards its performance, the cost evaluation and reliability test before the possible building of an industrial-scale unit. One of the ambitions of this dissertation is to provide an easily handled methodology of optimization where a large quantity of Brayton cycle layouts are reviewed and automatically optimized within. This step is almost an unrealistic task without the aid of rigorous equation of state for SC-CO_2, a stable process modeling environment, as well as a well-formulated optimization problem.

In Chapter 2, the Brayton process modeling is presented through two steps. Firstly, the equations of state which are able to represent SC-CO_2 are reviewed and presented. Considering that the operating conditions of a SC-CO_2 Brayton cycle could include the vicinity of its critical point, a rigorous selection procedure of an equation of state (EoS) for CO_2 is presented. Afterwards, in Chapter 3, by means of a simple recuperated Brayton cycle (RC) modeling and preliminary component design, the influence of EoS on the process performance and design of a SC-CO_2 Brayton cycle are analyzed and discussed. This investigation intends to understand the consequence of oversimplifications on EoS.

In order to find and propose a global optimum design and layout of SC-CO_2 Brayton cycle, optimization-based process synthesis is introduced in Chapter 4. Firstly, the notion of superstructure is introduced and the state-of-the-art of process synthesis is presented. Then the approach of superstructure optimization is detailed for a SC-CO_2 Brayton cycle design. This approach consists in formulating an optimization problem searching for best conventional continuous process parameters as well as the flowsheet topology. This methodology takes advantages of rigorous modeling of SC-CO_2 and of components (unit operations) in the commercial process simulator ProsimPlus™. Whereas the resolution of complex optimization problem is ensured by the metaheuristic optimizer MIDACO (Mixed Integer Distributed Ant Colony Optimization). This automatic process synthesis optimization enables to easily update the assumptions (and components), since the current state-of-the-art is still under development (Crespi et al., 2017; Brun et al., 2017).

Last but not least, in Chapter 5, the proposed optimization-based process synthesis approach is applied on an advanced superstructure of SC-CO_2 Brayton cycle under realistic industrial considerations. This advanced superstructure includes more than 1000 configurations of SC-CO_2 among which 11 configurations listed in Table 1.7 are also included. In addition, in-house built economic models on SC-CO_2 components enable to elaborate not only techno-economic assessment on already optimized SC-CO_2 Brayton cycles but also to realize a multi-objective optimization. The latter aims at minimizing the Levelized cost of electricity (LCOE) and capital investment cost (CAPEX) while maximizing the cycle performance (i.e., cycle efficiency).

Conclusions and general remarks are then drawn from this work and prospects for study and improvement of the developed tool are proposed.

CHAPTER 2

Thermodynamic model choice for CO_2

As highlighted in the introduction, the role of the selected thermodynamic model (equation of state) for CO_2 is decisive. The thermodynamic analysis can determine the feasibility of a given process (e.g., cycle thermal efficiency and temperature-entropy diagram), thus equation of state selection is the first step in process modeling that will affect all subsequent tasks in a process evaluation (Carlson, 1996; Hendriks et al., 2010).

Existing studies have pointed out that the property change of CO_2 near the critical point would result in a significant efficiency improvement (i.e., the compression work can be substantially decreased) (Dostal et al., 2004), along with a non-neglected influence in the turbomachinery design (Lee et al., 2016). However, a proper selection of equation of state for CO_2 has not been carried out. As an example, Dostal et al. (2004); Kato et al. (2004); Zhang et al. (2007); Jeong et al. (2011a); Lee et al. (2014) and (Serrano et al., 2014) all selected the Span Wagner equation of state (SW EoS) without justifying their choice. As a second example, the study performed by Mecheri and Le Moullec (2015) and Bai et al. (2018) selected Lee-Kesler-Plöker (LKP) equation of state for CO_2 properties prediction. Mecheri and Le Moullec (2015) compared deviations of different EoS on cycle efficiency where the Span Wagner (SW) equation of state was not among comparison candidates.

This chapter intends to introduce one elementary and important aspect of SC-CO_2 Brayton cycle modeling: the thermodynamic model of CO_2. The proper selection of EoS is carried for the temperature and pressure ranges of interest [300 K; 1373 K] and [7 MPa; 30 MPa], which is suggested by the different studies published as well as based on actual material constraint.

2.1 EQUATION OF STATE

In a close and 1-phase system with absence of chemical reaction, the **intensive state functions** that describe this system [temperature (T), pressure (P), molar volume (v), molar enthalpy (h),

molar entropy (s), molar internal energy (u), molar Gibbs energy (g), molar Helmholtz energy (a), molar heat capacity at constant volume and at constant pressure (c_v, c_p), speed of sound (w)...] can be represented by the knowledge of any two independent intensive variables. The mathematical equation that associates each function to two other variables is defined as an **equation of state (EoS)**. In practice, an EoS makes reference to the "volumetric equation of state" that is to the mathematical relation between P,v and T. Two families of EoS are encountered in chemical engineering thermodynamics:

1. the **volume-explicit EoS** in which the molar volume v is expressed as a function of T and P [$v(T,\ P)$]. .
2. the **pressure-explicit EoS** in which the pressure P is expressed as a function of T and v [$P(T,\ v)$]. This kind of EoS is capable of representing phase equilibria.

As a matter of fact, an equation of state dedicates to represent the real behavior of a pure fluid. More precisely, it only enables to estimate the difference between properties of a pure fluid in its actual state (exponent *) and properties of the fluid in the perfect-gas state (exponent $^\bullet$). This correction to be applied to the perfect-gas state is known as the residual function. The *residual* part of a state variable x is denoted as $x^{res(T,P)}$ for volume-explicit EoS and as $x^{res(T,v)}$ for pressure-explicit EoS.

To sum up, the knowledge of a volume-explicit or a pressure-explicit equation of state makes it possible to estimate all residual functions such as residual enthalpy (h), residual entropy (s), residual internal energy (u) or residual heat capacities (c_v, c_p).

✻ **Residual functions $x^{res}(T^*,\ P^*)$ from a volume-explicit EoS:**

$$x^{res}(T^*,\ P^*) = x^*(T^*,\ P^*) - x^\bullet(T^*,\ P^*) \tag{2.1}$$

Where:

$x \in (g,\ s,\ v,\ h,\ c_p,\ u,\ a,\ c_v)$

$x^*(T^*,\ P^*)$ is the property of the real pure fluid in its actual state: temperature T^*, pressure P^* and molar volume $v^*(T^*,\ P^*)_{\mathrm{EoS}}$ given by the EoS;

$x^\bullet(T^*,\ P^*)$ is the property in perfect-gas conditions. The perfect gas has the same temperature T^*, and the same pressure P^*as the real fluid. The molar volume of the perfect gas is $v^\bullet(T^*,\ P^*) = \frac{RT^*}{P^*}$. It is thus different from the molar volume of the pure real fluid in its actual state;

$v^*(T^*,\ P^*)$ is the volume-explicit equation of state.

The knowledge of the volume-explicit EoS makes it possible to calculate the residual Gibbs Energy by:

$$g^{res}(T,\ P) = \int_0^P [\underbrace{v^*(T,\ P)}_{\text{EoS}} - \frac{RT}{P}] \cdot dP \tag{2.2}$$

Knowing $g^{res}(T,\ P)$ it becomes possible to estimate all other residual state functions s^{res}, v^{res}, h^{res}, c_p^{res}, u^{res}, a^{res}, c_v^{res}.

Note that the volume-explicit equation of state can only represent P-v-T behavior of vapor phase since fixing the (T, P) variables leads to one single solution for the molar volume. Therefore, a volume-explicit EoS is not adapted for modeling systems containing liquid-vapor or more generally, two-phase equilibria.

✻ **Residual functions** $x^{res}(T^*,\ v^*)$ from a pressure-explicit EoS:

$$x^{res}(T^*,\ v^*) = x^*(T^*,\ v^*) - x^\bullet(T^*,\ v^*) \tag{2.3}$$

Where:

$x \in (a,\ s,\ P,\ h,\ c_p,\ u,\ g,\ c_v)$

$x^*(T^*,\ v^*)$ is the property of the real pure fluid in its actual state: temperature T^*, molar volume v^* and pressure $P^*(T^*,\ v^*)_{EoS}$ given by the EoS;

$x^\bullet(T^*,\ v^*)$ is defined as the property of the perfect-gas having the same temperature $T^*$and the same molar volume v^*as the real fluid. The pressure $P^\bullet$of the perfect gas is $P^\bullet = \frac{RT}{v}$;It is thus different from the pressure of the real fluid.

$P^*(T^*,\ v^*)$ is the pressure-explicit equation of state.

In a similar way, knowing the pressure-explicit EoS makes it possible to calculate the residual Helmholtz energy (see Eq. 2.4) from which all the other residual functions can be estimated (see Eq. 2.5)

$$a^{res}(T,\, v) = -\int_{+\infty}^{v} [\underbrace{P^*(T,\, v)}_{EoS} - \frac{RT}{v}] \cdot dv \tag{2.4}$$

$$\begin{cases} s^{res}(T,\, v) = -\left[\frac{\partial a^{res}(T,v)}{\partial T}\right]_v \\ P^{res}(T,v) = -\left[\frac{\partial a^{res}(T,v)}{\partial v}\right]_T \\ u^{res}(T,\, v) = a^{res}(T,\, v) + T \cdot s^{res}(T,\, v) \\ h^{res}(T,\, v) = u^{res}(T,\, v) + v \cdot P^{res}(T,\, v) \\ c_v^{res}(T,\, v) = \left[\frac{\partial u^{res}(T,v)}{\partial T}\right]_v \\ c_p^{res}(T,\, v) = c_v^{res} - T\frac{\left[\left(\frac{\partial P^{res}(T,\, v)}{\partial T}\right)\right]^2}{(\frac{\partial P^{res}(T,\, v)}{\partial v})_T} \end{cases} \tag{2.5}$$

Unlike volume-explicit EoS, pressure-explicit EoS can represent phase equilibrium and thus, critical phenomena can be estimated. Therefore, in the context of supercritical CO_2 analysis, only pressure-explicit EoS are considered.

The four major types of pressure-explicit EoS that are commonly used to predict CO_2 properties (as a non-polar pure component) are presented and discussed in the next sections. These four EoS types are:

- Cubic equations of state;
- Virial-type equations of state;
- Equation expressed in terms of Helmholtz energy;
- SAFT-type equations of state.

2.1.1 Cubic equation of state

The Cubic equations of state are applicable to both liquid, gas and more generally, multiphase state. It is called cubic because such equations can be written as a third degree polynomial in terms of molar volume at fixed T and P . For pure species, most of cubic EoS can be written in the following general form:

$$P(T,\, v) = \underbrace{\frac{RT}{v-b}}_{repulsive\,term} + \underbrace{\frac{-a(T)}{(v-r_1 b)(v-r_2 b)}}_{attractive\,term} \tag{2.6}$$

Where:

$a(T)$ is the attractive (or cohesive) pure-fluid parameter;

b is the molar co-volume of the considered molecule;

R is the gas constant.

Both parameters a and b can be calculated from the critical properties of studied fluid, thus, they depend on the studied component. Attention needs to be paid to b in its temperature independence. In fact, some non-physical inconsistencies have been observed when b is expressed as a temperature dependent function (Salim and Trebble, 1991; Kalikhman et al., 2010): isotherms in a pressure volume (Pv) plane will cross over at high temperature; also c_v (and/or c_p) will be negative at the infinite pressure. The component dependent parameters in cubic EoS write:

$$\begin{cases} a(T) = \frac{\Omega_a R^2 T_c^2 \alpha(T)}{P_c} \\ b = \frac{\Omega_b R T_c}{P_c} \end{cases} \tag{2.7}$$

Where:

T_c and P_c are experimental measured values of the critical temperature and pressure;

$\alpha(T)$ is the so-called **alpha function**, defined as $\alpha = \frac{a(T)}{a(T_c)}$. It is temperature dependent, except for the Van der Waals EoS for which $\alpha = 1$. By definition, alpha is equal to one at the critical temperature: $\alpha(T_c) = 1$;

r_1 and r_2 are universal constants (i.e., component independent parameters) of the EoS, they do not depend on the modeled component whereas $a(T)$ is component dependent;

Ω_a and Ω_b are universal constants of cubic EoS.

In Table 2.1, universal coefficients (r_1, r_2, Ω_a, Ω_b) are listed for some well known cubic equations of state. The combination of Table 2.1, Eqs. 2.6 and 2.7, along with an alpha function [see in section b], makes it possible to fully define a thermodynamic model.

a) Van der Waals equation of state

Table 2.1: EoS parameters used in three different cubic EoS

Equation	r_1	r_2	Ω_a	Ω_b
Van der Waals (VdW)	0	0	27/64	1/8
Redlich-Kwong (RK)	-1	0	0.42748	0.08664
Peng-Robinson (PR)	-1-$\sqrt{2}$	-1+$\sqrt{2}$	0.45724	0.07780

✻ Van der Waals EoS (1873)

In 1873, Johannes Diderik van der Waals (1873) has proposed a theoretical model that takes into account the repulsive and attractive effect in a real fluid:

$$(P + \frac{a_c}{v^2})(v - b) = RT \; or \; P = \frac{RT}{v - b} - \frac{a_c}{v^2} = P_{rep} + P_{attr} \tag{2.8}$$

$$\text{with} \begin{cases} a_c = \frac{27}{64} \frac{R^2 \cdot T_c^2}{P_c} \\ b = \frac{1}{8} \frac{R \cdot T_c}{P_c} \end{cases}$$

The Van der Waals equation is the cornerstone of cubic equations of state, but it is not quantitatively accurate in terms of critical compressibility factor (noted Z_c) and saturation properties prediction. The molar critical compressibility factor given in Eq. 2.9 is predicted as a universal value equal to 3/8 :

$$Z_c = \frac{P_c v_c}{RT_c} \tag{2.9}$$

However, the experimental values of Z_c varies between 0.24 and 0.29 for different hydrocarbons. Therefore, many researchers have attempted to modify the Van der Waals equation to improve its accuracy. Their efforts can be divided in two main categories: one concerning the parameters modification (both attractive and co-volume) and another concerning the volume translation.

b) Equations with attractive parameter dependent on temperature

✻ Clausius EoS (1880)

Clausius noted some limitations of the Van der Waals equation and suggested to make the attractive parameter temperature dependent:

$$P = \frac{RT}{v - b} - \frac{a(T)}{v^2} \tag{2.10}$$

$$\text{with} \begin{cases} a(T) = a_c \cdot \alpha(T) \\ a_c = \frac{27}{64} \frac{R^2 \cdot T_c^2}{P_c} \\ \alpha(T) = 1/T_r = T_c/T \\ b = \frac{1}{8} \frac{R \cdot T_c}{P_c} \end{cases}$$

Where T_r is called reduced temperature and defined as the ratio between the absolute temperature and the critical temperature.

✻ Redlich-Kwong EoS (1949)

Redlich and Kwong proposed a significant modification of the attractive term of the Van der Waals equation. They modified the attractive term by introducing a new temperature dependent alpha function and by replacing the polynomial term v^2 by $v(v+b)$. For a pure substance, the RK EoS is:

$$P = \frac{RT}{v-b} - \frac{a(T)}{v(v+b)} \tag{2.11}$$

$$\text{with} \begin{cases} a(T) = \Omega_a \frac{R^2 \cdot T_c^2}{P_c} \cdot \alpha(T) \, and \, \Omega_a \approx 0.42748 \\ b = \Omega_b R T_c / P_c \, with \, \Omega_b \approx 0.08664 \\ \alpha(T) = \sqrt{\frac{1}{T_r}} \end{cases}$$

✻ Soave-Redlich-Kwong (1972)

In 1972, Soave (1972) modified the expression of the attractive term $a(T)$ of the original equation by Redlich and Kwong . In the SRK attractive term, the alpha function $\alpha(T)$ depends on both the temperature and the acentric factor ω. The attractive term and the alpha function of the SRK EoS are :

$$\begin{cases} a(T) = \Omega_a \frac{R^2 \cdot T_c^2}{P_c} \cdot \alpha(T) \, and \, \Omega_a \approx 0.42748 \\ \alpha(T) = [1 + m(1 - \sqrt{T_r})]^2 \\ m(\omega) = 0.480 + 1.574\omega - 0.176\omega^2 \end{cases}$$

Where:

$m(\omega)$ is a component-dependent function, ωdenotes the experimental pure-component acentric factor;
$\omega = -\log_{10}(\frac{P^s(0.7T_c)}{P_0}) - 1$ was defined by Pitzer et al. (1955).

These modifications dramatically improve the prediction of pure component vapor-liquid properties: the SRK EoS is indeed much more accurate in the representation of liquid-vapor equilibrium than the RK EoS.

✻ Peng-Robinson (1976)

Peng and Robinson (1976) have developed a new EoS that improves the attractive term of the RK EoS and uses the Soave alpha function $\alpha(T)$. The aim of the PR EoS is to better represent the volumetric properties in the pure component liquid phase. The PR EoS is :

$$P = \frac{RT}{v-b} - \frac{a(T)}{v(v+b)+b(v-b)} \tag{2.12}$$

$$\text{With} \begin{cases} a(T) = \Omega_a \frac{R^2 \cdot T_c^2}{P_c} \cdot \alpha(T) \, and \, \Omega_a \approx 0.45724 \\ b = \Omega_b R T_c / P_c \, with \, \Omega_b \approx 0.07780 \\ \alpha(T) = [1 + m(\omega)(1 - \sqrt{T_r})]^2 \\ m(\omega) = 0.37464 + 1.57226\omega - 0.26992\omega^2 \end{cases}$$

c) Other modifications of the Van der Waals EoS attractive term

Besides the previously introduced cubic EoS, some other important efforts have been proposed in the dedicated literature to the modification of EoS attractive terms. The Schmidt-Wenzel and the Patel-Teja EoS (Schmidt and Wenzel, 1980; Patel and Teja, 1982) have the same repulsive term as the Van der Waals EoS but different attractive terms. In fact, in the Schmidt-Wenzel EoS, universal parameters are replaced by parameters that depend on ω. The Patel and Teja EoS involves a third parameter (noted c in Table 2.2). Both EoS have a component specific critical compressibility factor. Unfortunately, the predicted component specific critical compressibility factor deviates notably from the experimental critical compressibility factor. However, these modifications allow to have a better reproduction of the saturated liquid density on specific temperature ranges. For more details the reader is referred to their papers.

Table 2.2 compares the attractive term in the Redlich-Kwong, the Peng-Robinson, the Schmidt-Wenzel and the Patel-Teja EoS.

Table 2.2: List of attractive terms for other cubic equations of state

EoS	Year	Attractive term
Redlich-Kwong	1949	$\frac{a(T)}{v(v+b)}$
Peng-Robinson	1976	$\frac{a(T)}{v(v+b)+b(v-b)}$
Schmidt-Wenzel	1980	$\frac{a(T)}{v^2+(1+3\omega)v-3\omega b^2}$
Patel-Teja	1982	$\frac{a(T)}{v(v+b)+c(v-b)}$

d) Volume translation

Important deviations are frequently observed on liquid molar volume prediction when using conventional cubic EoS. To partially fix this issue, molar volumes must be translated of a constant quantity c (volume translation) as explained by Péneloux et al. (1982). By doing so, the new EoS better predicts liquid densities without deteriorating the vapor-liquid property predictions. Starting with the SRK EoS, the translated EoS writes:

$$P = \frac{RT}{v-b} - \frac{a(T)}{(v+c)(v+b+2c)} \tag{2.13}$$

With $c = \frac{RT_c}{P_c}(0.12 - 0.4077 \cdot Z_{RA})$

Where:

Z_{RA} is the Racket compressibility factor,

Nonetheless, such EoS (Péneloux et al., 1982; Mathias and Copeman, 1983) cannot accurately predict molar volume in the neighborhood of the pure-component critical point.

e) Alpha function

In this section, cubic EoS alpha function formulations are introduced. The **alpha functions** are generally classified in two types: the **generalized α functions** and the **parameterizable (component dependent parameter) α functions**.

The generalized alpha functions only depend on the knowledge of the acentric factor ω in addition to the reduced temperature (Soave, Twu et al., Boston–Mathias and Mathias-Copeman). When considering parameterizable alpha functions (Twu et al.), adjustable parameters (to be e.g., fitted on Liquid-Vapor equilibrium data) are required.

Alpha functions parameters are necessarily associated to specific cubic EoS. The alpha functions discussed below are generally combined with the Redlich–Kwong (RK) and Peng-Robinson (PR) EoS.

- The generalized Soave α function, (Soave, 1972) :

$$\alpha_{Soave}(T) = [1 + m(\omega)(1 - T_r^{0.5})]^2 \tag{2.14}$$

Where the $m(\omega)$ parameter is correlated to the acentric factor ω through the following generalized expression:

$$\begin{cases} m_{RK}(\omega) = 0.480 + 1.574\omega - 0.176\omega^2 \\ m_{PR}(\omega) = 0.37464 + 1.5422\omega - 0.26922\omega^2 \end{cases} \tag{2.15}$$

- The generalized Twu α function, (Twu et al., 1995):

$$\alpha_{gen.\,Twu}(T) = \alpha_0 + \omega(\alpha_1 - \alpha_0) \tag{2.16}$$

Where:

$$\begin{cases} \alpha_0 = T_r^{n_0(m_0-1)} \cdot exp[l_0(1 - T_r^{n_0 \cdot m_0})] \\ \alpha_1 = T_r^{n_1(m_1-1)} \cdot exp[l_1(1 - T_r^{n_1 \cdot m_1})] \end{cases}$$

The parameters $(l_0, l_1, m_0, m_1, n_0, n_1)$ are universal constants (same for all the compounds), Table 2.3.

Note that these aforementioned parameters are dependent to the chosen equation of state. Meanwhile, different sets of parameters have been proposed for the subcritical and supercritical regions. Table 2.3 shows the parameter values for the RK and PR EoS:

Table 2.3: Values of the parameters of the generalized Twu α function for the PR and RK EoS

EoS	Temperature	l_0	l_1	m_0	m_1	n_0	n_1
RK	$T_r \leq 1$	0.141599	0.500315	0.919422	0.799457	2.496441	3.291790
RK	$T_r > 1$	0.441411	0.032580	6.500018	1.289098	-0.200000	-8.000000
PR	$T_r \leq 1$	0.125283	0.511614	0.911807	0.784054	1.948150	2.812520
PR	$T_r > 1$	0.401219	0.024955	4.963070	1.248089	-0.200000	-8.000000

- The generalized Boston-Mathias α function, (Boston and Mathias, 1980):

For $T_r \leq 1 :\ \alpha(T)$ is given by Eq. 2.14 and 2.15

For $T_r > 1 :\ \alpha(T) = exp[c(1–T_r^d)]$

Where $d = 1 + (\frac{m}{2})$, $c = 1 - \frac{1}{d}$

- The parameterizable Mathias-Copeman function, (Mathias and Copeman, 1983):

$$\alpha_{MC}(T) = [1 + c_1(1 - \sqrt{T_r}) + c_2(1 - \sqrt{T_r})^2 + c_3(1 - \sqrt{T_r})^3]^2 \tag{2.17}$$

Where c_1, c_2, c_3 are adjustable parameters that are tabulated in the D.D.B data base (Dortmund Data Bank) for numerous pure constituents.

- The parameterizable Twu alpha function, (Twu et al., 1991):

Twu et al. (1991) have developed an alpha function involving an exponential form:

$$\alpha_{gen.Twu}(T) = T_r^{N(M-1)} \cdot exp[L(1 - T_r^{N \cdot M})] \tag{2.18}$$

Where, L,M,N are three pure component adjustable parameters .

Note that the first derivative of the alpha function ($\frac{\partial \alpha}{\partial T}$) is involved in the expression of the pressure-explicit residual enthalpy, while the second derivative ($\frac{\partial^2 \alpha}{\partial^2 T}$) is involved in the expression of the residual isobaric heat capacity. To sum up, as shown by Neau et al. (2009) and Privat et al. (2015), the alpha function choice is important both to predict Vapor-Liquid Equilibriums and derived properties.

2.1.2 Virial equation

The **virial EoS** is the sum of polynomial terms in pressure or density $(1/v)$, (Poling et al., 2001). This type of equation was first proposed by Thiesen in 1885 to represent the volumetric behavior of a sparse real fluid based on the ideal gas reference, (Sandler and Orbey, 1992). The virial EoS is only applicable to components in the gases phase. Such power series write:

$$z(T,v) = \frac{Pv}{RT} = 1 + \frac{B(T)}{v} + \frac{C(T)}{v^2} + \frac{D(T)}{v^3} + ... \tag{2.19}$$

$$z(T,P) = 1 + B'(T)\cdot P + C'(T)\cdot P^2 + D'(T)\cdot P^3 + ... \tag{2.20}$$

Where the temperature-dependent coefficients: $B(T)$ or $B'(T)$, $C(T)$ or $C'(T)$, . . . are respectively called the second, third, ... **virial coefficients**. The second virial coefficient represents the deviation between an ideal and real gas due to interactions between pairs of molecules. The third virial coefficient reflects the effects of interactions of molecules triplets, and so on.

Next subsections focus on two important types of virial equation : the Benedict-Webb-Rubin (BWR) EoS and the Lee Kesler Plöker (LKP) EoS.

✻BWR modified Starling – Nishiumi (BWRS)

The original Benedict-Webb-Rubin (BWR) equation of state, (Benedict et al., 1942), is an important virial equation of state. Starling (1971) proposed to modify the basic BWR EoS version using more parameters. Nishiumi and Saito (1975) developed a generalized and extended virial equation based on both Benedict EoS and Starling EoS. This extended formulation (noted BWRS in this report) is considered in the present study and is defined as follows:

$$P = \rho RT + (B_0 RT - A_0 - \frac{C_0}{T^2} + \frac{D_0}{T^3} - \frac{E_0}{T^4})\rho^2 + (b'RT - a' - \frac{d'}{T} - \frac{e'}{T^4} - \frac{f'}{T^{23}})\rho^3 + \alpha'(a' + \frac{d'}{T} + \frac{e'}{T^4} + \frac{f'}{T^{23}})\rho^6 + (\frac{c'}{T^2} + \frac{g'}{T^8} + \frac{h'}{T^{17}})\rho^3(1+\gamma'\rho^2)e^{(-\gamma'\rho^2)} \tag{2.21}$$

Where
$$\begin{cases}
\rho_c B_0 = A_1 + B_1\omega \\
\frac{\rho_c A_0}{RT_c} = A_2 + B_2\omega + 0.095\omega^3 \\
\frac{\rho_c C_0}{RT_c^3} = A_3 + B_3\omega \\
\rho_c^2\gamma = A_4 + B_4\omega \\
\rho_c^2 b = A_5 + B_5\omega \\
\frac{\rho_c^2 a}{RT_c} = A_6 + B_6\omega \\
\rho_c^3\alpha = A_7 + B_7\omega \\
\frac{\rho_c^2 c}{RT_c^3} = A_8 + B_8\omega \\
\frac{\rho_c D_0}{RT_c^4} = A_9 + B_9\omega \\
\frac{\rho_c^2 d}{RT_c^2} = A_{10} + B_{10}\omega \\
\frac{\rho_c E_0}{RT_c^5} = A_{11} + B_{11}\omega e^{(-3.8\omega)} \\
\frac{\rho_c^2 e}{RT_c^5} = A_{12} + B_{12}\omega + C_{12}\omega^2 + D_{12}e^{(E_{12}\omega + F_{12}\omega^2)} \\
\frac{\rho_c^2 f}{RT_c^{24}} = A_{13} + B_{13}\omega + C_{13}\omega^2 + D_{13}e^{(E_{13}\omega + F_{13}\omega^2)} \\
\frac{\rho_c^2 g}{RT_c^9} = A_{14} + B_{14}\omega + D_{14}e^{(E_{14}\omega)} \\
\frac{\rho_c^2 h}{RT_c^{18}} = A_{15} + B_{15}\omega + D_{15}e^{(E_{15}\omega)}
\end{cases}$$

The values for the universal parameters γ', α', A_j and $B_j(j = 1,2,...,15)$, C_j, and $F_j\,(j = 12,13)$, $D_j$and $E_j\,(j = 12,...,15)$, a', $b'...h'$are reported in the ProsimPlus™ software.

✻ Lee-Kesler-Plöker

The correlation of the second virial coefficient published by Pitzer and Curl (1957) has been widely used with great success. By incorporating a third parameter (acentric factor ω) in a linear expression of the compressibility, their EoS expression drives to important improvements in P-v-T predictions. Based on the same hypothesis, Lee and Kesler (1975) have established a linear interpolation for the compressibility factor by introducing two kinds of fluids:

- The “simple fluids” as argon, krypton and methane. Their acentric factor are equal to zero (ω=0).
- The “reference fluid” (heavy reference) as n-octane with an acentric factor value set to ω_R=0,3978.

Lee-Kesler-Plöker EoS is known as the most accurate enthalpy model for gases, (Li

et al., 2012). It is written in the following form:

$$z = z^0 + \frac{\omega}{\omega_R}(z^R - z^0) \tag{2.22}$$

Where $z^0$and z^R are functions of the BWR form: z^0 is for a simple fluid ($\omega = 0$) and z^R is for reference fluid.

$$z^0 \, or \, z^R = 1 + \frac{B}{v_r} + \frac{C}{v_r^2} + \frac{D}{v_r^5} + \frac{c_4}{T_r^3 v_r^2} + (\beta + \frac{\gamma}{v_r^2}) e^{(-\frac{\gamma}{v_r^2})} \tag{2.23}$$

Where: $v_r = \frac{P_c v}{R T_c}$, $B = b_1 - \frac{b_2}{T_r} - \frac{b_3}{T_r^2} - \frac{b_4}{T_r^3}$ $C = c_1 - \frac{c_2}{T_r} - \frac{c_3}{T_r^2}$, $D = d_1 + \frac{d_2}{T_r}$

The values of universal parameters: b_1, b_2, b_3, b_4, c_1, c_2, c_3, c_4, d_1, d_2, γ, β for both simple and reference fluids, are those extracted from the ProSimPlus™ software.

2.1.3 Equation of state expressed in terms of Helmholtz energy

Instead of considering generalized equations, adjustable (parameterizable) equations of state developed for CO_2, especially those expressed in terms of Helmholtz energy are also reviewed in this report. In 1994, Pitzer and Sterner (1994) have developed an equation of state for pure CO_2 involving 10 functional terms of residual Helmholtz energy and 28 adjustable coefficients. Another equation, the Span Wagner (SW) EoS, Span and Wagner (1996), is currently known as one of the most accurate equations of state available for pure CO_2, (Kim, 2007; Mazzoccoli et al., 2014; Yu et al., 2015). In their equation, the residual Helmholtz energy involves 42 functional terms with 188 adjustable coefficients. Kim (2007) simplified the SW EoS by decreasing the number of functional terms to 30. Their improvement leads to a more accurate representation in the vicinity of the critical point but the model is less accurate than the SW EoS in the liquid and vapor phases.

✻ Span Wagner

The Span Wagner EoS leads to precise prediction of pure CO_2 in terms of P-v-T, enthalpy, phase equilibrium properties and speed of sound prediction. Many CO_2 experimental data were used to model the Helmholtz energy. In addition, the functional terms of residual Helmholtz energy handle the derived properties (e.g., speed of sound and heat capacity) as continuous variable in subcritical, supercritical region as well as in the vicinity of the critical point.

The SW EoS can be written in the form:

$$\frac{A(\rho,T)}{(RT)} = \varphi(\delta,\tau) = \varphi^{\bullet}(\delta,\tau) + \varphi^{r}(\delta,\tau) \tag{2.24}$$

$$\varphi^{\bullet}(\delta,\tau) = ln(\delta) + a_1^{\bullet} + a_2^{\bullet}\tau + a_3^{\bullet}ln(\tau) + \sum_{i=4}^{8} a_i^{\bullet} ln[1 - e^{(-\tau\theta_i^{\bullet})}] \tag{2.25}$$

$$\varphi^{r} = \sum_{i=1}^{7} n_{i,j}\delta^{d_i}\tau^{t_i} + \sum_{i=8}^{34} n_i\delta^{d_i}\tau^{t_i}e^{-\delta^{c_i}} + \sum_{i=35}^{39} n_i\delta^{d_i}\tau^{t_i}e^{-\alpha_i(\delta-\varepsilon_i)^2-\beta_i(\tau-\gamma_i)^2} + \sum_{i=40}^{42} n_i\Delta^{b_i}\delta e^{-C_i(\delta-1)^2-D_i(\tau-1)^2} \tag{2.26}$$

Where,

$\delta = \frac{\rho}{\rho_c}$, $\tau = \frac{T_c}{T}$;

$\Delta = \{(1-\tau) + A_i[(\delta-1)^2]^{1/(2\beta)_i}\}^2 + B_i[(\delta-1)^2]^{a_i}$;

φ is the dimensionless Helmholtz function; $\varphi^{\bullet}$ represents the ideal gas part of the Helmholtz function and φ^{r} is the residual part of Helmholtz function;

$a_i^{\bullet}$, $\theta_i^{\bullet}$ are correlated parameters tabulated in the Table 2 in Annexes;

n_i, c_i, d_i, t_i, α_i, β_i, ϵ_i, γ_i, A_i, B_i, C_i, D_i are correlated parameters tabulated in the Table 3.

2.1.4 SAFT equation

In 1989, Chapman et al. (1989) proposed an equation of state called SAFT EoS (Statistical Associating Fluid Theory) in order to represent associating fluids.

In this theory, a molecule is a chain of m elementary segments (or monomers). The hard-sphere segment is defined as idealized segments that cannot overlap in space. This kind of EoS represents the contributions from the different inter-molecular forces (dispersion force, association force, ...).

✻ SAFT EoS

Two general forms of molar residual Helmholtz energy in the SAFT EoS are defined as follows, Polishuk et al., 2013:

$$\begin{cases} form\,1: \ \frac{a^{res}}{RT} = \frac{a-a^{\circ}}{RT} = \underbrace{\frac{a^{HS}}{RT} + \frac{a^{Disp\,seg}}{RT}}_{a^{Ref\,real\,seg}/RT} + \frac{a^{Chain\,of\,seg}}{RT} + \frac{a^{Assoc}}{RT} \\ form\,2: \ \frac{a^{res}}{RT} = \frac{a-a^{\circ}}{RT} = \underbrace{\frac{a^{HS}}{RT} + \frac{a^{Chain\,of\,HS}}{RT}}_{a^{Ref\,HS\,seg}/RT} + \frac{a^{Disp\,chain}}{RT} + \frac{a^{Assoc}}{RT} \end{cases} \tag{2.27}$$

Where, the residual hard-sphere term a^{HS} accounts for repulsive effects in a spherical-segment fluid.

a^{Assoc} stands for the contribution of inter-molecular association between real chains of segments.

In the form 1 of Eq. 2.27, the term $a^{Disp\,seg}$ represents the amount of Helmholtz energy to add to the residual hard-sphere Helmholtz energy (a^{HS}) in order to obtain the Helmholtz energy of real segments ($a^{ref\,real\,seg}$). Note that the reference fluid is made up of real segments (or real monomers) not bonded together. The term $a^{Chain\,of\,seg}$ represents the amount of Helmholtz energy due to the formation of covalent bonds between real segments.

In the second form of the EoS, the term $a^{Chain\,of\,HS}$ represents the amount of Helmholtz energy due to the formation of covalent bonds between hard-sphere segments. The reference fluid is made up of chains of hard spheres not yet subject to dispersion effects. Thus, chain terms a^{Chain} are added to a^{HS} to obtain $a^{Ref\,HS\,seg}$. The dispersion term $a^{Disp\,chain}$ represents the amount of Helmholtz energy to add to the Helmholtz energy of a hard-chain fluid (i.e. reference fluid) to obtain the Helmholtz energy of a real non-associating compound.

Generally speaking, three parameters per pure component are needed for non-associating and non-polar molecules: m, σ and $\frac{\varepsilon}{k_B}$, where m represents the average number of segment in a chain, σ is defined as the hard sphere diameter, $\frac{\varepsilon}{k_B}$ is the depth of pair potential characterizing the dispersion forces.

The popular forms of SAFT equations are PC (Perturbed-Chain)-SAFT , soft-SAFT, SAFT-VR (Variable-Range). The PC-SAFT EoS by Gross et al. (2001) is expressed using form 2 in Eq. 2.27. The soft-SAFT constructed by Blas and Vega (1997, 1998) relies on the first form of Eq. 2.27. The SAFT-VR by Gil-Villegas et al. (1997) is relying on the first form of Eq. 2.27. As a matter of readability, each SAFT-type EoS terms are not detailed in this report but can be easily found in the cited original papers.

The SAFT EoS better predicts liquid phase density in comparison with the cubic EoS. The data

of saturation vapor pressure and saturation liquid density are usually used to determine the pure-component SAFT parameters. However, since the SAFT EoS do not use the experimental values of T_c and P_c as input parameters, important deviations are usually observed on the predicted critical proprieties (T_c, P_c and v_c).

2.1.5 Representation of the critical region

Equations of state (e.g., cubic and SAFT type) do not accurately represent all the state variables (properties) in the vicinity of the critical point with a similar accuracy. Since our study includes this region; this chapter intends to evaluate the capacity of various EoS to predict properties in the critical region. As a matter of fact, near the vapor-liquid critical point of a substance, some non-classical behaviors are observed. For example, the experimental shape of the critical isotherm in the (c_v, P) (c_p, P) planes and the variation of the isothermal compressibility factor are significantly different from predictions by classical cubic EoS, (Poling et al., 2001). From a molecular point of view, that is because the molecular correlations are much longer ranged and fluctuate differently in this region. However, the classical theory of critical region in most of the EoS corresponds to a mean-field approximation, which neglects the local inhomogeneity (fluctuations) in density.

To overcome this deficiency, considerable studies have been done to develop equations that bridge two regions, from the "classical" region (classical behavior that occurs sufficiently far away from the critical point) to the "non-classical" critical point region. One approach is to use the crossover functions developed by Sengers and coworkers (Tang and Sengers, 1991; Anisimov et al., 1992; Kiselev, 1998), which are only applicable in the vicinity of a critical point. Such functions consider the long-scale fluctuations in density near the critical region in order to link the two regimes. However, their original method does not cover all conditions, recent efforts have led crossover functions applicable to subcritical, supercritical and critical regions by considering crossover functions as patch functions.

In this case, the crossover function is extended into a larger application range and is applied to cubic EoS (ex: Peng-Robinson EoS, Patel-Teja EoS) or SAFT type EoS outside the vicinity of the critical point, (Kiselev, 1998; Lee et al., 2007; Sun et al., 2005; Behnejad et al., 2015; Hu et al., 2003). Results show that this approach yields better property profiles in the critical region in comparison with the original cubic or SAFT EoS.

Another approach introduced by (Span and Wagner, 1996) is to improve the empirical expression of the properties that suffer from steep change in the critical point region: the specific heat capacity $c_p$and c_v as well as the speed of sound w. More precisely, it can be observed in

the equations listed below that when approaching the critical point, $(\frac{\partial p}{\partial \rho})_T^{-1}$ grows much faster than c_v. In Eq. 2.28, the specific isobaric heat capacity is dominated by the latter fraction. The fraction $(\frac{\partial p}{\partial \rho})_T$ becomes zero at the critical point, thus c_p is expected to grow towards infinity, which conforms to its realistic physical behavior. The residual part of Helmholtz function in the Span Wagner EoS enables c_v to have expected infinite behavior in the vicinity of the critical point. As a consequence, the expression of speed of sound in the Span Wagner EoS in Eq. 2.29 reduces towards zero when approaching the critical point.

$$\frac{c_p}{R} = \underbrace{-\tau^2(\varphi^\circ{}_{\tau\tau} + \varphi^r_{\tau\tau})}_{\frac{c_v}{R}} + \frac{\overbrace{(1+\delta\varphi^r_\delta - \delta\tau\varphi^r_{\delta\tau})^2}^{\approx(\frac{\partial p}{\partial T})^2_\rho}}{\underbrace{1+2\delta\varphi^r_\delta + \delta^2\varphi^r_{\delta\delta}}_{\approx(\frac{\partial p}{\partial \rho})_T}} \tag{2.28}$$

$$\frac{w^2}{RT} = \underbrace{1+2\delta\varphi^r_\delta + \delta^2\varphi^r_{\delta\delta}}_{\approx(\frac{\partial p}{\partial \rho})_T} - \frac{\overbrace{(1+\delta\varphi^r_\delta - \delta\tau\varphi^r_{\delta\tau})^2}^{\approx(\frac{\partial p}{\partial T})^2_\rho}}{\underbrace{\tau^2(\varphi^\circ{}_{\tau\tau} + \varphi^r{}_{\tau\tau})}_{-\frac{c_v}{R}}} \tag{2.29}$$

2.2 Discussions and Selection of EoS candidates

Each described EoS has more or less advantages and limitations. Conventional equations for non-polar fluid such as cubic EoS (Soave, 1972; Peng and Robinson, 1976) could successfully approximate all kinds of real fluid behavior with reasonable uncertainties and are relatively easy to compute. However, they have limited accuracy in predicting the liquid molar volumes (the liquid phase density and other properties involving the liquid molar volume). Empirical EoS, such as the virial-type EoS (Benedict et al., 1942; Starling, 1971; Nishiumi and Saito, 1975; Pitzer and Curl, 1957), predict liquid molar volumes more accurately than cubic EoS. On the other hand, the SAFT-type equations (Gross et al., 2001; Blas and Vega, 1997; Gil-Villegas et al., 1997) better predict liquid phase density than cubic EoS, but usually exhibit severe deviation in terms of critical property prediction (T_c , P_c and v_c). The salient advantage of SAFT-type EoS is lying in the possibility to account for association (presence of H bonds), it has been decided not to consider this class of EoS for the present study limited to pure (non-associating) CO_2. Specific adjustable EoS developed for CO_2, e.g., EoS expressed in terms of Helmholtz energy (Span and Wagner, 1996; Kim, 2007; Mazzoccoli et al., 2014; Yu et al., 2015), offer a priori a satisfactory prediction of each property in large regions of temperature and pressure.

In this thesis, only pure CO_2 is considered as working fluid. However, some other researchers

(Jeong et al., 2011a) studied the impact of modifying the CO_2 critical coordinates by mixing another gas, such as N_2, O_2, He, or Ar. In such a case, it would be recommended to use the well-established GERG 2008 EoS (Kunz and Wagner, 2012) (another Helmholtz-type EoS). For more details the reader is referred to their papers, this thesis will not go into details here.

Thereafter, in this dissertation, after having balanced the benefits of each equation, we intended to investigate as many as possible types of EoS. Six candidate EoS were eventually selected for the comparative study and are now sorted out according to their EoS class:

- *Cubic EoS:* the Peng-Robinson EoS (PR) using the classical Soave alpha function; the Peng-Robinson EoS combined with the Boston-Mathias alpha function (PR-BM), an alternative version of the PR EoS; the Soave Redlich-Kwong EoS (SRK) using the Soave alpha function;
- *Virial-type EoS:* the Lee-Kesler-Plöcker EoS (LKP), the Benedict-Webb-Rubin modified by Starling and Nushiumi (BWRS)
- *Helmholtz-type EoS:* the Span Wagner (SW) EoS.

In this study, the commercial software ProSimPlus™ was used to perform calculations with the PR, PR-BM, SRK, LKP and BWRS EoS, while Refprop (Lemmon et al., 2013) was considered to perform calculations with the SW EoS. For different SC-CO_2 Brayton cycle presented in Chapter 1, the temperature and pressure ranges of interest are [300 K; 1373 K] and [7 MPa; 30 MPa], respectively. Note that rounded values of the CO_2 critical point coordinates (304 K, 7.38 MPa) define the lowest bounds of the temperature and pressure domains investigated for testing EoS performances.

2.3 METHODS

2.3.1 Selection of properties for the comparison

In order to evaluate the accuracy of each EoS mentioned, a set of physico-chemical properties were selected for carrying out the comparison of EoS performances. The criteria used to select the properties are the following ones:

- Properties that are directly of interest for modeling the RC process were first considered. These are: (i) the **fluid density** which is used to estimate the volumetric flowrate of CO_2; this latter is an important input parameter for machinery sizing (e.g., compressor, turbine). (ii) **Heat capacities** are also required for the design of turbomachineries and were thus also selected. Although important for machinery sizing, transport properties such as

fluid viscosity were not considered because they cannot be directly calculated from EoS (they can however be estimated from correlations / theory requiring sometimes input parameters likely to be estimated from equations of state, e.g., density, residual entropy, etc.).

- Additional properties were also considered to enrich the set of properties considered for the comparison. By experience, derived EoS properties (that are properties involving the first or second EoS derivatives with respect to temperature or density, e.g. enthalpy, entropy, heat capacities, speed of sound, etc.) are a severe test for evaluating EoS performance and are thus of interest for our comparison. For this reason, the **speed of sound** was also included in the study in addition to the already-involved heat capacity. It is recalled that the expression of the speed of sound is given by: $w = \sqrt{vc_p/(Mc_v\kappa_T)}$ where v is the molar volume, c_p and c_v are the isobaric and isochoric heat capacities, M is the molecular weight and κ_T denotes the isothermal compressibility. It can be observed that a large number derived properties are involved in the expression of w.

2.3.2 Comparison steps

The capacity in predicting density, heat capacity and speed of sound of SC-CO_2 was tested out on temperature and pressure ranges of interest defined in Section 2.2. The procedure of comparison consists in five steps:

- Step 1: In section 2.4.1, the values of the critical temperature, critical pressure and critical density of pure CO_2 calculated by the various EoS are compared with the values found in the DIPPR (Design Institute for Physical Properties) 801 database available in the DIADEM software, (DIADEM, version 2015).

- Step 2: Then in section 2.4.2, the properties selected for the comparison (density, heat capacity and speed of sound) are calculated with all the studied EoS in the whole region of study (T=300-1373 K, P=7-30 MPa). This comparison is carried out with the available experimental data (Detherm database (Dortmund DataBank, 2015)). In particular, graphical comparison of six candidate EoS is performed in the vicinity of the critical point (T=300-310 K, P=7.38 MPa)

- Step 3: The comparison brought out in section 2.4.3 is a complementary step. The idea is to show a graphic representation of the EoS leading to the smallest mean absolute percentage error (MAPE) in previous step (T=300-1373 K, P=7-30 MPa).

- Step 4: Some unused experimental data which are out of domain of interest are tested out in comparison with the prediction of the final selected EoS (from step 2 and 3) in section 2.4.4. This step shows the prediction capacity of the selected EoS in wide ranges.

✻ Experimental data correction before comparison

For the complete temperature-pressure domain of study (i.e., 300-1373 K, 7-30 MPa), the aim is to use the data available in Detherm to proceed Step 2, Step 3 and Step 4 evaluation. However, author has noted that one set of density data referenced as "Nowak et al. (1997)" on density was wrongly entered in the Detherm software (10 "density" points). After an investigation, the pressures recorded in the original publication appear to not meet the range of our study, they are then crossed out.

Another set of data referenced in the publication of Tsuji et al. (1998) have been wrongly converted in terms of unit by the Detherm (68 "density" points). In this thesis, we recalculated the density based on the original published experimental compressibility factor (z), experimental temperature and pressure as well as Eq. 2.30:

$$z = \frac{P \cdot M}{\rho \cdot R \cdot T} \tag{2.30}$$

Where

P is the pressure in Pa;

T is the temperature expressed in K;

M is the molar mass of CO_2 expressed in kg/mol;

ρ is the density on kg/m^3

R is the gas constant equals to 8.314 J mol^{-1}K^{-1}.

After this conversion, this set of data shows a good consistency by comparison with other experimental data whereas the deviation before correction is 300%.

For the complete temperature-pressure domain of study (i.e., 300-1373 K, 7-30 MPa), Table 2.4 details the sources of experimental data and the amount of experimental data points used in this evaluation along with the temperature and pressure ranges.

For each considered property, the mean absolute percentage errors (MAPE) were used to quantify mean deviations between EoS predictions and experimental data. For a given property Y, the MAPE is defined as follows:

$$\mathrm{MAPE}(Y) = \frac{100}{n_{exp}} \sum_{i=1}^{n_{exp}} \left| \frac{Y_{exp,i} - Y_{EoS}(T_{exp,i}, P_{exp,i})}{Y_{exp,i}} \right| \tag{2.31}$$

Table 2.4: Temperature, pressure range and quantity of data applied in the entire EoS comparisons

Property	Temperature range (K)	Pressure range (MPa)	Amount of datapoints
Density	298.15-1033.15	6.98-20.00	2637
Heat capacity	283.01-573.15	7.00-20.10	359
Speed of sound	301.15-450.00	6.91-14.19	138

where n_{exp} is the number of experimental data on which the MAPE is evaluated, $Y_{exp,i}$ is the experimental value of the ith datapoint measured at given temperature $T_{exp,i}$ and pressure $P_{exp,i}$ and Y_{EoS} is the property calculated from EoS at given $T_{exp,i}$ and $P_{exp,i}$.

2.4 Results and discussion

2.4.1 Critical density

Table 2.5 provides the critical temperature (T_c), pressure (P_c) available in each EoS. Meanwhile, the critical density (ρ_c) was calculated by using their experimental values of T_c and P_c. The MAPE between EoS critical density prediction and the experimental data (DIADEM, version 2015) is also listed.

Table 2.5: MAPE (Mean absolute percentage errors) between EoS predictions and DIPPR experimental data in terms of critical density

	Critical temperature (T_c/K)	Critical Pressure (P_c/MPa)	Critical density (ρ_c/kg/m^3)	MAPE (ρ_c)
SW	304.13	7.3773	467.6	0.1%
PR	304.21	7.3830	416.9	10.9%
SRK	304.21	7.3830	385.4	17.7%
LKP	304.21	7.3830	468.5	0.1%
BWRS	304.21	7.3830	423.9	9.5%

Table 2.5 shows that the SW and LKP EoS exhibit the smallest overall deviations on critical density (0.1%) compared with the value in DIPPR database. The PR / PR-BM and BWRS EoS predict similar underestimated values of critical densities. The SRK EoS shows the biggest overall deviation (18%) which reflects its inadequacy to reproduce the critical density.

2.4.2 MAPE investigation of six candidate EoS

For each candidate EoS presented above, Table 2.6 shows the MAPE between EoS predictions and experimental data in the whole region of study (300-1373 K, 7-30 MPa) in terms of density (ρ), constant-pressure heat capacity (c_p) and speed of sound (w).

Table 2.6: MAPE (Mean absolute percentage errors) between EoS predictions and experimental data in terms of density, isobaric heat capacity and speed of sound for the SW, PR, PR-BM, SRK, LKP and BWRS EoS. The temperature and pressure ranges covered by the data are : 300-1373 K and 7-30 MPa, respectively. Values in bold indicate the most accurate predictions for a given property.

EoS	MAPE(ρ)	MAPE(c_p)	MAPE(w)
SW	**2.43%**	**3.95%**	**4.81%**
PR	4.48%	7.42%	28.89%
PR-BM	4.71%	7.30%	28.89%
SRK	8.85%	6.80%	30.66%
LKP	4.40%	5.61%	24.48%
BWRS	5.03%	8.85%	13.42%

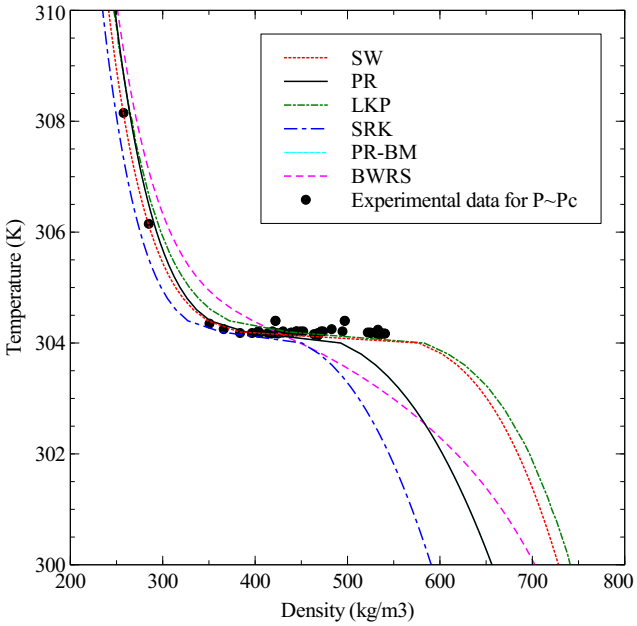

Figure 2.1: Comparison of the ability of the 6 candidate EoS to represent isobaric densities at the CO_2 critical pressure.

It can be observed that for each considered property, the SW EoS always leads to the most accurate predictions (lower than 4% for ρ and c_p). As a noticeable feature, the deviations between speed of sound data and SW EoS predictions are smaller than 5% while most of other EoS exhibit

deviations exceeding 20%. Let us mention that the superiority of the SW model can be observed both in the critical and supercritical regions. To support this statement, graphical illustrations of the capacity of the 6 candidate EoS to model near-critical data are now proposed through Figure 2.1 whereas Figure 2.5 deals with the modeling of supercritical data. At this step, let us note that the reproduction of near-critical data should be considered as a difficult challenge for an EoS. Figure 2.1 compares the predictions by the 6 candidate EoS in terms of density, speed of sound and constant-pressure heat capacity, in the vicinity of the CO_2 critical point. Experimental data-points are represented by black circles and EoS predictions by solid lines.

Figure 2.1 reports experimental density data measured at the CO_2 critical pressure in the temperature-density plane. Isobaric curves calculated from each of the six candidate EoS are shown. Most of them exhibit the typical horizontal inflection point characterizing the presence of the critical point on the critical isobar. As a noticeable exception, the BWRS EoS does not predict such horizontal inflection point indicating that this model underestimates the critical pressure of pure CO_2. In terms of ability for the models to reproduce near-critical density, it can be claimed that as expected, cubic EoS predictions (PR, PR-BM and SRK EoS) deviate notably from experimental data (MAPE $>$20%), contrary to the LKP and SW EoS which provide accurate density predictions in the critical region (especially if experimental uncertainties are taken into account).

Figure 2.2 shows speed of sound predictions for the six EoS. Important relative deviations (ranging between 16% and 41%) are observed for the PR, PR-BM, SRK, LKP, BWRS EoS. These models are not capable of accurately reproducing the V shape characterizing the critical isotherm in this plane indicating that derivative EoS properties are not properly estimated by these models in a near-critical region. On the contrary, the SW EoS seems to have the capacity both to predict the V shape and to quantitatively reproduce near-critical speed of sound data with a reasonable accuracy. Such results should be considered as excellent given that speeds of sound are notably sensitive to temperature and pressure variations in near-critical conditions and are thus highly difficult to predict in this region.

In a similar way, Figure 2.3 shows that the SW EoS *accurately* predicts constant-pressure heat capacities (MAPE = 0.5%) in a near-critical region. Heat capacities predicted by other EoS deviate from experimental data with a mean deviation of around 2%.

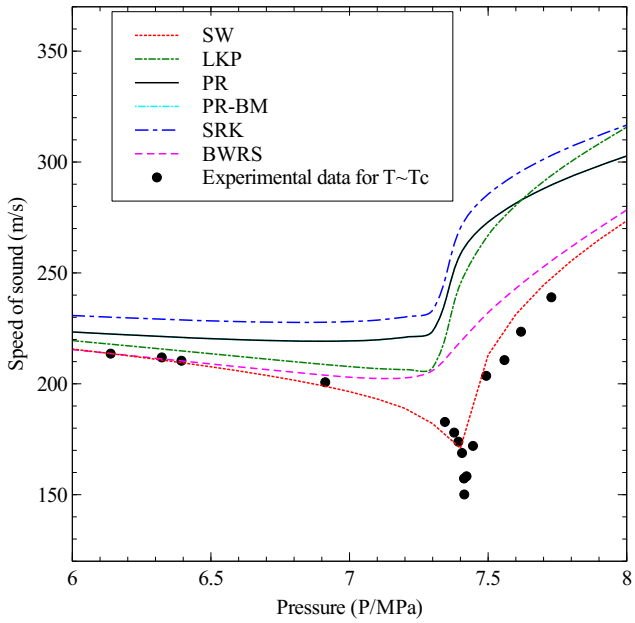

Figure 2.2: Comparison of the ability of the 6 candidate EoS to represent isothermal speeds of sound at the CO_2 critical temperature.

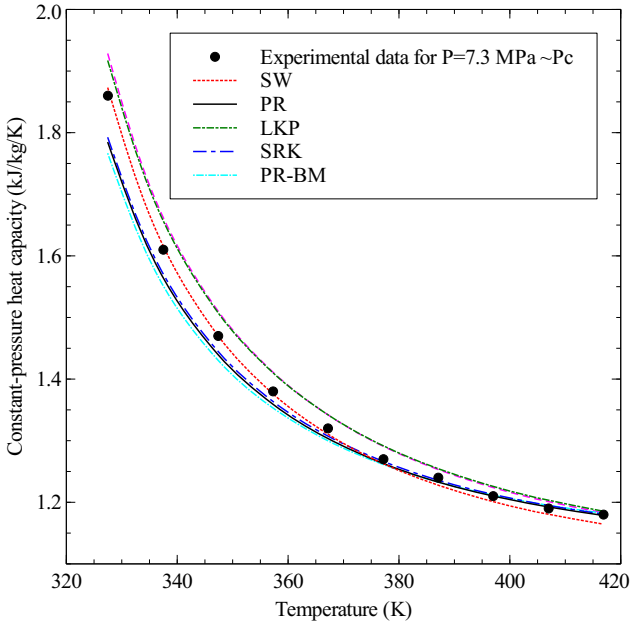

Figure 2.3: Comparison of the ability of the 6 candidate EoS to represent isobaric constant-pressure heat capacities at the CO_2 critical pressure.

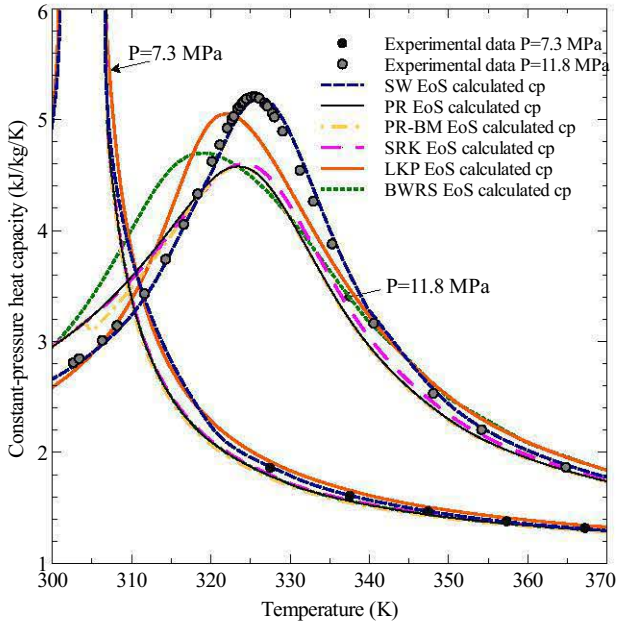

Figure 2.4: Graphical overview of the ability of the 6 candidate EoS to model isobaric heat-capacity data in the supercritical region

Figure 2.4 compares the 6 EoS in terms of constant pressure heat capacity prediction in the supercritical domain. It is recalled that when the pressure approaches the critical pressure (P_c) of pure CO_2, the constant-pressure heat capacity diverges. Above the critical pressure, the (constant pressure heat capacity versus temperature) curve exhibits a bell shape. While all model predictions seem equivalent at P_c ~ 7.3 MPa (Figure 2.1 (c)), the superiority of the SW EoS clearly appears at 11.8 MPa. This model outperforms the 5 other candidate EoS by providing deviations lower than 3%.

Eventually, the SW EoS appears as the most promising candidate out of the 6 candidate EoS at the end of step 2. For the next two steps of the comparison, this EoS can be considered as a reference EoS to compare with experimental data.

2.4.3 Graphic representation of SW EoS in the entire region of interest

A good correlation has been found between the SW EoS calculated density and experimental data, especially at high temperature and pressure, as showed in Figure 2.5 (a). The only area that provides important deviations (> 15%) is located at the critical region of CO_2 for temperatures in the range 300-305 K and pressures around 7.4 MPa, Figure 2.5 (b).

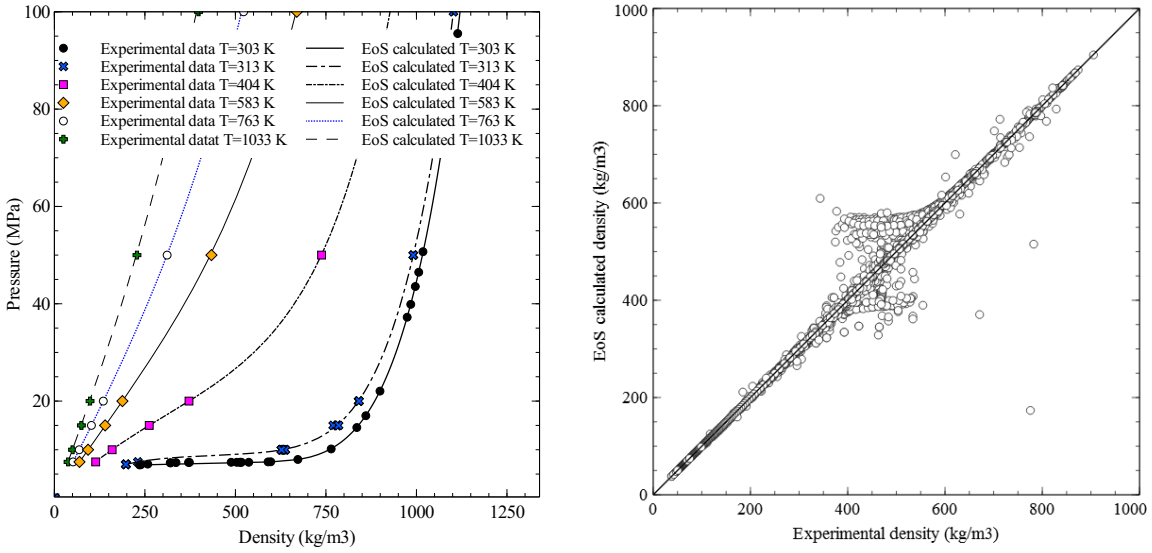

(a) (b)

Figure 2.5: Graphical overview of the ability of the SW EoS to model density in the supercritical region, 300 K< T <1373 K, 7 MPa< P <30 MPa. (a) plots experimental data on modeled curves and (b) shows the parity curve between experimental and EoS calculated density;,

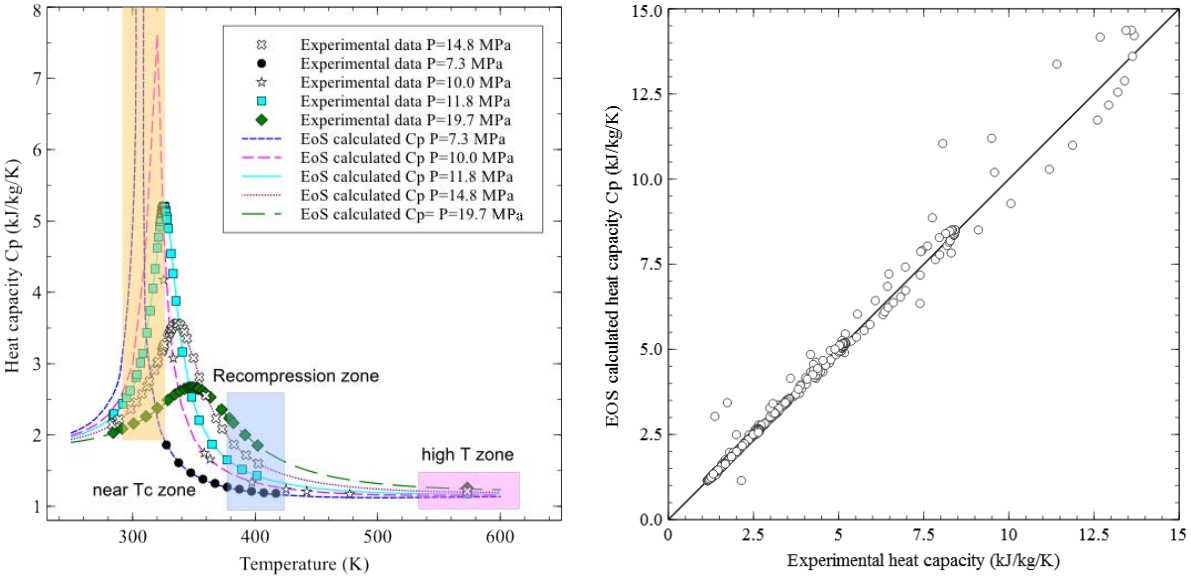

(a) (b)

Figure 2.6: Graphical overview of the ability of the SW EoS to model isobaric heat-capacity in the supercritical region, 300 K< T <1373 K, 7 MPa< P <30 MPa. (a) plots experimental data on modeled curves and (b) shows the parity curve between experimental and EoS calculated isobaric heat-capacity.

Figure 2.6 (a) qualitatively shows that the predicted isobaric heat capacity curves reproduce experimental data with a good accuracy. Note in Figure 2.6 (b) that the predicted heat capacity points are distributed along the parity line. The observation on relative deviation shows that the most important deviations are located in the vicinity of isobaric curves maxima. In this region, the relative mean deviation is about 30% while the relative mean deviation considering the entire data set is 1.7%.

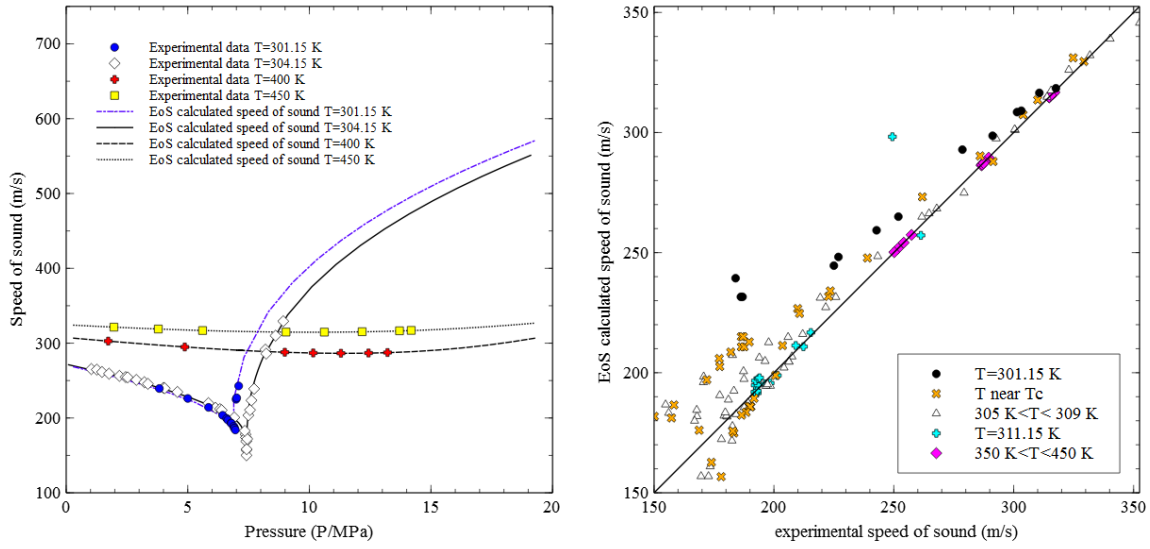

(a) (b)

Figure 2.7: Graphical overview of the ability of the 6 candidate EoS to model speed of sound in the supercritical region, 300 K< T <1373 K, 7 MPa< P <30 MPa. (a) plots the experimental data on modeled curves and (b) shows the parity curve between experimental and EoS calculated speed of sound.

Similar as for density and heat capacity, the SW EoS predicts accurately speeds of sound, especially at high pressures and temperatures, see Figure 2.7 (a) and (b). The mean relative deviation considering the entire data set is 4.8% and the biggest deviation can be observed around the CO_2 critical point. This step makes it possible to conclude that the SW EoS is not only interesting near the CO_2 critical point (see Step 2) but also predicts with a reasonable accuracy in all the other area of interest.

2.4.4 Comparison of the SW EoS with the unused experimental data sets

The step 1, 2 and 3 show that the SW EoS is able to accurately predict the CO_2 properties on entire area of interest. Since such Helmholtz type EoS has a wide application field in terms of temperature and pressure, some unused experimental data which are out of domain of interest are tested out. Especially data set published after 1994 and that were not employed during

the model calibration, as the SW EoS was published in 1994. Despite the resurgent interest in measuring the heat capacity and the speed of sound, the latest corresponding data recorded in the Detherm database are respectively dated from 1995 and 1998. The latest measured density data for CO_2 are dated 2013. Table 2.7 sums up the four latest (and appropriate for this study) sets of data and their global deviations.

Table 2.7: List of experimental data used in step 3

Property	Reference	T (K)	P (MPa)	Points	MAPE
ρ	Zolghadr et al. (2013)	313.15-393.15	0.34-17.20	250	3.13%
C_p	Dordain et al. (1995)	327-417	5.1-25.8	110	1.40%
w	Estrada-Alexanders and Trusler (1998)	220-450	0.51-9.27	61	0.02%
	Herget (1940)	301.15-311.15	0.888-10.1	196	3.67%

Figure 2.8, 2.9 and 2.10 show the parity plots between the latest sets of experimental data shown in Table 2.7 and the SW EoS calculated values. Satisfactory predictions in terms of density, heat capacity and speed of sound are achieved with the SW EoS in a broader applicability range for the CO_2.

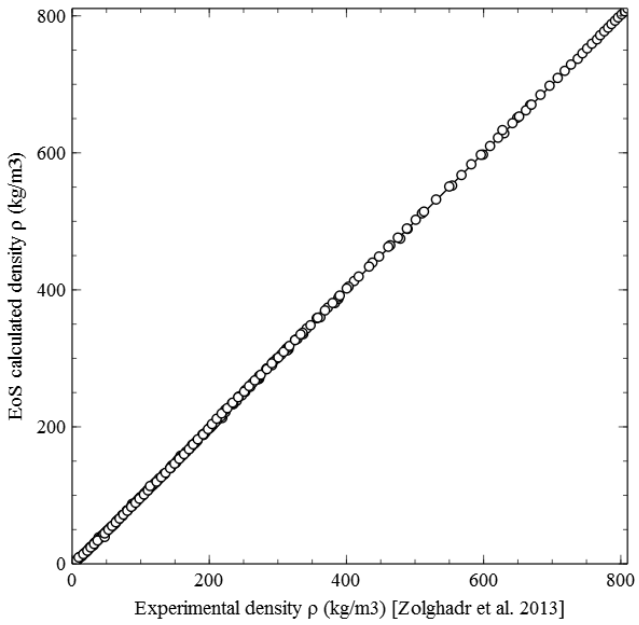

Figure 2.8: Parity plot of density, experimental data extracted from Zolghadr et al. (2013)

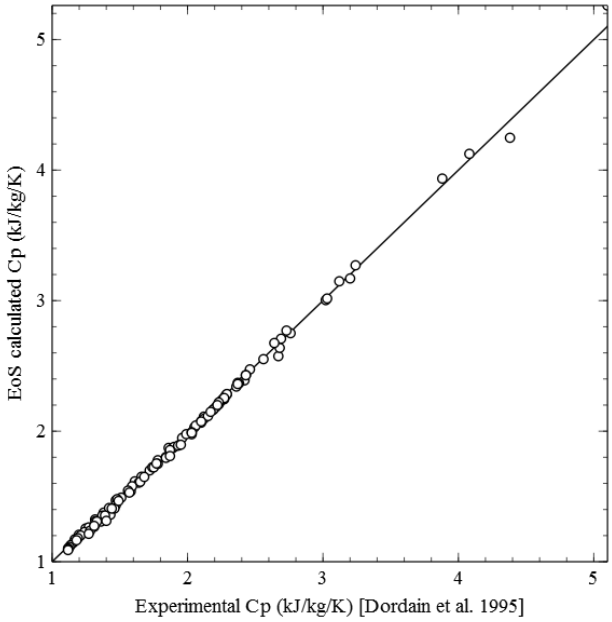

Figure 2.9: Parity plot of heat capacity, experimental data extracted from Dordain et al. (1995)

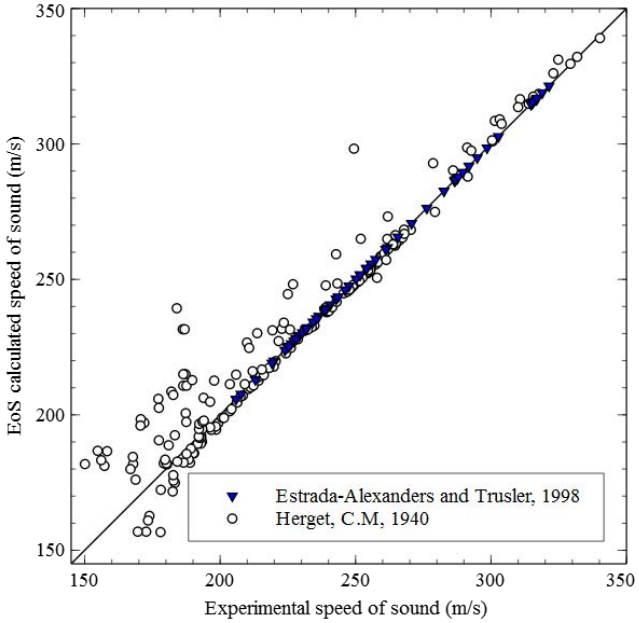

Figure 2.10: Parity plot of experimental data extracted from Estrada-Alexanders and Trusler (1998); Herget (1940)

In this chapiter, a rigorous selection procedure of an equation of state is presented for SC-CO_2. Different thermodynamic models that can be used to study the SC-CO_2 Brayton cycles have been compared in the entire temperature and pressure domains of interest (T = 300–1373 K, P = 7–30 MPa). In terms of pure-component behavior, among the six studied EoS, the Span Wagner EoS is the one that leads to the most accurate predictions of the CO_2 in the near-critical and supercritical regions.

For all the following chapters in this dissertation, SW EoS is applied and considered as the reference EoS for the modeling, simulation as well as optimization of SC-CO_2 Brayton cycle process.

CHAPTER 3

Modeling and design of recuperated SC-CO_2 Brayton cycle

In Brayton cycle, the fluid expansion is done in the 1-phase gas area which means that the working fluid still contains thermal energy at the expansion step outlet (high fluid temperature after expansion). It is thus intuitive to add a counter-current heat exchanger to recover the heat contained in this stream. This counter-current heat exchanger is denoted as *recuperator* in energy systems and the corresponding cycle configuration is known as *recuperated* Brayton cycle (RC). This cycle configuration is one of listed SC-CO_2 Brayton cycle in Chapter 1, it has high achievable efficiency despite of its simple layout (Çengel and Boles, 1989). The modeling and design on this RC cycle will serve as cornerstones for the intended superstructure optimization of a series of SC-CO_2 Brayton cycle.

On the other hand, though the selection of the thermodynamic model has been performed in the previous chapter, the impact of the final chosen thermodynamic model has not been yet globally quantified either in Brayton cycle process modeling nor unit operation (component) design.

Therefore, in this chapter, modeling, simulation, component (unit operation) design as well as sensibility analysis are performed with this SC-CO_2 RC cycle. Moreover, we intend to quantify the influence and uncertainty of chosen thermodynamic models on both process simulation and machinery sizing.

3.1 Process description of a recuperated SC-CO_2 Brayton cycle

The classical RC for SC-CO_2 proposed by Angelino (1969) is presented in Figure 3.1. It is composed of:

- [*a*-*b*] a non-isentropic compressor C1
- [*b*-*c*] the cold side of a heat exchanger called recuperator and denoted R1 (note that the pinch point of R1 is always located at the cold-side inlet)
- [*c*-*d*] the cold side of a heat exchanger absorbing a heat duty $\dot{Q}_{hot}$ from a heat source
- [*d*-*e*] a non-isentropic turbine
- [*e*-*f*] the hot side of the recuperator R1 (note that the pinch point of R1 is always located at the hot-side outlet)
- [*f*-*a*] the hot side of a heat exchanger evacuating a heat duty $\dot{Q}_{cold}$ to a heat sink

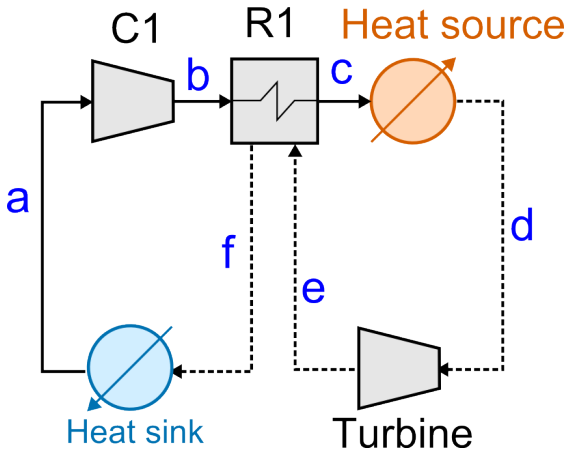

Figure 3.1: Base-case Recuperated Brayton Cycle (RC) layout.

A scientific publication is used to establish a guideline approach to set the parameter-design criteria for the cycle, (Mohagheghi and Kapat, 2013; Reyes-Belmonte et al., 2016). On absence of chemical reaction, the process model can be reduced to energetic balance, mass balance and thermodynamic aspects by ignoring e.g., mechanical or heat and mass transfer issues. The thermodynamic properties of SC-CO_2 are predicted by the SW EoS (the most accurate EoS for CO_2).

Compressor and turbine modeling proceed from a non-isentropic process of compression or expansion respectively, given by the following thermodynamic relations Eqs. 3.1 and 3.2.

$$\eta_{sC}(h_b - h_a) = (h_{b'} - h_a) \tag{3.1}$$

$$\eta_{sT}(h_d - h_{e'}) = (h_d - h_e) \tag{3.2}$$

Where η_{sC} is the isentropic efficiency of compression, listed in Table 3.1

η_{sT} is the isentropic efficiency of expansion, listed in Table 3.1

$h_{b'}$ is the enthalpy after isentropic compression and $h_{e'}$is the enthalpy after isentropic expansion. While normally the notation ' references to real gas compression, in this dissertation, it is used to represent isentropic compression for the readability of figures.

Energy conservation equation at the recuperator, given by Eq. 3.3, assumes that recuperators are insulated from its surroundings, the heat being exclusively exchanged between hot and cold streams.

$$h_c - h_b = h_e - h_f \tag{3.3}$$

The thermal pinch in R1 is defined as the minimal temperature difference within the recuperator. For the real-gas SC-CO_2, the high pressure low temperature stream b exiting the compressor has an isobaric heat capacity (c_p) that matches the bell shape illustrated in Figure 2.4 (see Section 2.4.2). The stream locating at the cold-side inlet of R1 thus holds a c_p two or three times higher than the hot-side outlet (stream f). Meanwhile the temperature and pressure range of stream c and e do not benefit this steep variation of c_p, this pinch is thus systematically located at the cold-side inlet (stream b) and hot-side outlet (stream f) for the RC configuration and consequently:

$$\Delta T_{pinch} = T_f - T_b \tag{3.4}$$

Pressure losses during heating or cooling processes (R1, heat sink, heat source) are assumed to be linear and dependent on a relative pressure loss $\%\Delta p$. This relation is given by Eq. 3.5 . Due to the high pressure in the cycle, the pressure drops (irreversibilities) in heat exchangers can not be neglected (Brun et al., 2017).

$$P_{out} = P_{in}(1 - \%\Delta p) \tag{3.5}$$

The mass flowrate is conserved during the entire process with the absence of chemical reaction and split. The mass flow rate of supercritical CO_2 can be calculated as the required flow rate to have a heat addition of $\dot{Q}_{hot}$, Eq. 3.6.

$$\dot{m} = \dot{Q}_{hot}/(h_c - h_d) \tag{3.6}$$

$$\bar{W}_{turbine} = h_d - h_e \tag{3.7}$$

$$\bar{W}_{compressor} = h_b - h_a \tag{3.8}$$

where h is the enthalpy per unit mass.

As defined in Chapter Introduction, the efficiency of the RC is calculated as the ratio of $\dot{W}_{net}$ and the heat duty $\dot{Q}_{hot}$ brought by the heat source (positively defined):

$$\text{RC cycle efficiency} = (\dot{m}\bar{W}_{turbine} - \dot{m}\bar{W}_{compressor})/\dot{Q}_{hot} \tag{3.9}$$

Table 3.1: Equipment data and fixed variables extracted from Mohagheghi and Kapat (2013)

Equipment data and fixed variables	Value
Turbine isentropic efficiency η_{sC}	0.9
Compressor isentropic efficiency η_{sT}	0.89
Pressure drop in every component (% of inlet pressure)	1
ΔT_{pinch} (K)	20
$\dot{Q}_{hot}$ (MW)	200
T_{in} compressor (K)	320
P_{in} compressor (MPa)	3.274
P_{out} compressor (MPa)	12
T_{it} turbine inlet temperature (K)	1373
Maximum stream temperature (K)	1373
Minimum stream temperature (K)	300
Maximum stream pressure (MPa)	30
Minimum stream pressure (MPa)	3.27

The resolution of established modeling equations (i.e., solution) requires information that is listed in Table 3.1. The internal irreversibilities of turbomachinery (isentropic efficiency) and pressure drops are equipment data (parameters), their values depend on the machinery state of the art. In this chapter, their values are set as those in the reference literature case of Mohagheghi and Kapat (2013). The compressor inlet temperature T_{in} was specified in order to satisfy two antagonistic objectives: on one hand, a low inlet temperature reduces the amount of energy needed for compressor work and thus increases the cycle efficiency; on the other hand, working in supercritical conditions induces a compressor-inlet temperature higher than the critical temperature of pure CO_2 (T_c=304.21 K). For this reason, T_{in} was set to 320 K including a safety margin of around 15 K with respect to T_c. In a similar way, the turbine inlet temperature

T_{it} was chosen as high as possible (for maximizing the turbine power generation) taking into account the maximal temperature that the turbine materials can endure and was finally set to 1373 K. The thermal pinch in R1 is generally admitted that this parameter has to be higher than 10 K in order to guaranty the feasibility of the heat transfer between the hot and cold sides. In the present case, a reasonable value of 20 K has been considered. The heat source duty is fixed to be $\dot{Q}_{hot}$ of 200 MW, the compressor inlet pressure P_{in} was set to 3.274 MPa and its outlet pressure P_{out} was set to 12 MPa, as set in the literature case of Mohagheghi and Kapat (2013).

3.2 SEQUENTIAL MODULAR SIMULATION

For the resolution of material and energy balances at the process scale, two main approaches are usually applied: (i) the equation-oriented approach and (ii) the modular sequential approach, Westerberg et al. (1979). The first approach is based on the writing and simultaneous resolution of the equations that make up all the unit operations of the process. It is denoted equations-oriented approach. The second approach uses unit operation models in a modular way and calls them successively in a flow-dependent sequence linking the unit operations to each other. It is defined as modular sequential approach.

Although the equations-oriented approach offers great robustness for the resolution of highly interconnected systems, its resolution necessitates some good initial point, which are not usually accessible in new process design, (Dowling and Biegler, 2015; Biegler, 2010). In addition, the equations-oriented method resolution needs some specialized solution procedures (based on experience). When accurate modeling is requested (particularly in the description of thermodynamic properties), the resolution involves a large number of variables and equations and it is thus not possible to benefit from the numerical methods specific to each unit operation, Biegler (2010). That is why, researchers frequently apply linear approximation or surrogate models in order to reduce compilation difficulties and errors (Chen and Grossmann, 2017). Yet such simplification implies compromises on solution quality (i.e., rigorousness).

On the other hand, the sequential modular approach that is widely used in steady-state process simulators (e.g., Aspen Plus ™, Pro / II ™, ProSim Plus ™) offers several advantages. In those process simulators, the specific unit model equations as well as specialized procedures for their solution are already contained in corresponding software module. Thus establishing the objective and constraint functions (in terms of unit and stream variables in the flowsheet) is relatively easy. Moreover, the initialization is usually straightforward. For large-scale process synthesis, the number of global variables (to be resolved) could be several thousands for

equations-oriented approach, but less than hundreds in modular sequential case, Biegler (2010). Many of them are actually deduced (within unit operation modular based on) from equipment specification data or (within sequentially resolved based on) from results of previous modules (operation unit). Those variables are "hidden" for users and as a result, less variables are to be handled by modeler.

The entire thesis intends to deal with SC-CO_2 Brayton cycle simulation and optimization with a rigorous thermodynamic representation of CO_2 without any approximation. Our ambition is to manage a large, arbitrarily complex process synthesis problem (detailed in chapter 4), where reliable initialization are not readily achievable. The application of process simulator can meet our demands with its relatively easy initialization and relatively user-friendly variable handling. The only weak area in modular approach is when the process has many, potentially nested, recycle loops and design specifications (Barton, 2010). The defined information sequence for the modular calculations as well as problem definition need to be treated carefully to prevent intermediate failure of process units (module). For the state-of-the-art process simulator, ProSimPlus™ is known to have many user options in the modular calculation sequences,i.e., practitioners can define by themselves in which order each unit operation is calculated by means of tear stream(s). As a result, ProSimPlus™ is chosen as the process simulator used in the entire dissertation.

3.3 METHODOLOGY FOR THE DESIGN OF COMPONENTS

A methodology is proposed for a pre-design of the recuperator and turbomachineries (compressor and turbine) consisting of (i) the evaluation of the UA product of the recuperator R1, (ii) the compressor rotor diameter and the turbine rotor diameter.

3.3.1 Estimation of the UA *product* in the recuperator R1

The product of the overall heat transfer coefficient (U) and the heat exchanger area (A) is a convenient way to specify the size and performance of a heat exchanger using a single parameter. The UA coefficient can be expressed using the Log Mean Temperature Difference (LMTD) formulation as follows (Hesselgreaves, 2001):

$$UA = \frac{\dot{Q}_{R1}}{\Delta T_{ml}} = \frac{\dot{m}\,\bar{Q}_{R1}}{\Delta T_{ml}} \tag{3.10}$$

Where $\Delta T_{ml} = \frac{\Delta T_{cold} - \Delta T_{hot}}{ln(\Delta T_{cold}/\Delta T_{hot})}$ is the so-called Log Mean Temperature Difference (LMTD) expressed in K, $\Delta T_{hot} = T_{hot\,inlet} - T_{cold\,outlet}$ is the inlet hot-side and outlet cold-side fluid temperature difference (i.e., $T_{stream\ e} - T_{stream\ c}$, following notations used in Figure 3.1), $\Delta T_{cold} = T_{hot\,outlet} - T_{cold\,inlet}$ is the outlet hot-side and inlet cold-side fluid temperature difference (i.e., $T_f - T_b$, following notations used in Figure 3.1), U is the overall heat transfer coefficient, A is the heat-exchanger area, $\dot{m}$ is the mass flowrate of pure CO_2 in the recuperator (note that the same flowrate $\dot{m}$ flows in the hot and cold sides of R1), $\bar{Q}_{R1}$ is the heat per unit mass in the recuperator and $\dot{Q}_{R1}$ is the heat duty transferred from the hot side to the cold side of the heat exchanger.

As mentioned in section 3.1, the thermal pinch ΔT_{pinch} is always located at the cold-side inlet and at the hot-side outlet; this parameter has been set to 20 K. As a consequence, $\Delta T_{cold} = \Delta T_{pinch} = 20\,\mathrm{K}$.

3.3.2 Turbomachineries

In this paragraph, the methodology used for the preliminary design of one-stage turbine and compressor is described. The *similarity concept* has been considered as an efficient sizing method to estimate in a simple way, some design parameters such as rotor diameters and maximum obtainable efficiency of turbomachineries (Balje, 1962a,b).

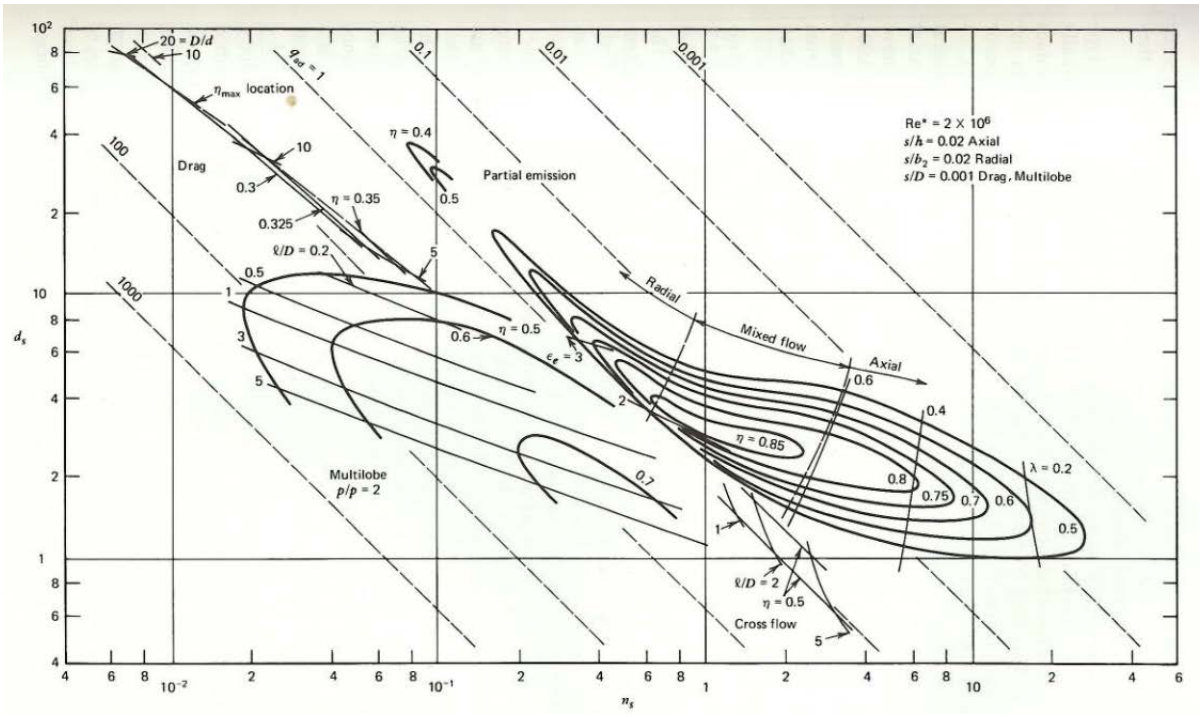

Figure 3.2: $n_s d_s$diagram for single stage compressors, extracted from Balje (1981)

The estimation of preliminary design is based on $n_s d_s$ diagrams as proposed by Balje (1981),

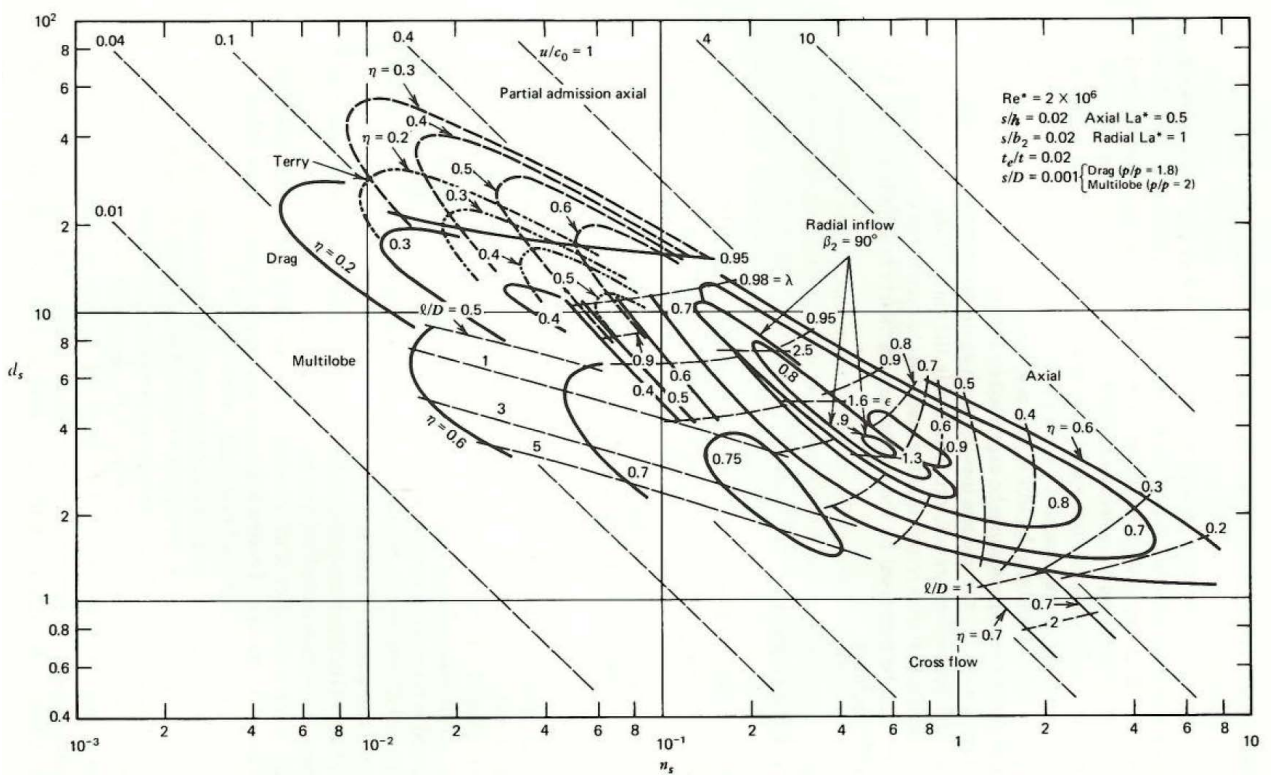

Figure 3.3: $n_s d_s$ diagram for single stage turbines or expanders, extracted from Balje (1981)

see Figure 3.2 and 3.3. Firstly, the dimensionless specific speed (n_s) needs to be calculated using the following definition, Eq.3.11:

$$n_\mathrm{s} = \frac{\omega_s \sqrt{\dot{V}}}{(g H_\mathrm{ad})^{3/4}} \tag{3.11}$$

where $\dot{V}$ is the volumetric flowrate (m^3/s) at the turbomachinery outlet (estimated from the mass flowrate $\dot{m}$ and the fluid density calculated from EoS), ω_s is the angular shaft speed (rpm), g is the gravitational constant (9.81 m/s²). H_ad is the adiabatic (and reversible) head ($\frac{\mathrm{J \cdot s^2}}{\mathrm{kg \cdot m}}$) defined by Balje (Balje, 1981) as:

$$H_{ad} = \frac{\bar{W}_{ad}}{g} = \begin{cases} \text{For a turbine: } \frac{\gamma}{\gamma-1}\frac{\bar{R}}{g}\left(\frac{T_{in}-T_{out}}{\eta}\right) \\ \text{For a compressor: } \frac{\gamma}{\gamma-1}\frac{\bar{R}}{g}\eta\left(T_{out}-T_{in}\right) \end{cases} \tag{3.12}$$

$\bar{W}_{ad}$ is the reversible work per mass unit, γ is the so-called *isentropic coefficient* defined as the ratio c_P/c_v of heat capacities (estimated from EoS), η denotes the isentropic efficiency and $\bar{R}$ is the gas constant per unit mass (i.e., gas constant divided by molecular weight $\mathrm{J/kg/K}$). T_{in} and T_{out} are the inlet and outlet temperatures of the turbomachinery returned by process simulation.

In our framework, given the size of turbomachinery, the maximum shaft speed for both turbine and compressor is assumed as $\omega_s = 7200\,\mathrm{rpm}$, as explained in (Fleming et al., 2013).

Then, by reading the corresponding $n_s d_s$ diagrams, the dimensionless specific diameter (d_s) is deducted. The preliminary estimation of rotor diameter D is then calculated by the d_s definition:

$$d_\mathrm{s} = \frac{D(gH_\mathrm{ad})^{1/4}}{\sqrt{\dot{V}}} \tag{3.13}$$

where D is the rotor diameter (m). The quantity d_s can be estimated with a (n_s-d_s) chart (Balje, 1981). The rotor diameter is then deduced from Eq.3.13.

Note that this method has been applied by the KAIST (Korea Advanced Institute of Science and Technology) institute to predesign turbomachineries involved in a SC-CO_2 Brayton cycle (Lee et al., 2012). In a similar way, it has been also used by the GE company for a base design of the main compressor and recompressor of SC-CO_2 Brayton cycles (Bidkar et al., 2016).

3.3.3 Sensitivity analysis

For each of the 6 candidate EoS described in previous section, a sensitivity analysis is performed by varying the compressor inlet (P_a) and outlet (P_b) pressures of the RC Brayton cycle.

The first step consists of screening the compressor inlet pressure when the compressor outlet pressure is fixed at a given value. Then the compressor outlet pressure is changed and step 1 is repeated. A hundred of different compressor outlet pressures were considered ranging between 10 and 24 MPa. This screening procedure permitted to determine the optimal values of P_a, denoted as $(P_a)_{opt}$, which maximize the cycle efficiency for a discrete set of P_b values. In section 3.4.3, the sensitivity results are illustrated in the form of optimal compressor ratios which are defined as $P_b/\,(P_a)_{opt}$.

3.4 Results and discussions

3.4.1 Process simulation results : influence of the thermodynamic model choice on cycle efficiency and other cycle performance indices

Before going into the influence of EoS on process performance, author would like to mention that no deviation (<0.1%) has been observed on ProSimPlus™ RC process simulation result in comparison to the literature results by Mohagheghi and Kapat (2013), who have also applied the SW EoS. This result indicates that the chosen simulator can perform steadily rigorous process simulation and property prediction, Figure 3.4.

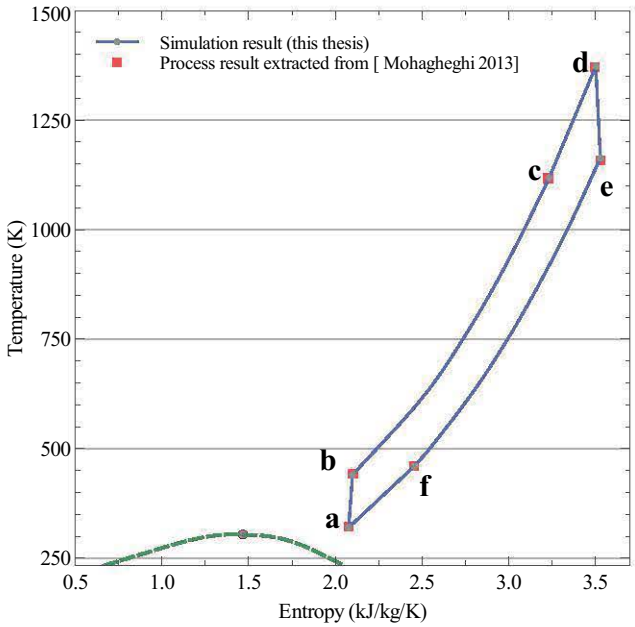

Figure 3.4: Simulation result of base-case SC-CO_2 Recuperated Brayton Cycle: Temperature-entropy diagram of process simulation as well as literature simulation of Mohagheghi and Kapat (2013).

Table 3.2 shows that the results of the process simulations performed for each of the 6 EoS, previously described. The main performance indices of the RC are provided (and in particular, the cycle thermal efficiency). It is recalled that the SW EoS has been identified as the reference model for near-critical and supercritical CO_2 on the basis of its capacity to reproduce physico-chemical properties of interest for the RC process. For the SW reference EoS, the cycle performance indices are explicitly shown; for the 5 remaining EoS (SRK, PR, PR-BM, LKP, BWRS), results are given in the form of relative deviations with respect to the values predicted by the reference model (SW EoS).

It can be observed that the mean relative deviation between the five EoS and the reference SW EoS is smaller than 2% in terms of thermal cycle efficiency. Similar results are observed for the heat duty exchanged between the hot and cold sides of the recuperator ($\dot{Q}_{R1}$), the turbine and compressor power works ($\dot{W}_{turbine}$ and $\dot{W}_{compressor}$). For all these properties, it can thus be concluded that the influence of the EoS choice is rather limited. However, depending on the EoS considered, amplified deviations ranging between 1% to 13% can be noticed on the hot terminal temperature difference in R1 ($\Delta T_{hot} = T_{hot\,inlet} - T_{cold\,outlet}$).

3.4.2 Influence of the thermodynamic model choice on component design

Table 3.2: RC performance indices: the process variables were specified as indicated in Table 3.1. The performance indices are explicitly provided for the reference EoS (SW). For the 5 other EoS, relative deviations with respect to the reference EoS are given.

		PR	PR-BM	SRK	LKP	BWRS
	SW (ref EoS)	(properties expressed in terms of relative deviations with respect to the SW EoS)				
RC cycle efficiency	0.557	-0.6%	-1.1%	-0.9%	-0.3%	-0.2%
Cycle net power $\dot{W}_{net}$	111 MW	-0.6%	-1.1%	-0.9%	-0.3%	-0.2%
ΔT_{hot}	44.8 K	+8.3%	+12.6%	+8.4%	+4.0%	+1.6%
$\dot{Q}_{R1}$	499 MW	-0.9%	-1.1%	-0.3%	-0.9%	-0.2%
Total mass flowrate $\dot{m}$	603 kg/s	-0.1%	-0.1%	-0.5%	-0.8%	-0.1%
$\dot{Q}_{heat\,sink}$	88.5 MW	+0.7%	+1.4%	+1.1%	+0.4%	+0.2%
Turbine Power $\dot{W}_{turbine}$	164 MW	-0.9%	-1.1%	-0.1%	-0.4%	-0.3%
Compressor power $\dot{W}_{compressor}$	52.8 MW	-1.6%	-1.1%	+1.5%	-0.5%	-0.7%

a) Recuperator: product UA In addition to the information already contained in Table 3.2 ($\dot{Q}_{R1}$, ΔT_{hot}, $\dot{m}$), Table 3.3 reports deviations observed on other properties characterizing R1 (ΔT_{ml}, $\bar{Q}_{R1}$) between the 5 EoS (PR, SRK, PR-BM, LKP and BWRS) and the reference EoS (SW). The relative deviation on coefficient UA is eventually indicated as well as the uncertainty ($\frac{\delta(UA)}{UA}$) estimated from Eq. 3.14:

To evaluate how the estimation of the UA coefficient is affected by the EoS choice, a propagation of uncertainty formula is used to relate the uncertainties on process variables and UA coefficient:

$$\delta(UA) = \sqrt{\left[\frac{\dot{m}}{\Delta T_{ml}}\delta(\bar{Q}_{R1})\right]^2 + \left[\frac{\dot{m}\,\bar{Q}_{R1}}{(\Delta T_{ml})^2}\delta(\Delta T_{ml})\right]^2 + \left[\frac{\bar{Q}_{R1}}{\Delta T_{ml}}\delta(\dot{m})\right]^2} \tag{3.14}$$

Where $\bar{Q}_{R1}$, ΔT_{ml} and $\dot{m}$ are estimated from the simulation of the RC for a given EoS, $\delta(\bar{Q}_{R1})$, $\delta(\Delta T_{ml})$ and $\delta(\dot{m})$ are considered as process variable uncertainties and are estimated as the difference between a given EoS and the reference SW EoS. The relative deviation on UA defined as $\frac{UA_{\mathrm{EoS}} - UA_{\mathrm{SW}}}{UA_{\mathrm{SW}}}$ is also used to discuss the results (see section 3.4.2).

Compared with the significant deviation observed on the hot pinch temperature, the deviation on the log mean temperature difference is rather low. Both the uncertainty and the relative deviation on UA reveal the importance of the EoS choice on the design of R1. Note that as expected, both criteria (uncertainty and relative deviation) lead to similar values. The deviations and uncertainties on UA are around 5% for most of EoS (except the BWRS EoS which is in better agreement with the SW EoS) and result from the combination of several factors:

Table 3.3: Influence of the EoS choice on recuperator (R1) key design features

EoS	SW (ref)	PR	PR-BM	SRK	LKP	BWRS
$\frac{(\dot{Q}_{R1})_{\text{EoS}}-(\dot{Q}_{R1})_{\text{SW}}}{(\dot{Q}_{R1})_{\text{SW}}}$ (%)	0	-0.9	-1.1	-0.3	-0.9	-0.2
$\frac{(\Delta T_{hot})_{\text{EoS}}-(\Delta T_{hot})_{\text{SW}}}{(\Delta T_{hot})_{\text{SW}}}$ (%)	0	+8.3	+12.6	+8.4	+4.0	+1.5
$\frac{(\Delta T_{ml})_{\text{EoS}}-(\Delta T_{ml})_{\text{SW}}}{(\Delta T_{ml})_{\text{SW}}}$ (%)	0	+4.6	+7.0	+4.7	+2.3	+0.9
$\frac{\dot{m}_{\text{EoS}}-\dot{m}_{\text{SW}}}{\dot{m}_{\text{SW}}}$ (%)	0	-0.1	-0.1	-0.5	-0.8	-0.1
$\frac{\bar{Q}_{R1,\text{EoS}}-\bar{Q}_{R1,\text{SW}}}{\bar{Q}_{R1,\text{SW}}}$ (%)	0	-0.8	-1.0	0.2	-0.1	-0.1
$\frac{(\text{UA})_{\text{EoS}}-(\text{UA})_{\text{SW}}}{(\text{UA})_{\text{SW}}}$ (%)	0	-4.5	-6.7	-5.0	-2.9	-1.0
$\frac{\delta(UA)}{UA}$ (%) (Eq. 3.14)	0	5.3	7.6	5.3	3.1	1.1

an overestimation of ΔT_{ml} , an underestimation of $\dot{m}$ and an underestimation of $\bar{Q}_{R1}$. As a consequence, a deviation of around 5% on the prediction of the heat exchange area will lead to a deviation on material mass. It this case, one can conclude that the EoS choice influences the sizing of the recuperator R1.

Tables 3.4 and 3.5 compare turbomachinery properties estimated from the 6 EoS considered.

In order to quantify how an EoS choice may impact turbomachinery design, the relative deviation $\frac{D_{\text{EoS}}-D_{\text{SW}}}{D_{\text{SW}}}$ between the SW EoS (reference EoS) and the five other EoS is defined.

The properties reported in these tables are: the deviations on mechanical power (for the turbine and compressor, respectively), the dimensionless parameters (n_s, d_s), the turbomachinery rotor diameter (D) and the relative deviation on rotor diameter ($\frac{D_{\text{EoS}}-D_{\text{SW}}}{D_{\text{SW}}}$).

Table 3.4: Influence of EoS choice on key design features of the turbine

	SW(ref)	PR	PR-BM	SRK	LKP	BWRS
$\frac{(\dot{W}_{turbine})_{\text{EoS}}-(\dot{W}_{turbine})_{\text{SW}}}{(\dot{W}_{turbine})_{\text{SW}}}$ (%)	0	-0.9%	-1.1%	-0.1%	-0.4%	-0.3%
n_s (dimensionless)	0.3773	0.3734	0.3721	0.3753	0.3768	0.3768
d_s (dimensionless)	5.410	5.567	5.615	5.491	5.431	5.430
$D\,(m)$	1.469	1.502	1.513	1.493	1.471	1.472
$\frac{D_{\text{EoS}}-D_{\text{SW}}}{D_{\text{SW}}}$ (%)	0	+2.3%	+3.0%	+1.6%	+0.2%	+0.2%

In Table 3.4, most of EoS tend to overestimate turbine diameters in comparison with the reference model (SW EoS). It can be observed that the turbine diameters calculated by the LKP and BWRS EoS are close to the ones predicted using the SW EoS (mean deviation $<$0.5%). Using the cubic EoS (PR, SRK, PR-BM), turbine diameters are overestimated of around 2% with respect to SW EoS predictions, which can be considered as reasonable.

Table 3.5: Influence of EoS choice on key design features of the compressor

	SW (ref)	PR	PR-BM	SRK	LKP	BWRS
$\frac{\left(\dot{W}_{compressor}\right)_{\mathrm{EoS}}-\left(\dot{W}_{compressor}\right)_{\mathrm{SW}}}{\left(\dot{W}_{compressor}\right)_{\mathrm{SW}}}$ (%)	0	-1.6%	-1.1%	1.5%	-0.5%	-0.7%
n_s (dimensionless)	0.4724	0.4711	0.4673	0.4765	0.4837	0.4774
d_s (dimensionless)	5.098	5.086	4.618	4.852	4.641	4.876
$D\,(m)$	0.926	0.915	0.828	0.886	0.847	0.887
$\frac{D_{\mathrm{EoS}}-D_{\mathrm{SW}}}{D_{\mathrm{SW}}}$ (%)	0	-1.2%	-10.6%	-4.3%	-8.5%	-4.2%

Unlike the turbine diameter, the compressor diameter is much more impacted by the EoS choice. A relative deviation around 10% is observed when the PR-BM and LKP EoS are applied. Among the 5 EoS compared to the SW EoS, the PR EoS exhibits the smallest deviations on the rotor diameter.

Finally, it is observed that the thermodynamic model choice has more influence on compressor sizing (Table 3.5) than on turbine sizing. This is certainly due to the fact that the compressor operates near the CO_2 critical point where most of EoS exhibit high deviations on physico-chemical property prediction. In particular, the ability of the EoS to reproduce accurately heat-capacity data in the near-critical region is a key issue to well estimate compressor rotor diameter (since heat capacity is involved in the rotor diameter calculations through the isentropic coefficient). To conclude, the EoS choice influences notably the compressor rotor sizing and consequently, the EoS choice could have non-negligible repercussions on process economic evaluation.

3.4.3 Sensibility analysis

b) Turbomachinery sizing Figure 3.5 represents the result of the aforementioned sensitivity procedures: the cycle efficiency is plotted as a function of the optimal compressor ratio: $P_b/\left(P_a\right)_{opt}$. For each EoS, a monotonically decreasing straight line is observed indicating that the maximal cycle efficiency is systematically obtained at the lowest value of the optimal compressor ratio for the given fixed constraints. In other words, the lower P_b is and the higher the optimal cycle efficiency is. This counter-intuitive result should be however qualified. In the present study, only energetic aspects are addressed. Economic limitations are not taken into account explaining why the optimal inlet compressor pressure seems to tend to zero. The incorporation of economic constraints (e.g., on the mass flowrate flowing into the cycle components) would bound the range of acceptable P_b values.

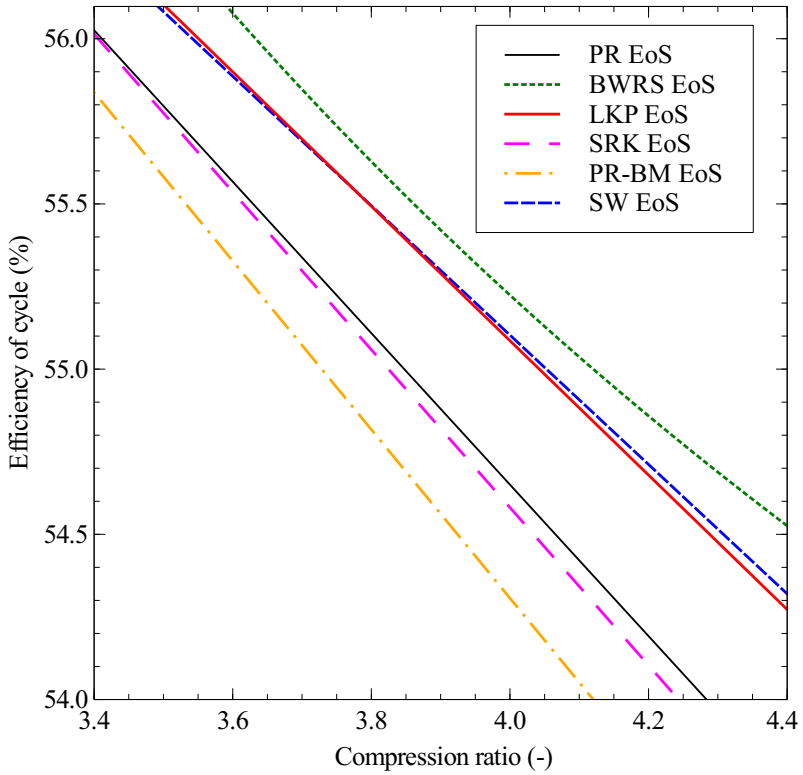

Figure 3.5: Cycle efficiency versus optimal compression ratio: $P_b/\left(P_a\right)_{opt}$ calculated from 6 EoS.

Regarding the result comparison for the 6 considered EoS, important discrepancy can be observed between the various models. While the LKP and SW EoS lead to similar predictions, the other four EoS (PR, BWRS, SRK and PR-BM EoS) exhibit more significant deviations.

- For a given efficiency value (e.g., 55%-pts), the required optimal compressor ratio predicted from different EoS varies from 3.7 to 4.1 (the reference SW EoS predicts 4.0). The mean deviation between the PR-BM EoS and the SW EoS reaches up to 10%.

- Meanwhile, for a fixed compression ratio (e.g., 4), the achievable cycle efficiency for the PR-BM EoS is no less than 1%-pts lower than the one predicted by the SW reference EoS.

Even though the deviation in RC cycle performance prediction is limited (from an energetic point of view), these differences observed above are not negligible from a “component design” (and thus economic) point of view. Moreover, acknowledgment of this influence is essential for the future superstructure optimization as well as techno-economic optimizations. With this comparison and confirmation, future assessments will not generate misleading results.

To sum up, on the modeling simulation results and the component-sizing of a specific SC-CO_2 Brayton cycle, this chapter highlights the impact of the selected EoS. For this highly recuperative simple cycle, the influence of the EoS choice is limited, which conforms with the results of Mecheri and Le Moullec (2015). However, from a component-sizing point of view, it has been found that certain deviations can be considered as high, leading to economic issues due to over or underestimation of equipment costs. For instance, a deviation of around 10% can be observed on the UA coefficient of the recuperator R1 depending on the EoS choice. This entails a 10% deviation on the estimation of the material mass required for R1. In a similar way, the impact of EoS on turbomachinery seems to be also significant. For example, the compressor rotor diameter predicted using the PR-BM EoS is 10% different from the one calculated using the SW EoS.

The section about the sensibility analysis shows that some optimal solutions can be found by manually screening the main variables of the process. Indeed, this method enables to assess global trends concerning the cycle behavior and to obtain a rather good set of variable values that enable to achieve high cycle performances. However, this methods is not self-sufficient since it does not take into account all the process constraints.

For example, the previous sensibility analysis shows that higher cycle efficiency seems to be achievable if the compression ratio is lower than 3.7, meaning that the minimal compression inlet pressure in lower than 3.27 MPa which is already the pressure lower bound of the study. In other words, the highest theoretical efficiency showed in the last figure higher than 55.7%-pts is infeasible (impossible/non-realistic), since the constraint on the lower pressure bound is violated. Yet this situation is unavoidable during the screening sensitivity procedure. In this context, the only way of finding the optimal solution by respecting given constraints is to perform a rigorous and well-defined optimization (with objective function, constraints) of the global process, as described in the following chapters.

CHAPTER 4

Superstructure optimization of SC-CO_2 Brayton cycle

One of the objectives of this thesis is to find the process configuration (process flowsheet) and its associated parameters that has the highest efficiency. A manual approach would be to perform a parametric optimization of each potential configuration of SC-CO_2 Brayton and compare their optimal efficiency, as discussed in Chapter "Introduction". On the other hand, a systematic way would be bring out **process synthesis** study, where generation of alternatives for system configurations and the selections of the devices and key parameters are directly guided by the specified criteria.

This chapter elaborates an automatic conceptual synthesis of SC-CO_2 Brayton cycle process through computer-aided **superstructure** optimization. By introducing firstly some vocabulary to understand the different approaches of process synthesis, a superstructure MINLP (Mixed Integer NonLinear Programming) optimization has been brought out for SC-CO_2 Brayton cycle. This chapter also includes results on methodology validation, and sensitivity analyses of bounds of optimized variable on superstructure optimization.

4.1 PROCESS SYNTHESIS

The term "Process Synthesis" is introduced since the late 1960's. Floudas (1998) has defined the **process synthesis** as to develop systematically process flowsheet(s) that transform the available raw material (input) into the desired products (output) and which meet the specified performance criteria (e.g. minimum cost). Its predetermined goal may also be minimizing environmental impact, minimizing energy consumption or maximizing process yield. Consequently, the application of process synthesis can offer both new directions and opportunities in meeting the challenges of sustainable development and productivity (Chen and Grossmann, 2017).

Process synthesis in chemical and energy fields has been upgraded significantly in the

last thirty years thanks to the progress made in mathematical programming and artificial intelligence . From 1950 til now, researches (both academic and industrial) on process synthesis continue to make progresses in many application areas as illustrated in Figure 4.1. While more attention has already been paid on heat exchanger systems and separation process, taking up 55% of actual papers on process synthesis, the General Flowsheet (entire system synthesis) design area seems to be rather steady and muted between 2000 and 2013 although the idea has been brought out in the 50's, (Grossmann and Daichendt, 1996; Chen et al., 2015).

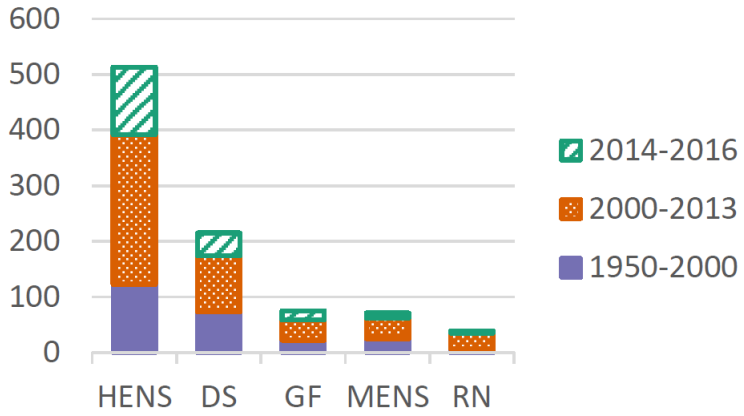

Figure 4.1: Process synthesis contributions from traditional areas of Heat Exchange Network Synthesis (HENS), Distillation Sequences (DS), General Flowsheets (GF), Mass Exchange Network Synthesis (MENS), and Reactor Networks (RN), statistic on 1270 process synthesis papers on Web of Science. Extracted from Chen and Grossmann (2017)

Three major lines of attack for process synthesis approaches have been classified by Floudas (1998) and Grossmann (1990): (a) the heuristic approach which relies on intuition and engineering knowledge, (b) the physical insight approach which relies on exploiting basic physical principles, (c) the optimization approach which relies on the use of mathematical programming techniques.

The first two methods are based on engineering experience and physical insight. Both rules-of-thumb and thermodynamic analysis (e.g. pinch analysis or entropy generation minimization) can be applied to quickly find some better solutions. While they can be very quickly in reducing the combinatorial problem, it is difficult to obtain a comprehensive and overall solution (especially for capital cost minimization). Hence those approaches only provide guidelines to improve the process configurations, (Linnhoff and Flower, 1978; Floudas, 1998; Grossmann, 1985).

On the other hand, the main idea of the last approach (c) is to formulate the synthesis

of a flowsheet as an optimization problem, i.e., **optimization-based process synthesis**. This methodology consists of having an explicit or implicit representation of a specified set of structure including the one meeting the target criterion (i.e., objective function). The specified set of process topology is denoted as **superstructure** and its explicit or implicit representation corresponds to **modeling of superstructure**. Its main advantage lies in providing a more systematic framework for handling a variety of process-synthesis problems, which gives a global view of different features. Though the steady state and dynamic behavior of many chemical and energy systems can nowadays be described in detail, the ability to robustly solve large, industrially-relevant optimization problems remains limited (Chen and Grossmann, 2017).

The difficulties lie mainly in the non-convexity and non-linearity of process synthesis problems. It has been noted in the study of Quesada and Grossmann (1995), that even simple flowsheet structures such as mixers and splitters can give rise to non-convex nonlinear expressions in the form of mass balances (in case of multi-component stream). Incorporation of process thermodynamics and transport phenomena further complicate the global optimum research though their precision are know to influence directly the results of process synthesis. Those aforementioned issues may partially explain the muted statistic on General Flowsheets area as such systems can encompass almost all of traditional area (e.g. heat exchanger network, distillation and reactor). Hence the dissemination of optimization-based process synthesis into the industrial community is still relatively low, (Barnicki and Siirola, 2004; Quaglia et al., 2015).

Forehead mentioned argument means that the ability of optimization algorithms as well as the formulation of the problem are important (Floudas, 1998; Grossmann, 1985). In addition, the detail of modeling and the computational expense need to be considered.

4.2 OPTIMIZATION-BASED PROCESS SYNTHESIS

In optimization-based process synthesis, one of the main steps is to define the flowsheet which contains all the process configuration alternatives, i.e., a superstructure. In a defined **superstructure**, the selection of the process unit as well as their interconnections are performed by discrete decision variables. On the other hand, design parameters and operating conditions are continuous decision variables in the superstructure. With the presence of both discrete and continuous variables, the optimization-based process synthesis is therefore defined as mixed integer nonlinear programming (MINLP) problem .

Discussions elaborated in previous chapter demonstrated that modular sequential process simulator is more advantageous (compared with equations-oriented approach) to be applied

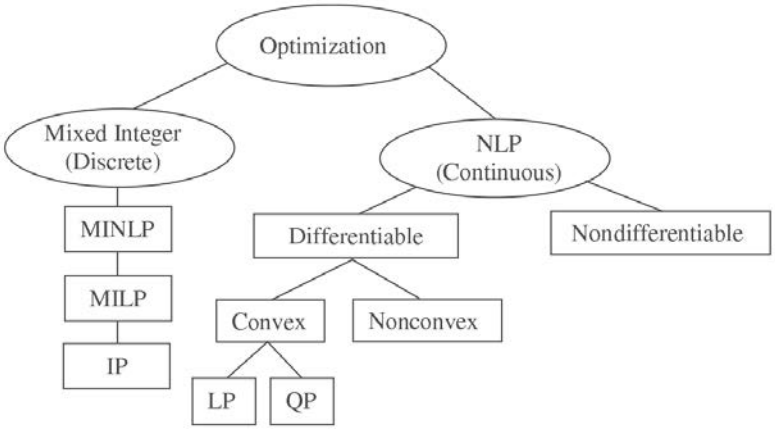

Figure 4.2: Classes of optimization problems, including Mixed Integer Non Linear Programming (MINLP), Non Linear Programming (NLP), Mixed Integer Linear Programming (MILP), Integer Programming (IP), Linear Programming (LP) and Quadratic Programming (QP). Figure extracted from Biegler (2010).

considering the closed loop and recycle nature in the SC-CO_2 Brayton cycle process. In the same concept, it has been decided to continue performing the superstructure MINLP optimization within ProSimPlus™. Such kind of optimization based on simulator results is thus denoted as *simulator-based optimization* in this thesis.

✻ Motivation of Simulator-based optimization

The idea of interfacing MINLP algorithm with simulator has been firstly brought up by Harsh et al. (1989). They interfaced an outer approximation MINLP procedure with Flowtran™ simulator. Later on, efforts have been made to apply Aspen Plus™ or Aspen Hysys™ in different kinds of optimization-based processes synthesis problem, such as distillation systems, (Bravo-Bravo et al., 2010; Leboreiro and Acevedo, 2004; Gutiérrez-Antonio and Briones-Ramírez, 2009; Caballero et al., 2005) and retrofit of chemical processes, (Diwekar et al., 1992; Gross and Roosen, 1998; Brunet et al., 2012; Chen et al., 2015). Meanwhile, Ebsilon Professional™, a process simulation software, is applied by Wang et al. (2014a) for the energy conversion system application. A recent contribution of Corbetta et al. (2016) was focused on interfacing the process simulator SimSci PRO/II™ with GAMS in order to optimize both process configuration and parameter.

Though the commercial process simulators applied in the cited studies also provide reliable and rigorous modeling environments, their calculation procedure focus on using MINLP resolution as master layer and the simulator is successively called by MINLP solver. More computational efforts are necessary since the main program of MINLP solver is responsible for

generating initial simulation point, testing the simulation convergence as well as finding the optimal solution. In such cases, the communication between process simulator and MINLP algorithms involves additional interfaces. This kind of interfaces are not universal meaning that resuming one of cited studies introduces a personalized supporting tools construction. Therefore, simulator-based optimization is still a young area where further developments are still needed to reveal the full potential of this approach.

The motivation of our simulator-based MINLP optimization study is to propose for the first time (to the best of authors's knowledge) a methodology in which the entire optimization loop is handled by the simulator and both continuous variables and discrete integer variables are optimized simultaneously, Figure 4.3. In addition, ProSimPlus™ can manage many external MINLP solver by its reversal communication module thus no supporting interface needs to be constructed. Users can furthermore use all the unit operations available in the process simulator software to configure the superstructures (graphical representation) they wish to study.

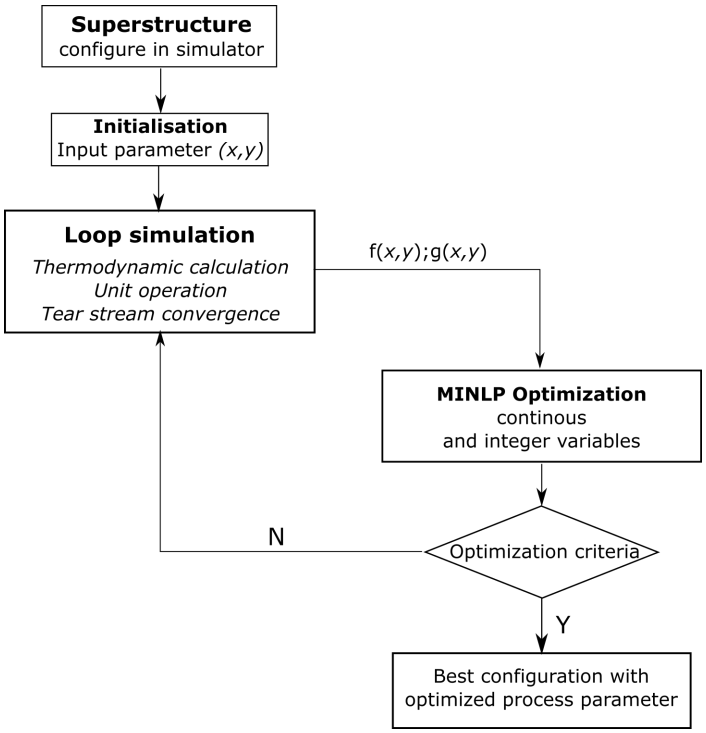

Figure 4.3: Program structure of simulator-based superstructure optimization proposed in this thesis

✻Optimization unit in ProsimPlus™

In ProsimPlus™, the optimization unit (OPTI) has predefined communication interfaces which makes it possible to select an external dynamic library (.dll) and manage the entire simulation and optimization loops.

The .dll should implement communication interfaces and is statically or dynamically linked with the chosen external algorithm. The OPTI retrieves the values of the objective function as well as the values of the equality and inequality constraints and passes them automatically to the external dynamic library. The latter makes these value available to the external algorithm, which calculates the new values of the optimization variables.

The deducted new values of optimization variables are then available to each unit operation through information streams (virtual stream in dot) exiting optimization unit. They are the new values used for the next simulation.

A customizable table of parameters, available in the graphical user interface of the optimization unit, allows to access to the parameters of the external algorithm, Figure 4.4. The figure illustrates in ProSimPlus™ a simple two reactors problem of Diwekar et al. (1992)

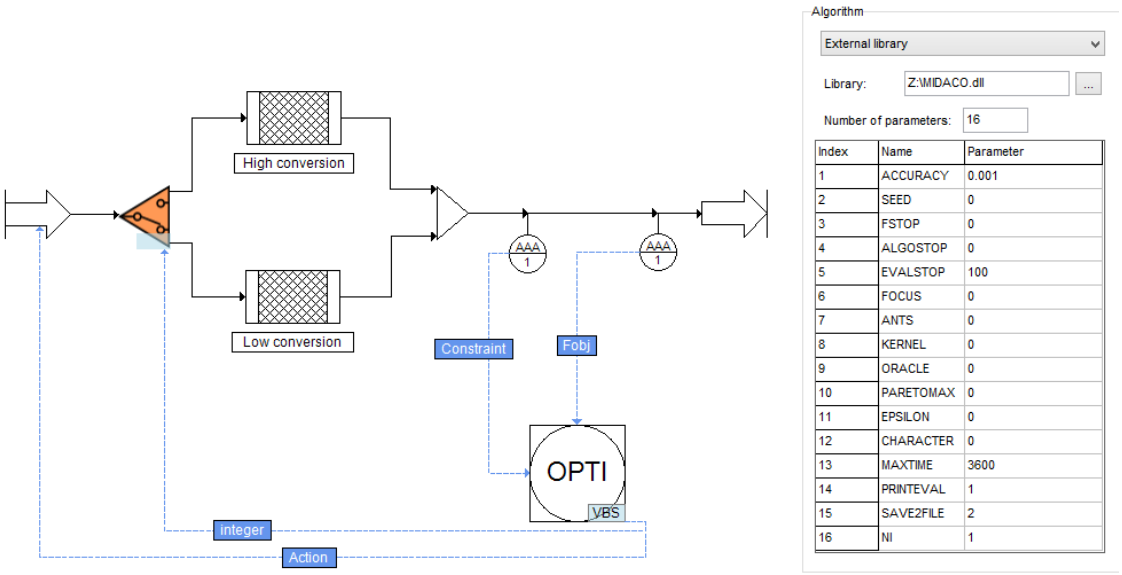

Figure 4.4: Illustration superstructure graphic representation (left) and optimization unit (right) in ProSimPlus, case of a Two Reactors Problem (blue dashed lines are information streams: 1 objective function, 1 constraint, 1 integer decision and 1 continuous variables)

✻ Algorithms for solving MINLP problem

The resolution of MINLP problem is broadly classified into deterministic and stochastic ones,

(Bussieck and Vigerske, 2014; Schlüter, 2012). MINLP problems involve nonlinear objective function and/or nonlinear constraints. Depending on convexity of MINLP problems, two categories of problems are considered: convex MINLP and nonconvex MINLP. Convex MINLP involves minimizing a convex objective function over a convex feasible region. In a non-convex MINLP, the objective function and/or the feasible region are not convex, (Trespalacios and Grossmann, 2014).

The early MINLP algorithms development are based on deterministic methods, e.g., Branch and Bound (BB) (Gupta and Ravindran, 1985), Outer Approximation (OA) (Duran and Grossmann, 1984) and Generalized Benders Decomposition (GBD) (Geoffrion, 1972). The idea is to build resolution by combining one (or several) algorithms from Linear Programming (LP), Integer Programming (IP), and Nonlinear Programming (NLP).

Branch and Bound (BB) type methods use NLP (Non Linear Programming) relaxation, i.e., NLP problems are often formulated and solved at a lower level for fixed values of the discrete variables. Higher level only manages the branching of the decision tree over the discrete search space, (Gupta and Ravindran, 1985). The OA methods and the GBD methods, on the other hand, usually perform a linear relaxation (gradient-based linearizations), transforming MINLP problem into solving MILP (Mixed Integer Linear Problem) master problem and NLP subproblem (Chen and Grossmann, 2017; Schlüter, 2012).

An earliest commercial solver that could solve MINLP problems was SCICONIC based on BB method in the mid 1970's (Forrest and Tomlin, 2007). Later on, Viswanathan and Grossmann (1990) developed DICOPT (DIscrete and Continuous OPTimizer), a general purpose algorithm for convex MINLP based on the outer approximation method of Duran and Grossmann (1984). Since then, numerous academic and commercial efforts have been made on deterministic solvers development. Some known general purpose solvers for the global MINLP solution are alphaBB (α-Branch-and-Bound) (Adjiman et al., 2000); BARON (Branch-And-Reduce Optimization Navigator) (Tawarmalani and Sahinidis., 2002), BONMIN (Basic Open-source Nonlinear Mixed Integer Programming) (Bonami et al., 2008), MISQP (Mixed Integer Sequential Quadratic Programming) (Exler et al., 2012); MILANO (Mixed-Integer Linear and Nonlinear Optimizer) (Benson, 2011), COUENNE (Convex Over and Under ENvelopes for Nonlinear Estimation) (Belotti et al., 2009), (Bussieck and Vigerske, 2014).

The above solvers can achieve global optimal results for convex problem but some of them are exclusive for nonconvex problem. In addition, state-of-the-art solvers for deterministic optimization have been highly integrated to several well-developed high-level algebraic modeling environments, e.g., GAMS, NEOS and AMPL, tailored for complex, large-scale

applications.

On the other hand, during the last decades, attempts have been made to apply stochastic algorithms, especially the nature-inspired algorithms, for example Genetic Algorithms (Cheung et al., 1997; Deb et al., 2002; Tayal et al., 1999), Particle Swarm Optimization (Kennedy and Eberhart, 1995), Tabu search (Glover, 1989) or Ant Colony Optimization (ACO) algorithms (Dorigo, 1992), Figure 4.5. Stochastic methods can solve a MINLP problem without derivative information. In that case, they do not require explicit information of the mathematical model either for the objective function or constraints, which means its application would be suitable in modular simulator (Vazquez-Castillo et al., 2009). In addition, the most significant advantage of stochastic approaches is their robustness regarding critical function properties (like non-convexity or discontinuities).

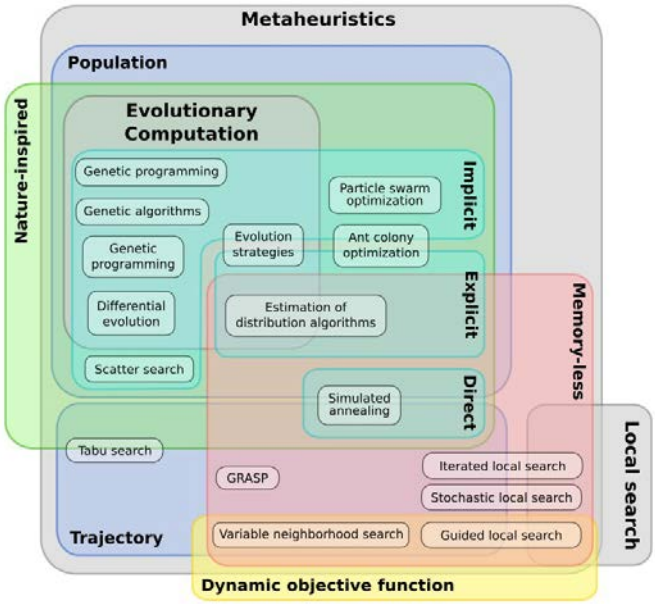

Figure 4.5: Classification of different stochastic algorithm. Extracted from Nojhan (2007)

✻ Mixed Ant Colony Optimization (MIDACO) optimizer

The basic idea of Ant Colony Optimization (ACO) proposed by Dorigo (1992) is to mimic the biological behaviour of ants randomly exploring food and trailing its path back home with a chemical pheromone when they successful find a food source. Overtime the shortest path is the path traveled frequently by ants and thus has the most concentrated pheromones, Figure 4.6.

For most of stochastic algorithms, the proof-of-convergence in general case study remains limited due to its young history. Nevertheless, Schlüter (2012) has successfully performed a

comparison of MIDACO(Mixed Integer Distributed Ant Colony Optimization) with BONMIN, COUENNE and MISQP through100 benchmark problems, Schlüter et al. (2012). The results show that MIDACO manages to find the (already) best known and sometimes even a better global solution with a promising CPU time. Moreover, in the review of Bussieck and Vigerske (2014), MIDACO has been chosen as one of state-of-the art nature-inspired stochastic solver.

In addition, as constraints handling is known as difficult part for natural inspired algorithm, Schlüter and Gerdts (2010) introduced in MIDACO an advanced penalty approach (Oracle penalty function) to transform constrained MINLP problem to unconstrained MINLP. This approach uses one parameter Ω, oracle parameter, which corresponds directly to the global optimal objective function value $\phi(x, y)$. Currently this method has also been integrated in some other academic natural inspired MINLP algorithm (Munawar et al., 2011; Gebreslassie and Diwekar, 2015; Dong et al., 2013), showing its promising constraints handling capacity.

In the context of MINLP superstructure optimization of a SC-CO_2Brayton cycle, one challenge is to solve the highly non linear non-convex problem. Meanwhile, finding a good initial starting point for the optimization problem can be another major challenge as for Brayton cycle's recycle loop and closed nature. With the reverse communication available in MIDACO, ProSimPlus™ optimization block can call this external solver without additional user effort. That is why we intend to use stochastic MIDACO in this thesis, though the theoretical analysis and industrial application of stochastic methods is still a young field, (Schlüter, 2012).

In addition, MIDACO solver can deal with multi-objective optimization, in order to include more than one criterion (objective), such as cycle efficiency, cost or environmental impact. In this chapter only mono-objective optimization is illustrated while in the next chapter more details will be shown on a multi-objective optimization.

4.3 OPTIMIZATION-BASED PROCESS SYNTHESIS PROCEDURE

4.3.1 Modeling of the superstructure

Thermodynamic and unit operation modeling

The modeling of a superstructure can be divided into three steps before the mathematical formulation. The first step consists of the modeling of the thermodynamic behavior of CO_2 and the modeling of all the unit operations. In the third chapter, it was demonstrated that the choice of the equation of state (EoS) had an impact not only on thermodynamic property prediction but also consequently on process simulation, sizing, and optimization. As explained in the

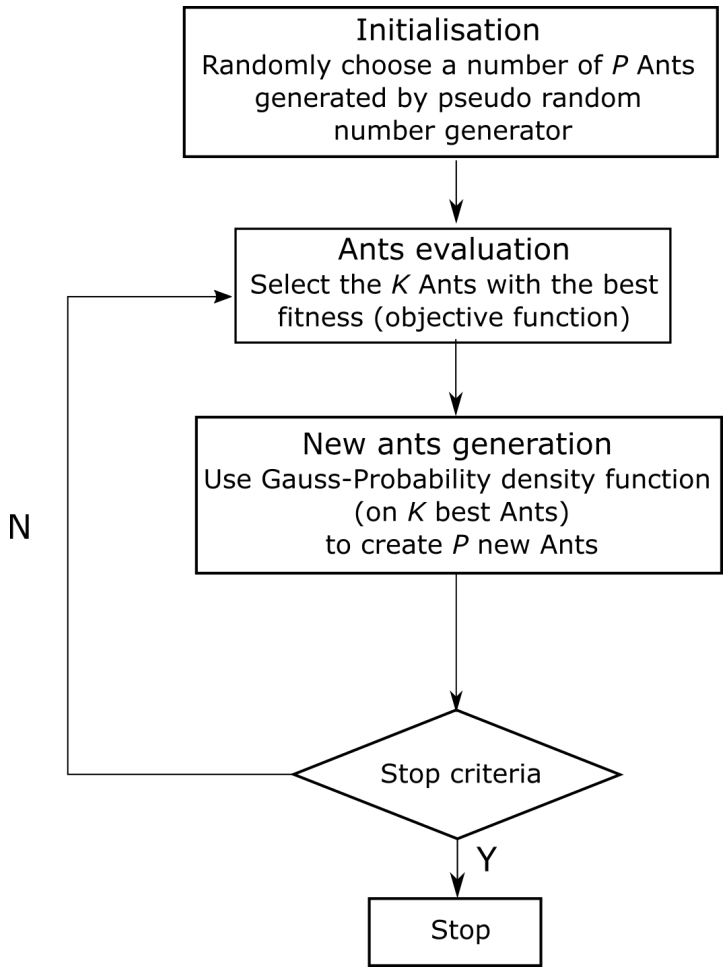

Figure 4.6: Ant Colony Optimization procedure. P stands for Population size, K stands for Kernel size in multi-kernel Gauss PDF's, Schlüter (2012)

previous section, application of commercial modular sequential simulator benefits directly from the rigorous modeling environment of thermodynamic properties representation (SC-CO_2) as well as the basic mass, energy balances and certain featured equations associated with unit operations characteristic variables.

Thus, for the present study, the Span-Wagner EoS has been still chosen in ProSimPlus™ simulator environment as thermodynamic model for the CO_2 property prediction while unit operations modeling is guaranteed by the process simulator.

Connectivity modeling

Superstructure is a superior process flowsheet which combines as many promising process configuration as possible (Ahadi-Oskui et al., 2010). According to this definition, connections between some unit operations must be arranged in order to reproduce the largest possible set of different flowsheets (including the classical ones), and to do so, it must be possible to switch

the paths and equipment encompassed. That is why flow switcher is introduced to switch on or off any of these connections.

In this thesis, flow switchers make it possible to virtually remove unit operations by simply setting their flow rate to zero. Flow switcher is more or less similar to a typical flow split, instead of having continuous separation ratio, a multipath (2 or more) decision switcher makes it possible to select a preferential path. In this chapter, only dual-paths switchers are used (while triple-paths switchers are used in the next chapter).

Principal flow switcher is illustrated in Figure 4.7. The switcher level y_i is defined as an integer decision variable as following:

$$S_1 = S_3,\ if\ y_i = 1 \tag{4.1}$$

$$S_1 = S_3,\ if\ y_i = 2 \tag{4.2}$$

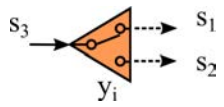

Figure 4.7: Decision switcher S_k denotes the molar mass or mass flowrate of stream k; y_i is the integer decision variable.

Note that in process simulators, the absolute zero flow at unit operation inlet is not permitted. As a consequence, the "zero flow" in the present study is set as a pseudo zero flow with a molar flowrate equals to 10^{-15} mol/s.

Superstructure generation

The last step before optimization is to generate the superstructure . According to Quaglia et al. (2015), the development of superstructure integrates alternative collection approach, insight-based synthesis approach and combinatorial synthesis approach. The first two methods consist in listing the known processing Brayton cycle configurations based on previous experiences (review listed in Chapter "introduction") and using engineering insights to contain new solutions and exclude infeasible or non-conventional alternatives. The combination of different alternatives following switcher positions permits to enlarge the searching space of alternative flowsheet and thus is likely to include innovative design solutions.

As an example in this chapter, a first superstructure -denoted SS1- is used (see Figure 4.8), is composed of two different blocks: the heat source & electricity production block and the

heat integration block. From right to left, the first logical switcher *SW1* alternate between a Brayton cycle with and without reheating. The second and third switchers *SW2 SW3* determine the existence of an extra heat recuperator meanwhile they select the flow that will be heated in this recuperator. This "simple" superstructure (2^3=8 structural alternatives) is used here to validate the superstructure optimization approach.

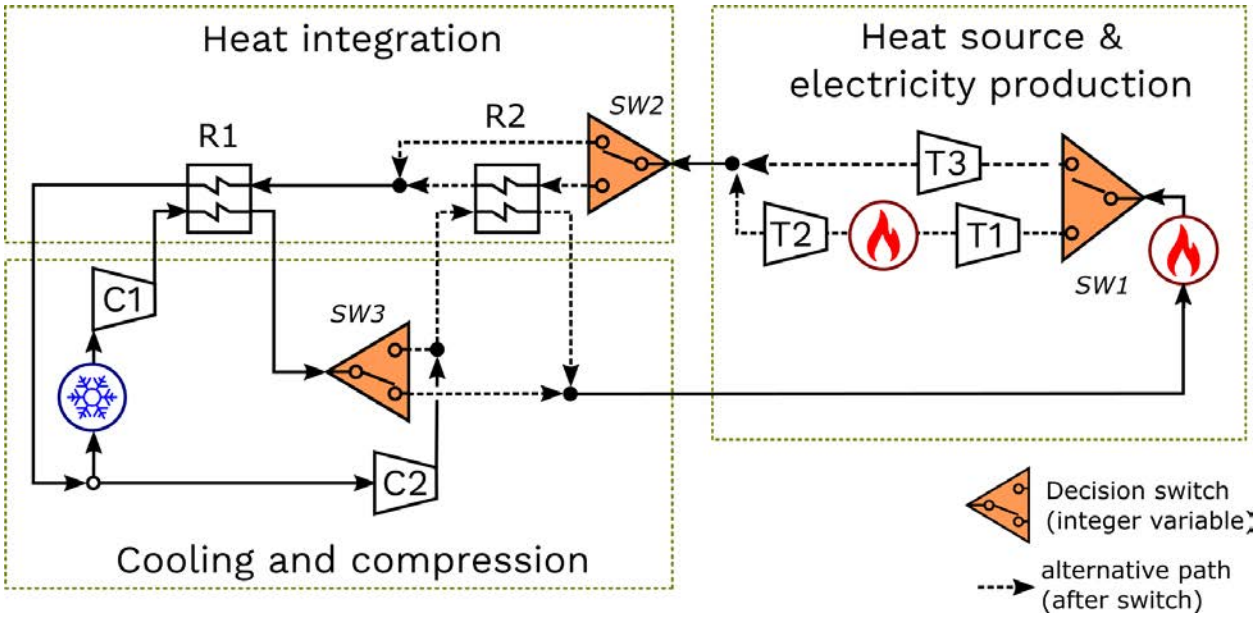

Figure 4.8: Example of superstructure for SC-CO_2 Brayton cycle SS1 (2^3=8 structural alternatives)

4.3.2 General mathematical problem formulation

Once generated a large set of alternative flowsheets by means of a superstructure, the mathematical optimization problem can be properly defined including the definition of an objective function (Quaglia et al., 2015). Non-convex functions appear because of the rigorousness of unit operations and thermodynamic model used in this thesis, thus increasing the risk of non-convergence. The closed and recycled nature of Brayton cycles is another difficulty which increases the risk of failure of the process simulation and/or the structure optimization. Eventually, the presence of flow switchers induces discontinuous objective functions entailing additional convergence difficulties. As a consequence, some enforcement strategy is proposed in this part to master the difficult convergence cases.

Enforcement strategy

The success of an optimization algorithm is known to be strongly influenced by the problem formulation and the selection of variables, even when using a stochastic optimizer. It is important to formulate the problem in a way that ensures fast and easy convergences of the simulation and that lead to all process variables including calculated ones ranging between their lower and upper bounds (Corbetta et al., 2016). In this study, in order to improve the simulation and optimization convergence, four enforcement have been carried out: a) feasible path b) fictive unit c) separation of multi-streams operations and d) process parameter specification.

a) Feasible path

As mentioned, a sequential modular simulation, tear stream(s) is chosen in this work in order to handle a process with existence of recycle loop. A tear stream is defined as any stream (not necessarily the recycle stream) that "break open" the calculation loops during the simulation by considering the so-called tear variables (temperature, flowrate, pressure), (Biegler, 2010).

Simulator such as ProSimPlus™ will update tear variables (temperature, pressure and mass flowrate) to solve the tear equations (equations which serve to break every calculation loop) until two consecutive iterations lead to tear equation resolution within the specified tolerance. The convergence of simulation (i.e., feasibility) refers to the meet of criterion on tear stream equations. In ProSimPlus™, the tear variables can also be handled by the phase simulation, denoted *feasible path*. Tear stream(s) are proposed to ProSimPlus™ users following an automatic procedure, (Sargent and Westerberg, 1964; Tarjan, 1972; Motard and Westerberg, 1981; Upadhye and Grens, 1975). In SS1, the tear stream is chosen as the cold stream leaving from recuperator R2 and entering in the boiler.

However, it is also possible to consider the tear streams variables as a part of the variables to be optimized, by physically breaking the tear streams. This method is denoted *infeasible path*. In such case, tear equations become equality constraints to be solved and tear variables are to be optimized during optimization.

The application of feasible path then helps to reduce the number of optimized variables and reducing the computing effort. In this superstructure optimization, the feasible path approach has been chosen. A comparison between feasible and infeasible path will be brought out in Section 4.4.1.

b) Fictive unit

Another ingenuity in the formulation step is to add a fictive unit after each turbine in the Brayton

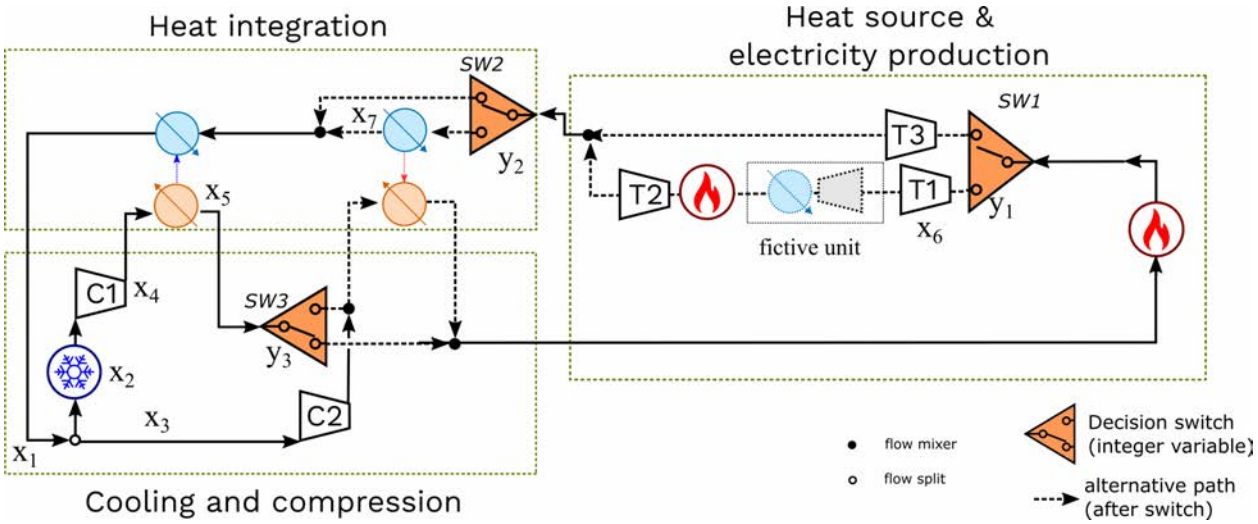

Figure 4.9: Superstructure of SC-CO_2 Brayton cycle after feasibility modification (2^3=8 structural alternatives)

cycle. An optimizer searching for the ratio of turbine (P_{in}/P_{out}) does not see the infeasible engineering scenario leading to obtain an outlet pressure lower than main compressor inlet pressure (ratio<1). An inequality constraint could indeed reduce the frequency of this scenario, yet adding constraints can increase the non-convexity character of the objective function since both mentioned pressures are optimized variables. In this case, a fictive compressor and a fictive cooler are introduced (Figure 4.9) so that when the aforementioned scenario takes place, the fictive compressor will compress CO_2 to raise up the compressor outlet pressure and the fictive cooler will regulate the stream temperature to obtain the same stream temperature as before the fictive compression. The required work of the fictive compressor is then included as electricity consumption in the objective function, as detailed in Section 4.3.2. This formulation tip is not merely a simple penalty consideration but an engineer practitioner advisement.

c) Separation of multi-streams operations

The recuperators in the SC-CO_2 Brayton superstructure are counter-current heat exchangers. It is recalled that in the previous chapter, thermal pinch in a counter-current heat exchanger is defined as the minimal temperature difference between the hot and cold sides of heat exchanger. A usual counter-current heat exchanger in process simulator works with specification on inlet (both cold side and hot side) streams temperature and the pinch temperature. Another way would be specifying the quantity of exchanged heat duty, the inlet temperature of at least one stream at heat exchanger and the minimal pinch temperature. In either case, a sequential modular process simulation needs 3 specifications, though some of

them are process information given by other modules in the process. Hence, a conventional counter-current heat exchanger resolution necessitates additional iterations in an entire calculation loop .

In the present case, counter-current exchangers are treated differently by dividing the so-called recuperator by a hot-side inlet stream cooled by a simple "cold sink" and a cold-side inlet stream warmed by a "hot source", Figure 4.9. Both cold sink and hot source are simple heat exchanger. The combination of them becomes a counter-current heat exchanger by setting the sum of their quantity of heat exchanged equals to zero ($-\dot{Q}_{hot\ source} + \dot{Q}_{cold\ sink} = 0$).

This modification enables to avoid additional simulation iterations introduced by the counter-current exchanger, especially it reduces the occurrence of diverging iteration processes. The optimization itself benefits from the relaxation of counter-current exchanger, although two additional parameters (outlet streams temperatures) and four inequality constraints (minimum pinch temperatures) are added.

d) Process variable specification

Table 4.1: Values of fixed process variables, equipment data and constraints used in the superstructure SS1

Hypothesis on fixed variables and Equipment data	
T_{it} turbine inlet temperature (K)	893.15
T_{it} turbine inlet temperature after reheating (K)	893.15
CO_2 flowrate before main cooling (kg/s)	6000
ΔT_{pinch} (K)	10
Turbine isentropic efficiency	0.9
Compressor isentropic efficiency	0.89
Pressure drop in every component (% of inlet pressure)	1
Constraints	
g_1 on R1 cold end temperature difference (K)	$(\Delta T - 10) \geqq -0.5$
g_2 on R1 hot end temperature difference (K)	$(\Delta T - 10) \geqq -0.5$
g_3 on R2 hot end temperature difference (K)	$(\Delta T - 10) \geqq -0.5$
g_4 on R2 cold end temperature difference(K)	$(\Delta T - 10) \geqq -0.5$
g_5 on ratio of main compressor C1 (-)	$(P_2/P_1 - 1) \geq -0.025$

Design of the SC-CO_2 Brayton cycle depicted by SS1 requires the determination of 10 continuous and integers optimized variables, such as equipment temperature, pressure, flow switchers decision variables, as listed in Table 4.2 and showed in Figure 4.9. The bounds of variables are based on the state-of-art ultra-supercritical steam (USC-steam) Rankine cycle condition 30 MPa/893.15 K. Table 4.1 lists the modeling equipment data and assumptions such

Table 4.2: List of optimized variables and their bounds considered in SS1

Optimized continuous variables x	Bounds
P_{in} compressor (MPa)	$x_1 \in 3.3 - 10$
$T_{cooling}$(K)	$x_2 \in 304.35 - 373.15$
Flow to Recompression (%)	$x_3 \in 10^{-6} - 0.5$
P_{out} compressor (MPa)	$x_4 \in 3.3 - 30$
Ratio= P_{in} / P_{out} of turbine T1 (-)	$x_6 \in 1 - 5$
T_{R1}cold stream out (K)	$x_5 \in 304.35 - 893.15$
T_{R2} hot stream out (K)	$x_7 \in 304.35 - 893.15$
Optimized integer variables y	
SW1	$y_1 \in \{1,\ 2\}$
SW2	$y_2 \in \{1,\ 2\}$
SW3	$y_3 \in \{1,\ 2\}$

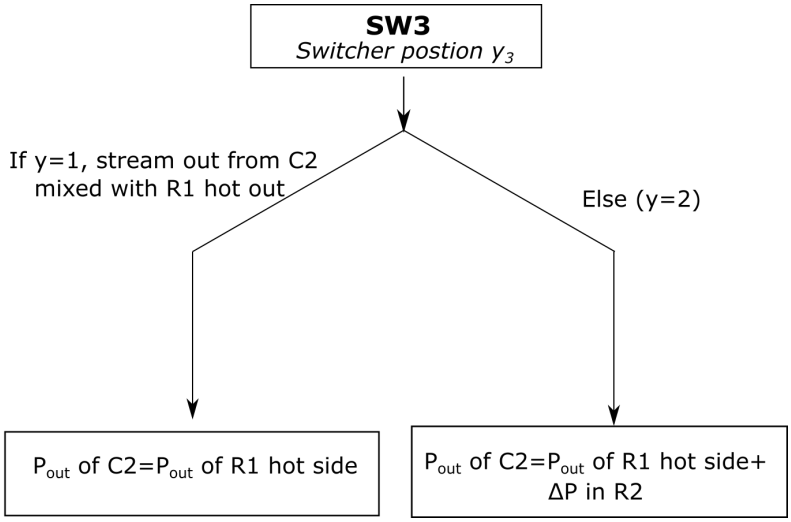

Figure 4.10: Logical rule for recompressor C2

as isentropic efficiency of turbomachinery, minimal pinch temperature and the pressure drop.

The calculated variables, on the other hand, are still considered in the problem formulation. Their existence is identified as a tip to reduce the number of optimized variables. In SS1, they are the "final turbine" (T3 or T2) outlet pressure and the compressor outlet pressure in compressor C2 (which is equal to the pressure of the other stream in the mixer). The specification of these variables necessitates logical rules since their values depends on the process layout (i.e. dependent on integer variables), illustrated respectively in Figure 4.10 and 4.11.

Such specifications can firstly avoid optimizing variables that are dependent to the other optimized variables. The research of their optimal value can easily get out of bounded as their upper and lower bound depends also on both continuous and integer variables. In the case of SS1 optimization, the aforementioned specification enables to avoid the optimization of

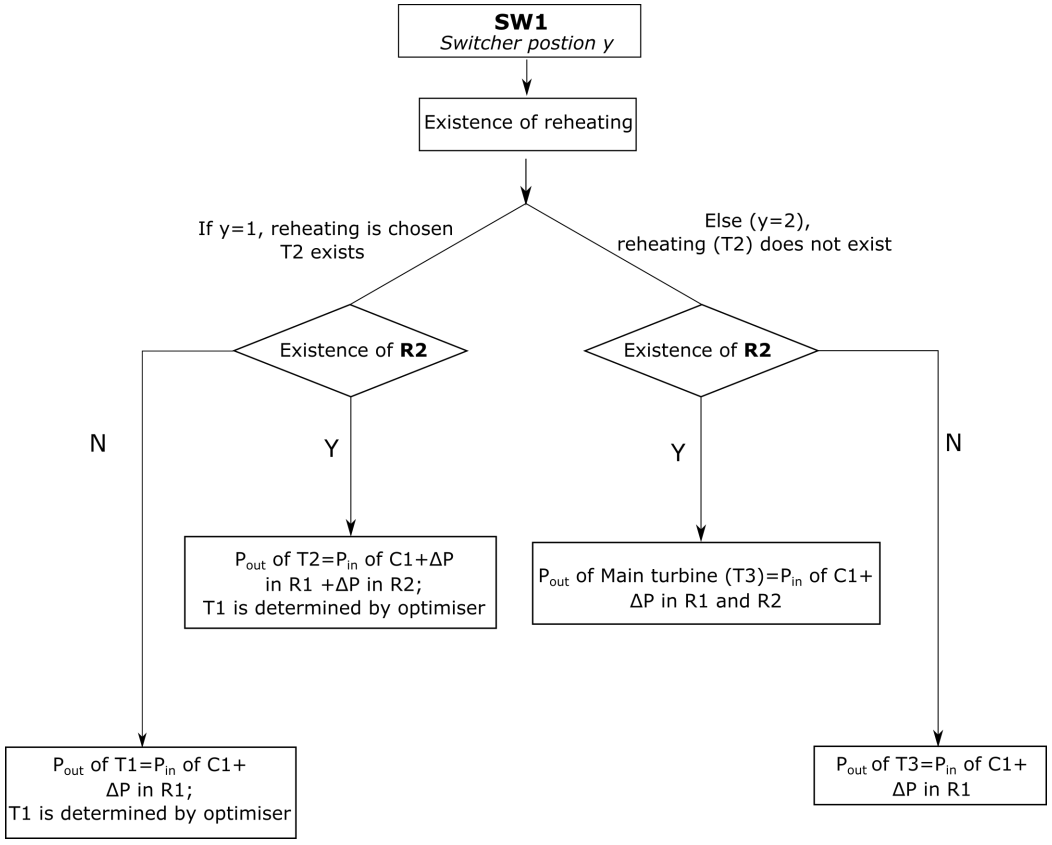

Figure 4.11: Logical rule for turbine after reheating

the "final turbine" pressure and the pressure of re-compression, leading to a reduction of the number of optimized variables (initially 10).

Objective function

Within the superstructure SS1 optimization, the cycle efficiency is seen as main indicator of the energy performance:

$$\eta_{\text{cycle}} = \dot{W}_{net} / \sum \dot{Q}_{hot} \tag{4.3}$$

The net power generated by the coupled system {turbine + compressor} (fictive unit included) is defined by the relation: $\dot{W}_{net} = \sum \dot{W}_{turbine} - \sum \dot{W}_{compressor}$ (note that all the power terms $\dot{W}$ involved in this definition are positively defined). The heat duty $\sum \dot{Q}_{hot}$ is defined by the heat source in main heating and reheating (positively defined).

Optimal design for these sequences means to have an energy system that produces electricity with an as high as possible cycle efficiency. The superstructure optimization problem is then expressed as :

$$\underset{x,y}{Min}\ \phi(x,y) = -\eta_{\text{cycle}} \qquad (x \in \mathbb{R}^{n_{con}},\ y \in \mathbb{Z}^{n_{int}}) \tag{4.4}$$

$$s.t.\ g(x) \geq 0 \tag{4.5}$$

$$x_{min} \leq x \leq x_{max} \tag{4.6}$$

$$y_{min} \leq y \leq y_{max} \tag{4.7}$$

where $g(x)$ is the vector of inequality constraints; $x = [x_1, ..., x_7]$ is continuous optimized variable vector and $y = [y_1,\ y_2,\ y_3]$ is flow switcher decision variables (optimized variables).

The three discrete variables result in 2^3=8 structural alternatives, yet 2 redundant structure are identified by author. Thus, this SS1 represents 6 distinctive process configurations of SC-CO_2 Brayton cycle.

4.4 RESULTS

4.4.1 Preliminary comparison of the feasible and the infeasible approach

In Section 4.3.2, it is mentioned that the *feasible path* is applied in our methodology for tear stream functions. However, it is possible to open the loop physically by setting tear stream parameters as optimized variables. The optimization problem is therefore different as three variables and corresponding equality constraints are added. This approach is named *infeasible path.* At each iteration optimization, the entire process loop itself is not necessarily converged since all constraints are awaited to be respected only at the end of optimization (Biegler and Cuthrell, 1985).

$$\underset{x,y}{Min}\ \phi(x,y) = -\eta_{\text{cycle}} \qquad (x \in \mathbb{R}^{n_{con}},\ y \in \mathbb{Z}^{n_{int}}) \tag{4.8}$$

$$s.t.\ g(x) \geq 0 \tag{4.9}$$

$$h(x,y) = 0 \tag{4.10}$$

$$x_{min} \leq x \leq x_{max} \tag{4.11}$$

$$y_{min} \leq y \leq y_{max} \tag{4.12}$$

where $h(x,y)$ is the equality constraints introduced by tear variables; $x = [x_1, ..., x_{10}]$ and $y = [y_1,\ y_2,\ y_3]$ are optimized variables.

Before showing the results of our optimization strategy, this preliminary comparison between feasible approach and infeasible approach has been performed to confirm the assumption on optimization robustness.

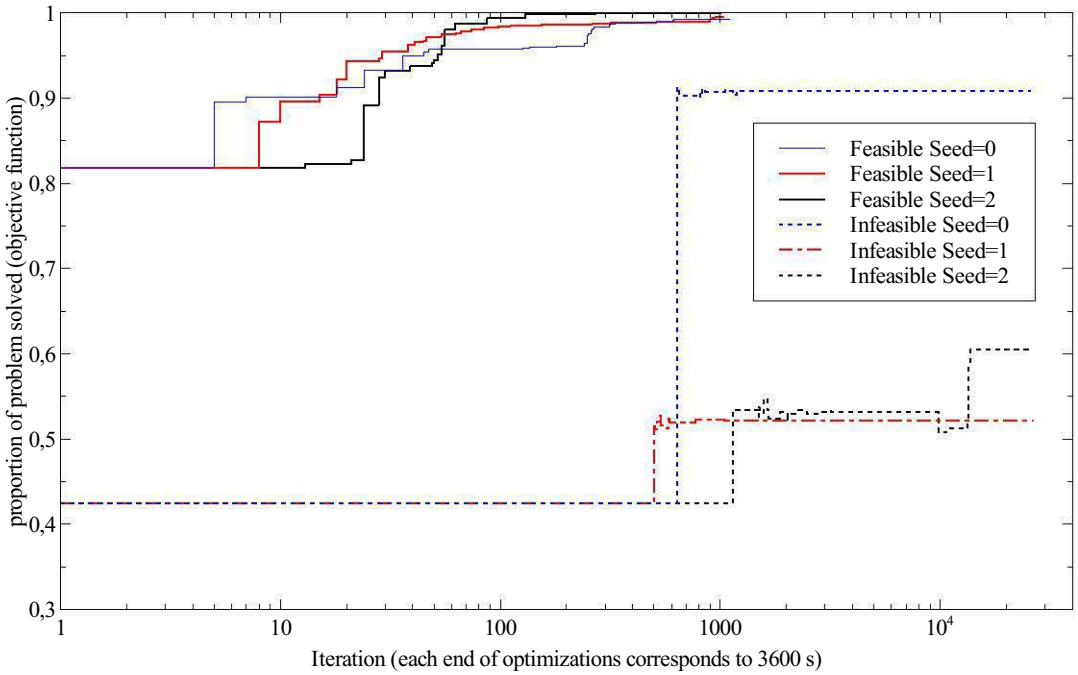

Figure 4.12: Relative performance comparison between Feasible Path approach and Infeasible path approach optimization evolution comparison. Feasible path optimization represented with solid lines and Infeasible path optimization represented with dashed dot lines. Note that the constraints of infeasible path optimization are not necessary respected in the presented curves.

Taking the same SC-CO_2 Brayton cycle superstructure as in Figure 4.9 for example, Figure 4.12 shows the evolution rate between two approaches. Note that for 1 hour optimization, the *infeasible path* optimization has more calculation iterations. This can be explained by the reduced simulation time since the tear equations are no more respected for simulation loop. However, for the *infeasible path* optimization, less steps of objective function evolution are observed compared with *Feasible path* approach. In addition, the constraints function only began to be satisfied at the end of 1000 iterations indicating that it takes much more time to get one result with constraints respected (especially tear equation constraints). Those observations confirm that the *infeasible path* optimization requires more computing efforts for the additional equality constraints resolution within such a non-convex MINLP optimization. The Black-Box nature of ACO does not require the explicit form of constraints thus MIDACO has difficulty to see which optimized variables are related to the equality constraints, especially when the

mass balance of tear stream (as well as entire process) can vary in a wide range. Theoretically, *infeasible path* optimization will find the same optimum as feasible path optimization. However, feasible path is capable of finding optimum in less computing time. Therefore, in a non-convex constrained MINLP problem with Black-box algorithm, it is recommended to favor the *feasible path* and let the simulator to handle the equality constraints.

4.4.2 Superstructure Optimization of SC-CO_2 Brayton cycle

Schlüter et al. (2012) have illustrated that stochastic algorithms such as MIDACO has intriguing advantages of blackbox optimization over deterministic ones. This means that the objective and constraint functions and their properties (discontinuities, non-convexity) can be completely unknown, which fits well with the complex real-world optimization application. In return, much more function (objective and constraints) evaluations are required than in deterministic methods.

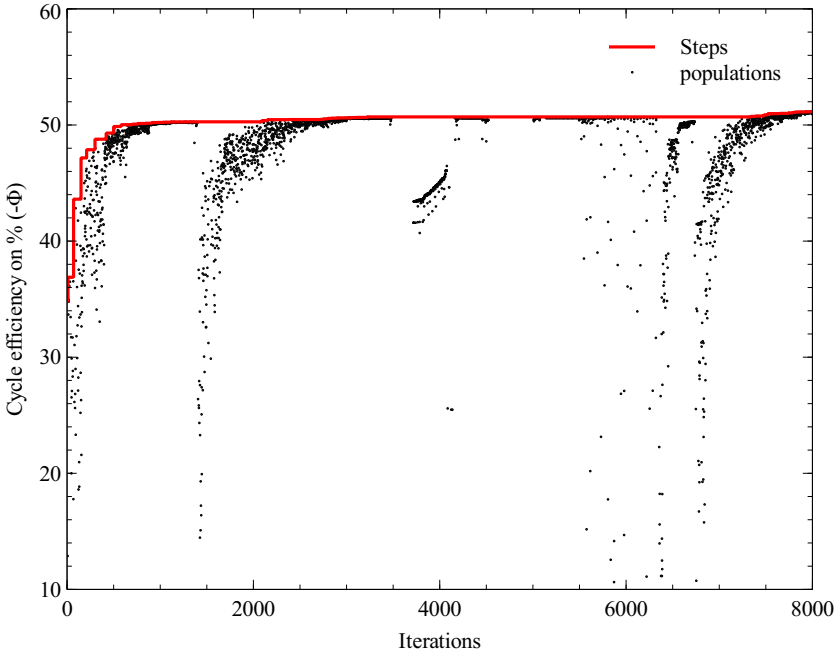

Figure 4.13: Optimization progress of SC-CO_2 Brayton cycle

Figure 4.13 shows the optimization progress over time by population representation (only the population satisfying the constraints is presented). It has been noticed the population generated by the first 1500 iteration has quickly evolved to a cycle efficiency of 50% ($-\phi$). The iterations afterwards are brought out with a new series of population which leads to a small improvement of 0.2%-pt on objective function. This observation indicates that MIDACO makes progress in

optimal function research by generating genuine new populations.

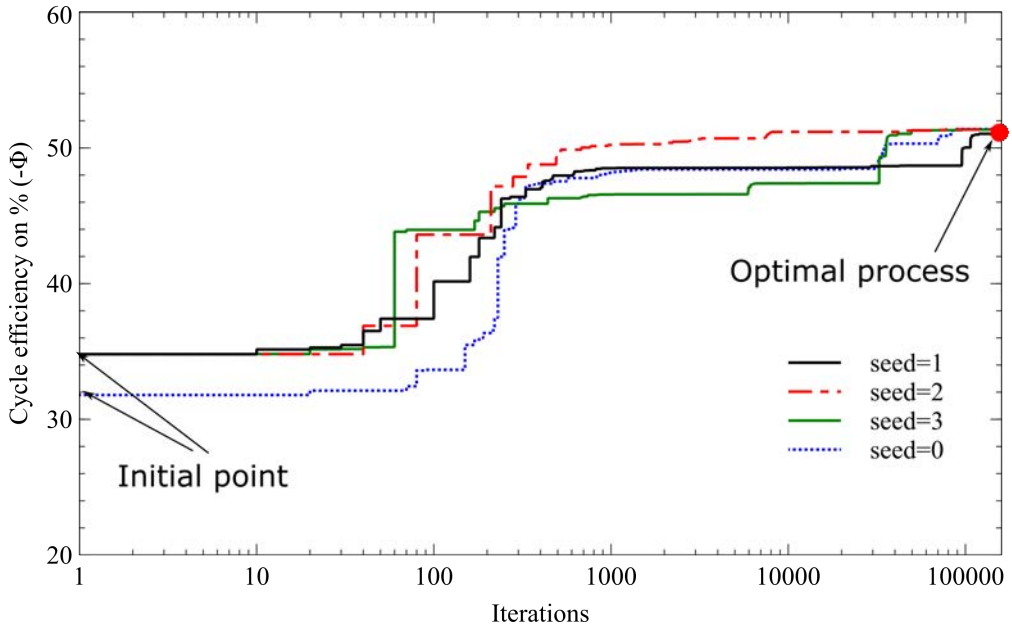

Figure 4.14: Optimization progress of four runs with different random seeds

In fact, the random character of the initial ant colony is controlled by a pseudo-random number generator using an initial seed in MIDACO. By modifying the seed value, different initial populations can be generated.

The evolution of four optimizations with different initial population is presented in Figure 4.14. It can be noted that different random seeds lead to diverse progress of optimization. After 160 000 generations (iterations), the structural result of the best individual is identical (i.e., identical set of {y}), see Table 4.3. In addition, similar sets of {x} are obtained for four different runs indicating that the optimal process (both its configuration and operation conditions) are the best known solution to the defined optimization problem. Note that some seeds have evolved more quickly towards better individuals than some others, it is thus recommended to run several times the same optimization with different seeds.

With all the constraints satisfied, the optimal process layout with cycle efficiency as high as 51.4% is composed of two compressors, two recuperators, and one reheat (thus two turbines), Figure 4.15. Compared with the initial proposal of SC-CO_2 Brayton cycle by Feher and Angelino, (Feher, 1967; Angelino, 1969), the optimal process configuration has an enforced heat integration. Figure 4.15 and Table 4.3 indicate that all the exchangers have reached a minimal accepted thermal pinch. The temperature difference between hot outgoing stream and the cold inlet stream is denoted as “cold end temperature difference”, and the temperature difference

Table 4.3: Results for superstructure optimization of SC-CO_2 Brayton cycle SS1

Results	Variable range	seed=1	seed=2	seed=3	seed=0
Best cycle efficiency (%)		51.38	50.93	51.36	51.34
Integer variables y		$\{1,1,1\}$	$\{1,1,1\}$	$\{1,1,1\}$	$\{1,1,1\}$
P_{in} compressor (MPa)	$x_1 \in 3.3-10$	7.50	7.66	7.63	7.57
$T_{cooling}$(K)	$x_2 \in 304.35-373.15$	304.35	304.74	304.35	304.39
Flow to Recompression C2 (%)	$x_3 \in 10^{-6}-0.5$	0.34	0.33	0.34	0.34
P_{out} compressor (MPa)	$x_4 \in 3.3-30$	30.00	30.00	30.00	30.00
Ratio turbine T1 (-)	$x_6 \in 1-5$	1.92	2.04	1.91	1.99
T_{R1}cold stream out (K)	$x_5 \in 304.35-893.15$	495.03	503.96	488.12	490.36
T_{R2} hot stream out (K)	$x_7 \in 304.35-893.15$	504.56	513,.58	497.63	499.94
Constraints ($\geqq 0$)					
g_1 on R1 cold end (K)	$(\Delta T-10) \geqq -0.5$	-0.46	-0.49	-0.41	-0.45
g_2 on R1 hot end (K)	$(\Delta T-10) \geqq -0.5$	0.00	4.58	0.00	-0.3
g_3 on R2 hot end (K)	$(\Delta T-10) \geqq -0.5$	35.05	38.29	36.72	36.08
g_4 on R2 cold end (K)	$(\Delta T-10) \geqq -0.5$	-0.46	-0.41	-0.49	-0.41
g_5 on ratio of compressor C1 (-)	$(P_2/P_1-1) \geq -0.025$	59.97	58.36	58.60	59.26

between hot inlet stream and the cold outgoing stream is denoted as "hot end temperature difference" (10 ± 0.5 K is the lower bound considered for both ends). It can be concluded that the efficiency can be further improved by relaxing the constraint on minimal pinch. Furthermore, entropy loss is avoided at mixer since its inlet streams 3' and 3" show identical temperature and pressure (iso-entropy) before mixing.

For the continuous process variables such as main cooling temperature ($T_{cooling}$) and the outlet compressor pressure (P_{out} compressor), their optimal values reach respectively the lower and upper bound stipulated in this study. Table 4.3 indicates that at the optimum, the cooling temperature tends to 304.35 K while the optimal compressor outlet pressure reaches 30 MPa. This trend is rather logical since efficiency of an ideal Brayton cycle is determined by its temperature of heat source (T_{it}) and heat release ($T_{cooling}$). As explained in the Chapter 1, the cycle efficiency can be improved by increasing the average temperature of heat addition and decreasing the average temperature of the heat release.

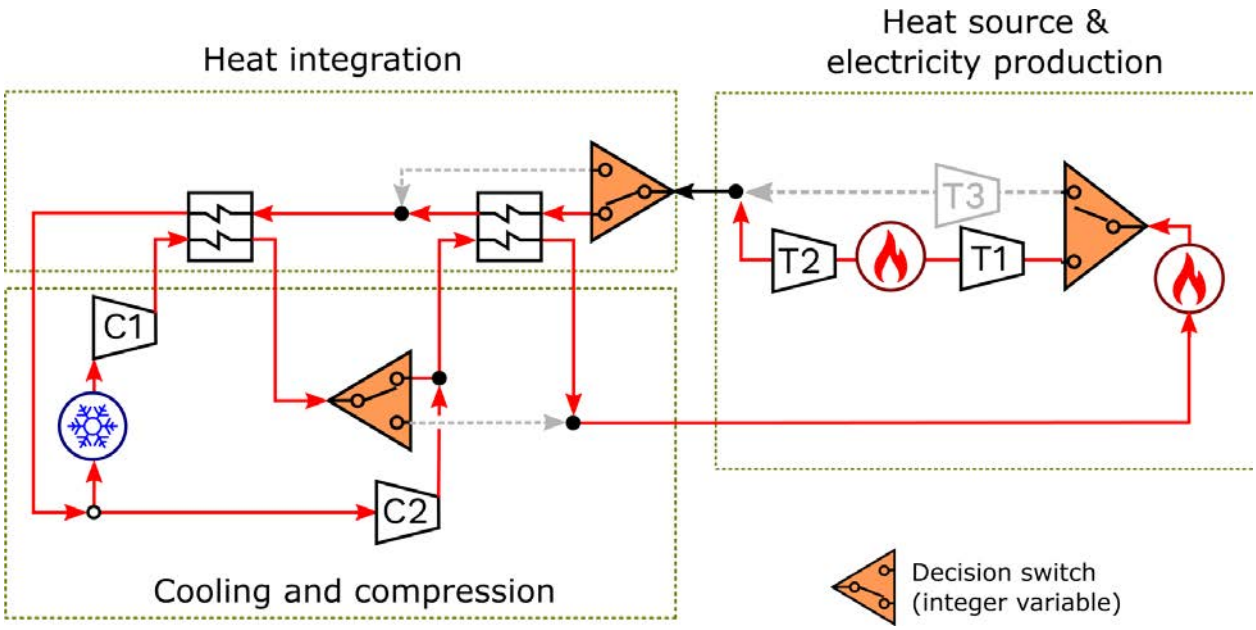

a) optimal process y={1,1,1} in superstructure

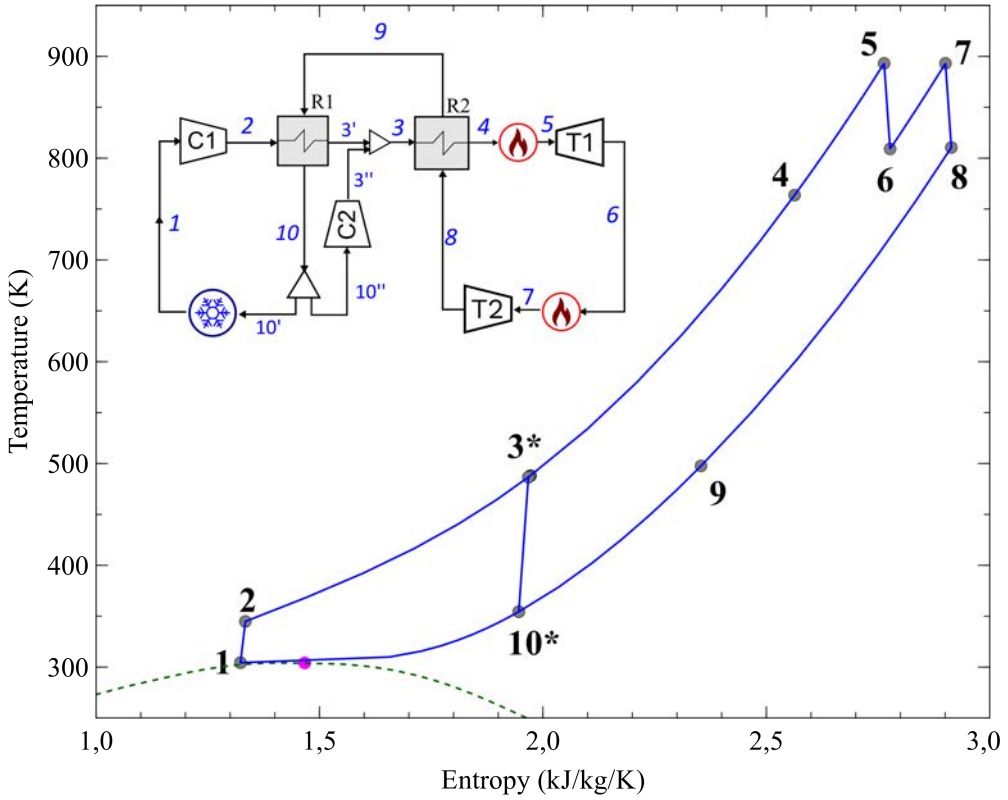

b) Temperature-Entropy diagram of optimal process

Figure 4.15: Process synthesis result: optimal flowsheet for the SC-CO_2 Brayton cycle

4.4.3 Result validation by six Non Linear Problem optimizations

In this section, the objective is to validate the described "superstructure optimization methodology". The optimization approach described in Section 4.3 is able to perform NLP (Non Linear Problem) optimization by fixing the structure of each process candidate (fixed $\{y_1, y_2, y_3\}$) in the defined superstructure. The eight possible process layouts generated by $\{y_1, y_2, y_3\}$ are reduced to six in Figure 4.16 by eliminating two redundancies.

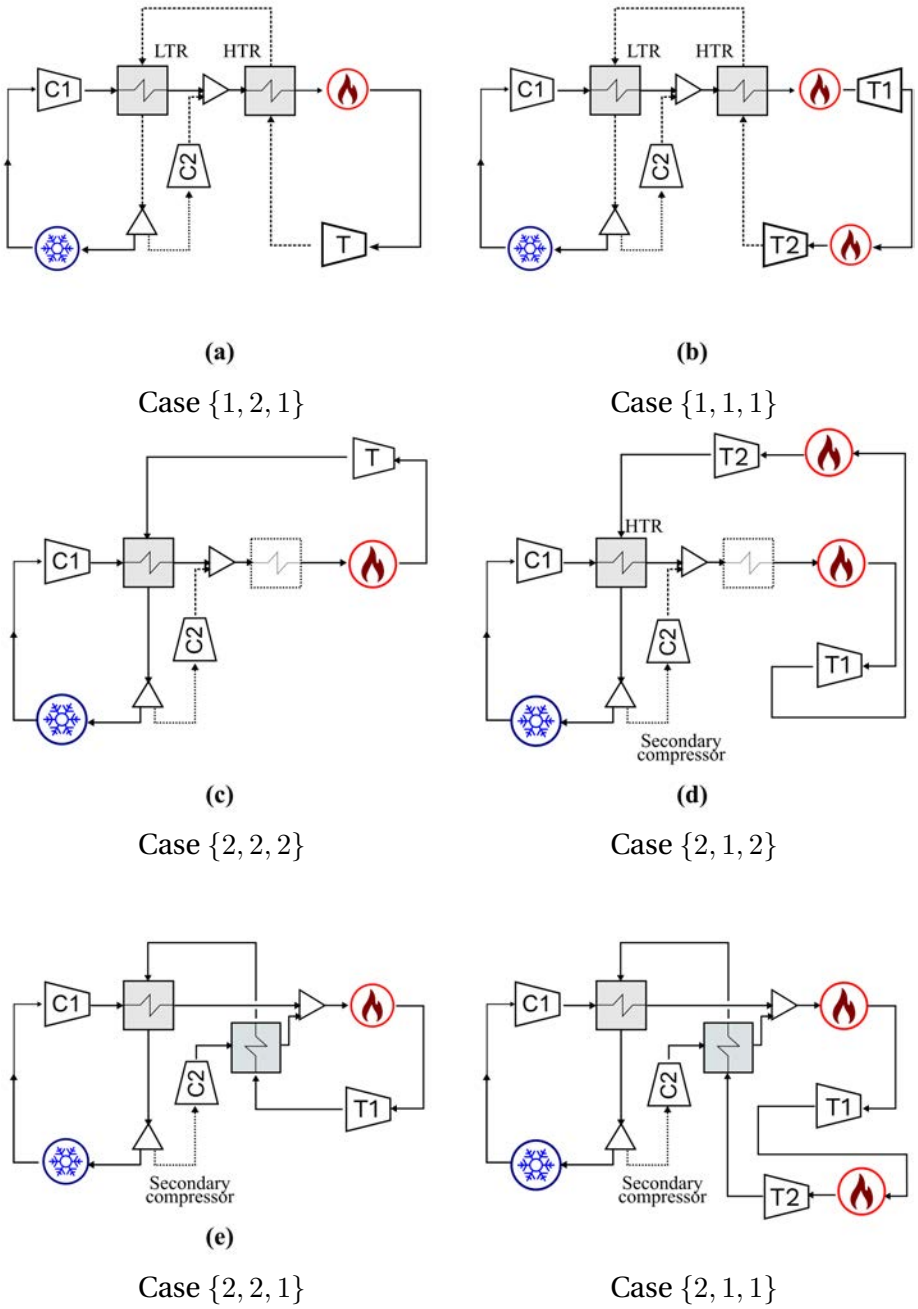

Figure 4.16: Illustration of SC-CO_2 Brayton cycles presented in the defined superstructure

Table 4.4: Non Linear Problem (NLP) optimization result of six process configurations

Configuration	$\{1,2,1\}$	$\{1,1,1\}$	$\{2,2,2\}$	$\{2,1,2\}$	$\{2,2,1\}$	$\{2,1,1\}$
Best cycle efficiency (%)	49.55	51.33	47.39	48.63	47.61	48.90
P_{in} compressor (MPa) x_1	7.61	7.46	7.47	7.44	7.48	7.49
$T_{cooling}$ (K) x_2	304.35	304.35	304.35	304.35	304.35	304.35
Flow to Recompression (%) x_3	0.34	0.34	0.25	0.20	0.25	0.23
P_{out} compressor (MPa) x_4	30	30	30	30	30	30
Ratio main turbine (-) x_6	-	1.91	-	1.91	-	1.65
T_{R1} cold stream out (K) x_5	488.34	497,76	717.04	795.89	660.60	707.16
T_{R2} hot stream out (K) x_7	498.09	507.39	-	-	670.29	716.74
Constraints (≥ 0)						
g_1 on R1 cold end (K)	-0.50	-0.41	-0.41	-0.49	-0.38	-0.45
g_2 on R1 hot end (K)	-0.25	-0.37	-0.49	-0.49	-0.31	-0.42
g_3 on R2 hot end (K)	32.02	33,84	-	-	18.38	0.25
g_4 on R2 cold end (K)	0.02	-0,42	-	-	163.74	210.23
g_5 on ratio of compressor C1 (-)	58.83	60,44	60,29	60,60	60.20	60.15
Some key process variables (result)						
P_{out} main turbine (MPa) (T1 or T3)	7.84	-	7.62	-	7.71	-
P_{out}T2 (MPa)	-	7.69	-	7.59	-	7.71
T_{R1} hot stream out (K)	354.80	360.67	359.69	361.66	359.09	359.12
T_{R2} cold stream out (K)	688.77	763.73	-	-	699.27	778.43
CO_2 flowrate in boiler (kg/s)	9208.78	9206.14	7903.31	7643.94	8132.55	7937.07

Table 4.4 summarizes the objective function, optimized variables, constraints and calculated parameters results of each layout. By comparing the cycle efficiency, the configuration$\{1,1,1\}$ is indeed the most energy-optimal process among all the six cycles. By comparing the left row (without reheating) and the right row layouts (with reheating) in Figure 4.16, it has been noticed that the introduction of reheating helps to rise efficiency by 1.3%-pt as expected. For different process configurations, all the obtained optimal main cooling temperatures ($T_{cooling}$) are at their lower boundary. In addition, the compressor outlet pressure (P_{out} compressor) is at its upper bound which enables to get more mechanical work during the expansion in turbine. Unlike the cooler temperature and compressor outlet pressure, other optimized variables such as flow to recompression (x_3) and recuperator temperatures vary when the process changes.

Note that a wide range of main compressor inlet pressure is considered in this study, the lower boundary of inlet pressure is lower than the CO_2 critical pressure. However, the results in Table 4.4 indicate that as long as the main cooling temperature is higher than the CO_2 critical temperature, the optimal main compressor (C1) inlet pressures are optimized to be close to the critical pressure of CO_2 for diverse SC-CO_2 Brayton cycles.

To conclude, this study validates the optimum found in superstructure optimization to be

the best known process by comparing every Brayton cycle configuration included in the SS1 superstructure.

4.4.4 Sensitivity analysis

The purpose of this part is to analysis the influence of $T_{cooling}$ (as well as minimal stream temperature) and T_{it} (turbine inlet temperature) on superstructure optimization since they are indicators for ideal Brayton cycle efficiency. This section is achieved by performing respectively a SS1 superstructure optimization by each different $T_{cooling}$ and T_{it}. The same optimization approach described in Section 4.3 is applied to look for optimal process configuration as well as the corresponding operation parameter.

Impact of the main cooling temperature

The minimal stream temperature listed in Table 4.1 is changed to be respectively 308.15 K, 318.15 K and 328.15 K. The optimal process layout for different optimization turned out to be configuration {1, 1, 1} (Figure 4.16 (b)), indicating that for the studied superstructure, main cooling temperature $T_{cooling}$ does not influence the choice of optimal layout of SC-CO_2 Brayton cycle. Figure 4.17 shows the results of temperature entropy diagrams for four different temperatures.

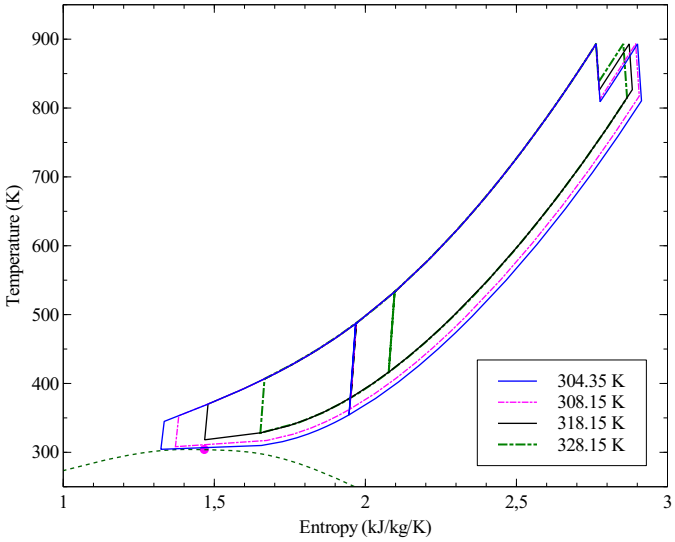

Figure 4.17: Temperature-Entropy diagram for different cooling temperatures

It can be observed that all the main compressor outlet pressures are identical and reach the upper bound (30 MPa). The higher $T_{cooling}$ gets, the smaller surface is observed in the T-S

diagram. A monotonically decreasing trend is observed in Figure 4.18 (a) when $T_{cooling}$ increases: by increasing the temperature by 24 K, the cycle efficiency decreases by 7%-pt, which could give an insight for practitioners what to expect with their own cooling condition.

Further comparisons are illustrated by Figure 4.18 (b) (c), showing that both the optimal flow fraction and optimal main compressor inlet pressure are sensitive to the change of the main cooling temperature. As the cooling temperature rises, optimal inlet compressor pressure increases. For cooling temperature higher than 318 K, the optimal inlet compressor pressure is limited by its upper acceptable value (10 MPa). While $T_{cooling}$ rises, a monotonically decreasing relationship is observed on flow fraction before recompressor. Results in Figure 4.18 (b) (c) indicate that the entire component sizing would be different as main cooling temperature changes.

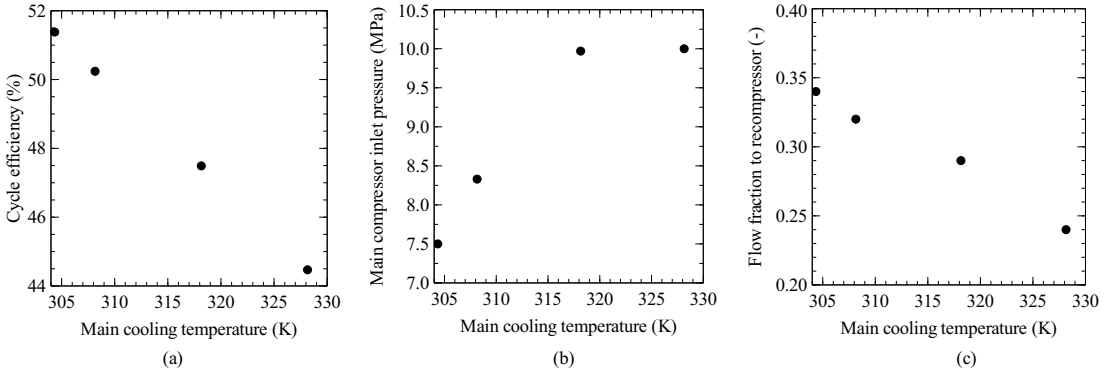

Figure 4.18: Influence of cooling temperature on a) cycle efficiency b) compressor inlet pressure c) fraction of flow pass to recompression

Impact of the Turbine Inlet Temperature

Similarly to previous sensitivity study, during this assessment, the boundary of maximum stream temperature and the set of turbine inlet temperature T_{it} are considered differently within optimization compared with the initial hypothesis. Different T_{it} lead to identical best process layout which is the configuration {1, 1, 1}. Both Figure 4.19 and 4.20(a) illustrate that there is a monotonically increasing relationship between turbine inlet temperature T_{it} and the cycle efficiency. Rising up the T_{it} by 220 K results in a 9%-pt improvement in cycle efficiency. The influence of inlet turbine temperature on optimal main compressor outlet pressure is limited. For different T_{it} , the optimal main compressor outlet pressure is 30 MPa.

Nevertheless, unlike the case of main cooling temperature, the main compressor inlet pressure and flow fraction are less impacted by the boiler temperature change. A relative

deviation around 2.6% is observed on different optimal main compressor inlet pressure and the deviation rises up to 4.2% in terms of flow fraction (to the recompression). To conclude, boiler temperature impacts the efficiency without significantly modifying component sizing.

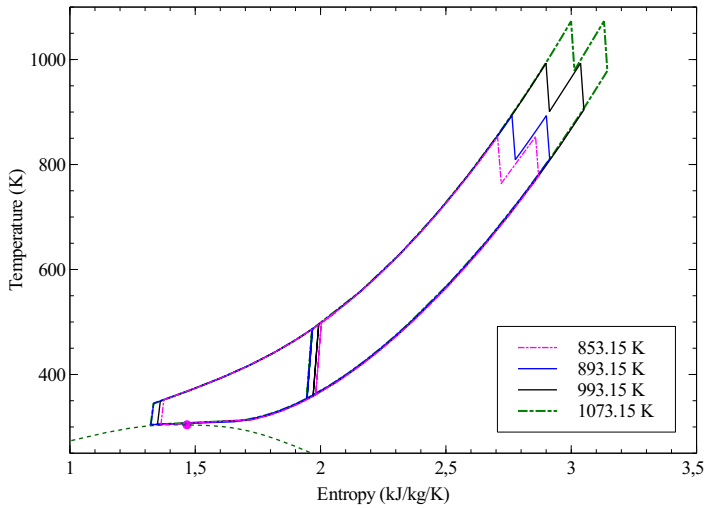

Figure 4.19: Temperature-Entropy diagram for different boiler temperatures

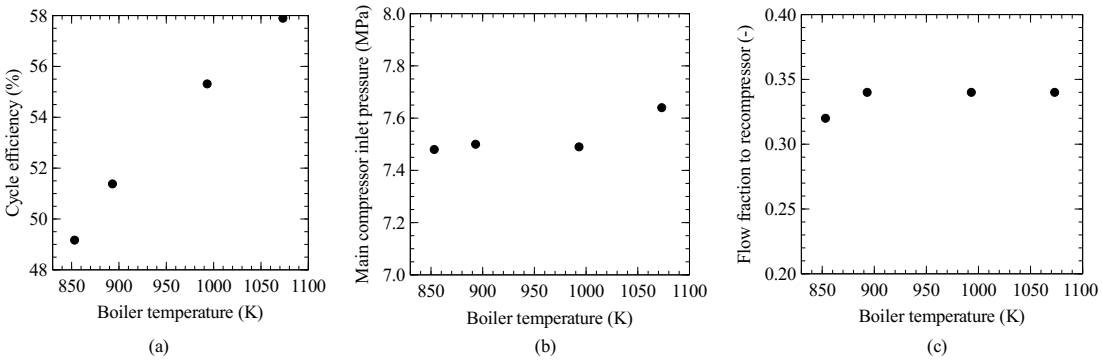

Figure 4.20: Influence of inlet turbine temperature on a) cycle efficiency b) compressor inlet pressure c) fraction of flow pass to recompression

In this chapter, the optimization of a superstructure that depicts a SC-CO_2 Brayton cycle has been presented. This approach enables to systematically study numerous configurations under the same modeling environment and hypotheses. The proposed simulator-based optimization uses a commercial process simulator to manage the entire Mixed Non Linear Programming (MINLP) optimization, where the optimizer MIDACO searches simultaneously both continuous variables (process variables) and the discrete integer variables (process layout). The results show the potential application of this methodology since any unit operation that is available in the simulator can be used to design the superstructure.

An industrial-scale problem usually has additional constraints arising in practice (e.g. new restrictions on some variables), or even modified objective function (e.g. new cost model developed). The practical management of variables, constraints and their bounds makes it easy to review some performed assessments when necessary.

In the next chapter, this validated methodology will be utilized on an industrial scale superstructure of SC-CO_2 Brayton cycle in the application of advanced coal-fired power plant, where both mono-objective and multi-objective optimization will be carried out.

CHAPTER 5

Energy and economic optimization based synthesis: SC-CO_2 Brayton cycle for coal-fired plant application

While the superstructure built in the previous chapter (SS1) includes only a few number of SC-CO_2 cycle architectures, a more sophisticated superstructure (denoted SS2) is now created to include many more configurations such as those reviewed in Chapter 1. In particular, the "preheating" design configuration proposed by Mecheri and Le Moullec (2015) for coal-fired power plant application has been considered in this new superstructure. The SS2 has been built to fit actual and more realistic industrial constraints. This chapter conducts a complete SS2 optimization for SC-CO_2 Brayton cycle in industrial conditions, in terms of both energy (mono-objective) and economics (multi-objective). As the energy mono-objective optimization reveals the electric production performance of an innovative power cycle, in-house economic correlations help to access an important technology global criterion, the Levelized Cost Of Electricity (LCOE).

5.1 SUPERSTRUCTURE IN INDUSTRIAL CONDITIONS

In the power cycle definition, the heat source serves only for heat addition at a constant temperature while in the coal-fired plant, the thermal energy (both radiative and convective) received by SC-CO_2 is provided by the coal combustion in the boiler.

In this dissertation, issues related to the association of a SC-CO_2 Brayton cycle with a coal-fired boiler are not considered. It is assumed that a similar technology as the current "state-of-the-art coal boiler" (Ultra SuperCritical-steam boiler) can be combined with the studied SC-CO_2 Brayton cycles. In this context, some USC-steam boiler specification and constraints are described. The temperature in such boiler is around 1673.15 K (1400 °C); approximately half the total heat duty is delivered at this temperature through radiative heat transfer, the other half is the sensible heat of flue gas leaving the boiler (Le Moullec, 2013a). Yet, the flue gas temperature

can reach around 823.15 K (550 °C) after the evaporator in furnace, steam superheater, and steam reheater. The economizer and the air-heater are back-end heat exchangers used to recover this unexploited energy in the flue gas. The economizer saves fuel usage by extracting the low-grade heat (to heat the water), reducing also the heat loss to the atmosphere through. The air heater on the other hand, uses the heat from the flue gas to heat the primary and secondary air that enters into the furnace, lowering the air or coal humidity (Rayaprolu, 2009).

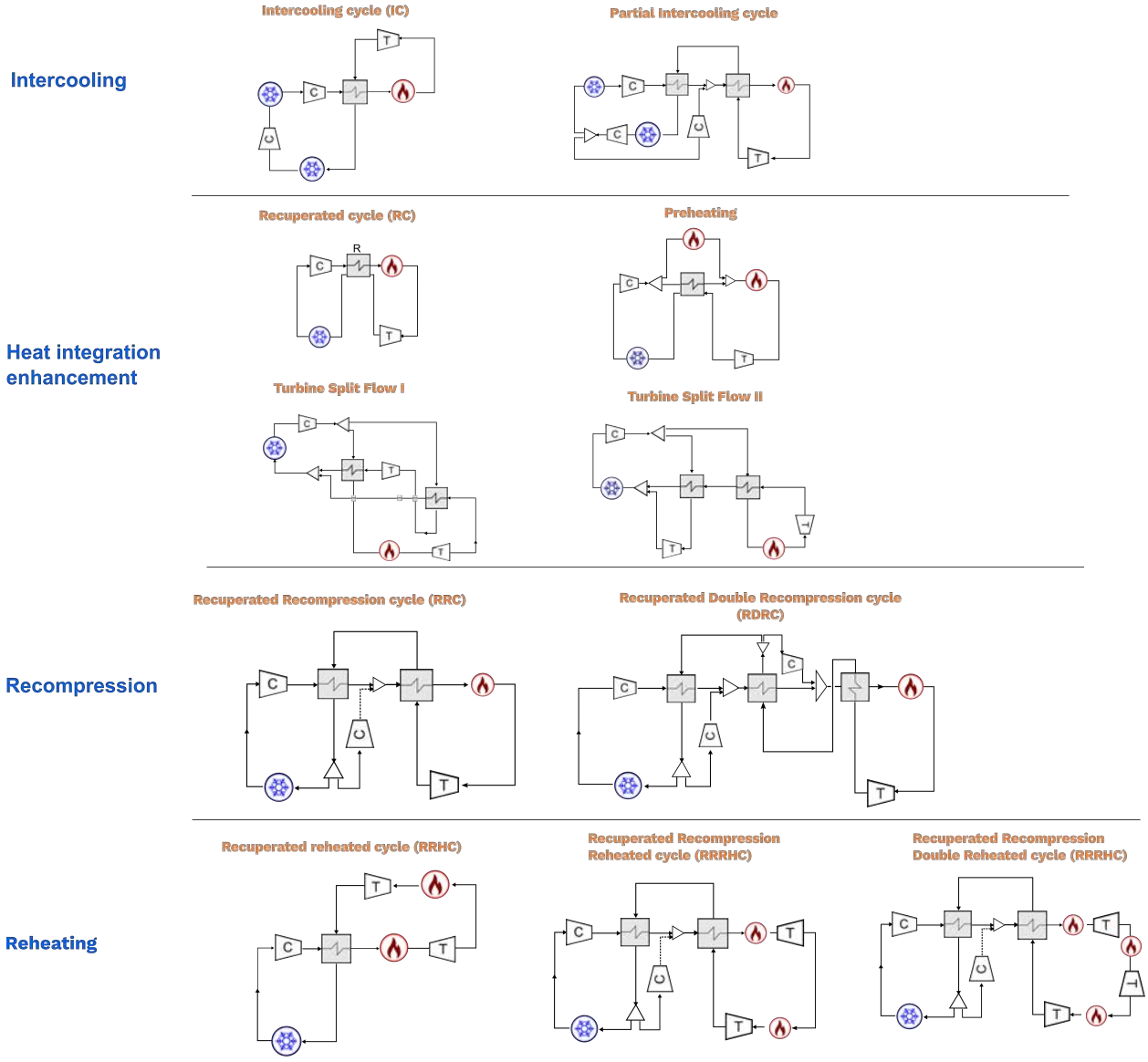

Figure 5.1: Classification of individual process modifications of SC-CO_2 Brayton cycle taken into account in the superstructure SS2 (Angelino, 1968; Mecheri and Le Moullec, 2015; Crespi et al., 2017)

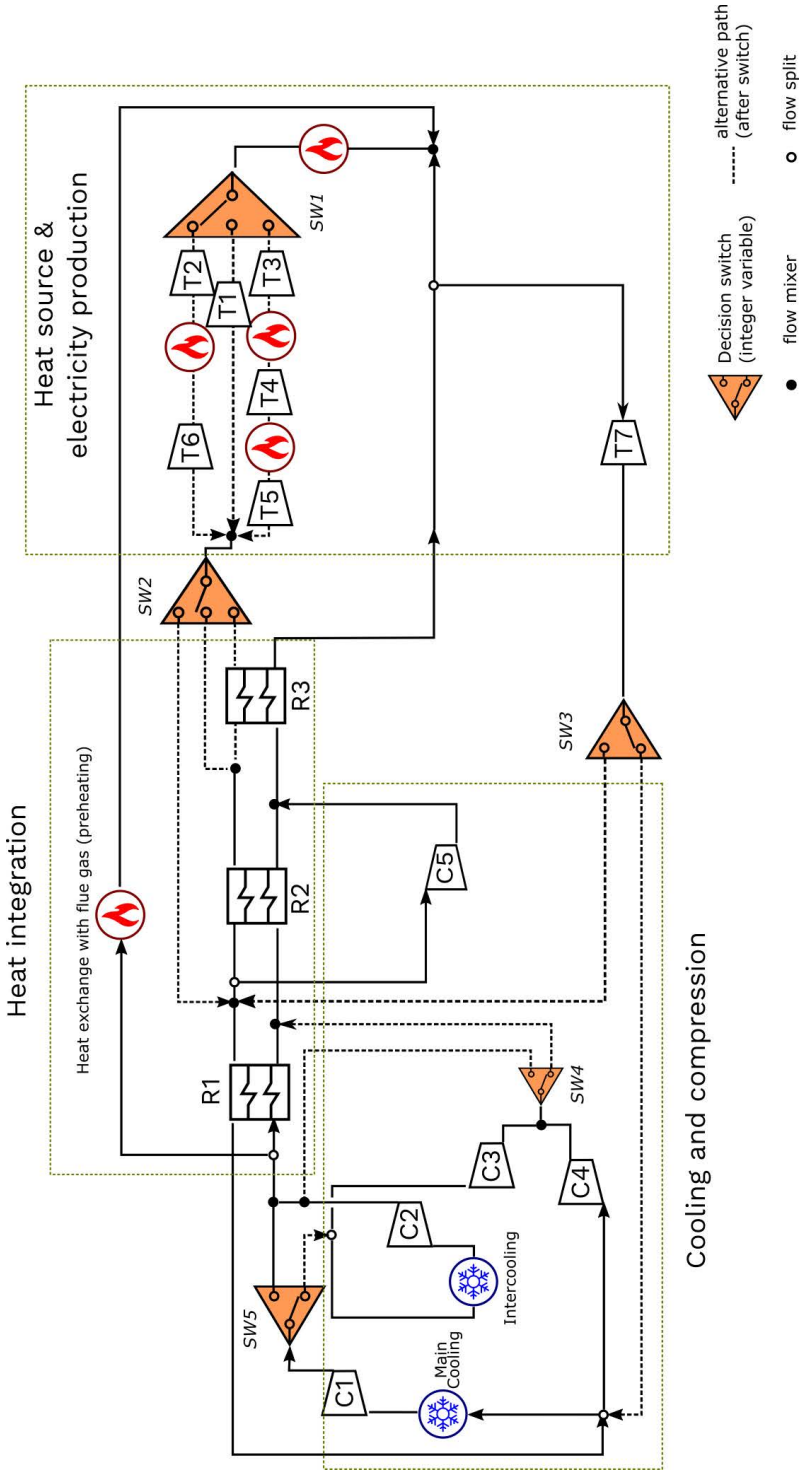

Figure 5.2: Superstructure SS2 for SC-CO_2 Brayton cycle ($2^7 \times 3^2 = 1152$ structural alternatives)

Similar application of flue gas has been considered by Mecheri and Le Moullec (2015) as well as Le Moullec (2013b) in the case of SC-CO_2 coal-fired plant. They proposed that the economizer and air-heater block in SC-CO_2 coal-fired application can preheat a partial flow of CO_2 in order to limit the loss on boiler. In this thesis, hypothesis of $(\frac{\dot{Q}_{\text{flue gas}}}{\sum \dot{Q} - \dot{Q}_{\text{flue gas}}} - 9\% = 0)$ has been made on the thermal energy that SC-CO_2 can be recovered by heat exchanging with the flue gas in comparison with the boiler thermal energy. As a part of mathematical formulation, this statement is considered as an equality constraint.

Another particularity of this superstructure is to take into account, as much as possible, the known configurations of a SC-CO_2 Brayton cycle. In a review conducted by Crespi et al. (2017) concerning SC-CO_2 Brayton cycle, a list of 42 different stand-alone Brayton cycle configurations is proposed. The construction of this second superstructure (SS2) has taken 11 of them into account (Figure 5.1). Note that the cycle configurations listed in the literature review are not all considered because some of them are transcritical cycles (with liquid CO_2). On the other hand, different heat sources could have some atypical cycle configuration. For example, for the fusion reactor, two main heaters (heat addition by heat source) are in parallel. Therefore, such specific configurations have not been taken into account for the industrial case regarding coal-combustion

The superstructure SS2 shown in Figure 5.2 is composed of three different blocks: the heat source & electricity production block, the heat integration block and the cooling compression block. From right to left, the first logical switcher *SW1* alternates between a Brayton cycle with (single or double) reheating or without. Reheating is a potential action to raising the electricity production in turbines. The second switchers *SW2* situated in the heat integration block determines the existence of recuperators R2 and R3 whereas R1 must be present in any final process configuration. *SW3* can also be categorized in heat integration block as it looks for a better position to inject flow in turbine T7 (if it exists) for energy recovery. Similar to *SW3*, *SW4* tries to recover the energy carried by compressed flow. Finally, *SW5* enables superstructure SS2 to have an intercooling system (or a partial intercooling) at choice to reduce the compressor consumption.

Together with the combination of logical switches and flow splitters, the SS2 in Figure 5.2 represents at once over 1000 layouts of SC-CO_2 Brayton cycle. This large searching space will lead to an advanced process structural optimization with a global view and some innovative design solutions may occur.

By employing the methodology proposed in the previous chapter, the enforcement strategy leads to a modified superstructure illustrated in Figure 5.3. Each counter-current heat exchanger

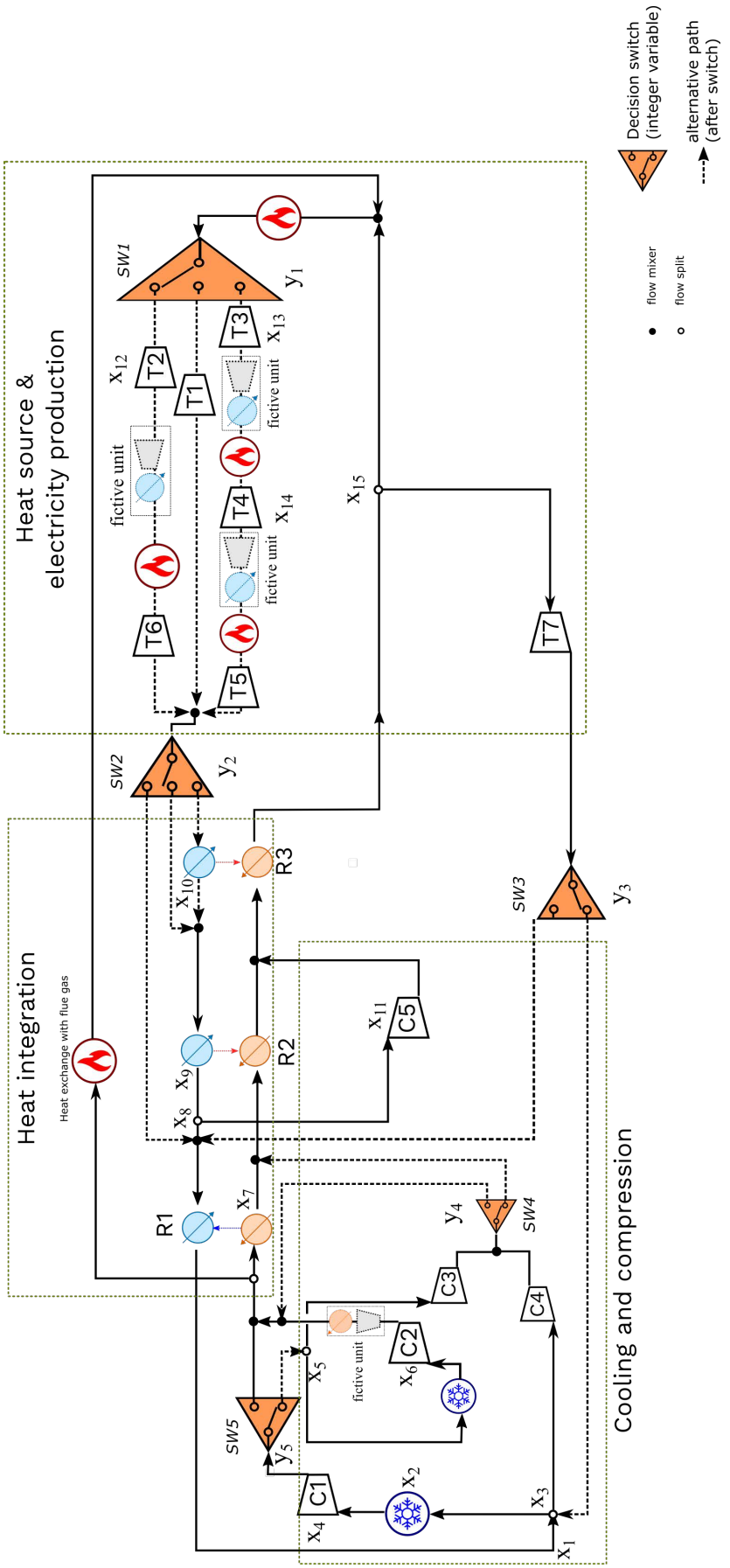

Figure 5.3: Superstructure SS2 of SC-CO_2 Brayton cycle after feasibility modification ($2^7 \times 3^2 = 1152$ structural alternatives)

is represented by two simple unit operations which are the basic heat exchanger block (one representing the "cold" side of the heat exchanger, and the other one the "hot" side with $-\dot{Q}_{hot\ side} + \dot{Q}_{cold\ side} = 0$).

In addition, for turbines T2, T3 and T4, fictive units of “compressor+cooler” are added. For compressor C2 that compresses a stream being intercooled, a fictive unit of “turbine+heater” is employed. After the "feasibility modification" step, the superstructure SS2 results in 32 unit operations (Figure 5.3).

- In this chapter three major assessments are performed by using the SS2. First, a mono-objective optimization of the SS2 is done in order to find cycle layouts that achieve the best performance (i.e. energy aspect optimization). In this case, the “cycle efficiency” is the objective to maximize.

- In a second step, an in-house economic model is directly used to access the LCOE of the optimized cycle layout(s) obtained in the first step. As a result, this step is not an optimization but an application of the economic model on the “mono-objective optimization” results.

- The last step is to perform a multi-objective optimization by taking both cycle “energetic” and “economic” performances into account. The results of this last step (multi-objective) are then compared to the results of the “mono-objective” and discussions are brought out.

5.2 MONO-OBJECTIVE SUPERSTRUCTURE OPTIMIZATION OF SC-CO_2 BRAYTON CYCLE

5.2.1 General mathematical problem formulation for energy mono-objective optimization

Similar specification rules as in the previous chapter are applied so that some unit operations (components) in the superstructure SS2 are not necessarily managed by the external optimizer.

Firstly, all the “final turbines” (last turbine before entering *SW2* or *SW3*) are deducted by logical rules. Consequently, the outlet pressure of turbine T6, T1, T5 and T7 are deducted from the knowledge of other optimized variables. For example, the outlet pressure of turbine T7 is specified to be equal to either that of hot stream leaving R2 or that of stream entering the main cooling.

In addition, compressors C3 and C4 are logically defined so that their outlet pressure are equal

to the other stream in the mixer. Therefore, by adopting the enforcement rule described in the previous chapter, optimization of 32 unit operations in Figure 5.3 reduced in optimizing a total of 21 variables among which 5 are discrete integer variables (note that triple-paths switchers present), Table 5.2.

In the context of coal-fired plant, assumptions are made in the similarity with the state-of-the-art USC-steam coal-fired plant, which allows steam to achieve 30 MPa and 893.15 K (620 °C). The thermal pinch in R1, R2 and R3 is set to be higher than 10 K in order to guaranty the feasibility of the heat transfer between the hot and cold sides. As explained in Chapter 3, the brutal change of isobaric heat capacity in Brayton cycle enables to have minimal pinch either at cold end (hot outgoing stream and the cold inlet stream side) or hot end (cold outgoing stream and the hot inlet stream side). Otherwise cross temperature profile will occur and the simulation will not be converged. Therefore, for R1 and R2, two inequality constraints are considered for each of them. As for R3, its cold end temperature difference is not imposed supposing the influence of C5 on temperature is limited as its flow fraction is limited to be lower than 50%.

Table 5.1: Values of fixed process variables, equipment data and constraints used in the superstructure SS2

Hypothesis on fixed variables and Equipment data	
T_{it} turbine inlet temperature (K)	893.15
T_{it} turbine inlet temperature after reheating (K)	893.15
CO_2 flowrate before main cooling (kg/s)	6000
MinimumΔT_{pinch} (K)	10
Turbine isentropic efficiency (-)	0.9
Compressor isentropic efficiency (-)	0.89
Pressure drop in every component (% of inlet pressure)	1
Constraints	
g_1 on R1 hot end temperature difference (K)	$(\Delta T - 10) \geqq -0.5$
g_2 on R1 cold end temperature difference (K)	$(\Delta T - 10) \geqq -0.5$
g_3 on R2 cold end temperature difference (K)	$(\Delta T - 10) \geqq -0.5$
g_4 on R2 hot end temperature difference(K)	$(\Delta T - 10) \geqq -0.5$
g_5 on R3 hot end temperature difference(K)	$(\Delta T - 10) \geqq -0.5$
g_6 on ratio of main compressor C1 (-)	$(\mathrm{P}_2/\mathrm{P}_1 - 1) \geq -0.025$
g_7 on on flue gas (-)	$\frac{\dot{Q}_{\text{flue gas}}}{\sum \dot{Q} - \dot{Q}_{\text{flue gas}}} - 9\% = 0$

Table 5.2: List of optimized variables and their bounds considered in SS2

Optimized continuous variables x	Bounds
P_{in} compressor C1 (MPa)	$x_1 \in 3.3 - 10$
$T_{cooling}$(K)	$x_2 \in 304.35 - 373.15$
Flow to Recompression C4 (%)	$x_3 \in 10^{-6} - 0.5$
P_{out} compressor C1 (MPa)	$x_4 \in 3.3 - 30$
Flow to recompression C3 (%)	$x_5 \in 10^{-6} - 0.5$
P_{out} compressor C2/MPa	$x_6 \in 3.3 - 30$
T_{R1}cold side out (K)	$x_7 \in 304.35 - 893.15$
Flow to recompression C5 (%)	$x_8 \in 10^{-6} - 0.5$
T_{R2} hot side out (K)	$x_9 \in 304.35 - 893.15$
T_{R3} hot side out (K)	$x_{10} \in 304.35 - 893.15$
P_{out} compressor C5/MPa	$x_{11} \in 3.3 - 30$
Ratio turbine T2 (-)	$x_{12} \in 1 - 5$
Ratio turbine T3 (-)	$x_{13} \in 1 - 5$
Ratio turbine T4 (-)	$x_{14} \in 1 - 5$
Flow fraction passing to T7 (%)	$x_{15} \in 10^{-6} - 0.5$
Flow fraction of CO_2 preheated by flue gas (%)	$x_{16} \in 10^{-6} - 0.5$
Optimized integer variables y	
SW1	$y_1 \in \{1,\ 2,\ 3\}$
SW2	$y_2 \in \{1,\ 2,\ 3\}$
SW3	$y_3 \in \{1,\ 2\}$
SW4	$y_4 \in \{1,\ 2\}$
SW5	$y_5 \in \{1,\ 2\}$

Note that a relative pressure drop is more realistic in industrial conditions, the pressure drop is set to be 1% of inlet stream pressure (identical to Chapter 3 and 4). Other assumptions, equipment data and constraints considered in the mono-objective optimization are listed in Table 5.1. To sum up, seven inequality constraints and one equality constraint have also been considered.

For the first optimization of this advanced superstructure, the cycle efficiency is still seen as main indicator of the energy performance, Eq 5.1.

$$\begin{aligned} \underset{x,y}{Min}\ \phi(x,y) &= -\eta_{\text{cycle}} \qquad (x \in \mathbb{R}^{n_{con}},\ y \in \mathbb{Z}^{n_{int}}) \\ s.t.\ h(x) &= 0 \\ g(x) &\geq 0 \\ x_{min} \leq x &\leq x_{max} \\ y_{min} \leq y &\leq y_{max} \end{aligned} \tag{5.1}$$

where $\eta_{\text{cycle}} = \frac{\dot{W}net}{\sum \dot{Q}}$

$g(x)$ is the vector of inequality constraints; with $\sum \dot{Q} = \dot{Q}_{\text{heat}} + \dot{Q}_{\text{reheating}}(\text{if exist})$.

$x = [x_1, ..., x_{20}]$ is the vector of continuous optimized variables

$y = [y_1,\ y_2,\ y_3\ y_4\ y_5]$ is the vector of flow switcher decision variables.

$h(x)$ is the equality constraint ($\frac{\dot{Q}_{\text{flue gas}}}{\sum \dot{Q} - \dot{Q}_{\text{flue gas}}} - 9\% = 0$), but in the formulation, it is managed by the simulation phase and not by the optimizer.

$g(7)$ is specified as an indicator of constraint convergence (of $h(x)$). In case of non-convergence at simulation phase, optimizer will see it as a non-respected inequality constraint.

5.2.2 Results

The optimization progress of 200,000 iterations and four seeds are illustrated in Figure 5.4, it can be seen that the four runs have converged towards very close cycle efficiencies. Two promising structural results (respectively denoted “Case A” and “Case B”) with simultaneously optimized process parameters are obtained. Case A: y= {1 2 1 1 1} which has a cycle efficiency of 55.99% (Figure 5.5 a). Case B: y= {3 2 1 1 1} reaches a net efficiency of 55.58% (Figure 5.6 a).

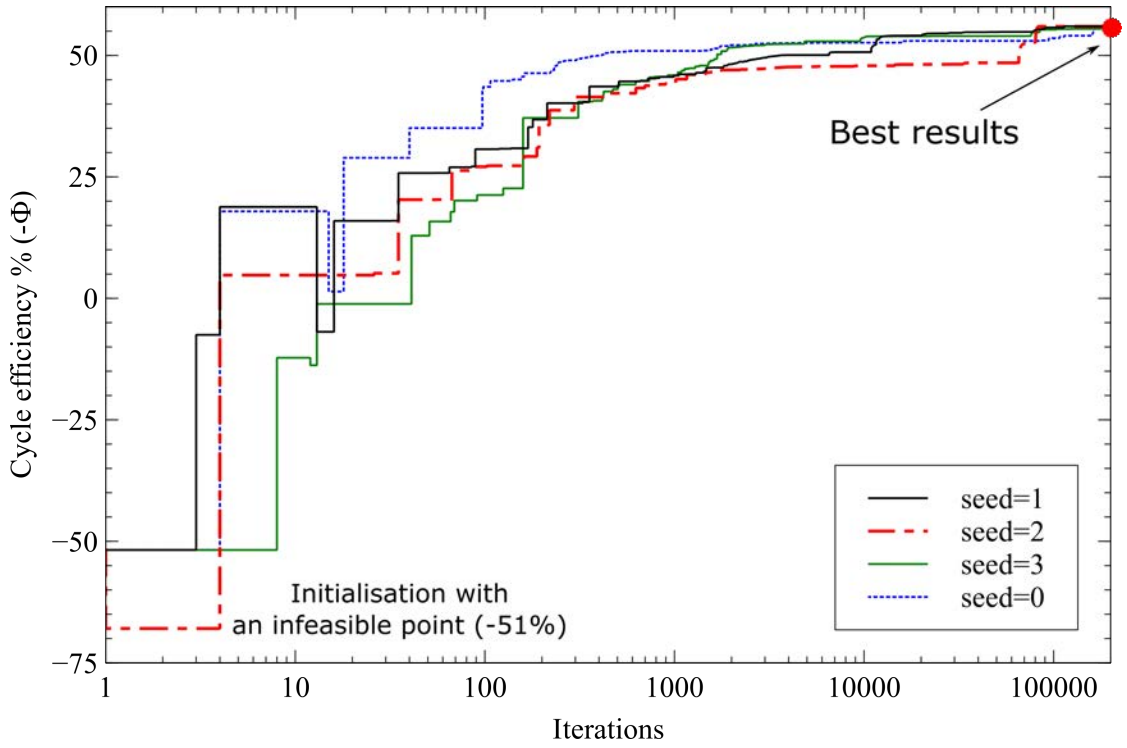

Figure 5.4: Energy performance optimization progress of four runs with different random seeds

As the main structure difference between two best results sits on the reheating mode, the configuration Case B in Figure 5.5 a) is called “double reheating-double recompression-preheating” Brayton cycle, while the configuration Case A in 5.6 a) is denoted as “single reheating-double recompression-preheating” Brayton cycle. Case A is slightly more efficient than Case B thanks to the double reheating, which leads to a higher turbine power production, and thus higher net power, Table 5.3.

Note that neither the boiler power capacity nor the mass flowrate of SC-CO_2 in boiler is fixed during the optimization, it is possible that the final optimized Brayton cycle has different industrial scale. For example, the Case A and B have similar but different power capacity. The power density of the Case A is higher than that of the Case B (Table 5.3), explaining the 0.41%-pts higher cycle efficiency.

In addition, as can be noticed for the temperature entropy diagram, Figures 5.5 and 5.6, no entropy loss is found at mixer (before stream 4 and before stream 3 in either case). Although streams such as 4’, 4” before mixing has optimized variables on terms of pressure or temperature, optimization leads them to identical temperature and pressure (iso-entropy) before entering the mixer. As this trend has already been observed for the optimization SS1, we can finally conclude the iso-entropy as an indicator for end of optimization (at least competitive results).

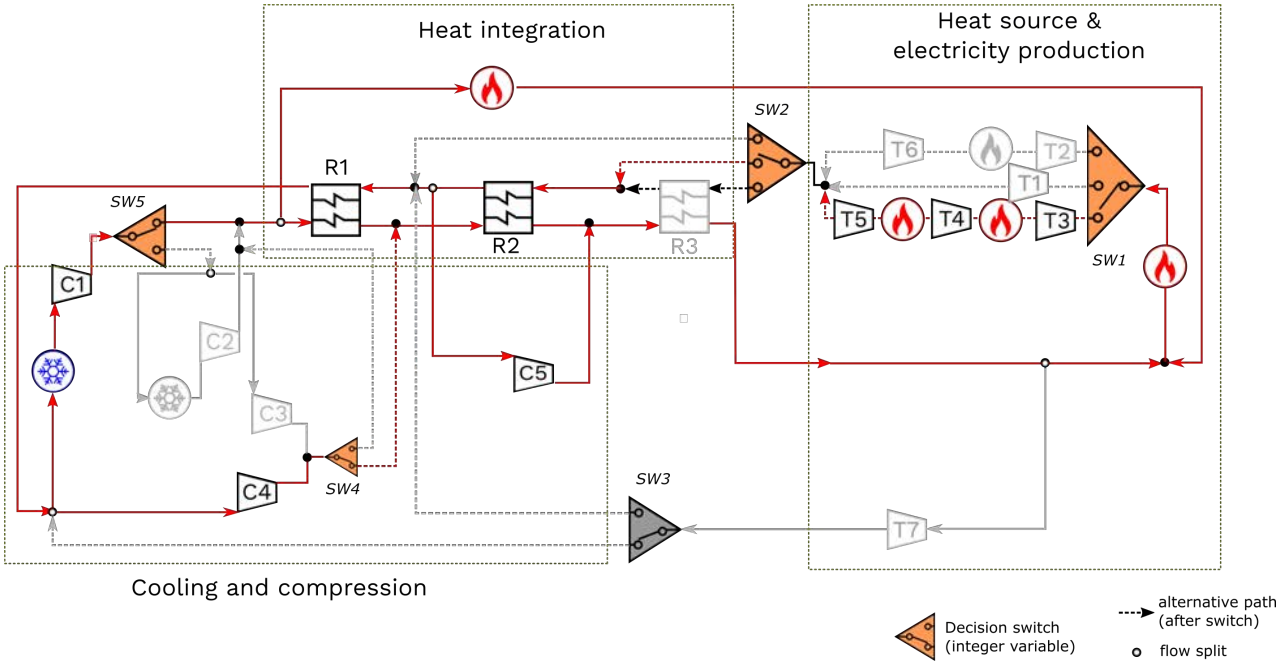

a) Optimal process y={1, 2, 1, 1, 1} in superstructure

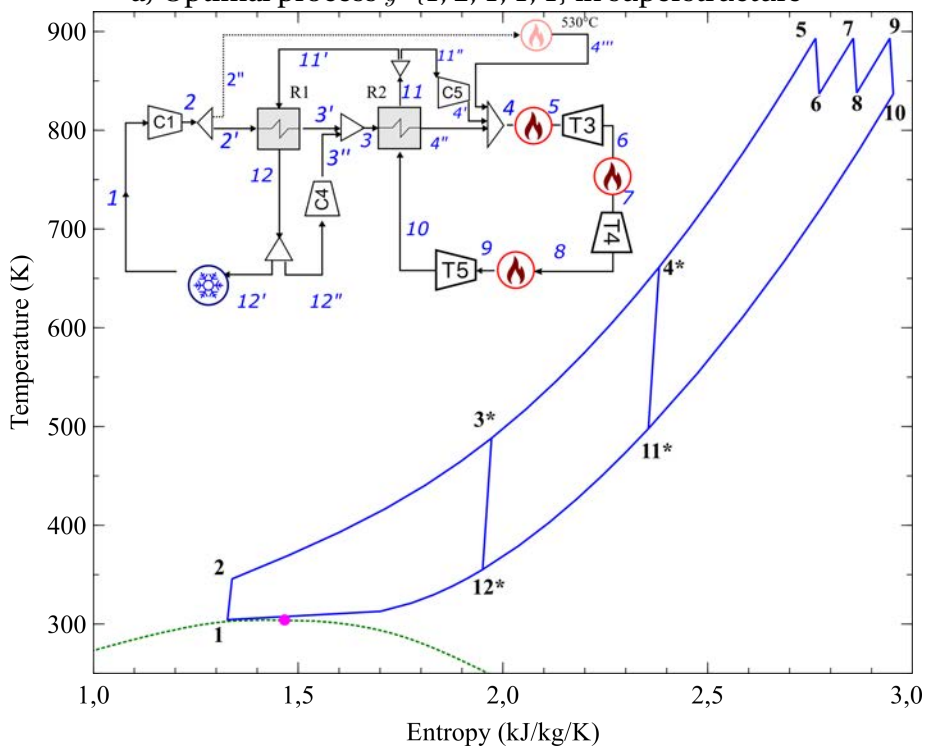

b) Temperature-Entropy diagram of optimal process

Figure 5.5: Energy performance optimization based process synthesis result of the SC-CO_2 Brayton cycle: a) optimal flowsheet denoted Case B, b) Temperature-Entropy diagram

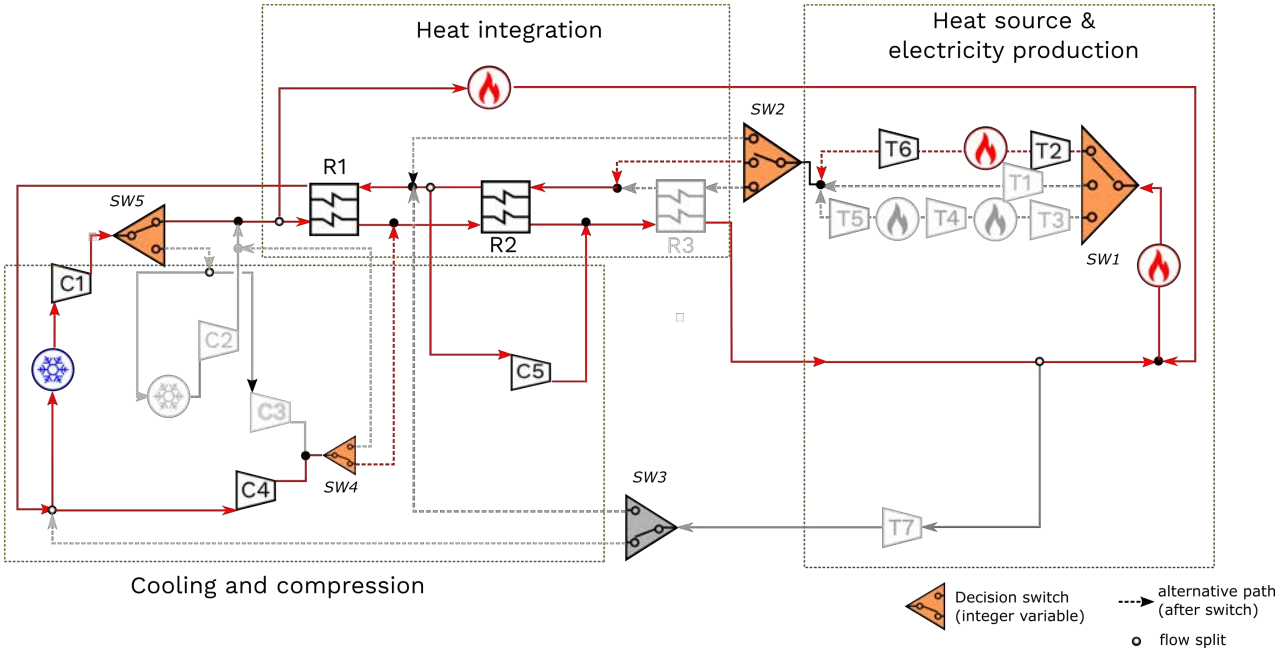

a) Optimal process y={3, 2, 1, 1, 1} in superstructure

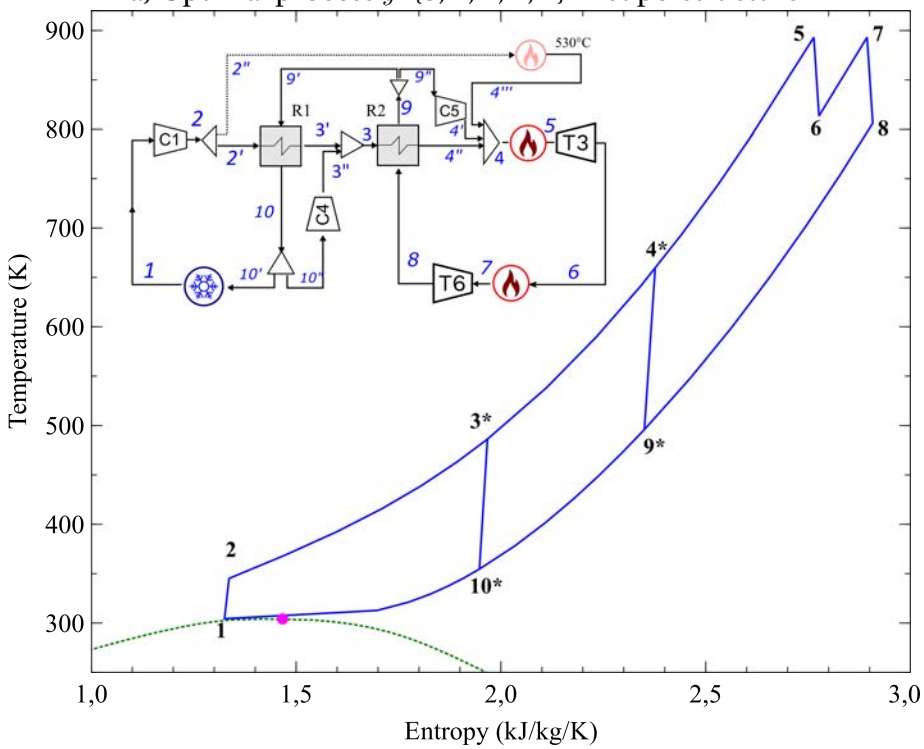

b) Temperature-Entropy diagram of optimal process

Figure 5.6: Energy performance optimization based process synthesis result of the SC-CO_2 Brayton cycle: a) optimal flowsheet denoted Case A b) Temperature-Entropy diagram

As listed in the Table 5.3, final constraints indicate that both recuperators R1 and R2 have reached their minimal thermal pinch lower bound in either case (i.e., $10-0.5$ K). It can be noticed that at the end of optimization, the Case A has the minimal temperature difference at both cold end (hot outgoing stream and the cold inlet stream side) and hot end (hot outgoing stream and the cold inlet stream side) of recuperator R1, indicating a better heat integration has occured in R1 in comparison with the Case B.

For the continuous process variables such as the main cooling temperature ($T_{cooling}$) and the outlet compressor pressure (P_{out} compressor), their optimal value respectively reaches (as for the SS1 optimization situation) the lower and the upper bounds stipulated in this study. Table 5.3 indicates that at the optimum, the cooling temperature tends to 304.35 K while the optimal compressor outlet pressure reaches 30 MPa. The same remarks have been brought out for superstructure SS1 and SS2, indicating that for this framework (determined assumptions and process specification), optimizer performs a research for minimizing the heat release temperature ($T_{cooling}$) and maximizing the pressure of stream (P_{out} main compressor) entering the heat source. Note that setting the main cooling temperature as low as possible and the main compressor C1 outlet pressure as high as possible are common actions taken by process engineers: these actions based on thermodynamic analysis (e.g., T-S diagram) and definition can improve the power cycle efficiency. However, the author prefers to leave those variables to be optimized instead of fixing their values by intuition. This observation can be regarded as an indicator of global optimal point (or at least a local optimum).

Table 5.3: Results for superstructure optimization of SC-CO_2 Brayton cycle

		Case A	Case B
Cycle efficiency (%-pts)	Variable range	55.99	55.58
Integer variables y		{1 2 1 1 1}	{3 2 1 1 1}
P_{in} compressor C1 (MPa)	$x_1 \in 3.3-10$	7.60	7.62
$T_{cooling}$(K)	$x_2 \in 304.35-373.15$	304.35	304.35
Flow to Recompression C4 (%)	$x_3 \in 10^{-4}-50\%$	30	30
P_{out} compressor C1 (MPa)	$x_4 \in 3.3-30$	30.00	29.92
Flow to recompression C3 (%)	$x_5 \in 10^{-6}-0.5$	-	-
P_{out} compressor C2 (MPa)	$x_6 \in 3.3-30$	-	-
T_{R1}cold side out (K)	$x_7 \in 304.35-893.15$	486.69	486.22
Flow to recompression C5 (%)	$x_8 \in 10^{-4}-50\%$	7.7	8.4
T_{R2} hot side out (K)	$x_9 \in 304.35-893.15$	496.25	495.92
T_{R3} hot side out (K)	$x_{10} \in 304.35-893.15$	-	-
P_{out} compressor C5(MPa)	$x_{11} \in 3.3-30$	3.79	3.77
Ratio turbine T2 (-)	$x_{12} \in 1-5$	-	1.84
Ratio turbine T3 (-)	$x_{13} \in 1-5$	1.53	-
Ratio turbine T4 (-)	$x_{14} \in 1-5$	1.53	-
Flow fraction passing to T7 (%)	$x_{15} \in 10^{-4}-50\%$	10^{-4}	10^{-4}
Flow fraction of CO_2 preheated by flue gas (%)	$x_{16} \in 10^{-4}-50\%$	5.04	5.33
Constraints ($\geqq 0$)			
g_1 on R1 hot end ΔT (K)	$(\Delta T-10) \geqq -0.5$	-0.48	-0.50
g_2 on R1 cold end ΔT (K)	$(\Delta T-10) \geqq -0.5$	-0.50	-0.269
g_3 on R2 cold end ΔT (K)	$(\Delta T-10) \geqq -0.5$	-0.48	-0.489
g_4 on R2 hot end ΔT (K)	$(\Delta T-10) \geqq -0.5$	-0.50	-0.498
g_5 on R3 hot end ΔT (K)	$(\Delta T-10) \geqq -0.5$	-	-
g_6 on ratio of main compressor C1 (-)	$(P_2/P_1-1) \geq -0.017$	2.95	2.95
g_7 on on flue gas	$\frac{\dot{Q}_{\text{flue gas}}}{\sum \dot{Q}-\dot{Q}_{\text{flue gas}}}-9\%=0$	-1.4×10^{-6}	-3.0×10^{-6}
Key process parameter (result at the end of optimization)			
CO_2 flowrate in boiler (kg/s)	-	9499.83	9572.31
Power in turbines (MW)	-	1854	1840
Work in compressors (MW)	-	582	591
Power capacity of boiler (MW)	-	2272	2249
Power density (kW/kg/s)		133.90	130.48

For the performed energy-objective optimization, it has been assumed that the heat recovered from the flue gas to the cycle is free of charge, intending to focus only on the cycle efficiency and excluding the boiler influence on the cycle. However, in the consideration of an entire power plant, the flue gas is not free of charge and thus the definition of cycle efficiency needs to be adjusted. The adjusted cycle efficiency is $\eta_{\text{cycle}} = \frac{\dot{W}net}{\sum \dot{Q}}$ with $\sum \dot{Q} = \dot{Q}_{\text{heat}} + \dot{Q}_{\text{reheating}}(\text{if exist}) + \dot{Q}_{\text{flue gas}}$. This new adapted definition of the objective function indicates that previous assumption on the flue gas leads to an overestimated best cycle efficiency. After this update, the best obtained cycle efficiency became 51.37%-pts (Case A) and 50.94%-pts (Case B). This more realistic objective function is adopted for the section 5.3 (application of economic model on the Case A and B layouts) and 5.4 (multi-objective optimization of SS2).

5.2.3 Sensitivity analysis

The purpose of this part is to analyze the influence of the main cooling temperature $T_{cooling}$ (as well as minimal stream temperature) and turbine inlet temperature T_{it} on the superstructure optimization results since they are indicators for ideal Brayton cycle efficiency. The same optimization approach described in Section 5.2 is applied to look for optimal process configuration as well as the corresponding operation parameter. In other words, this step is done by completing "mono-objective" optimization of SS2 for each new values of $T_{cooling}$ and T_{it}.

Main cooling temperature

The minimal stream temperature listed in Table 5.1 is changed to be respectively 308.15 K, 318.15 K and 328.15 K. These new optimizations of SS2 lead to the same two best cycle configurations as obtained above (Case A and B). The optimal process layout is thus concluded to be not sensitive to the cooling temperature under the circumstance of defined assumptions. However, the cycle performance varies with the cooling temperature.

A monotonically decreasing trend is observed in Figure 5.7 (a). The cycle efficiency decreases by 8%-pts when $T_{cooling}$ is increased by 24 K. Further comparisons on optimal main compressor inlet pressure are illustrated on the Figure 5.7 (b) the optimal inlet compressor pressure increases with the cooling temperature. It has been noticed that the highest optimal inlet compressor pressure is actually limited by its upper bound as defined in the Table 5.2. Finally, the main cooling temperature has a limited influence on other process variables such as the flow fraction passing to compressor C4 and the flow fraction passing to compressor C5, Figure 5.7 (c) and (d).

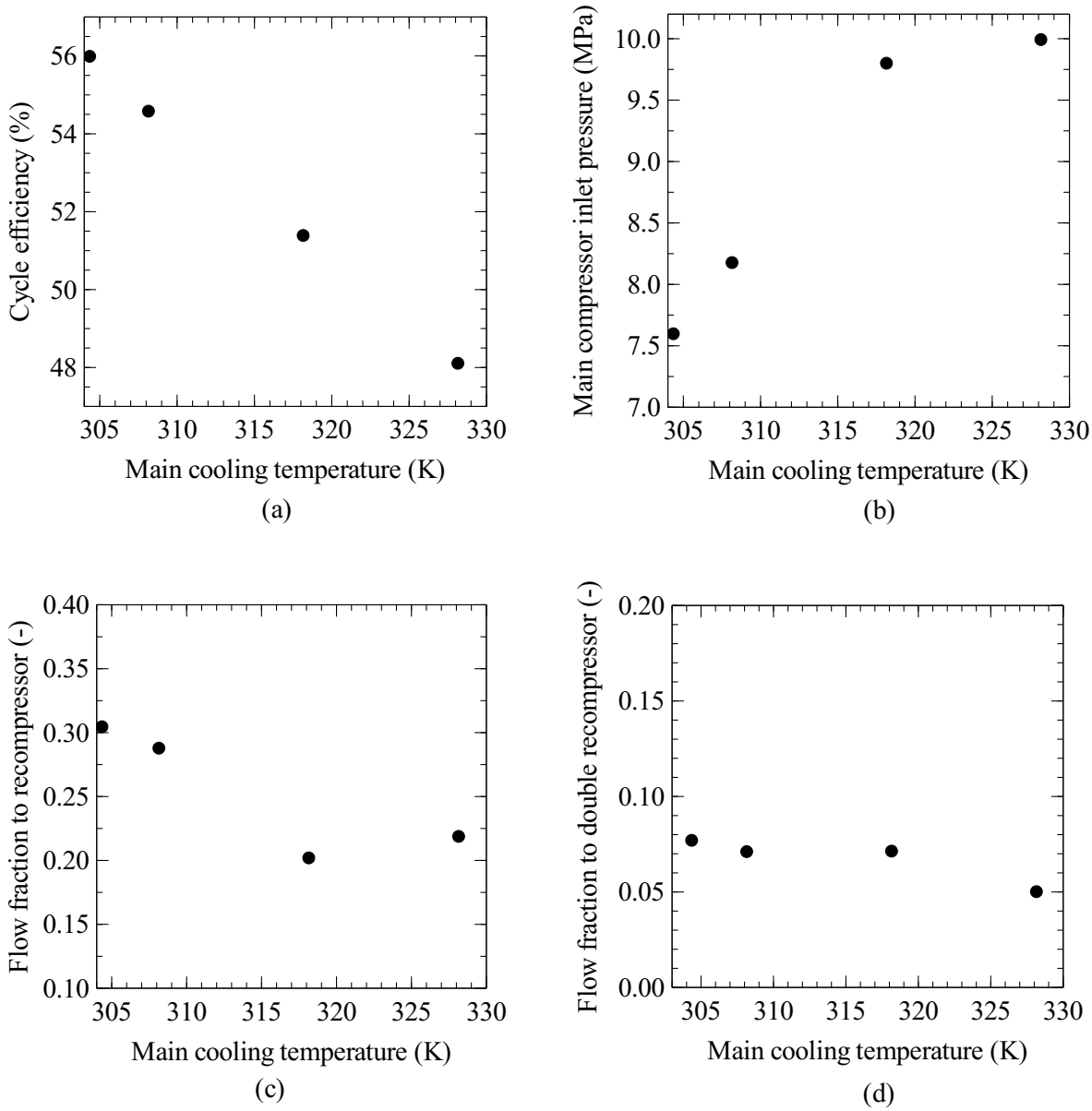

Figure 5.7: Influence of cooling temperature on a) cycle efficiency; b) compressor inlet pressure; c) fraction of flow passing to compressor C4; d) fraction of flow passing to double compressor C5.

Inlet Turbine Temperature

During the assessment of inlet turbine temperature, the boundary of maximum stream temperature and the set of inlet turbine temperature T_{it} are respectively switched to 853.15 K, 993.15 K and 1073.15 K, all other parameters being similar to those used in the initial optimization.

✻ Another promising configuration

Optimizations performed with T_{it} at 993.15 K and 1073.15 K result in a different best process configuration (denoted Case C) (y={3, 1, 1, 1, 1}). It is a single reheating double recompression SC-CO_2 Brayton cycle with three recuperators, Figure 5.8.

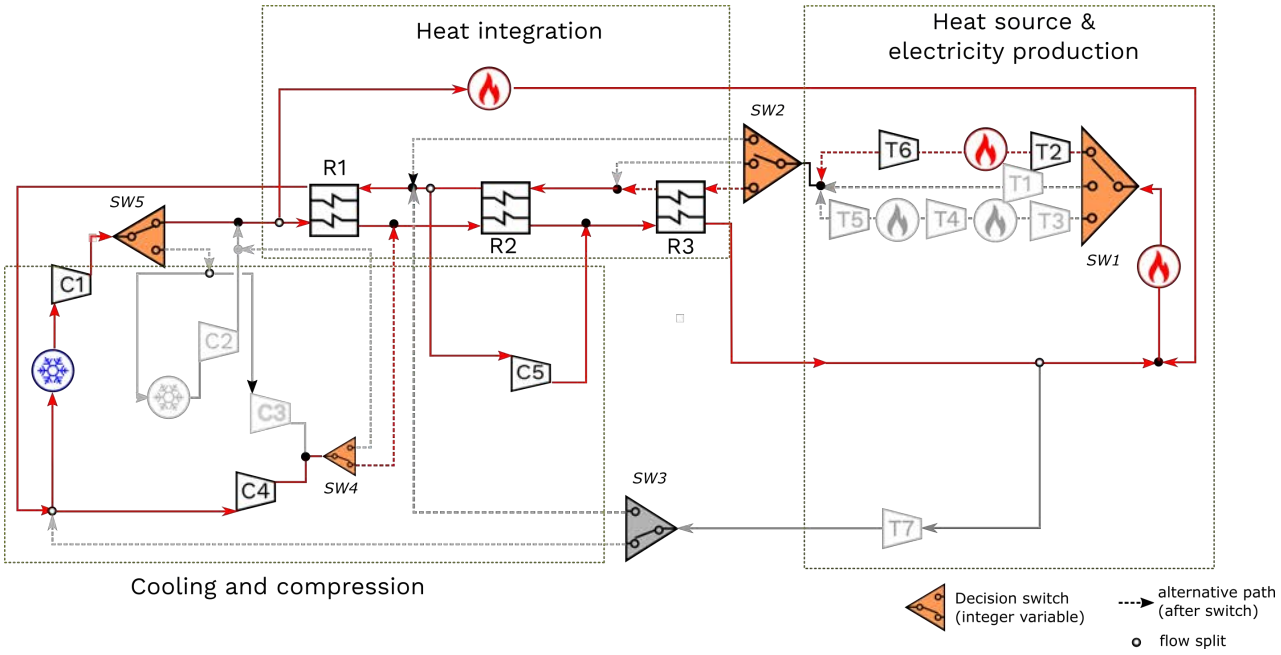

Figure 5.8: Energy optimal process y={3, 1, 1, 1, 1} in the superstructure during higher inlet turbine temperature sensitivity analysis (Case C)

This implies that for higher turbine inlet temperature, more heat is at disposal in hot stream for heat integration.

✻ Sensitivity on process variables

Figure 5.9(a) illustrate that there is a monotonically increasing relationship between turbine inlet temperature T_{it} and the cycle efficiency. Rising the T_{it} by 220 K results in a 9%-pts improvement in cycle efficiency (similar to the sensitivity observed in SS1). The influence of turbine inlet temperature on optimal main compressor outlet pressure is limited. For different T_{it} , the optimal main compressor outlet pressure stays at 30 MPa.

Nevertheless, unlike the case of main cooling temperature, the main compressor inlet pressure and the two aforementioned flow fractions are less impacted by the boiler temperature change.

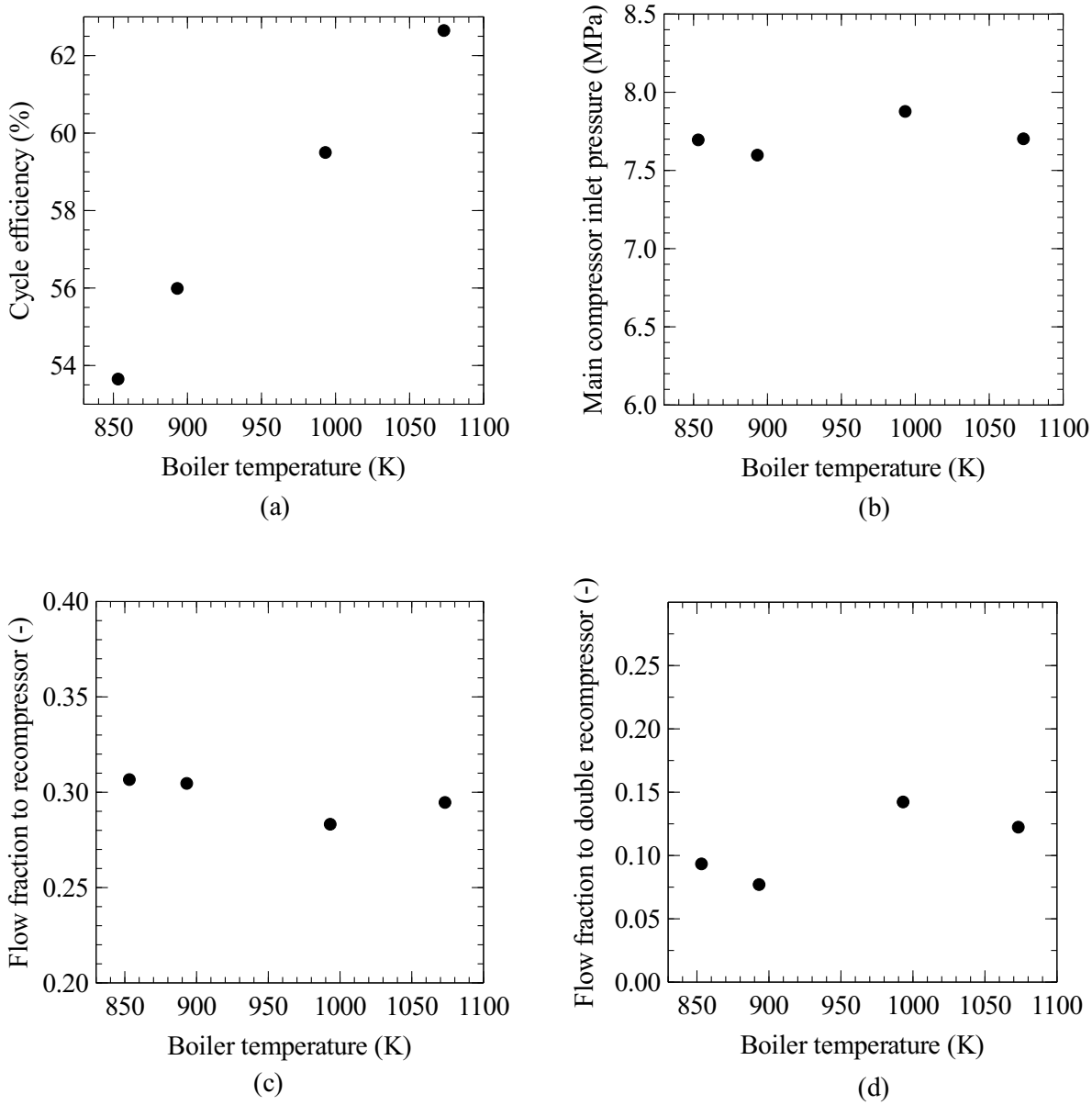

Figure 5.9: Influence of inlet turbine temperature on a) cycle efficiency b) compressor inlet pressure c) fraction of flow pass to compressor C4; d) fraction of flow passing to double compressor C5.

5.3 TECHNO-ECONOMIC ANALYSIS OF SC-CO_2 BRAYTON CYCLE

The techno-economic analysis plays an important role on the path from conception of technology to commercial embodiment. While the conception studies provide specific information on the theoretical process design and component sizing, the techno-economic analysis delivers a deep understanding of costs related to both equipment and performance (efficiency) of the technology. Conducting a techno-economic analysis can then provide useful "cycle economic performance indicator" for decision makers. One of the indicators often applied in the energy field is the levelized cost of electricity (LCOE) as it provides unbiased evaluation of a technology, (Brun et al., 2017).

For the SC-CO_2 Brayton cycle, very few economic information is available given that many of components are still under development and are not readily commercialized. Although published related studies are believed to be highly speculative (Brun et al., 2017), this dissertation tries to perform LCOE calculations that reflect envelop of cost in the literature. The LCOE assessed at conception stage serves as an important technology design criteria. Given that the LCOE results highly depend on the chosen "economic model" (assumptions, costs estimations...), the purpose of this section is not to provide the most accurate or reliable economic approach but to use economic models that enable to make a valid comparison and optimization within comparable system assumptions (section 5.4). In this context, an in-house economic model is used to perform the economic assessment of optimized cycles from the previous section.

5.3.1 Economic Approach adopted by EDF R&D for SC-CO_2 Brayton cycle

N.B. the provided cost functions and indicators (CAPEX, LCOE) do not necessarily reflect the EDF's vision on cost of SC-CO_2 equipment but provides information on relative costs and their dependence with equipment design and operating parameter.

The cost of SC-CO_2 equipment

The methodology to calculate SC-CO_2 Brayton cycle investment costs (CAPEX), operational expenditure costs (OPEX) and levelized cost of electricity (LCOE) is a combination of in-house EDF and literature cost correlations (Driscoll, 2004; Driscoll and Hejzlar, 2004; Caputo et al., 2005; Carlson et al., 2014; Kumar et al., 2015; Shiferaw et al., 2016; Dennis, 2017; Brun et al., 2017; Hinze et al., 2017; Park et al., 2018). These three costs can be expressed as a function of the cost of main components of the SC-CO_2Brayton cycle (C_{EQP}). The component cost is based on

"power function" (Eq. 5.2 and 5.3), improved by in-house correlations to take into account the impact of the high-temperature high pressure on materials, by introducing two factors f_P and f_T, (Mecheri and Wang, 2018).

$$\text{For turbomachinery}: \quad C_{\text{EQP}} = a \times (\mid W \mid)^b \times f_P \times f_T \tag{5.2}$$

$$\text{For heat exchanger}: \quad C_{\text{EQP}} = a \times (UA)^b \times f_P \times f_T \tag{5.3}$$

Where "a" and "b" are empirical parameters that depend on the considered component, Table 5.4.

The factor f_P is related to the maximum component pressure and f_T is related to the maximum component temperature. The following relationships (established in-house) enable to represent the variation of material cost when it occurs an expensive high grade/quality material for relatively high temperature and/or pressure:

$$f_T = \begin{cases} 1 & if\ T_{max} < 673\,\text{K} \\ 5.32 - 0.0238 \times T_{max}(\text{°C}) + 0.00003 \times T_{max}^2(\text{°C}) & if\ T_{max} \geq 673\,\text{K} \end{cases} \tag{5.4}$$

$$f_P = \begin{cases} 1 & if\ P_{max} < 10\,\text{MPa} \\ 0.8 + 0.02 \times P_{max}(\text{bar}) & if\ P_{max} \geq 10\,\text{MPa} \end{cases} \tag{5.5}$$

Table 5.4: Parameters for SC-CO_2 Brayton cycle component cost calculation

Component	a	b
Recuperator	500	1
Chiller	200	1
Turbine	201000	0.8
Compressor	160000	0.8
Boiler (including gas clean up treatment)	562000	1

Capital expenditure (CAPEX) calculation

The most commonly considered methodology to calculate the investment costs (CAPEX) is to decompose the total investment (Eq. 5.6) into:

- the installed equipment cost C_{EQP},

- the direct cost (C_{direct}) including the cost of main equipment, the cost of secondary equipment (pipes, valves, civil engineering, instrumentation and control, etc.), the transportation cost, the land cost, the civil and structure cost,

- and the indirect cost $C_{indirect}$, as it represents engineering, supervision and plant start-up costs.

$$\text{CAPEX}[\$] = \sum C_{\text{EQP}} + C_{direct} + C_{indirect} \tag{5.6}$$

with

$$C_{direct} = C_{piping} + C_{\text{I\&C}} + C_{land} + C_{civil} \tag{5.7}$$

Where C_{piping}, $C_{\text{I\&C}}$, C_{land} and C_{civil} are expressed on function of equipment cost $\sum C_{\text{EQP}}$, using the assumptions listed in Table 5.5 and $C_{indirect}$ is assumed to be $8\% \times (\sum C_{\text{EQP}} + C_{direct})$.

Table 5.5: The in-house economic assumption and index for SC-CO_2 Brayton cycle economic analysis. Based on (Caputo et al., 2005; Kumar et al., 2015; Park et al., 2018)

Content	Unit	Value
Piping	% $\sum C_{\text{EQP}}$	3
I&C (Instrumentation and Control)	% $\sum C_{\text{EQP}}$	5
Land	% $\sum C_{\text{EQP}}$	3
Civil and Transportation	% $\sum C_{\text{EQP}}$	15
Coal price (C_{fuel})	\$/MWh_{th}	10
Currency	\$2017	-
Plant availability ($Hour_{year}$)	h	7884
Plant lifetime (n)	year	40
Discount rate (a)	%	8

The flue gas clean up is included in the boiler equipment cost.

Operational expenditure (OPEX) calculation

The annual operating costs can be divided in three main parts:

$$\text{OPEX} = \text{OPEX}_{\text{O\&M}} + \text{OPEX}_{var} + \text{OPEX}_{fuel}$$

With:

- The fixed operating and maintenance (O&M) cost is defined as a function of the CAPEX: $\text{OPEX}_{\text{O\&M}}[\$/year] = 0.03 \times \text{CAPEX}$

- The variable O&M cost corresponds to consumables, license fees and taxes. This cost is estimated as 3.5 $ /MWh for the considered coal-fired power plant:$\mathrm{OPEX}_{var}[\$/year] = 3.5 \times P_e \times \mathrm{Hour}_{year}$

- The operating cost related to the fuel, OPEX_{fuel}, which depends directly on the net power plant energy production as well as the cost of coal on the market. Here, we will take a coal cost (C_{fuel}) of 10 $ / MWh (about 55 € per ton of coal), including loading costs. $\mathrm{OPEX}_{fuel}[\$/year] = \mathrm{C}_{fuel} \times \sum \dot{Q}/\eta_{boiler} \times \mathrm{Hour}_{year}$

The following assumptions and definitions are taken into account for the OPEX calculation:

Hour_{year} is the number of working hours per year. This value is estimated as 7884 h/year in this dissertation, Table 5.5.

P_e is the electrical generation capacity of the power plant, expressed on MWe. $P_e = \eta_{alt}.\eta_{aux}.W_{net}$

$\eta_{alt} = 0.99$, $\eta_{aux} = 0.97$. These values are estimated by the similarities to the steam coal-fired plant.

W_{net} is the net electrical power produced by the SC-CO_2 Brayton cycle.

$\sum \dot{Q}$ is the thermal power received by SC-CO_2 in the entire power cycle. This heat duty including the heat transfer in the furnace wall, suspension part as well as flue gas. $\sum \dot{Q} = \dot{Q}_{\mathrm{heat}} + \dot{Q}_{\mathrm{reheating}}(\mathrm{if\ exist}) + \dot{Q}_{\mathrm{flue\,gas}}$

η_{boiler} is the boiler efficiency. Considering the similarities between the future SC-CO_2 boiler and the state-of-the-art steam boiler, this boiler efficiency is assumed to be 94%.

LCOE calculation

The Levelized Cost Of Electricity (LCOE) is an aggregated indicator of the overall process costs levelized during the power plant lifetime. It encompasses annualized cost of the investment (CAPEX) using a discount rate, the operational costs, and the obtained electric production.

In this study, the LCOE of the considered power plant is expressed as following:

$$\mathrm{LCOE} = \frac{\mathrm{CAPEX} \times f_a + \mathrm{OPEX}}{P_e \times \mathrm{Hour}_{year}} \tag{5.8}$$

Where f_a is the discount factor that takes into account both the risk aversion of the investor and the investment distribution over the plant lifetime. This quantity depends on the discount rate a and the plant lifetime n (listed in Table 5.5) and is defined by the following relation:

$$f_a = \frac{a(1+a)^{n-1}}{(1+a)^n - 1} \tag{5.9}$$

For a 40 year lifetime power plant with a discount rate of 8%, the discount factor (f_a) is 0.0776. Thus, the discount lifetime of the project ($1/f_a$) is 13 years.

The use of LCOE enables to quantify several trade-offs, such as:

- CAPEX / OPEX trade-offs. For example: "is it worth to increase the investment (e.g. increasing surfaces in heat exchangers) to reduce the operational cost (e.g. by increasing the cycle efficiency)?"
- Production / annual cost trade-offs. For example: "is it worth to spend additional annualized cost (numerator in Eq. 5.8) to increase the production (denominator in eq. 5.8)?"

Therefore, the properties of LCOE makes it a very relevant objective function for optimization in industrial conditions.

5.3.2 LCOE result of the two best energy optimization results

Using the assumptions listed in the above methodology, the power plant with optimized configuration Case A and Case B have a LCOE respectively equals to 62.3 and 60.9 $/MWh, Table 5.6.

Table 5.6: Techno-economic results of two best energy-objective optimized processes (Case A and B)

Content	Unit	Case A	Case B
Cycle efficiency (with penalty introduced by the flue gas utilization)	%	51.37	50.94
Net power plant efficiency LHV ($\eta_{plant} = \eta_{boiler} \times \eta_{cycle} \times \eta_{alt} \times \eta_{aux}$)	%	46.37	45.98
Share of CAPEX in LCOE	$/MWh	26.84	25.69
Share of OPEX in LCOE	$/MWh	35.42	35.16
LCOE	$/MWh	62.26	60.86

By looking into the annual investment (CAPEX on M$/year) in Figure 5.10, the raised turbine and boiler investment costs in Case A are a direct consequence of double reheating configuration. The investment of the recuperators in Case A is 16% higher than that of Case B indicating that larger recuperators are needed to recover the heat duty available in the last turbine outlet stream.

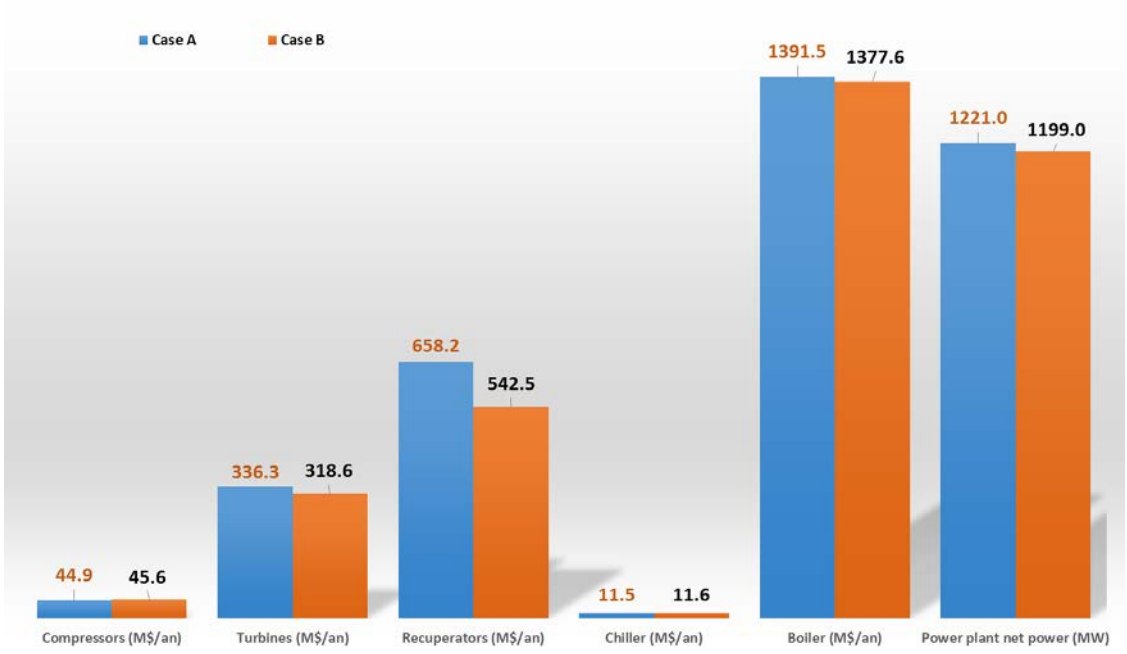

Figure 5.10: Investment cost (CAPEX) of different component on M$/year: Compressors, Turbines, Recuperators, Chiller and Boiler. The last bar chart on the right represents the net production of power plant.

For the two studied cycle layouts, the investment cost of boiler has the most important share among all the equipment (over 40% of the total CAPEX). Thus, future expected innovation on the boiler design will certainly influence the total investment of such a SC-CO_2 power plant. It can be noticed that chillers have low investment costs, because of assumption based on cooling water free of charge. In other circumstances (e.g., in the desert), the cold utility may be expensive.

It is only with the levelized cost of electricity calculation that the compromise between energy and economic aspect is revealed. While the Case A has a higher cycle efficiency in comparison with Case B, its specific investment cost (i.e., CAPEX expressed on $/MWh), its discounted operating cost (i.e., OPEX expressed on $/MWh) and its levelized cost of electricity are higher in comparison with that of Case B, Table 5.6.

Figure 5.11 illustrates the cost share of LCOE on CAPEX (orange) and OPEX (blue) for the two aforementioned processes. In power production industry, new projects planned are usually long term investments, explaining the high ratio share of OPEX in either figure. Though the assumptions on techno-economic analysis may be updated in the future, the importance of OPEX in power industry as well as the global vision of technology provided by the LCOE is highlighted.

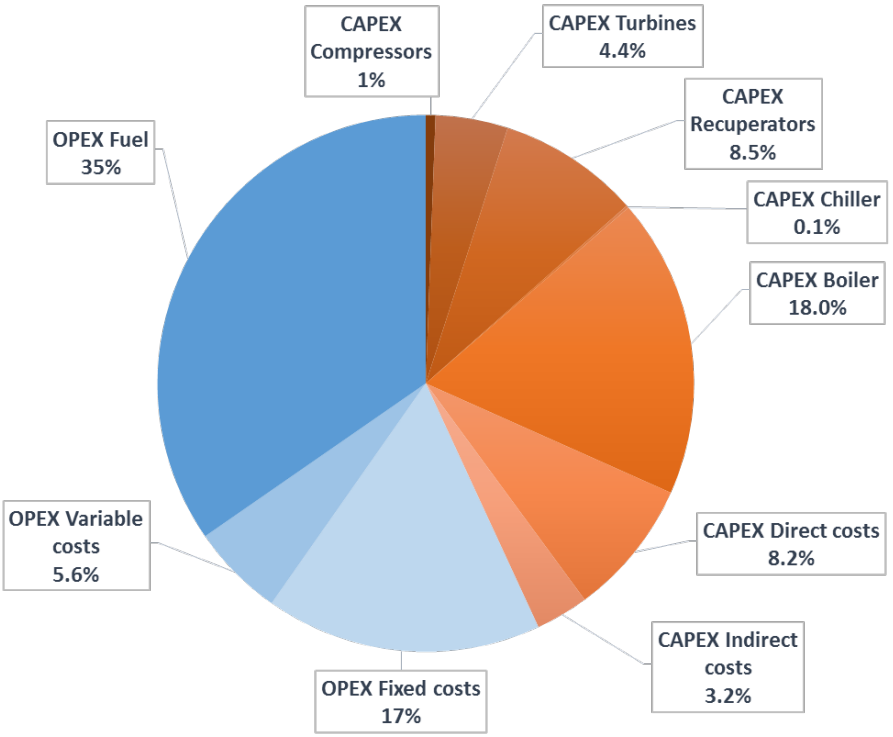

{1 2 1 1 1} Double reheating double recompression

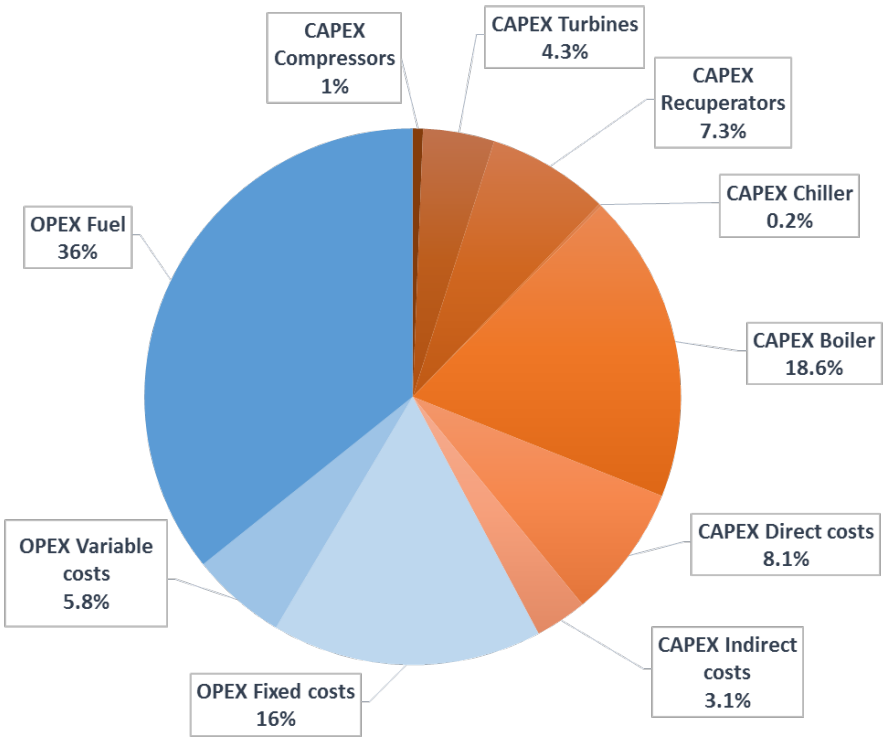

{3 2 1 1 1} Single reheating double recompression

Figure 5.11: Cost share ratio for the two best coal-fired SC-CO_2 power plants (up: Case A, down: Case B)

5.4 MULTI-OBJECTIVE SUPERSTRUCTURE OPTIMIZATION OF SC-CO_2 BRAYTON CYCLE

The process synthesis in industrial conditions usually involves more than a single criterion (objective function), decisions need to be taken in the presence of trade-offs between two or more conflicting objectives. Taken the SC-CO_2 Brayton cycle as example, to reveal its potential in industrial deployment, it is necessary to maximize its cycle efficiency while minimizing the LCOE and CAPEX. When more than one objective function are to be optimized simultaneously, the optimization problem is called multi-objective optimization.

Unlike mono-objective optimization, there is no single solution that simultaneously optimizes the energetic and the economic objectives. The best solutions, often called "Pareto set", "Pareto front" or "non-dominated set", are a group of solutions that cannot further improve any of the objective functions without degrading one or more of the other objective values.

In MIDACO, the multi-optimization is solved by an approach called Utopia–Nadir–Balance decomposition proposed by Schlueter et al. (2015), which is similar to the weighted global criterion method (reviewed in Marler and Arora (2004)). A single super-objective is also formulated based on adding weighing factor to the multiple objectives. However, the Utopia–Nadir–Balance decomposition deployed in MIDACO enables to have a weighing method evolving on function of optimization. It takes into account the best individual of each single objective (Utopia) and the worst individual (Nadir) as well as an indicator of decision maker's preferences (Balance). The Utopia and Nadir are generated within MIDACO, while the Balance (the importance of each objective) is chosen by the user (Schlueter et al., 2015). In a benchmark example carried out by Schlueter et al. (2015), Utopia–Nadir–Balance decomposition leads to a better approximated Pareto front, indicating this method holds advantages over weighted global criterion method.

5.4.1 General mathematical problem formulation for energy aspect optimization

Instead of choosing two conflicting objectives in multi-objective optimization (e.g., efficiency and total investment CAPEX), or carrying out a many-objective optimization (considering all the potential energy and economic criterion); in this dissertation, decision has been made on optimizing three different objectives among which one overall objective function is prioritized (by setting the Balance parameter in MIDACO equals to 1).

Here the levelized cost of electricity (LCOE) is chosen to be the overall objective function

for the following two reasons: a) it is a key criterion that reveals the viability of technology for decision maker ; b) its calculation incorporates the plant electricity production, the power plant efficiency η_{plant}, CAPEX and OPEX. In a mathematics point of view, it is suitable to be chosen as an overall objective function.

As a result, the superstructure multi-objective optimization problem is formulated to minimize LCOE, maximize the plant efficiency and minimize the investment cost CAPEX. The mathematical formulation is expressed as:

$$\begin{aligned} \underset{x,y}{Min}\ & f_1(x,y),\ f_2(x,y),\ f_3(x,y) \qquad (x \in \mathbb{R}^{n_{con}},\ y \in \mathbb{Z}^{n_{int}}) \\ & s.t.\ h(x) = 0 \\ & g(x) \geq 0 \\ & x_{min} \leq x \leq x_{max} \\ & y_{min} \leq y \leq y_{max} \end{aligned} \tag{5.10}$$

where

$f_1 = \text{LCOE}$

$f_2 = -\eta_{\text{cycle}} = \frac{\dot{W}net}{\sum \dot{Q}}$ with $\sum \dot{Q} = \dot{Q}_{\text{heat}} + \dot{Q}_{\text{reheating}}(\text{if exist}) + \dot{Q}_{\text{flue gas}}$

$f_3 = \text{CAPEX}$

The calculation of the power plant LCOE and CAPEX is based on methodology and assumptions introduced in Section 5.3.

In this section, the minimal recuperator pinch ΔT_{pinch} constraint is relaxed (not necessarily fixed at 10 K anymore). Technically, recuperators with temperature pinch value between 2 K and 4 K are already commercialized but their cost is relatively high. An appropriate formulated techno-economic analysis in Section 5.3 would successfully take the rising cost into account during the multi-objective optimization. Therefore, the constraints on temperature difference (cold side and hot side) of recuperators $g_i (i = 1, ..., 5)$ are merely the lowest physical boundary possible for heat exchangers in power production system. $\Delta T_{pinch} \geq 2\,\text{K}$ is set for the aforementioned constraints.

Two other inequality constrains are added respectively for the LCOE lower bound g_8 and the power plant efficiency upper bound g_9, Table 5.7, in order to restrain the exploration within a feasible region.

$h(x)$ is the equality constraint ($\frac{\dot{Q}_{\text{flue gas}}}{\sum \dot{Q} - \dot{Q}_{\text{flue gas}}} - 9\% = 0$) considered in the simulation phase managed by the simulator. Meanwhile, this information is recuperated in the inequality

constraint g_7 as an indicator of constraint convergence. In case of non-convergence of this equality constraint at simulation phase, the optimizer will consider it as a non-respected inequality constraint.

$x = [x_1, ..., x_{20}]$ is continuous optimized variable vector and $y = [y_1, y_2, y_3\, y_4\, y_5]$ is flow switcher decision variable vector (optimized variables). Their considered bounds are listed in Table 5.8.

Table 5.7: Values of fixed process variables, equipment data and constraints used in the superstructure SS2 multi-objective optimization

Hypothesis on fixed variables and Equipment data	
T_{it} turbine inlet temperature (K)	893.15
T_{it} turbine inlet temperature after reheating (K)	893.15
CO_2 flowrate before main cooling (m/s)	6000
MinimumΔT_{pinch} (K)	2
Turbine isentropic efficiency	0.9
Compressor isentropic efficiency	0.89
Pressure drop in every component (% of inlet pressure)	1
Constraints	
g_1 on R1 hot end (K)	$(\Delta T - 2) \geqq -0.001$
g_2 on R1 cold end (K)	$(\Delta T - 2) \geqq -0.001$
g_3 on R2 cold end (K)	$(\Delta T - 2) \geqq -0.001$
g_4 on R2 hot end (K)	$(\Delta T - 2) \geqq -0.001$
g_5 on R3 hot end (K)	$(\Delta T - 2) \geqq -0.001$
g_6 on ratio of main compressor C1 (-)	$(P_2/P_1 - 1) \geq -3.3 \times 10^{-5}$
g_7 on on flue gas	$\frac{Q_{\text{flue gas}}}{\sum Q - Q_{\text{flue gas}}} - 9\% = 0$
g_8	$\text{LCOE} \geq 0$
$g_9$on upper bound of power plant efficiency	$\eta_{plant} < 65\%$

Table 5.8: List of optimized variables and their bounds considered in SS2 multi-objective optimization

Optimized continuous variables x	Bounds
P_{in} compressor C1 (MPa)	$x_1 \in 3.3 - 10$
$T_{cooling}$(K)	$x_2 \in 304.35 - 373.15$
Flow to Recompression C4 (%)	$x_3 \in 10^{-6} - 0.5$
P_{out} compressor C1 (MPa)	$x_4 \in 3.3 - 30$
Flow to recompression C3 (%)	$x_5 \in 10^{-6} - 0.5$
P_{out} compressor C2/MPa	$x_6 \in 3.3 - 30$
T_{R1}cold side out (K)	$x_7 \in 304.35 - 893.15$
Flow to recompression C5 (%)	$x_8 \in 10^{-6} - 0.5$
T_{R2} hot side out (K)	$x_9 \in 304.35 - 893.15$
T_{R3} hot side out (K)	$x_{10} \in 304.35 - 893.15$
P_{out} compressor C5/MPa	$x_{11} \in 3.3 - 30$
Ratio turbine T2 (-)	$x_{12} \in 1 - 5$
Ratio turbine T3 (-)	$x_{13} \in 1 - 5$
Ratio turbine T4 (-)	$x_{14} \in 1 - 5$
(1-Flow Split to T7)/%	$x_{15} \in 10^{-6} - 0.5$
Flow split to flue gas economizer (%)	$x_{16} \in 10^{-6} - 0.5$
Optimized integer variables y	
$SW1$	$y_1 \in \{1,\ 2,\ 3\}$
$SW2$	$y_2 \in \{1,\ 2,\ 3\}$
$SW3$	$y_3 \in \{1,\ 2\}$
$SW4$	$y_4 \in \{1,\ 2\}$
$SW5$	$y_5 \in \{1,\ 2\}$

5.4.2 Results and discussions

The left column in Figure 5.12 shows the formation and evolution of the Pareto as a function of iterations. The right column in the figure lists the corresponding best SC-CO_2 Brayton cycle configurations at different iteration. The initialization of multi-objective optimization is Case B (with LCOE equals to 60.9 \$/MWh) which is one of best points obtained in Section 5.2. At end of 10 000 iterations, it is likely that a preliminary non-dominated set is formed with an optimal LCOE of 56.2 \$/MWh. However, some better compromises between the LCOE and the efficiency are generated at iteration 40 000, and gradually get more densely populated between iteration 40 000 and iteration 65 800 (end of optimization).

The final results of the Pareto front are illustrated by Figures 5.13, 5.14 and 5.15, where historic points during optimization are also plotted (gray points). The 3D representation reflects more clearly the existence of at least one local Pareto Front, which is probably a result of non-convexity introduced by integer variables. The best LCOE point is situated on the Pareto front (surface) and achieves 52.3 \$/MWh. This reduction of 8 \$/MWh represents approximately 67.5 M\$/year for a

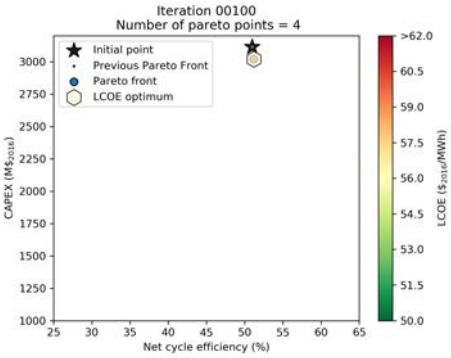

Iteration 100

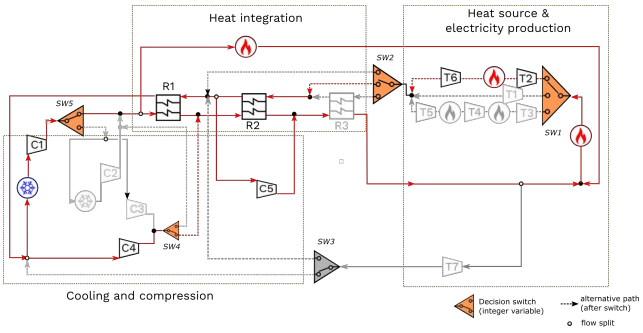

y={3, 2, 1, 1, 1}
single reheating double recompression configuration

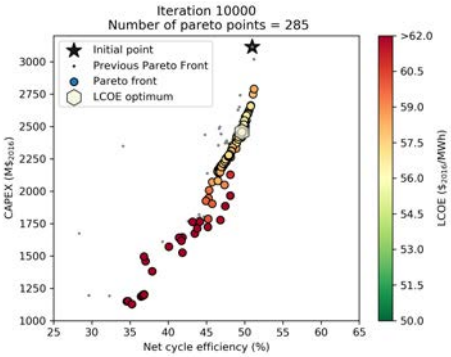

Iteration 10000

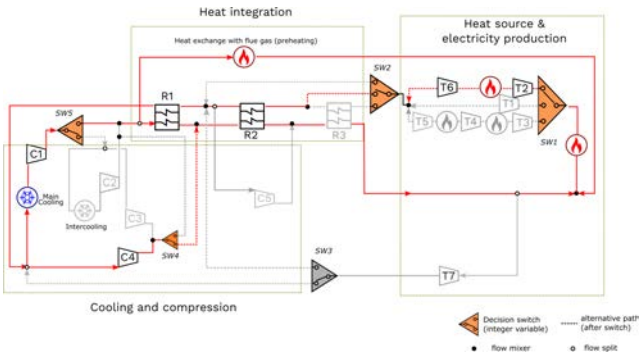

y={3, 2, 1, 1, 1}
single reheating single recompression configuration

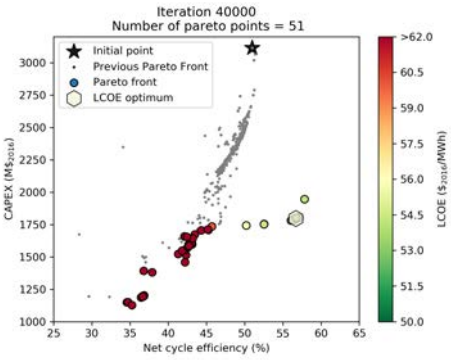

Iteration 40000

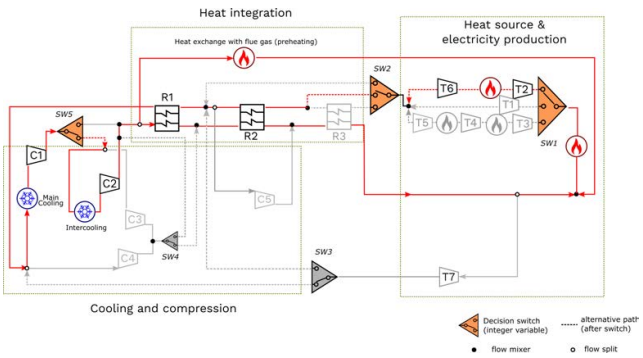

y={3, 2, 1, 1, 2}
single reheating intercooling configuration

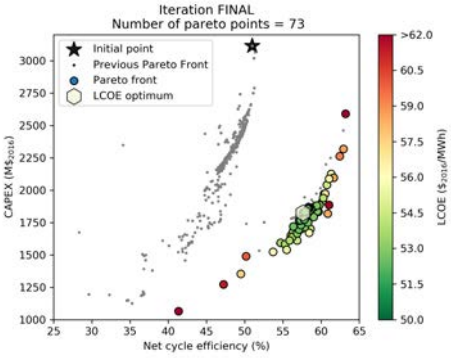

Iteration 65800

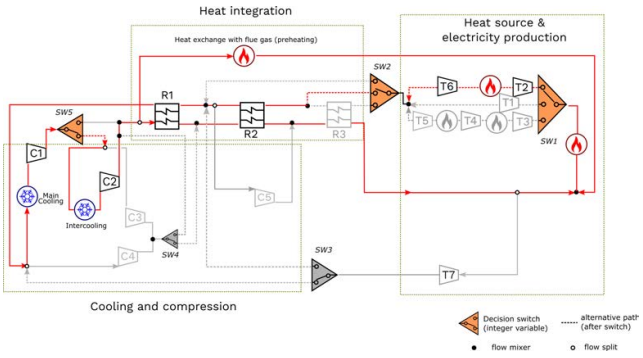

y={3, 2, 1, 1, 2}
single reheating intercooling configuration

Figure 5.12: Evolution of Pareto front on function of iteration as well as instantaneous best process configuration

1000 MWe power plant. With a 40 year life time, the optimized power plant benefice a saving of 2700 M$.

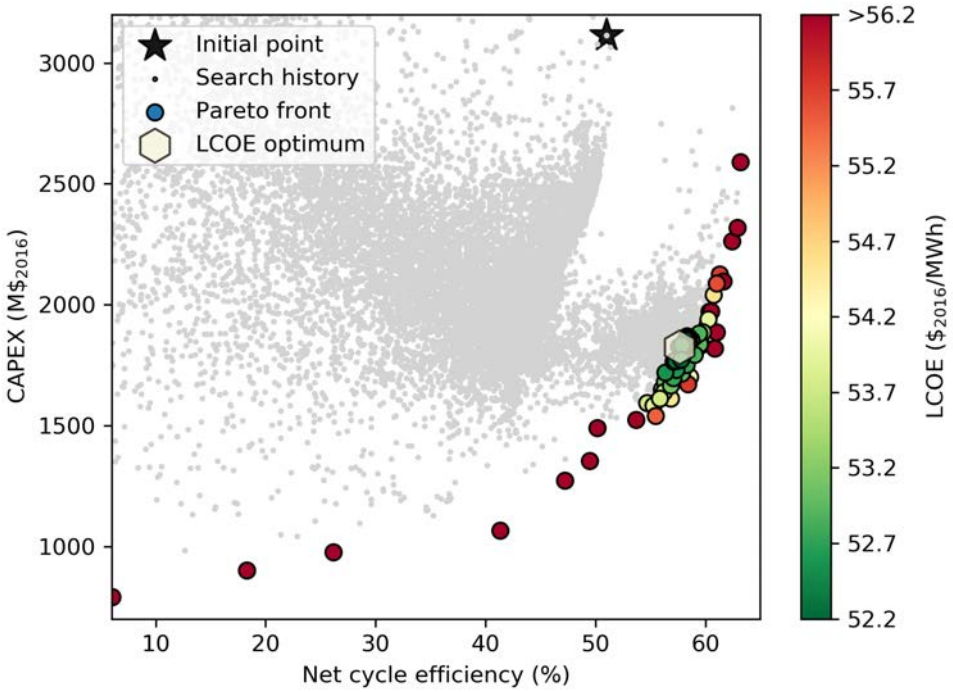

Figure 5.13: Investment cost versus plant efficiency versus LCOE (color axis) at different generation

The results justified the choice of overall objective function LCOE in a multi-objective optimization. Finding the best compromise between cycle efficiency and CAPEX can not satisfy the decision maker's LCOE criterion. Although such bi-objective optimization will also eventually lead to a Pareto front, choosing one appropriate point will be an impossible task since OPEX should not be neglected. On the other hand, if the multi-objective optimization proceed with CAPEX, OPEX and cycle efficiency without any discrimination, a complex normalization will be necessary since they do not have the same order of magnitude. One last situation would be comparing the performance between a LCOE mono-objective optimization and the multi-objective optimization brought out in this thesis.

Despite the successful energy mono-objective optimization, the involvement of techno-economic correlation raises the complexity of optimization problem. Without a proper comparison, it is difficult to judge but author thinks mono-objective optimization on LCOE in such a superstructure may occur difficulty in global optimum search.

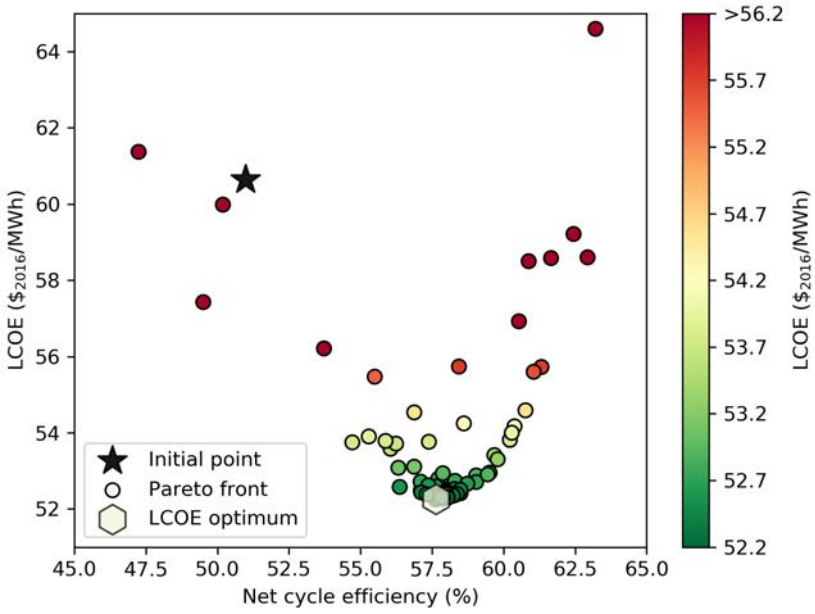

Figure 5.14: 2D cut of Pareto front representing LCOE vs Efficiency

Although there is no obvious evolution of the cost share ratios between “mono-objective” and “multi-objective” optimization (Figure 5.17), the absolute investment cost of different types of equipment have evolved before and after the optimization, Figure 5.16. Their specific OPEX ($/MWh) and CAPEX ($/MWh) have been respectively reduced by 17% and by 12%, Table 5.9. Given the final promising configuration illustrated in Figure 5.18, the chiller investment has increased due to the use of an intercooler. Meanwhile, the optimal configuration excludes compressors C4 and C5, which explains the declined CAPEX on compressors.

Compared with the “mono-objective” optimization result, the “multi-objective” optimization leads to a coal-fired power plant with lower power production (from 1199 MW to 845 MW, Figure 5.16), but with higher efficiency (51.4%-pts raised to 57.6%-pts). The observed LCOE reduction of 15% (from 61 to 52 $/MWh) indicates that a good compromise between energy and economic point of view has been found.

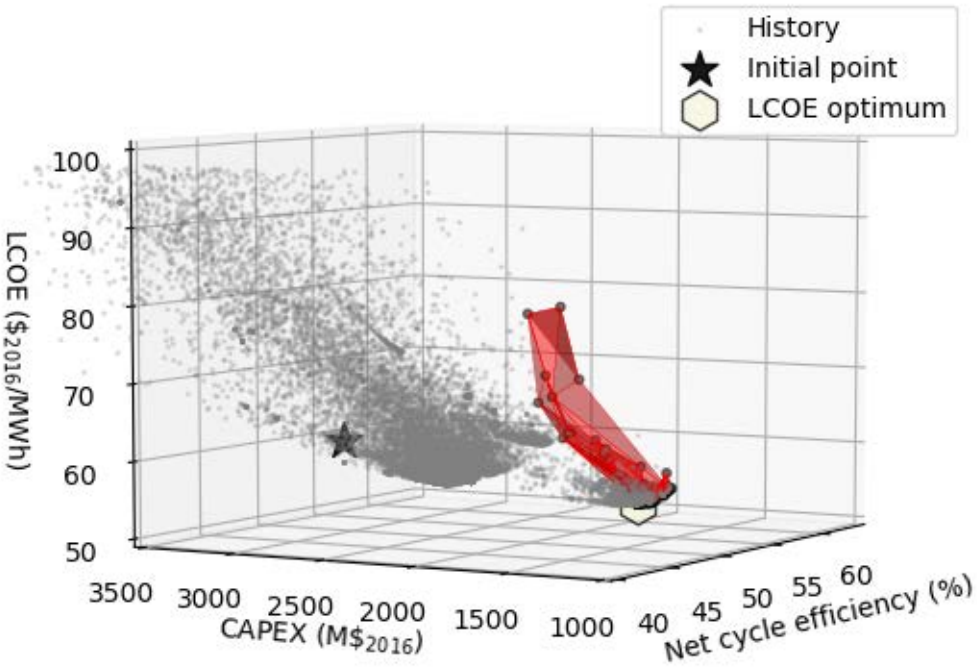

Figure 5.15: 3D representation of optimization iteration process. Axis are the three objective functions: LCOE, CAPEX and net cycle efficiency)

Table 5.9: Techno-economic results of energy-optimal process and LCOE-optimal process

Content	Unit	Initialization (Case B)	Best result
Cycle efficiency (with penalty introduced by flue gas)	%-pts	50.94	57.62
Net power plant efficiency LHV ($\eta_{plant} = \eta_{boiler} \times \eta_{cycle} \times \eta_{alt} \times \eta_{aux}$)	%-pts	45.98	52.01
Production electricity	MWh/year	9 453 871	6 659 504
CAPEX total	$/MWh	25.69	21.31
OPEX total	$/MWh	35.16	30.95
LCOE	$/MWh	60.86	52.26

On the Temperature-Entropy diagram of the "multi-objective" optimal process (Figure 5.19), the compression ratio in compressor C2 is as low as 1.02 (reaching its lower bound). The low temperature high pressure stream exiting C2 favored the heat integration on R1, where its minimal pinch temperature ΔT_{pinch} reaches 5 K. This pinch situating on the hot end of

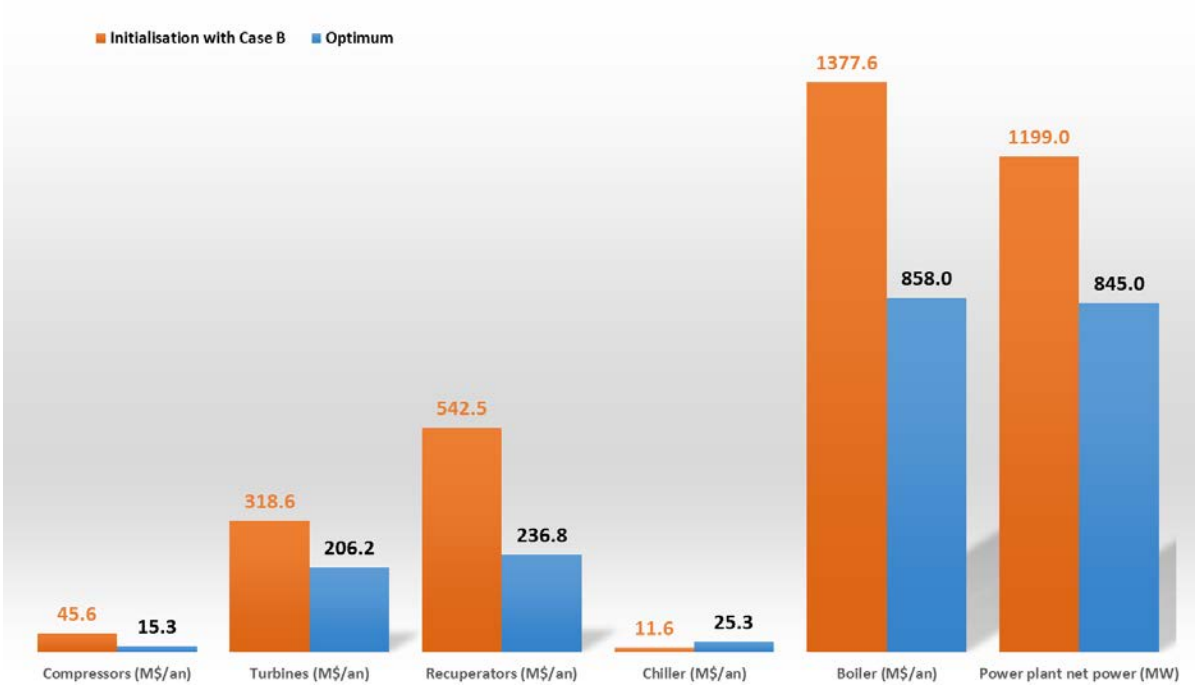

Figure 5.16: Comparison of investment between initialization (energy-optimal) and the LCOE-optimal achieved after the multi-optimization in coal-fired SC-CO_2 power plant application

recuperator R1 is lower than the assumption set in energy mono-objective optimization (10 K minimal pinch), explaining the higher cycle efficiency compared with the SS2 mono-objective optimization. This implies that despite of high cost of heat exchanger, optimization favored a reduced pinch for R1 while the minimal pinch for R2 is set to 20 K.

Together with the CAPEX on recuperator, the final optimal SC-CO_2 Brayton cycle process achieved a good compromise between the energetic role of the recuperator (improvement of cycle performance thanks to the heat integration) and their cost impact (efficient recuperators are expensive).

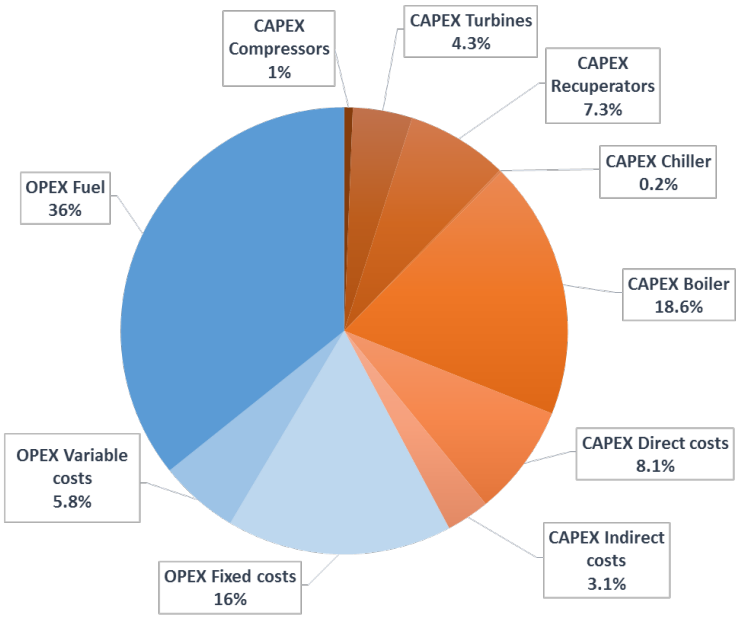

Initial share ratio of LCOE

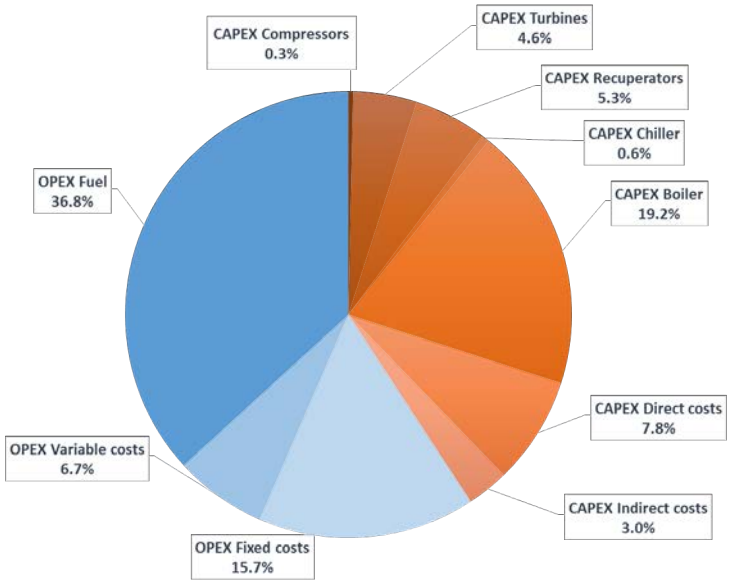

Optimized share ratio of LCOE

Figure 5.17: Multi-optimization result: cost share ratio for the LCOE-optimal coal-fired SC-CO_2 power plant

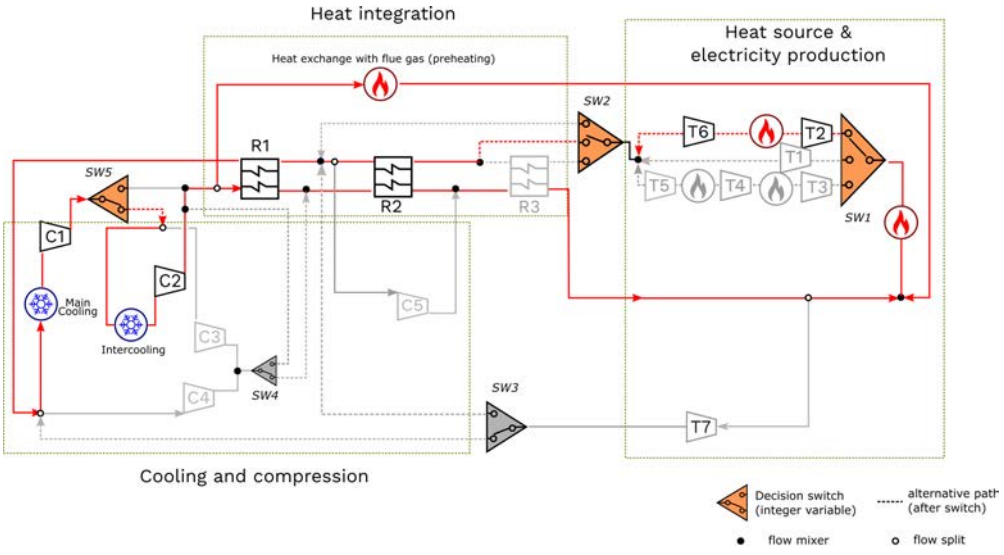

Figure 5.18: optimal process y={3, 2, 1, 1, 2} found for the best LCOE on the Pareto Front

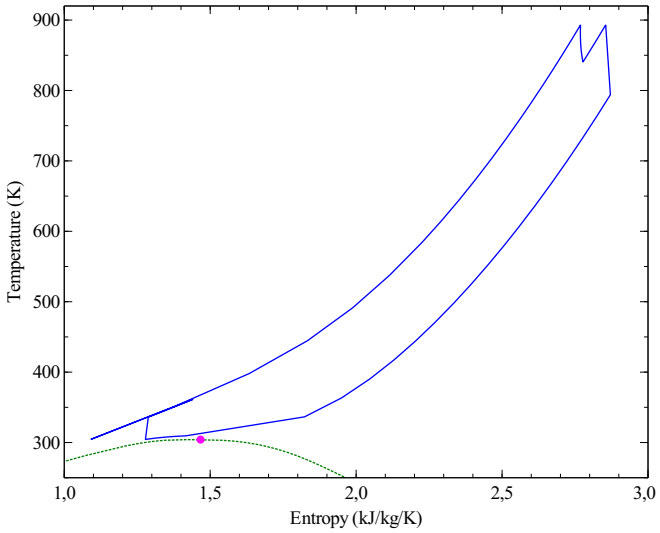

Figure 5.19: Temperature-Entropy diagram of optimal process

To sum up, this chapter deals with a large-scale mono-objective as well as a multi-objective optimization on the superstructure SS2. The implementation of the latter has applied in-house techno-economic correlations.

The construction of superstructure SS2 enables to review larger amount of cycle configuration. Considering the context of coal-fired plant, during the conception phase, the utilization of flue gas has been included as a "free of charge" heat duty. The most promising Brayton cycle has been found to be a “double reheating double recompression-reheating” layout with a best cycle efficiency up to 56.0%-pts. However, when taking into account the flue gas into the total boiler heat duty, the newly defined cycle efficiency is penalized to 51.4%-pts. This reduction implies that certain industrial constraints imposed by the heat source has negative influence on the cycle energy performance. Given that the “working fluid preheating” by flue gas might not exist with other heat sources (such as solar or nuclear applications), additional optimization calculations have been done and show that the SS2 optimization without “working fluid preheating” step (under the same optimization conditions) can find a net cycle efficiency of 52.1%-pts.

By applying the in-house established techno-economic analysis method, the optimal “double reheating-double recompression-preheating” layout (Case A) leads to a LCOE up to 61 $/MWh. And the “single reheating-double recompression-preheating” layout (Case B) has a LCOE that reaches 62 $/MWh.

The performed multi-objective optimization leads to a Pareto front representing the trade-off between economic and energy criteria. The “overall LCOE objective function” helps to find a specific solution which is the most cost-effective (lowest LCOE cycle layout). The most promising configuration evolved to a “single reheating-intercooling-preheating” configuration with a cycle efficiency of 57.2%-pts (with relaxed temperature pinch minimal constraint) and a LCOE of 52.3 $/MWh. From the decision maker’s point of view, this difference enables to save about 68 M$/year.

For the different assumptions, variables bounds as well as different objectives, the constructed superstructure optimization leads to different optimal processes. The proposed methodology can be thus seen as a powerful automatic tool in technology performance and economic evaluation.

CHAPTER 6

Conclusion and perspectives

Highly energy-efficient and cost-effective power cycles for both residential and industrial sectors have become urgent challenges to respond to energy need and to sustainable development. The future trends of power plant are expected to have higher heat integration, higher temperature and pressure levels and possible mixed heat sources. In this context, conceptual process synthesis could be a crucial tool to lead the system configuration without actual manually study each possibility.

For innovative power cycles (here the SC-CO_2 Brayton cycle), one of the principal obstacles in technology deployment is to prove its feasibility, viability and potential in realistic industrial conditions. Researchers in different laboratories or industries are trying to make progress in the construction and control of turbomachinery. In this context, the purpose of this dissertation is to provide a conception and optimization of SC-CO_2 Brayton cycle to assess the potential of this technology for coal-fired power plants.

CO_2 in the vicinity of its critical point or in its supercritical state has some abrupt changes in its physical properties. The isobaric heat capacity of CO_2 approaches infinity at its critical point but also it has bell shape evolution on function of temperature in the supercritical region. The speed of sound has a specific V shape characterizing the critical isotherm in the plane (speed of sound, temperature). A proper selection of equation of state (EoS) has been carried out to have an accurate model to reproduce the aforementioned property variations. By comparing the density, the isobaric heat capacity for six different equations of state (EoS), the Span Wagner (SW) EoS has been identified as the most accurate equations of state for CO_2. While isobaric heat capacity is a regular comparison criterion, the speed of sound is rarely considered for equation of state (EoS) selection. The comparison results imply that the speed of sound can be a severe validation criterion in pure fluid EoS selection.

The proper selection of EoS for the CO_2 property prediction is actually the first step but a very fundamental one for all the SC-CO_2 Brayton cycle studies, yet the deviation of possible EoS for

SC-CO_2 has never been quantified. The next phases of modeling, simulation and preliminary design of a recuperated SC-CO_2 Brayton cycle (RC cycle) are all subsequent tasks that depends on the precision of the chosen EoS. It has been found that certain deviation (uncertainty) on simulation results due to the EoS applied has impacts on equipment sizing and/or optimization result, hence leading to process design and economic issues. However, for the studied SC-CO_2 RC cycle, the influence of the EoS choice is limited, which conforms with the conclusion of Mecheri and Le Moullec (2015).

The optimization based process synthesis applied in this thesis is a Mixed Integer Non Linear Programming (MINLP) superstructure approach. The simulator-based superstructure MINLP optimization explores a set of structural alternatives embedded in a user-defined superstructure and identifies the optimal solution among all through ProSimPlus, a commercial process simulator. The implementation of this approach in a commercial simulator facilitated the graphical building of a superstructure. Moreover, the proposed methodology enables for the first time (to the best of author's knowledge) handling the entire optimization loop within a simulator: both continuous variables and discrete integer variables are optimized simultaneously by optimizer. The application of Mixed Ant Colony Optimization (MIDACO) optimizer in this thesis profits from its black-box and stochastic nature, which enables the future application of MINLP optimization in non-differential problems.

For the industrial context of coal-fired power plant, the usage of low grade flue gas is imposed during the conceptual phase of superstructure. The most energetic promising Brayton cycle (among 1000 alternatives) has been found to be a double reheating-double recompression-reheating layout with a best net cycle efficiency up to 51.4%-pts, which is the best known SC-CO_2 Brayton cycle under same working conditions. However, when not taking into account the flue gas into superstructure optimization (e.g., other heat sources do not require flue gas for CO_2 preheating), the best cycle efficiency rises to 52.1%-pts. This reduction implies that certain industrial constraints imposed by the heat source could have negative influence on the cycle energy performance.

The techno-economic analysis plays an important role on the path from the conception of technology to commercial embodiment. The in-house techno-economic models on SC-CO_2 Brayton cycle components enable access to the capital expenditure (CAPEX), operational expenditure (OPEX) and levelized cost of electricity (LCOE). The latter incorporates other terms as well as cycle performance. For the multi-objective optimization, the LCOE is prioritized as this overall objective function and the two other objectives are CAPEX and cycle efficiency. This kind of implementation helps to identify a specific best rational solution point on the Pareto

front instead of a set of points. Meanwhile it avoids normalizing each objective when their weight in the decision making is not clear.

An initial point of (60.9 $/MWh LCOE, 3124 M$ CAPEX, 51%-pts net cycle efficiency) is considered, which is the best result obtained in the mono-objective optimization. The multi-objective optimization leads to (52.3 $/MWh LCOE, 1826 M$ CAPEX, 57%-pts net cycle efficiency) with a Brayton cycle configuration evolved to "single reheating intercooling-preheating" configuration. This reduction of 8 $/MWh on LCOE represents approximately 67.5 M$/year for a 1000 MWe power plant. With a 40 year life time, the optimized power plant benefices a saving of 2700 M$. As a result, the optimized LCOE, as well as the Pareto only well reflect the trade-off between economic and energy criteria, but also reveal the potential of this technology in economic performance.

Discussion

From the optimization method point of view, progressive studies on the design or/and structural optimization of SC-CO_2 performed can be classified into:

1) parametric screening of the main compressor inlet and outlet pressure for the RC cycle configuration (Chapter 3);

2) Non Linear Programming (NLP) optimization for fixed structural design is applied to validate the superstructure MINLP optimization methodology (Chapter 4).

3) The superstructure MINLP optimization on SS1 and SS2 to find promising parametric and structural design that lead to the most efficient SC-CO_2 Brayton cycle (Chapters 4 and 5).

The features of the aforementioned three studies for SC-CO_2 Brayton cycle are compared in Table 6.1. The sensibility analysis can quickly give engineers the trend of cycle efficiency on function of several parameters and thus quickly improve the objective (e.g., efficiency). However, the scanning procedure enables to vary one parameter at one while the other parameters to be studied are fixed. Consequently, this method can only be guidelines to find effective measures for technology performance improvement but hardly can provide a global optimum that takes all the constraints into account. The NLP optimization with whether derivative-based or derivative-free solver is well disseminated in academics and industry, yet it only deals with continuous variables and does not allow to optimize automatically process configuration. The MINLP superstructure method carried out in this dissertation, on the other hand, explores the most promising (either energy aspect or techno-economic aspect) SC-CO_2 Brayton cycle process configuration within the defined superstructure. It is able to propose new structural alternatives and has a large searching space thanks to the combination of switcher

positions. This methodology is also employed for the multi-objective MINLP superstructure optimization. A Pareto front is generated which enables rational decision making. MINLP superstructure optimization can then be seen as a powerful tool in technical and economic performance of technology.

The building of the superstructure needs indeed expert knowledge to decide which structural alternatives should be included. However, the other two types of optimization obligate also certain experience on technology itself. Strategies proposed in this thesis help to reduce the number of variables to be optimized, the constraints to be considered as well as to improve convergence of optimization. However, the superstructure may take a large number of meaningless structures into account, thus computational effort is relatively large.

Terms	Optimization by sensibility analysis	NLP Optimization	Superstructure MINLP Optimization
Structure space definition	Specific structure	Specific structure	Superstructure
Optimization variable	1 at a time	continuous variable	continuous and integer variable
Way to find optimum	Simulation & Graphical comparison	MIDACO	MIDACO
(Near-) global optimal solution?	×	✓	✓
Required development time	+	++	+++

Table 6.1: Comparisons between the methodologies employed in this thesis for the analysis and synthesis of thermal power plants

Future work

The simple cost estimation in this dissertation provides "cycle economic performance indicator" for decision makers. However, further cost sensitivity analysis on some specific component would enlighten the industrial employment path for SC-CO_2 Brayton cycle. For example, it would be interesting to carry out multi-objective techno-economic optimization with scenarios "high cost exchanger" or "high cost turbomachinery" in order to compare with the "reference" scenario proposed in this thesis.

In addition, the uncertainty involved in the component cost model should be evaluated. Involving hazard factor for innovative but low maturity component in the entire LCOE calculation would indicate reliability of the final economic indicator (Neveux et al., 2017). For example, if the compressor is the most innovative component of the entire processes, during the LCOE calculation, a higher uncertainty will be introduced compared with the chiller, which is a component with mature technology.

The present thesis only deals with superstructure within energy systems. With the established methodology, it is possible to optimize and evaluate other known or unknown (grassroot) processes (e.g., distillation) in both performance and economic feature. In particular, it would be interesting to carry out a superstructure MINLP optimization for the state-of-the-art USC-steam power plant. We may wonder if the actual process configuration can still be improved? Do the "rule of thumb" engineering methods have already brought the current USC-steam power cycle to the highest achievable energetic and economic performances?

One of future perspectives on the methodology development concerns implementation of exergy-based analysis as one final step (post analysis) after multi-objective optimization. Although exergy analysis considers both the quality and quantity of energy, it is recommended to consider this approach as post result analysis to understand the choice of optimizer. Note that global optimizations often achieve good compromise in an overall situation, but not necessarily exergy minimization in every component.

A simple component sizing as well as simplified component cost models have been employed during the economic assessments in this thesis. Future improvement on cost estimation can be expected following the state-of-the-art evolution. The simulator-based process synthesis methodology elaborated enables to easily adjust constraints or cost model within the framework.

Last but not least, automatic structural evolution is expected to be one of future perspectives. The superstructure definition is found to be usually difficult and error-prone and impossible process alternatives are also considered during the optimization. Proposing a generic conception of structure evolution without any manual input for technology specification would be a promising solution.

Bibliography

C.S. Adjiman, I.P. Androulakis, and C.A. Floudas. Global optimization of mixed-integer nonlinear problems. *AIChE Journal*, 46(9):1769–1797, 2000.

T. Ahadi-Oskui, S. Vigerske, I. Nowak, and G. Tsatsaronis. Optimizing the design of complex energy conversion systems by branch and cut. *Computers & Chemical Engineering*, 34(8):1226 – 1236, 2010.

Y. Ahn and J.l. Lee. Study of various brayton cycle designs for small modular sodium-cooled fast reactor. *Nuclear Engineering and Design*, 276:128 – 141, 2014.

Y. Ahn, S.J. Bae, M. Kim, S.K. Cho, S. Baik, J.I. Lee, and J.E. Cha. Review of supercritical CO_2 power cycle technology and current status of research and development. *Nuclear Engineering and Technology*, 47(6):647 – 661, 2015.

A.D. Akbari and S.M.S. Mahmoudi. Thermoeconomic analysis & optimization of the combined supercritical CO_2 (carbon dioxide) recompression Brayton/organic Rankine cycle. *Energy*, 78: 501–512, 2014.

N. Alpy, L. Cachon, D. Haubensack, J. Floyd, N. Simon, L. Gicque, G. Rodriguez, M. Saez, and G. Laffont. Gas cycle testing opportunity with ASTRID, the french sfr prototype. *The 4th International Symposium-Supercritical CO_2 Power Cycles*, 2014.

J.B. Ang. CO_2 emissions, energy consumption, and output in france. *Energy Policy*, 35(10):4772 – 4778, 2007.

G. Angelino. Carbon dioxide condensation cycles for power production. *ASME. J. Eng. Power.*, 1968.

G. Angelino. Real gas effects in carbon dioxide cycles. *ASME Paper*, No. 69-GT-103:1–12, 1969.

M.A. Anisimov, S.B. Kiselev, J.V. Sengers, and S. Tang. Crossover approach to global critical phenomena in fluids. *Physica A: Statistical Mechanics and its Applications*, 188(4):487 – 525, 1992.

M. Aritomi, T. Ishizuka, Y. Muto, and N. Tsuzuki. Performance test results of the supercritical CO_2 compressor for a new gas turbine generating system. *ASME. International Conference on Nuclear Engineering, 18th International Conference on Nuclear Engineering*, 2010.

N. Armaroli and V. Balzani. *Energy for a Sustainable World*. Wiley-VCH Verlag GmbH & Co. KGaA, 2010. ISBN 9783527633593.

Z. Bai, G. Zhang, Y. Li, G. Xu, and Y. Yang. A supercritical CO_2 brayton cycle with a bleeding anabranch used in coal-fired power plants. *Energy*, 142:731–738, 2018.

O.E. Balje. A study on design criteria and matching of turbomachines: Part a Similarity relations and design criteria of turbines. *Transactions of the ASME*, Series A, 1962a.

O.E. Balje. A study on design criteria and matching of turbomachines: Part b Compressor and pump performance and matching of turbocomponents. *Transactions of the ASME*, Series A, 1962b.

O.E. Balje. *Turbomachines: A Guide to Design, Selection and Theory*. Wiley, 1981. ISBN 0471060364.

S.D. Barnicki and J.J. Siirola. Process synthesis prospective. *Computers & Chemical Engineering*, 28(4):441 – 446, 2004.

P.I. Barton. The sequential modular strategy for steady-state process simulation. Technical report, Departement of Chemical Engineering,Massachussetts Institute of Technology, 2010.

H. Behnejad, H. Cheshmpak, and A. Jamali. The Extended Crossover Peng-Robinson Equation of State for Describing the Thermodynamic Properties of Pure Fluids. *Journal of Statistical Physics*, 158(2):372–385, 2015.

P. Belotti, J. Lee, L. Liberti, F. Margot, and A. Wächter. Branching and bounds tighteningtechniques for non-convex MINLP. *Optimization Methods and Software*, 24(4-5): 597–634, 2009.

M. Benedict, G.B. Webb, and L.C. Rubin. An Empirical Equation for Thermodynamic Properties of Light Hydrocarbons and Their Mixtures II. Mixtures of Methane, Ethane, Propane, and n-Butane. *The Journal of Chemical Physics*, 10(12):747–758, 1942.

H.Y. Benson. Mixed integer nonlinear programming using interior-point methods. *Optimization Methods and Software*, 26(6):911–931, 2011.

S.M. Besarati, K. Atashkari, A. Jamali, A. Hajiloo, and N. Nariman-Zadeh. Multi-objective thermodynamic optimization of combined Brayton and inverse Brayton cycles using genetic algorithms. *Energy Conversion and Management*, 51(1):212–217, 2010.

R.A. Bidkar, G. Musgrove, M. Day, C.D. Kulhanek, T. Allison, A.M. Peter, D. Hofer, and J. Moore. Conceptual designs of 50 MWe and 450 MWe supercritical CO_2 turbomachinery trains for power generation from coal. part 2: Compressors. *The 5th International Symposium - Supercritical CO_2 Power Cycles*, pages 1–17, 2016.

L.T. Biegler. *Nonlinear Programming: Concepts, Algorithms, and Applications to Chemical Processes*. 2010. ISBN 978-0-89871-702-0.

L.T. Biegler and J.E. Cuthrell. Improved infeasible path optimization for sequential modular simulators-ii: the optimization algorithm. *Computers & Chemical Engineering*, 9(3):257 – 267, 1985.

M. Binotti, M. Astolfi, S. Campanari, G. Manzolini, and P. Silva. Preliminary assessment of sCO_2 cycles for power generation in csp solar tower plants. *Applied Energy*, 204:1007 – 1017, 2017.

F.J. Blas and L.F. Vega. Thermodynamic behaviour of homonuclear and heteronuclear Lennard-Jones chains with association sites from simulation and theory. *Molecular Physics*, 92(1):135–150, 1997.

F.J. Blas and L.F. Vega. Prediction of binary and ternary diagrams using the statistical associating fluid theory (saft) equation of state. *Industrial & Engineering Chemistry Research*, 37(2):660–674, 1998.

P. Bonami, L.T. Biegler, A.R. Conn, G. Cornuéjols, I.E. Grossmann, C.D. Laird, J. Lee, A. Lodi, F. Margot, N. Sawaya, and A. Wächter. An algorithmic framework for convex mixed integer nonlinear programs. *Discrete Optimization*, 5(2):186 – 204, 2008. In Memory of George B. Dantzig.

P.M. Boston and P.M. Mathias. Phase equilibria in a third-generation process simulator. In *The 2nd International Conference on Phase Equilibria and Fluid Properties in the Chemical Process Industries*, pages 823–849, West Berlin, 1980.

BP. British petroleum company energy outlook 2017 edition, 2017. URL `https://www.bp.com/`.

C. Bravo-Bravo, J.G. Segovia-Hernández, C. Gutiérrez-Antonio, A.L. Durán, A. Bonilla-Petriciolet, and A. Briones-Ramírez. Extractive dividing wall column: Design and optimization. *Industrial & Engineering Chemistry Research*, 49(8):3672–3688, 2010.

K. Brun, P. Friedman, and R. Dennis. *Fundamentals and Applications of Supercritical Carbon Dioxide (sCO_2) Based Power Cycles*. 2017.

R. Brunet, J.A. Reyes-Labarta, G. Guillén-Gosálbez, L. Jiménez, and D. Boer. Combined simulation optimization methodology for the design of environmental conscious absorption systems. *Computers & Chemical Engineering*, 46(Supplement C):205 – 216, 2012.

M.R. Bussieck and S. Vigerske. MINLP solver software, 2014.

J.A. Caballero, D. Milan-Yanez, and I.E. Grossmann. Rigorous design of distillation columns: Integration of disjunctive programming and process simulators. *Industrial and Engineering Chemistry Research*, 44(17):6760–6775, 2005.

L. Cachon, C. Biscarrat, F. Morin, D. Haubensack, E. Rigal, I. Moro, F. Baque, S. Madeleine, G. Rodriguez, and G. Laffont. Innovative power conversion system for the french sfr prototype, astrid. *American Nuclear Society*, 2012.

A.C. Caputo, M. Palumbo, P.M. Pelagagge, and F. Scacchia. Economics of biomass energy utilization in combustion and gasification plants: effects of logistic variables. *Biomass and Bioenergy*, 28(1):35 – 51, 2005.

E.C. Carlson. Don't gamble with physical properties for simulations. *Chemical Engineering Progress*, pages 35–46, 1996.

M.D Carlson, A.K. Kruizenga, C. Schalansky, and D.F. Fleming. Sandia progress on advanced heat exchangers for sCO_2 brayton cycles. *The 4th International Symposium -Supercritical CO_2 Power Cycles*, 2014.

J. Cha, T. Lee, J. Eoh, S. Seong, S. Kim, D. Kim, M. Kim, T. Kim, and K. Suh. Development of a supercritical CO_2 Brayton energy conversion system coupled with a sodium cooled fast reactor. *Nuclear Engineering and Technology*, 41(8):1025–1044, 2008.

R. Chacartegui, J.M. Muñoz de Escalona, D. Sánchez, B. Monje, and T. Sánchez. Alternative cycles based on carbon dioxide for central receiver solar power plants. *Applied Thermal Engineering*, 31(5):872–879, 2011.

W.G. Chapman, K.E. Gubbins, G. Jackson, and M. Radosz. Saft: Equation-of-state solution model for associating fluids. *Fluid Phase Equilibria*, 52:31 – 38, 1989.

Q. Chen and I.E. Grossmann. Recent developments and challenges in optimization-based process synthesis. *Annual Review of Chemical and Biomolecular Engineering*, 8:249–283, 2017.

Y. Chen, J.C. Eslick, I.E. Grossmann, and D.C. Miller. Simultaneous process optimization and heat integration based on rigorous process simulations. *Computers & Chemical Engineering*, 81:180 – 199, 2015. Special Issue: Selected papers from the 8th International Symposium on the Foundations of Computer-Aided Process Design (FOCAPD 2014), July 13-17, 2014, Cle Elum, Washington, {USA}.

W. Cheng, W. Huang, and Y. Nian. Global parameter optimization and criterion formula of supercritical carbon dioxide brayton cycle with recompression. *Energy Conversion and Management*, 150:669 – 677, 2017.

B.K.S. Cheung, A. Langevin, and H. Delmaire. Coupling genetic algorithm with a grid search method to solve mixed integer nonlinear programming problems. *Computers & Mathematics with Applications*, 34(12):13 – 23, 1997.

J. Cho, H. Shin, H. Ra, G. Lee, C. Roh, B. Lee, and Y. Baik. Research on the development of a small-scale supercritical carbon dioxide power cycle experimental test loop. *The 5th International Symposium - Supercritical CO_2 Power Cycles*, 2016.

M. Corbetta, I.E. Grossmann, and F. Manenti. Process simulator-based optimization of biorefinery downstream processes under the Generalized Disjunctive Programming framework. *Computers & Chemical Engineering*, 88(Supplement C):73 – 85, 2016.

F. Crespi, G. Gavagnin, D. Sánchez, and G.S. Martínez. Supercritical carbon dioxide cycles for power generation: A review. *Applied Energy*, 195:152 – 183, 2017.

K. Deb, A. Pratap, S. Agarwal, and T. Meyarivan. A fast and elitist multiobjective genetic algorithm: NSGA-II. *IEEE Transactions on Evolutionary Computation*, 6(2):182–197, Apr 2002.

R. Dennis. Overview of supercritical carbon dioxide based power cycles for stationary power generation. *Advanced Turbines and Supercritical CO_2 Power Cycles Programs*, 2017.

D. Hofer . Phased approach to development of a high temperature CO_2 power cycle pilot test facility . *The 5th International Symposium - Supercritical CO_2 Power Cycles*, 2016.

DIADEM. DIPPR 801 database. version 2015.

U.M. Diwekar, I.E. Grossmann, and E.S. Rubin. An MINLP process synthesizer for a sequential modular simulator. *Industrial & Engineering Chemistry Research*, 31(1):313–322, 1992.

DOE. US department of energy project profile: 10-megawatt supercritical carbon dioxide turbine, 2015.

M. Dong, X. Cheng, and Q. Niu. A constrained particle swarm optimization algorithm with oracle penalty method. *Applied Mechanics and Materials*, 303-306:1519–1523, 2013.

L. Dordain, J.Y. Coxam, J.R. Quint, J.P.E. Grolier, E.W. Lemmon, and S.G. Penoncello. Isobaric heat capacities of carbon dioxide and argon between 323 and 423 K and at pressures up to 25 MPa. *Journal of Supercritical Fluids*, 8(3):228–235, 1995.

M. Dorigo. *Optimization, learning and natural algorithms*. PhD thesis, 1992.

Dortmund DataBank. Database supplied in detherm by dechema company. 2015.

V. Dostal, M.J. Driscoll, and P. Hejzlar. *A supercritical carbon dioxide cycle for next generation nuclear reactors*. PhD thesis, MIT, 2004.

A.W. Dowling and L.T. Biegler. A framework for efficient large scale equation-oriented flowsheet optimization. *Computers & Chemical Engineering*, 72:3 – 20, 2015.

M.J. Driscoll. Supercritical CO_2 Plant Cost Assessment. Technical report, MIT, 2004.

M.J. Driscoll and P. Hejzlar. 300 MWe supercritical CO_2 plant layout and design. Report, 2004.

M.T. Dunham and B.D. Iverson. High-efficiency thermodynamic power cycles for concentrated solar power systems. *Renewable and Sustainable Energy Reviews*, 30:758–770, 2014.

M.A. Duran and I.E. Grossmann. An outer-approximation algorithm for a class of mixed-integer nonlinear programs. *Mathematical Programming*, 35:307–339, 1984.

Y. Çengel and M.A. Boles. *thermodynamics: An Engineering Approach*. 5th edition edition, 1989.

A.F. Estrada-Alexanders and J.P.M. Trusler. Speed of sound in carbon dioxide at temperatures between (220 and 450) K and pressures up to 14 MPa. *Journal of Chemical Thermodynamics*, 30(12):1589–1601, 1998.

O. Exler, T. Lehmann, and K. Schittkowski. A comparative study of sqp-type algorithms for nonlinear and nonconvex mixed-integer optimization. *Mathematical Programming Computation*, 4(4):383–412, Dec 2012.

E.G. Feher. The supercritical thermodynamic power cycle Douglas Paper No.4348. In *Proceedings of the Intersociety Energy Conversion Engineering Conference*, pages 13–17, Miami Beach, August 1967.

D. Fleming, A. Kruizenga, J. Pasch, T. Conboy, and M. Carlson. Corrosion and erosion behavior in supercritical CO_2 power cycles. *ASME. Turbo Expo: Power for Land, Sea, and Air, Volume 3B*, 2014.

D.D. Fleming, T.M. Conboy, J.J. Pasch, G.A. Rochau, R.L. Fuller, T.V. Holschuh, and S.A. Wright. Scaling Considerations for a Multi-Megawatt Class Supercritical CO_2 Brayton Cycle and Commercialization. Technical Report SAND2013-9106, Sandia National Laboratories, 2013.

C.A. Floudas. *Nonlinear and Mixed-Integer Optimization. Fundamentals and Applications*, volume 12. Jan 1998.

J. Floyd, N. Alpy, A. Moisseytsev, D. Haubensack, G. Rodriguez, J. Sienicki, and G. Avakian. A numerical investigation of the sCO_2 recompression cycle off-design behaviour, coupled to a sodium cooled fast reactor, for seasonal variation in the heat sink temperature. *Nuclear Engineering and Design*, 260:78 – 92, 2013.

J.J.H. Forrest and J.A. Tomlin. Branch and bound, integer, and non-integer programming. *Annals of Operations Research,*, (1):81–87, 2007.

R.L. Fuller. Closed Brayton Cycle Power Conversion Unit for Fission Surface Power Phase I Final Report, 2010.

P. Garg, P. Kumar, and K. Srinivasan. Supercritical carbon dioxide Brayton cycle for concentrated solar power. *Journal of Supercritical Fluids*, 76:54–60, 2013.

B.H. Gebreslassie and U.M. Diwekar. Efficient ant colony optimization for computer aided molecular design: Case study solvent selection problem. *Computers & Chemical Engineering*, 78:1 – 9, 2015.

A.M. Geoffrion. Generalized benders decomposition. *Journal of Optimization Theory and Applications*, 10:237–260, 1972.

A. Gil-Villegas, A. Galindo, P.J. Whitehead, S.J. Mills, G. Jackson, and A.N. Burgess. Statistical associating fluid theory for chain molecules with attractive potentials of variable range. *The Journal of Chemical Physics*, 106(10):4168–4186, 1997.

A.A. Gkountas, A.M. Stamatelos, and A.I. Kalfas. Recuperators investigation for high temperature supercritical carbon dioxide power generation cycles. *Applied Thermal Engineering*, 125 (Supplement C):1094 – 1102, 2017.

F. Glover. Tabu search part i. *ORSA Journal on Computing*, 1(3):190–206, 1989.

B. Gross and P. Roosen. Total process optimization in chemical engineering with evolutionary algorithms. *Computers & Chemical Engineering*, 22(Supplement 1):S229 – S236, 1998. European Symposium on Computer Aided Process Engineering-8.

J. Gross, , and G. Sadowski. Perturbed-chain saft: An equation of state based on a perturbation theory for chain molecules. *Industrial & Engineering Chemistry Research*, 40(4):1244–1260, 2001.

I.E. Grossmann. Mixed-integer programming approach for the synthesis of integrated process flowsheets. *Computers & Chemical Engineering*, (9), 1985.

I.E. Grossmann. MINLP optimization strategies and algorithms for process synthesis. *Foundations of computer-aided process design*, 1990.

I.E. Grossmann and M.M. Daichendt. New trends in optimization-based approaches to process synthesis. *Computers & Chemical Engineering*, 20(6):665 – 683, 1996. Fifth International Symposium on Process Systems Engineering.

J. Guo. Design analysis of supercritical carbon dioxide recuperator. *Applied Energy*, 164:21 – 27, 2016.

O.K. Gupta and A. Ravindran. Branch and bound experiments in convex nonlinear integer programming. *Management Science*, 31(12):1533–1546, 1985.

C. Gutiérrez-Antonio and A. Briones-Ramírez. Pareto front of ideal petlyuk sequences using a multiobjective genetic algorithm with constraints. *Computers & Chemical Engineering*, 33(2): 454 – 464, 2009.

H. Hagi. *Optimisation rationnelle des performances énergétiques et environnementales d'une centrale à charbon pulvérisé fonctionnant en oxy-combustion.* PhD thesis, 2014.

M.G. Harsh, P. Saderne, and L.T. Biegler. A mixed integer flowsheet optimization strategy for process retrofits-the debottlenecking problem. *Computers & Chemical Engineering*, 13(8):947 – 957, 1989.

E. Hendriks, G.M. Kontogeorgis, R. Dohrn, J.C. de Hemptinne, I.G. Economou, L.F. Zilnik, and V. Vesovic. Industrial requirements for thermodynamics and transport properties. *Industrial & Engineering Chemistry Research*, 22:11131–11141, 2010.

J.Y. Heo, M.S. Kim, S. Baik, S.J. Bae, and J.I. Lee. Thermodynamic study of supercritical CO_2 brayton cycle using an isothermal compressor. *Applied Energy*, 206:1118 – 1130, 2017.

C.M. Herget. Ultrasonic velocity in carbon dioxide and ethylene in the critical region. *Journal of Chemical Physics*, 8(7):537–542, 1940.

J.E. Hesselgreaves. *Compact Heat Exchangers*. Pergamon, Oxford, 2001.

J.F. Hinze, G.F. Nellis, and M.H. Anderson. Cost comparison of printed circuit heat exchanger to low cost periodic flow regenerator for use as recuperator in a s-CO_2 brayton cycle. *Applied Energy*, 208:1150 – 1161, 2017.

N. Holaind, G. Bianchi, M. De Miol, S.S. Saravi, S. A. Tassou, A. Leroux, and H. Jouhara. Design of radial turbomachinery for supercritical CO_2 systems using theoretical and numerical CFD methodologies. *Energy Procedia*, 123:313 – 320, 2017. Proceedings of 1st International Conference onSustainable Energy and Resource Use in Food ChainsincludingSymposium on Heat Recovery and Efficient Conversion and Utilisation of Waste HeatICSEF 2017, 19-20 April 2017, Windsor UK.

Z. Hu, J. Yang, and Y. Li. Crossover SAFT equation of state for pure supercritical fluids. *Fluid Phase Equilibria*, 205(1):1–15, 2003.

IEA. Technology roadmap: High-efficiency, low-emissions coal-fired power generation, 2012. URL `https://www.iea.org/`.

IEA. World energy outlook special briefing for COP21, 2015a. URL `https://www.iea.org/`.

IEA. Key world statistic : Indicators for 2015, 2015b. URL `https://www.iea.org/`. Consulted on 6th Februrary 2015.

IEA. World energy outlook 2017, 2017. URL `https://www.iea.org/`.

B.D. Iverson, T.M. Conboy, J.J. Pasch, and A.M. Kruizenga. Supercritical CO_2 Brayton cycles for solar-thermal energy. *Applied Energy*, 111:957–970, 2013.

M.Z. Jacobson. Review of solutions to global warming, air pollution, and energy security. *Energy & Environmental Science*, 2008.

W.S. Jeong, J.I. Lee, and Y.H. Jeong. Potential improvements of supercritical recompression CO_2 brayton cycle by mixing other gases for power conversion system of a SFR. *Nuclear Engineering and Design*, 241(6):2128–2137, 2011a.

W.S. Jeong, J.I. Lee, and Y.H. Jeong. Potential improvements of supercritical recompression co2 brayton cycle by mixing other gases for power conversion system of a sfr. *Nuclear Engineering and Design*, 241:2128–2137, 2011b.

V. Kalikhman, D. Kost, and I. Polishuk. About the physical validity of attaching the repulsive terms of analytical EOS models by temperature dependencies. *Fluid Phase Equilibria*, 293: 164–167, 2010.

Y. Kato, T. Nitawaki, and Y. Muto. Medium temperature carbon dioxide gas turbine reactor. *Nuclear Engineering and Design*, 230(1-3):195–207, 2004.

J. Kennedy and R. Eberhart. Particle swarm optimization. In *Neural Networks, 1995. Proceedings., IEEE International Conference on*, volume 4, pages 1942–1948 vol.4, Nov 1995.

S. Kim, Y. Cho, M.S. Kim, and M. Kim. Characteristics and optimization of supercritical CO_2 recompression power cycle and the influence of pinch point temperature difference of recuperators. *Energy*, 2018.

S.G. Kim, Y. Lee, Y. Ahn, and J.I. Lee. CFD aided approach to design printed circuit heat exchangers for supercritical CO_2 brayton cycle application. *Annals of Nuclear Energy*, 92:175 – 185, 2016.

Y. Kim. Equation of state for carbon dioxide. *Journal of Mechanical Science and Technology*, 21 (5):799–804, 2007.

S.B. Kiselev. Cubic crossover equation of state. *Fluid Phase Equilibria*, 147(1-2):7 – 23, 1998.

R. Kumar, A.Kr. Sharma, and P.C Tewari. Cost analysis of a coal-fired power plant using the npv method. *Journal of Industrial Engineering International*, 2015.

O. Kunz and W. Wagner. The gerg-2008 wide-range equation of state for natural gases and other mixtures: An expansion of gerg-2004. *Journal of Chemical & Engineering Data*, 57(11):3032–3091, 2012.

Y. Le Moullec. Conceptual study of a high efficiency coal-fired power plant with CO_2 capture using a supercritical CO_2 brayton cycle. *Energy*, 49:32 – 46, 2013a.

Y. Le Moullec. Conception of a pulverized coal fired power plant with carbon capture around a supercritical carbon dioxide Brayton cycle. *Energy Procedia*, 37:1180–1186, 2013b.

J. Leboreiro and J. Acevedo. Processes synthesis and design of distillation sequences using modular simulators: a genetic algorithm framework. *Computers & Chemical Engineering*, 28 (8):1223 – 1236, 2004.

B. Lee and M. Kesler. A generalized thermodynamic correlation based on three-parameter corresponding states. *AIChE Journal*, 21(3):510–527, 1975.

J. Lee, J.I Lee, Y. Ahn, S.G. Kim, and J.E. Cha. Conceptual design of supercritical CO_2 Brayton cycle radial turbomachinery for SMART application. *Transactions of the Korean Nuclear Society Autumn Meeting*, pages 1–2, 2012.

J. Lee, J.I. Lee, H.J. Yoon, and J.E. Cha. Supercritical carbon dioxide turbomachinery design for water-cooled small modular reactor application. *Nuclear Engineering and Design*, 270:76–89, 2014.

J. Lee, S. Cho, J. Cha, and J. Lee. Sensitivity study of S-CO_2 compressor design for different real gas approximations. *ASME Turbo Expo: Power for Land, Sea, and Air, Volume 9.*, pages 1–9, 2016.

S. Lee, B. Park, and J. Chung. Numerical studies on thermal hydraulic performance of zigzag-type printed circuit heat exchanger with inserted straight channels. *Applied Thermal Engineering*, 123:1434 – 1443, 2017.

Y. Lee, M.S. Shin, J. Yeo, and H. Kim. A crossover cubic equation of state near to and far from the critical region. *Journal Chemical Thermodynamics*, 39(9):1257–1263, 2007.

E.W. Lemmon, M.L. Huber, and M.O. McLinden. NIST standard reference database 23: Reference fluid thermodynamic and transport properties-refprop, version 9.1, 2013.

C. Li, W. Jia, and X. Wu. Application of Lee-Kesler equation of state to calculating compressibility factors of high pressure condensate gas. *Energy Procedia*, 14:115 –120, 2012.

M. Li, H. Zhu, J. Guo, K. Wang, and W. Tao. The development technology and applications of supercritical CO_2 power cycle in nuclear energy, solar energy and other energy industries. *Applied Thermal Engineering*, 126:255 – 275, 2017.

Y. Li, S. Liao, and G. Liu. Thermo-economic multi-objective optimization for a solar-dish Brayton system using NSGA-II and decision making. *Electrical Power and Energy Systems*, 64:167–175, 2015.

B. Linnhoff and J.R. Flower. Synthesis of heat exchanger networks: I. systematic generation of energy optimal networks. *AIChE Journal*, 24(4):633–642, 1978.

H.A. Long, T. Wang, and A. Thomas. Evaluation of using supercritical rankine cycles in integrated coal gasification combined cycles (igcc). *ASME. Turbo Expo: Power for Land, Sea, and Air, Volume 3: Coal, Biomass and Alternative Fuels; Cycle Innovations; Electric Power; Industrial and Cogeneration Applications; Organic Rankine Cycle Power Systems*, 2017.

Y. Ma, M. Liu, J. Yan, and J. Liu. Thermodynamic study of main compression intercooling effects on supercritical CO_2 recompression brayton cycle. *Energy*, 140(Part 1):746 – 756, 2017.

Z. Ma and C. Turchi. Advanced supercritical carbon dioxide power cycle configurations for use in concentrating solar power system. In *The 3th International Symposium-Supercritical CO_2 Power Cycles*, 2011.

J. Mahaffey, A. Kalra, M. Anderson, and K. Sridharan. Materials corrosion in high temperature supercritical carbon dioxide. *The 4th international symposium supercritical CO_2 power cycles*, 2014.

M. Marchionni, G. Bianchi, K.M. Tsamos, and S.A. Tassou. Techno-economic comparison of different cycle architectures for high temperature waste heat to power conversion systems using CO_2 in supercritical phase. *Energy Procedia*, 123:305 – 312, 2017. Proceedings of 1st International Conference onSustainable Energy and Resource Use in Food ChainsincludingSymposium on Heat Recovery and Efficient Conversion and Utilisation of Waste Heat 2017, 19-20 April 2017, Windsor UK.

R.T. Marler and J.S. Arora. Survey of multi-objective optimization methods for engineering. *Structural and Multidisciplinary Optimization*, 26(6):369–395, Apr 2004.

P.M. Mathias and T.W. Copeman. Extension of the Peng-Robinson equation of state to complex mixtures: Evaluation of the various forms of the local composition concept. *Fluid Phase Equilibria*, 13:91 – 108, 1983.

M. Mazzoccoli, B. Bosio, E. Arato, and S. Brandani. Comparison of equations-of-state with P-ρ-T experimental data of binary mixtures rich in CO_2 under the conditions of pipeline transport. *Journal of Supercritical Fluids*, 95:474–490, 2014.

C.F. McDonald and D.G. Wilson. The utilization of recuperated and regenerated engine cycles for high-efficiency gas turbines in the 21st century. *Applied Thermal Engineering*, 16(8):635 – 653, 1996.

M. Mecheri and Y. Le Moullec. Supercritical CO_2 Brayton cycles for coal-fired power plants. *Energy*, 103:758–771, 2015.

M. Mecheri and H. Wang. Challenges in using fuel-fired heaters for sCO_2 closed brayton cycle. *The 6th International Supercritical CO2 Power Cycles Symposium*, 2018.

A. Meshram, A.K. Jaiswal, S.D. Khivsara, J.D. Ortega, C. Ho, R. Bapat, and P. Dutta. Modeling and analysis of a printed circuit heat exchanger for supercritical CO_2 power cycle applications. *Applied Thermal Engineering*, 109:861 – 870, 2016. Special Issue: Solar Energy Research Institute for India and the United States (SERIIUS) - Concentrated Solar Power.

D. Milani, M.T. Luu, R. McNaughton, and A. Abbas. Optimizing an advanced hybrid of solar-assisted supercritical CO_2 brayton cycle: A vital transition for low-carbon power generation industry. *Energy Conversion and Management*, 148:1317 – 1331, 2017.

M. Mohagheghi and J. Kapat. Thermodynamic optimization of recuperated S-CO_2 brayton cycles for solar tower applications. *Proceedings of ASME Turbo Expo 2013: Turbine Technical Conference and Exposition*, pages 1–11, 2013.

A. Moisseytsev and J.J. Sienicki. Transient accident analysis of a supercritical carbon dioxide Brayton cycle energy converter coupled to an autonomous lead-cooled fast reactor. *Nuclear Engineering and Design*, 238(8):2094–2105, 2008.

A. Moisseytsev and J.J. Sienicki. Investigation of alternative layouts for the supercritical carbon dioxide brayton cycle for a sodium-cooled fast reactor. *Nuclear Engineering and Design*, 239 (7):1362–1371, 2009.

R.L. Motard and A.W. Westerberg. Exclusive tear sets for flowsheets. *AIChE Journal*, 27(5):725–732, 1981.

A. Munawar, M. Wahib, M. Munetomo, and K. Akama. Advanced genetic algorithm to solve MINLP problems over gpu. In *2011 IEEE Congress of Evolutionary Computation (CEC)*, pages 318–325, June 2011.

E. Neau, O. Hernández-Garduza, J. Escandell, C. Nicolas, and I. Raspo. The soave, twu and boston-mathias alpha functions in cubic equations of state: Part i. theoretical analysis of their variations according to temperature. *Fluid Phase Equilibria*, 276(2):87 – 93, 2009.

T. Neises and C. Turchi. A comparison of supercritical carbon dioxide power cycle configurations with an emphasis on CSP applications. *Energy Procedia*, 49:1187–1196, 2014.

T. Neveux, O. Authier, M. Kanniche, and F. Siros. Uncertainties in techno-economic evaluation of innovative processes - effect of technology maturity and preparation effort. *Presentation at the 30th SFGP Congress*, 2017.

H. Nishiumi and S. Saito. An improved generalized BWR equation of state applicable to low reduced temperatures. *Journal of Chemical Engineering of Japan*, 8(5):356–360, 1975.

Nojhan. Classification of metaheuristics, 2007. URL `http://metah.nojhan.net/post/2007/10/12/Classification-of-metaheuristics`. consulted on January 2018.

P. Nowak, T. Tielkes, R. Kleinrahm, and W. Wagner. Supplementary measurements of the P-ρ-T relation of carbon dioxide in the homogeneous region at T=313 K and on the coexistence curve at T=304 K. *Journal of Chemical Thermodynamics*, 29(8):885 – 889, 1997.

S. Park, J. Kim, M. Yoon, D. Rhim, and C. Yeom. Thermodynamic and economic investigation of coal-fired power plant combined with various supercritical CO_2 brayton power cycle. *Applied Thermal Engineering*, 130:611 – 623, 2018.

N.C. Patel and A.S. Teja. A new cubic equation of state for fluids and fluid mixtures. *Chemical Engineering Science*, 37(3):463 – 473, 1982.

D. Peng and D. Robinson. A new two-constant equation of state. *Industrial & Engineering Chemistry Fundamentals*, 15(1):59–64, 1976.

M. Persichilli, A. Kacludis, E. Zdankiewicz, and T. Held. Supercritical CO_2 power cycle developments and commercialization: Why S-CO_2 can displace steam. In *Power-Gen India & Central Asia 2012*, pages 19–21, Pragati Maidan, New Delhi, India, April 2012.

H.S. Pham. *Investigation of the supercritical CO_2 cycle : mapping of the thermodynamic potential for different applications; further understanding of the physical processes, in particular through simulations and analysis of experimental data*. PhD thesis, 2015.

K.S. Pitzer and R.F. Curl. The volumetric and thermodynamic properties of fluids. iii. empirical equation for the second virial coefficient 1. *Journal of the American Chemical Society*, 79(10): 2369–2370, 1957.

K.S. Pitzer and S.M. Sterner. Equations of state valid continuously from zero to extreme pressures for H_2O and CO_2. *Journal of Chemical Physics*, 101(4):3111–3116, 1994.

K.S. Pitzer, D.Z. Lippmann, R.F. Curl, C.M. Huggins, and D.E. Petersen. The Volumetric and Thermodynamic Properties of Fluids. II. Compressibility Factor, Vapor Pressure and Entropy of Vaporization. *Journal of the American Chemical Society*, 77(13):3433–3440, 1955.

A. Péneloux, E. Rauzy, and R. Fréze. A consistent correction for Redlich-Kwong-Soave volumes. *Fluid Phase Equilibria*, 8(1):7 – 23, 1982.

B.E. Poling, J.M. Prausnitz, and J.P. OConnell. *The properties of gazes and liquids*. McGrawHill, fifth edition edition, 2001.

I. Polishuk, R. Privat, and J.N. Jaubert. Novel methodology for analysis and evaluation of SAFT-Type equations of state. *Industrial & Engineering Chemistry Research*, 52(38):13875–13885, 2013.

R. Privat, M. Visconte, A. Zazoua-Khames, JN. Jaubert, and R. Gani. Analysis and prediction of the alpha-function parameters used in cubic equations of state. *Chemical Engineering Science*, 126:584 – 603, 2015.

J. Qi, T. Reddell, and K. Qin. Supercritical CO_2 radial turbine design performance as a function of turbine size parameters. *ASME Turbo Expo: Power for Land, Sea, and Air, Volume 9.*, June 2016.

A. Quaglia, C.L. Gargalo, S. Chairakwongsa, G.S., and R. Gani. Systematic network synthesis and design: Problem formulation, superstructure generation, data management and solution. *Computers & Chemical Engineering*, 72(Supplement C):68 – 86, 2015.

I. Quesada and I.E. Grossmann. Global optimization of bilinear process networks with multicomponent flows. *Computers & Chemical Engineering*, 19(12):1219 – 1242, 1995. An International Journal of Computer Application in Chemical Engineering.

A.R. Ravishankara, J.S. Daniel, and R.W. Portmann. Nitrous oxide (N_2O): The dominant ozone-depleting substance emitted in the 21st century. *Science*, 326(5949):123–125, 2009.

K. Rayaprolu. *Boilers for Power and Process*. CRC Press, 2009. ISBN 9781420075366.

M.A. Reyes-Belmonte, A. Sebastián, M. Romero, and J. González-Aguilar. Optimization of a recompression supercritical carbon dioxide cycle for an innovative central receiver solar power plant. *Energy*, 112:17 – 27, 2016.

W.G. Le Roux, T. Bello-Ochende, and J.P. Meyer. A review on the thermodynamic optimisation and modelling of the solar thermal Brayton cycle. *Renewable and Sustainable Energy Reviews*, 28:677–690, 2013.

W.G. Le Roux, T. Bello-Ochende, and J.P. Meyer. The efficiency of an open-cavity tubular solar receiver for a small-scale solar thermal Brayton cycle. *Energy Conversion and Management*, 84:457–470, 2014.

A. Rovira, J. Muñoz-Antón, M. J. Montes, and J. M. Martínez-Val. Optimization of Brayton cycles for low-to-moderate grade thermal energy sources. *Energy*, 55:403–416, 2013.

RPB. Human population: Population growth, 2018. URL `http://www.prb.org/`. consulted on January 2018.

P.H. Salim and M.A. Trebble. A modified trebble-bishnoi equation of state: thermodynamic consistency revisited. *Fluid Phase Equilibria*, 65:59 – 71, 1991.

S.I. Sandler and H. Orbey. *Equations of State, Models for thermodynamic and Phase Equilibria Calculations*. University of Delaware, 1992.

R.W.H. Sargent and A. W. Westerberg. Speed-up in chemical engineering design. *Transactions of the Institution of Chemical Engineers*, pages 190–197, 1964.

J. Sarkar. Second law analysis of supercritical CO_2 recompression Brayton cycle. *Energy*, 34(9): 1172–1178, 2009.

J. Sarkar and S. Bhattacharyya. Optimization of recompression s-CO_2 power cycle with reheating. *Energy Conversion and Management*, 50(8):1939 – 1945, 2009.

M. Schlüter. Nonlinear mixed integer based optimization technique for space applications. *PhD Thesis*, 2012.

M. Schlüter and M. Gerdts. The oracle penalty method. *Journal of Global Optimization*, 47(2): 293–325, Jun 2010.

M. Schlüter, M. Gerdts, and J.J Rückmann. A numerical study of MIDACO on 100 MINLP benchmarks. *Optimization*, 61(7):873–900, 2012.

M. Schlueter, C.H. Yam, T. Watanabe, and A. Oyama. Many-objective optimization of interplanetary space mission trajectories. In *2015 IEEE Congress on Evolutionary Computation*, pages 3256–3262, May 2015.

G. Schmidt and H. Wenzel. A modified van der Waals type equation of state. *Chemical Engineering Science*, 35(7):1503 – 1512, 1980.

I.P. Serrano, J.I. Linares, A. Cantizano, and B.Y. Moratilla. Enhanced arrangement for recuperators in supercritical CO_2 brayton power cycle for energy conversion in fusion reactors. *Fusion Engineering and Design*, 89(9-10):1909 – 1912, 2014. Proceedings of the 11th International Symposium on Fusion Nuclear Technology-11 (ISFNT-11) Barcelona, Spain, 15-20 September, 2013.

D. Shiferaw, J. Montero Carrero, and R. Le Pierres. Economic analysis of sCO_2 cycles with PCHE recuperator design optimisation. *The 5th International Symposium - Supercritical CO_2 Power Cycles March 28-31, 2016, San Antonio, Texas*, 2016.

A. Shiu and P. Lam. Electricity consumption and economic growth in china. *Energy Policy*, 32 (1):47 – 54, 2004.

R. Singh, M.P. Kearney, and C. Manzie. Extremum-seeking control of a supercritical carbon-dioxide closed Brayton cycle in a direct-heated solar thermal power plant. *Energy*, 60:380–387, 2013a.

R. Singh, S.A. Miller, A.S. Rowlands, and P.A. Jacobs. Dynamic characteristics of a direct-heated supercritical carbon-dioxide brayton cycle in a solar thermal power plant. *Energy*, 50:194 – 204, 2013b.

C. Sánchez, R. Juárez, J. Sanz, and M. Perlado. Design and analysis of helium Brayton power cycles for HiPER reactor. *Fusion Engineering and Design*, 88(9-10):2679–2683, 2013.

S. Sánchez-Orgaz, A. Medina, and A. Calvo Hernández. Thermodynamic model and optimization of a multi-step irreversible Brayton cycle. *Energy Conversion and Management*, 51(11):2134–2143, 2010.

G. Soave. Equilibrium constants from a modified Redlich-Kwong equation of state. *Chemical Engneering Science*, 27(6):1197–1203, 1972.

R. Span and W. Wagner. A new equation of state for carbon dioxide covering the fluid region from the triple-point temperature to 1100 K at pressures up to 800 MPa. *Journal of Physical and Chemical Reference Data*, 25(6):1509–1558, 1996.

K.E. Starling. Thermo data refined for LPG, part 1 : Equation of state and computer prediction. *Hydro. Process.*, pages 101–104, 1971.

L. Sun, S.B. Kiselev, and J.F. Ely. Multiparameter crossover equation of state: generalized algorithm and application to carbon dioxide. *Fluid Phase Equilibria*, 233(2):204–219, 2005.

S. Tang and J.V. Sengers. Proceedings of the 2nd international symposium on supercritical fluids thermodynamic behavior of fluids in the supercritical region. *The Journal of Supercritical Fluids*, 4(4):209 – 214, 1991.

R. Tarjan. Depth-first search and linear graph algorithms. *SIAM Journal on Computing*, 1(2): 146–160, 1972.

M. Tawarmalani and N.V. Sahinidis. *Convexification and Global Optimization in Continuous and Mixed-Integer Nonlinear Programming: Theory, Algorithms, Software, and Applications*, volume 65. Kluwer Academic Publishers, 2002. ISBN 978-1-4020-1031-6.

M.C. Tayal, Y. Fu, and U.M. Diwekar. Optimal design of heat exchangers: A genetic algorithm framework. *Industrial & Engineering Chemistry Research*, 38(2):456–467, 1999.

D. Thimsen. Closed brayton power cycles using supercritical carbon dioxide as the working fluid. Technical report, Electric Power Research Institute, 2014.

F. Trespalacios and I.E. Grossmann. Review of mixed-integer nonlinear and generalized disjunctive programming methods. *Chemie Ingenieur Technik*, 86(7):991–1012, 2014.

T. Tsuji, S. Honda, T. Hiaki, and M. Hongo. Measurement of the P-V-T relationship for carbon dioxide+n-butane and carbon dioxide+i-butane in the vicinity of the critical point. *Journal of Supercritical Fluids*, 13(1):15–21, 1998.

N. Tsuzuki, Y. Kato, and T. Ishiduka. High performance printed circuit heat exchanger. *Applied Thermal Engineering*, 27(10):1702 – 1707, 2007. Heat transfer and sustainable energy technologies.

C.S. Turchi, Z. Ma, and J. Dyreby. Supercritical carbon dioxide power cycle configurations for use in concentrating solar power systems. *ASME. Turbo Expo: Power for Land, Sea, and Air, Volume 5*, 2012.

C.H. Twu, D. Bluck, J.R. Cunningham, and J.E. Coon. A cubic equation of state with a new alpha function and a new mixing rule. *Fluid Phase Equilibria*, 69:33 – 50, 1991.

C.H. Twu, J.E. Coon, and J.R. Cunningham. A new generalized alpha function for a cubic equation of state part 1. Peng-Robinson equation. *Fluid Phase Equilibria*, 105(1):49 – 59, 1995.

UNCC. Global warming potentials, 2018. URL `http://unfccc.int/ghg_data/`. consulted on 2015.

R.S. Upadhye and E.A. Grens. Selection of decompositions for chemical process simulation. *AIChE Journal*, 21(1):136–143, 1975.

J.D. van der Waals. *Over de continuiteit van den gas-en Vloeistoftoestand*. PhD thesis, Leiden, Holland., 1873.

J.A. Vazquez-Castillo, J.A. Venegas-Sánchez, J.G. Segovia-Hernández, H. Hernández-Escoto, S. Hernández, C. Gutiérrez-Antonio, and A. Briones-Ramírez. Design and optimization, using genetic algorithms, of intensified distillation systems for a class of quaternary mixtures. *Computers & Chemical Engineering*, 33(11):1841 – 1850, 2009.

L. Vesely and V. Dostal. Research on the effect of the pinch point shift in cycles with supercritical carbon dioxide. In *The 4th International Symposium-Supercritical CO_2 Power Cycles*, Pittsburgh, Pennsylvania, 2014.

L Vesely, V Dostal, and P Hajek. Design of experimental loop with supercritical carbon dioxide. *ASME. International Conference on Nuclear Engineering, Volume 3: Next Generation Reactors and Advanced Reactors; Nuclear Safety and Security*, 2014.

J. Viswanathan and I.E. Grossmann. A combined penalty function and outer-approximation method for MINLP optimization. *Computers & Chemical Engineering*, 14(7):769 – 782, 1990.

J. Wang, Z. Sun, Y. Dai, and S. Ma. Parametric optimization design for supercritical CO_2 power cycle using genetic algorithm and artificial neural network. *Applied Energy*, 87(4):1317 – 1324, 2010.

K. Wang, Y. He, and H. Zhu. Integration between supercritical CO_2 brayton cycles and molten salt solar power towers: A review and a comprehensive comparison of different cycle layouts. *Applied Energy*, 195:819 – 836, 2017.

L. Wang, Y. Yang, C. Dong, T. Morosuk, and G. Tsatsaronis. Parametric optimization of supercritical coal-fired power plants by MINLP and differential evolution. *Energy Conversion and Management*, 85(Supplement C):828 – 838, 2014a.

L. Wang, Y. Yang, C. Dong, T. Morosuk, and G. Tsatsaronis. Systematic optimization of the design of steam cycles using MINLP and differential evolution. *Journal of Energy Resources Technology*, 136:031601–12, 2014b.

N.T. Weiland and C.W. White. Techno-economic analysis of an integrated gasification direct-fired supercritical CO_2 power cycle. *Fuel*, 212:613 – 625, 2018.

P.S. Weitzel. Steam generator for advanced ultra supercritical power plants 700c to 760c. *ASME 2011 Power Conference, Volume 1*, pages 281–291, 2011.

A.W. Westerberg, H.P. Hutchinson, R.L. Motard, and P. Winter. *Process flowsheeting*. Cambridge University Press, 1979.

S.A. Wright, M.E. Vernon, and P.S. Pickard. Concept design for a high temperature helium brayton cycle with interstage heating and cooling, 2006.

S.A. Wright, R.F. Radel, M.E. Vernon, G.E. Rochau, and P.S. Pickard. Operation and analysis of a supercritical CO_2 Brayton cycle. Technical report, Sandia National Laboratories, Albuquerque and Livermore, 2010.

S.A. Wright, T.M. Conboy, Parma E.J., Lewis T.G., and Rochau G.A. Summary of the Sandia supercritical CO_2 development program. In *The 3th International Symposium-Supercritical CO_2 Power Cycles*, 2011.

S. Yu, L. Chen, Y. Zhao, H. Li, and X. Zhang. A brief review study of various thermodynamic cycles for high temperature power generation systems. *Energy Conversion and Management*, 94:68–83, 2015.

X. Zhang, H. Yamaguchi, and D. Uneno. Experimental study on the performance of solar rankine system using supercritical CO_2. *Renewable Energy*, 32(15):2617–2628, 2007.

H. Zhao and P.F. Peterson. Multiple reheat helium Brayton cycles for sodium cooled fast reactors. *Nuclear Engineering and Design*, 238(7):1535–1546, 2008.

Y. Zhao, B. Wang, J. Chi, and Y. Xiao. Parametric study of a direct-fired supercritical carbon dioxide power cycle coupled to coal gasification process. *Energy Conversion and Management*, 156:733 – 745, 2018.

A. Zolghadr, M. Escrochi, and S. Ayatollahi. Temperature and composition effect on CO_2 miscibility by interfacial tension measurement. *Journal of Chemical Engineering Data*, 58(5): 1168–1175, 2013.

List of publication and communication

Journal Paper:

Q. Zhao, M. Mecheri, T. Neveux, JN. Jaubert, “On the selection of a proper equation of state for the modeling of a supercritical CO_2 Brayton cycle: consequences on the process design”, Industrial & Engineering Chemistry Research, 2017

Conference Paper:

Q. Zhao, M. Mecheri, T. Neveux, P. Guittard, JN. Jaubert, “Superstructure optimization (MINLP) within ProSimPlus Simulator”, Proceedings of the 28th European Symposium on Computer Aided Process Engineering June 10 to 13 , 2018, Graz, Austria.

Q. Zhao, M. Mecheri, T. Neveux, R. Privat, JN. Jaubert, “Design of SC-CO2 Brayton Cycles using MINLP Optimization within a Commercial Simulator”, the 6th International Supercritical CO2 Power Cycles Symposium, 2018, Pittsburgh, Pennsylvania. USA

Q. Zhao, M. Mecheri, T. Neveux, R. Privat, JN. Jaubert, "Thermodynamic model investigation for supercritical CO_2 Brayton cycle for coal-fired power plant application", the 5th International Symposium Supercritical CO_2 Power Cycles, 2016, San Antonio, Texas. USA

Conference Poster:

Q. Zhao, M. Mecheri, T. Neveux, JN. Jaubert, Framework for superstructure optimization: process synthesis of supercritical CO_2 Brayton cycle, 10th Word Congress of Chemical Engineering (WCCE), 2017, Barcelona, Spain

Q. Zhao, M. Mecheri, T. Neveux, JN. Jaubert, Parametric optimization of Supercritical CO_2 Brayton cycle by MINLP approach, SFGP 2017, Nancy, France

Q. Zhao, M. Mecheri, T. Neveux, JN. Jaubert, Framework for design optimization: process development of supercritical CO_2 Brayton cycle for coal-fired power plant, 20st Conference on Process Integration, Modelling and Optimisation, 2016, Prague, Czech Republic.

Appendices

SPAN WAGNER EQUATION OF STATE COEFFICIENT

i	$a°_i$	$\theta_i°$	i	$a°_i$	$\theta_i°$
1	8.37304456		5	0.62105248	6.11190
2	-3.70454304		6	0.41195293	6.77708
3	2.50000000		7	1.04028922	11.32384
4	1.99427042	3.15163	8	0.08327678	27.08792

Table 2: Values of coefficients in correlation equation, Eq. 2.25

Table 3: Values of coefficients in correlation equation, Eq. 2.26

i	n_i	d_i	t_i					
1	$0.38856823203161 \times 10^{0}$	1	0.00					
2	$0.29385475942740 \times 10^{1}$	1	0.75					
3	$-0.55867188534934 \times 10^{1}$	1	1.00					
4	$-0.76753199592477 \times 10^{0}$	1	2.00					
5	$0.31729005580416 \times 10^{0}$	2	0.75					
6	$0.54803315897767 \times 10^{0}$	2	2.00					
7	$0.12279411220335 \times 10^{0}$	3	0.75					
i	n_i	d_i	t_i	c_i				
8	$0.21658961543220 \times 10^{1}$	1	1.50	1				
9	$0.15841735109724 \times 10^{1}$	2	1.50	1				
10	$-0.23132705405503 \times 10^{0}$	4	2.50	1				
11	$0.58116916431436 \times 10^{-1}$	5	0.00	1				
12	$-0.55369137205382 \times 10^{0}$	5	1.50	1				
13	$0.48946615909422 \times 10^{0}$	5	2.00	1				
14	$-0.24275739843501 \times 10^{0}$	6	0.00	1				
15	$0.62494790501678 \times 10^{-1}$	6	1.00	1				
16	$-0.12175860225246 \times 10^{0}$	6	2.00	1				
17	$-0.37055685270086 \times 10^{0}$	1	3.00	2				
18	$-0.16775879700426 \times 10^{-1}$	1	6.00	2				
19	$-0.11960736637987 \times 10^{0}$	4	3.00	2				
20	$-0.45619362508778 \times 10^{-1}$	4	6.00	2				
21	$0.35612789270346 \times 10^{-1}$	4	8.00	2				
22	$-0.74427727132052 \times 10^{-2}$	7	6.00	2				
23	$-0.17395704902432 \times 10^{-2}$	8	0.00	2				
24	$-0.21810121289527 \times 10^{-1}$	2	7.00	3				
25	$0.24332166559236 \times 10^{-1}$	3	12.00	3				
26	$-0.37440133423463 \times 10^{-1}$	3	16.00	3				
27	$0.14338715756878 \times 10^{0}$	5	22.00	4				
28	$-0.13491969083286 \times 10^{0}$	5	24.00	4				
29	$-0.23151225053480 \times 10^{-1}$	6	16.00	4				
30	$0.12363125492901 \times 10^{-1}$	7	24.00	4				
31	$0.21058321972940 \times 10^{-2}$	8	8.00	4				
32	$-0.33958519026368 \times 10^{-3}$	10	2.00	4				
33	$0.55993651771592 \times 10^{-2}$	4	28.00	5				
34	$-0.30335118055646 \times 10^{-3}$	8	14.00	6				
i	n_i	d_i	t_i	α_i	β_i	γ_i	ε_i	
35	$-0.21365488688320 \times 10^{3}$	2	1.00	25	325	1.16	1.00	
36	$0.26641569149272 \times 10^{5}$	2	0.00	25	300	1.19	1.00	
37	$-0.24027212204557 \times 10^{5}$	2	1.00	25	300	1.19	1.00	
38	$-0.28341603423999 \times 10^{3}$	3	3.00	15	275	1.25	1.00	
39	$0.21247284400179 \times 10^{3}$	3	3.00	20	275	1.22	1.00	
i	n_i	a_i	b_i	β_i	A_i	B_i	C_i	Di
40	$-0.66642276540751 \times 10^{0}$	3.500	0.875	0.300	0.700	0.3	10.0	275
41	$0.72608632349897 \times 10^{0}$	3.500	0.925	0.300	0.700	0.3	10.0	275
42	$0.55068668612842 \times 10^{-1}$	3.000	0.875	0.300	0.700	1.0	12.5	275

SUPERSTRUCTURE SS2 IN COMMERCIAL SIMULATOR PROSIMPLUS

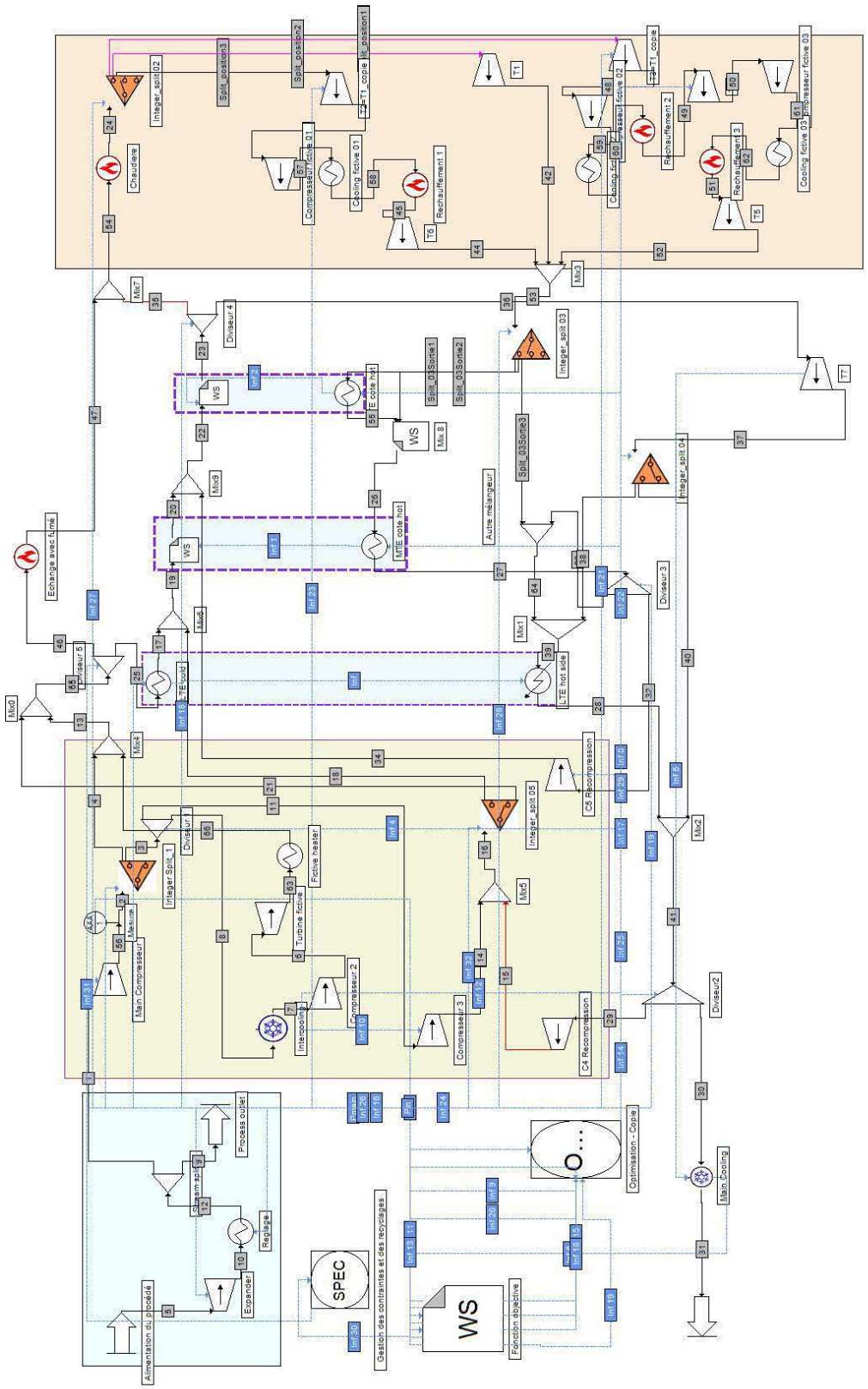

Figure 1: Illustration of SS2 superstructure in simulator, with presence of OPTI unit and information streams

UTOPIA-NADIR-DECOMPOSITION

The decomposition approach considered in MIDACO is the so called Utopia and Nadir information. The individual objective $f_i(x)$ is transformed to a target function T_j by using the Balance (user defined objective prioritization), the Utopia U_i (global minimum of individual objective $f_i(x)$), and Nadir N_i (the worst objective function value for the respective $f_i(x)$) represents the global minimum of the respective objective. The target function for each j-th subproblem in MIDACO is defined as follows:

$$T_j(x) = \sum_{i=1}^{M} w_i^j \cdot \frac{f_i(x) - U_i}{N_i - U_i} + B_j(x)$$

The set of single objective problems given by $T_1, ..., T_M$ therefore decomposes the original multi-objective problem.

Where w_i^j is a weight [0,1], in form of matrix;
$d_i^j(x) = w_i^j \cdot \frac{f_i(x)-U_i}{N_i-U_i}$;
and $B_j(x) = \sum_{i=1}^{M} ||d_i^j(x) - D_j(x)||$.

MIDACO PARAMETER

Table 4 listed all the values of user-defined parameters in MIDACO for SS1 mono-objective optimization, SS2 mono-objective optimization, SS2 multi-objective optimization.

The accuracy corresponds to the permitted constraint absolute violation value. Different SEED choice make MIDACO to have various random number generator. FSTOP is one of the stop criterion for optimizer. For example, when the objective function is lower than -60, the optimization stops. EVALSTOP is set for the maximum optimization iteration. ORACLE is the parameter of Oracle penalty function for constraints handling. The idea is to have a value that approaches the best function objective but not too close to it. Finding a proper MIDACO value needs some background knowledge (approximate range) on the studied optimization problem. Other optimizer parameters have the MIDACO default value, 0.

Table 4: MIDACO Parameter used for SS1, SS2, 0 represents for solver default value

Parameter N°	Term	Value used in this dissertation		
		SS1	SS2	SS2 multi-objective
Parameter (1)	ACCURACY	0.5	0.5	0.5
Parameter (2)	SEED	[0;1;2;3]	[0;1;2;3]	[0;1;2]
Parameter (3)	FSTOP	-60	-60	-60
Parameter (4)	ALGOSTOP	0	0	0
Parameter (5)	EVALSTOP	150 000	200 000	200 000
Parameter (6)	FOCUS	0	0	0
Parameter (7)	ANTS	0	0	0
Parameter (8)	KERNEL	0	0	0
Parameter (9)	ORACLE	-40	-45	-45
Parameter (10)	PARETOMAX	0	0	0
Parameter (11)	EPSILON	0	0	0
Parameter (12)	CHARACTER	0	0	0
Parameter (13)	MAXITIME	0	0	0
	Balance	-	-	0

MIDACO PARAMETER SENSIBILITY

The following sensitivity assessment is elaborated to find appropriate parameter set for a more robust optimization. According to MIDACO Manuel, where ORACLE can improve the constraints handling, the optimizer performance on large scale problems can generally benefit from tuning the following parameter: FOCUS, ANTS, KERNEL. The following different

assessments try to evaluate different set of MIDACO parameters.

Table 5: MIDACO Parameter sensitivity study, 0 represents for solver default value

Parameter N°	Term	Value in this dissertation denoted “Reference”	Sensitivity case I “Default”	Sensitivity case II “Soft”
Parameter (1)	ACCURACY	0.5	0.5	0.5
Parameter (2)	SEED	[1;2;3]	[1;2;3]	[1;2;3]
Parameter (3)	FSTOP	-60	0	-56
Parameter (4)	ALGOSTOP	0	0	0
Parameter (5)	EVALSTOP	40000	40000	40000
Parameter (6)	FOCUS	0	0	100
Parameter (7)	ANTS	0	0	0
Parameter (8)	KERNEL	0	0	0
Parameter (9)	ORACLE	-40	0	-50
Parameter (10)	PARETOMAX	0	0	0
Parameter (11)	EPSILON	0	0	0
Parameter (12)	CHARACTER	0	0	0
Parameter (13)	MAXITIME	0	0	0

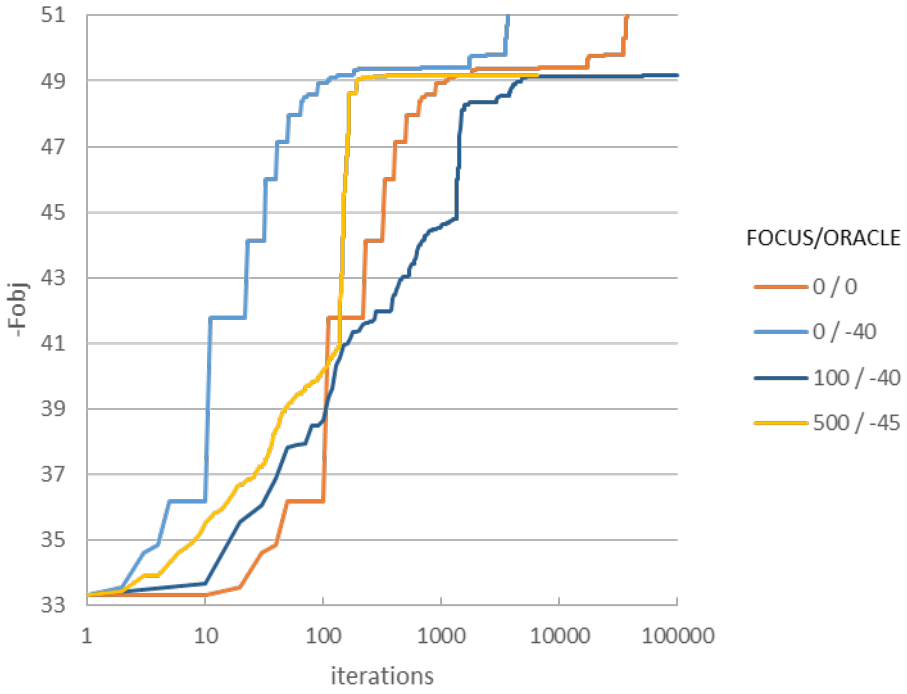

Figure 2: Focus/Oracle parameter influence in SS1 optimization

Figure 2 illustrates the sensitivity analysis brought out using “default” set parameter (in Table 5) with different sets of FOCUS/ORACLE. It is noted that the chosen 0/-40 leads to a more quickly research in objective. A better optimum is achieved within less iterations.

Meanwhile, the SS1 optimization is found to be not influenced by the ANT/KERNEL parameters, while other parameters are at “Reference”. For 10 different sets of ANT/KERNEL, the optimization steps vary but the default set has a better objective function evolution within 100 000 iterations.

Figure 4 and Figure 5 illustrate the optimization performance and constraints violation for “Soft” parameter set, “Default” parameter set and “Reference set”, the latter is applied in SS1 optimization this dissertation. The Soft set of combination Focus/Oracle accelerates the constraints fulfillment in comparison with the “default” set. However, the soft set FOCUS does not help in the research of objective function.

To sum up, although this sensitivity analysis is a posterior study on SS1 optimization, the choice of the solver user-defined parameter appears to be an appropriate parameter selection.

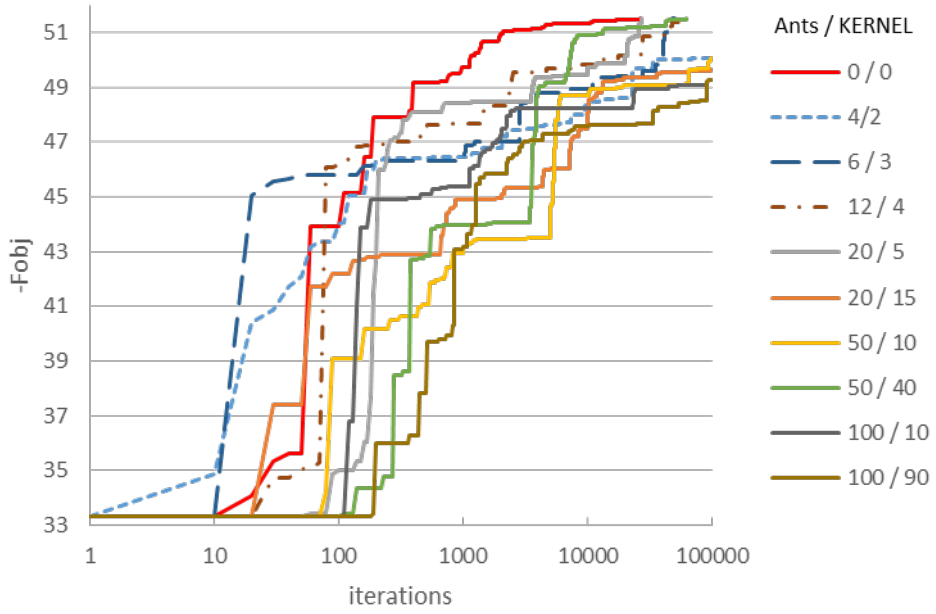

Figure 3: Ants/KERNEL parameter influence in SS1 optimization

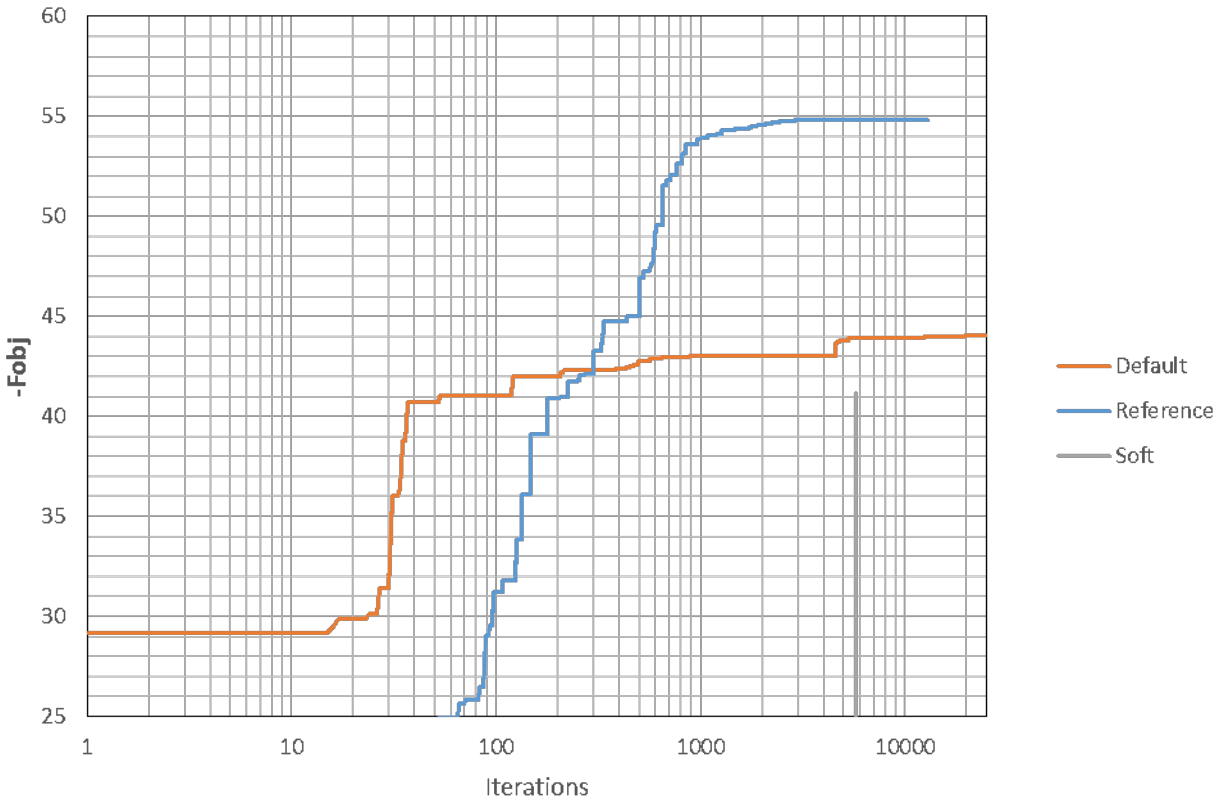

Figure 4: Comparison of objective function between “Default”, “Reference” and “Soft” set

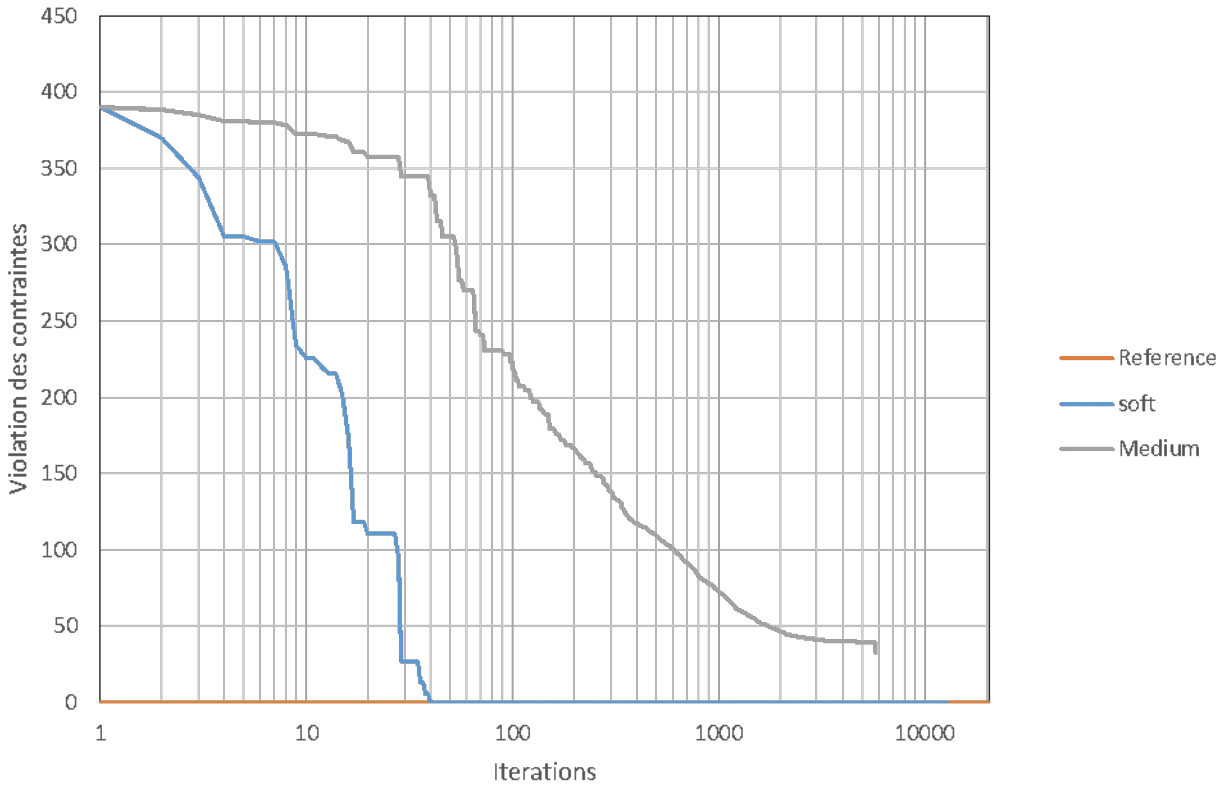

Figure 5: Comparison of constraint handling between “Default”, “Reference” and “Soft” set

THE STATE-OF-THE-ART SC-CO2 COMPONENT (TEST LOOP SCALE)

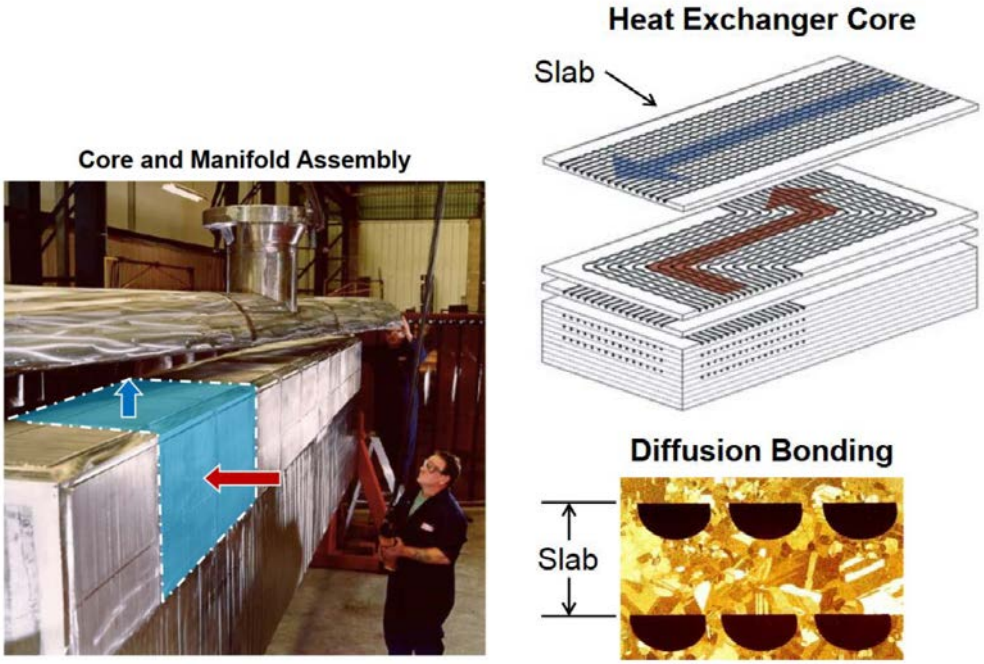

Figure 6: Printed Circuit Heat Exchangers for SC-CO_2 test loop. Photo extracted from Sandia National Laboratory

Figure 7: Scale of compressor for SC-CO_2 10 MWe test loop, photo extracted from GE company

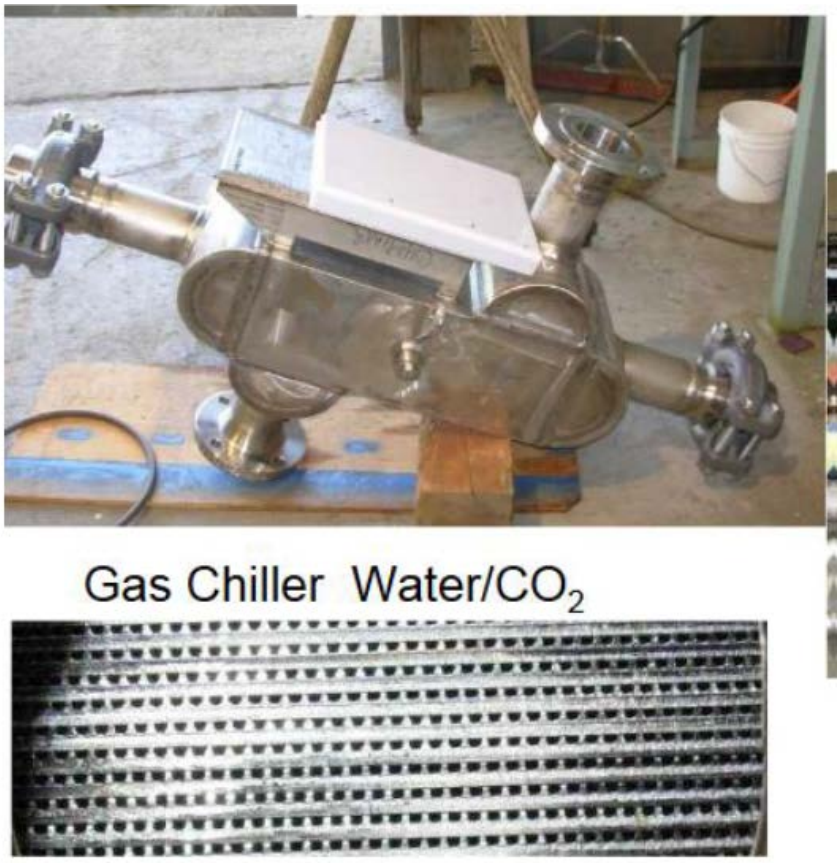

Figure 8: Several kWth SC-CO_2 chiller for main cooling. Photo extracted from Sandia National Laboratory

• **Résumé en anglais**

Conception and optimization of supercritical CO_2 Brayton cycles for coal-fired power plant application

Efficiency enhancement in power plant can be seen as a key lever in front of increasing energy demand. Nowadays, both the attention and the emphasis are directed to reliable alternatives, i.e., enhancing the energy conversion systems. The supercritical CO_2 (SC-CO_2) Brayton cycle has recently emerged as a promising solution for high efficiency power production in nuclear, fossil-thermal and solar-thermal applications.

Currently, studies on such a thermodynamic power cycle are directed towards the demonstration of its reliability and viability before the possible building of an industrial-scale unit. The objectives of this PhD can be divided in two main parts:

• A rigorous selection procedure of an equation of state (EoS) for SC-CO_2 which permits to assess influences of thermodynamic model on the performance and design of a SC-CO_2 Brayton cycle.

• A framework of optimization-based synthesis of energy systems which enables optimizing both system structure and the process parameters.

The performed investigations demonstrate that the Span-Wagner EoS is recommended for evaluating the performances of a SC-CO_2 Brayton cycle in order to avoid inaccurate predictions in terms of equipment sizing and optimization.

By combining a commercial process simulator and an evolutionary algorithm (MIDACO), this dissertation has identified a global feasible optimum design –or at least competitive solutions– for a given process superstructure under different industrial constraints. The carried out optimization firstly base on cycle energy aspects, but the decision making for practical systems necessitates techno-economic optimizations. The establishment of associated techno-economic cost functions in the last part of this dissertation enables to assess the levelized cost of electricity (LCOE). The carried out multi-objective optimization reflects the trade-off between economic and energy criteria, but also reveal the potential of this technology in economic performance.

Key words: Supercritical CO_2, Brayton power cycle, Superstructure, Optimization, MINLP, Ant Colony Optimization

---

• **Résumé en français**

Conception et optimisation du cycle de Brayton au CO_2 supercritique dans l'application des centrales à charbon

L'amélioration des systèmes énergétiques est considérée comme un levier technologique pour répondre aux défis liés à la croissance de la demande d'électricité et des émissions des gaz à effet de serre. Les futures centrales devraient présenter une intégration thermique plus flexible et des sources de chaleur mixtes possibles. Une des solutions fiables consiste à utiliser un cycle de Brayton au CO_2 supercritique (CO_2-SC), un tel cycle à haut rendement est théoriquement prometteur pour les applications nucléaires, fossiles et solaires thermiques.

• Un des principaux obstacles au déploiement du cycle de Brayton au CO_2-SC est de justifier sa faisabilité, sa viabilité et son potentiel à l'échelle industrielle. Dans ce contexte deux axes de recherche ont été identifiées :

• Une sélection rigoureuse de l'équation d'état qui permet de représenter les propriétés d'intérêt du CO_2-SC. Une nouvelle méthodologie pour l'optimisation des centrales électriques, permettant de sélectionner automatiquement le procédé optimal parmi une grande quantité de configurations possibles (dénomme superstructure).

Les résultats de la première partie de cette thèse mettent en lumière que l'équation de SW est pertinente pour limiter l'impact de l'imprécision de l'équation d'état sur le dimensionnement du procédé.

Dans cette thèse, un simulateur de procédé commercial, ProSimPlus a été combiné avec un solveur type évolutionnaire (MIDACO) afin d'effectuer des optimisations superstructure. Premièrement, le critère d'optimisation est de maximiser le rendement énergétique du procédé. Dans un deuxième temps, on cherche simultanément à minimiser les coûts du procédé. Pour ce faire, des fonctions de coût internes à EDF ont été utilisées afin de permettre l'estimation des coûts d'investissement (CAPEX), des dépenses opérationnelles (OPEX) et du coût actualisé de l'électricité (LCOE).

Mots clés: Supercritical CO_2, cycle de Brayton, Production d'énergie, Superstructure, Optimization, MINLP, Ant Colony Optimization